UNIVERSITY OF OKLAHOMA

GRADUATE COLLEGE

EFFECTS OF RESIDENT WATER AND NON-EQUILIBRIUM ADSORPTION ON THE PRIMARY AND ENHANCED COALBED METHANE GAS RECOVERY

A DISSERTATION

SUBMITTED TO THE GRADUATE FACULTY

in partial fulfillment of the requirements for the

degree of

Doctor of Philosophy

By

HOSSEIN JAHEDIESFANJANI
Norman, Oklahoma
2006

UMI Number: 3212014

UMI Microform 3212014

ProQuest Information and Learning Company
300 North Zeeb Road
P.O. Box 1346
Ann Arbor, MI 48106-1346

EFFECTS OF RESIDENT WATER AND NON-EQUILIBRIUM ADSORPTION ON THE PRIMARY AND ENHANCED COALBED METHANE GAS RECOVERY

A DISSERTATION APPROVED FOR THE
MEWBOURNE SCHOOL OF PETROLEUM AND GEOLOGICAL ENGINEERING

BY

_____

Dr. FARUK CIVAN (CHAIR)

_____

Dr. ROY M. KNAPP

_____

Dr. SUBHASH N. SHAH

_____

Dr. JAMES M. FORGOTSON Jr

_____

Dr. SAMUEL O. OSISANYA

ACKNOWLEDGMENT

I would like to express my sincere appreciation and gratitude to my parents, Asad and Mansoureh for their continuous support and all the beautiful moments that they have provided to me by their candle-like burning to illuminate my future.

I wish to thank to the members of my doctoral committee: Dr. Roy M. Knapp, Dr. Subhash N. Shah, Dr. Samuel O. Osisanya, Dr. James M. Forgotson Jr, and in particular, **Dr. Faruk Civan** under whose supervision this dissertation work was performed, for his professional, fatherly manner, and timely help in managing and directing this study.

Special thanks are due to the ConococoPhilips Company at Bartlesville, Oklahoma, and especially Mr. David Zornes for the fellowship provided to perform this work.

Finally, the best thanks are due to my fiancée Roya for her lovely presence in my life.

Hossein Jahediesfanjani

Norman, Oklahoma

May 2006

Table of Content Page

List of Tables Page

List of Figures Page

ABSTRACT

The major part of the gas in coalbed methane and shale gas reservoirs is stored as the adsorbed gas in the coal and organic materials of the black shale internal surfaces. The sorption sites in both reservoirs are composed of several macropores that contain very small pore sizes. Therefore, the adsorption/desorption is very slow process and follows a non-equilibrium trend. The time-dependency of the sorption process is further affected by the reservoir resident water. Water can diffuse into the matrix and adsorption sites, plug the pores and affect the reservoir gas production.

This study presents an experimental and theoretical procedure to investigate the effects of the resident water and time-dependency of the sorption process on coalbed and shale gas primary and enhanced recovery by simultaneous CO_2/N_2 injection. Series of the experiments are conducted to construct both equilibrium and non-equilibrium single and multi-component isotherms with the presence of water. A novel and rapid data interpretation technique is developed based on the non-equilibrium adsorption/desorption thermodynamics, mass conservation law, and volume filling adsorption theory. The developed technique is implemented to construct both equilibrium and non-equilibrium multi-component multi-phase isotherms from the early time experimental measurements. The non-equilibrium isotherms are incorporated in the coalbed methane/shale gas reservoir simulations to account for the time-dependency of the sorption process.

The experimental results indicate that the presence of water in the sorption system reduces both carbon dioxide and nitrogen adsorption rates. Reduction in the

adsorption rate for carbon dioxide is more than nitrogen. The results also indicate that the resident water reduces the adsorption ability of low rank coals more than high rank ones. The results of the multi-component sorption tests indicate that increasing the initial mole fraction of the nitrogen gas in the injected CO_2/N_2 mixture will increase the net carbon dioxide sequestration rate on coals in the presence of water. The optimum CO_2/N_2 ratio that can result in the maximum carbon dioxide sequestration rate can be obtained by conducting the experiments for various CO_2/N_2 ratios.

The results of applying the developed non-equilibrium interpretation technique for several literature and in-house data indicate that both the equilibrium and non-equilibrium isotherms can be constructed in shorter time period (around 70 times less than the time required with the equilibrium techniques) and with higher accuracy using this method. The developed isotherms account for the presence of the resident water and hence increase the obtained isotherm accuracy.

The results of incorporating the non-equilibrium isotherms instead of the equilibrium ones in the coalbed/shale gas reservoir simulation indicate that ignoring the time-dependency of the sorption process can lead to significant reservoir recovery prediction error especially in high rank coals that contain tighter pore sizes. Various coalbed/shale primary and enhanced gas production scenarios are considered to demonstrate the flexibility and ability of this technique in accurate reservoir simulation.

CHAPTER 1

INTRODUCTION

The increasing request for the energy has raised the concern of providing the new energy resources to answer the world's energy demands. The lack of the new conventional hydrocarbon reserves and high oil and natural gas prices have led the oil and gas industry to consider the unconventional hydrocarbon resources. The economical oil and gas production from the unconventional resources by the conventional methods is not yet possible. They usually require unconventional techniques to be produced within the economical limits. The questions of whether the production from any unconventional resource is economical and estimation of the true and recoverable reserves have to be answered prior to any investments.

Coalbed methane and shale gas reservoirs are two of the major unconventional natural gas resources not only in the United States but also in some other countries in Europe, Japan, and some parts of Asia. The gas storage and transport mechanisms in both coalbed methane and shale gas reservoirs are somewhat similar. In both reservoirs some part of the gas (over 90% in coalbed methane and around 50% in shale gas reservoirs) is stored as the adsorbed gas. Therefore, to estimate the true reserves and also to accurately simulate the gas transfer in the reservoir a thorough knowledge of the gas adsorption mechanism is essential.

The adsorption mechanism is a complicated and slow process. The gas molecules first approach the solid surface and then are adsorbed on the solid

internal surfaces due to the van der Waals attraction forces. The adsorbed gas builds a new liquid-like state. This state exhibits different thermodynamic, physical, and chemical properties than the free gas. To fully understand the solid-gas interactions and hence the adsorption/desorption mechanisms require a comprehensive knowledge of the various components in contact with each other, and the possible interactions and thermodynamics of the whole system. The majority of the coalbed methane and shale gas reservoirs are initially water saturated. Water can diffuse through the matrix structure in both liquid and vapor forms, and adsorb on the solid surfaces. The gas phase is usually a mixture of various gases such as methane, carbon dioxide, nitrogen, oxygen, and some heavier hydrocarbons. Each of the components has different affinity to different solid surfaces. Therefore, studying the adsorption phenomenon is a complicated task.

Statement of the Problem

An isotherm is usually used to express the ability of the solid to hold gas at various pressure levels at a constant temperature. Different isotherms have been introduced in the literature to model the adsorption behavior of various gases at different adsorbents. Each isotherm is based on some simplifying assumptions that may not be the representative of the reality. The Langmuir isotherm is the most popular one in the coalbed methane and shale gas industry. Langmuir and several other isotherms introduced, and evaluated in the literature, are called the equilibrium isotherms. They only represent the equilibrium and final adsorbed gas

amount at each pressure. Hence, they do not represent the intermediate non-equilibrium stages, experienced in coalbed and shale gas reservoirs.

The gas and liquid adsorption and desorption are slow and time-dependent processes. This creates difficulties especially in the laboratory in constructing an equilibrium isotherm for a given system of coal/gas. Establishing an equilibrium isotherm may take weeks and sometimes several months. Therefore, despite significant improvements in the isotherm development, and coalbed and shale gas reserve evaluation and reservoir modeling techniques, the difficulty of developing a rapid method to establish both equilibrium and non-equilibrium isotherms has not been resolved. Moreover, the available isotherms consider only two phases-gas and coal. In general, the influence of the resident water in the isotherm development has been ignored due to the complexity of the sorption phenomenon in multi-phase systems.

Objectives

The overall objective of this study is to develop a procedure to obtain both equilibrium and non-equilibrium isotherms for the multi-phase system of coal-water and multi-component gas and implement to improve the coalbed and shale gas reservoir simulation. The developed procedure should also reduce the time required to construct an isotherm by taking the early-time non-equilibrium sorption data points and projecting them to the equilibrium state. It is demonstrated that the present approach improves the quality of the presently available coalbed methane and shale gas reservoir simulators by accounting for the dynamics of the

adsorption/desorption processes occurring in the reservoir. The present study accomplishes the above-mentioned objectives by carrying out the following four steps:

1. Experimental studies for measurement of the adsorbed gas volume with and without the presence of water under equilibrium and non-equilibrium conditions.
2. Theoretical studies for development of the equilibrium and non-equilibrium gas isotherms with and without the presence of water.
3. Validation of the equilibrium and non-equilibrium gas isotherms with and without the presence of water.
4. Improving the coalbed methane and shale gas reservoir simulation by replacing the equilibrium isotherms with non-equilibrium isotherms.

The presentation of this study is carried out in the following chapters:

1. Chapter one is an introduction, describing the importance of the problem and general objectives of the current study.
2. Chapter two reviews the coalbed methane and shale gas reservoir characteristics. This helps better understanding the nature of these reservoirs, fluid (gas and water) transportation mechanisms, and the similarities and differences of both coalbed methane and shale gas reservoirs.
3. Chapter three reviews the nature of the adsorption/desorption phenomenon, and the available equilibrium and non-equilibrium theories. This will give the reader a thorough knowledge of the adsorption/desorption processes, the

theory behind the available isotherms, and the thermodynamics of the adsorption/desorption phenomena.

4. Chapter four describes the experimental studies conducted for measurement of the adsorbed gas volume in coal with and without the presence of water under non-equilibrium condition. An experimental set-up is prepared to generate the necessary data and to test the model developed in Chapter five. Series of the non-equilibrium sorption experiments are conducted for the system of pure CO_2 and pure N_2, mixture of CO_2/N_2 with and without water on coal, and the generated data are reported.
5. Chapter five presents theoretical studies for development of equilibrium and non-equilibrium gas isotherms with and without the presence of water. The details of the developed model are presented.
6. Chapter six presents the validation of the procedure used in obtaining the equilibrium and non-equilibrium gas isotherms with and without the presence of water. Series of the literature and in-house generated experimental data are used to evaluate, modify, and validate the developed model.
7. Chapter seven presents the implementations of the developed multi-component non-equilibrium gas adsorption in coal with the presence of water in improving the coalbed methane and shale gas reservoir simulation quality. Series of the primary and enhanced gas production are presented under various CO_2/N_2 injection scenarios.

8. Chapter eight presents the conclusions obtained based on this study and the recommendations offered to expand and improve upon the results of the current study.

CHAPTER 2

REVIEW OF THE FUNDAMENTAL CHARACTERISTICS OF COALBED METHANE AND SHALE GAS RESERVOIRS

The coalbed methane and shale gas reservoirs are unconventional gas reservoirs having specific characteristics. Both coalbed and shale gas reservoirs are naturally fractured and water saturated reservoirs. The extension, direction, and properties of the natural fractures may be different in different reservoirs. The naturally fractured reservoirs are usually divided into two distinct sections as the matrix and fracture. Matrix is usually a low permeability and high porosity block that contains and stores the major fraction of the fluid in a reservoir. The natural fractures are the high permeability and low porosity channels throughout the reservoir that enhance fluid and hydrocarbon transfer in the reservoir.

The mechanism of the fluid storage in the matrix structure in coalbed methane and shale gas reservoirs is different than the conventional reservoirs. Because, the porosity and width of the present fractures are very limited and restricted, the volume of the hydrocarbon stored in the fracture system is not significant in compared to the matrix storage capacity. Gas is stored in such reservoirs in the following forms.

1. Gas adsorption on the coal or shale internal surfaces.
2. Gas storage in the free matrix pore volume.
3. Gas storage as dissolved gas in water.

4. Gas storage in the fracture pore volume.

The major gas storage mechanisms in coalbed methane and shale gas reservoirs are gas adsorption and storage in the free matrix pore volume. The process of adsorption is a very complicated process. This is discussed in more detail in the next chapter. The majority of the coalbed methane and shale gas reservoirs are water saturated at their initial state. The water is mainly available in the natural fracture system and can hardly diffuse into the matrix due to the very tight matrix structure and very small pore size. Moreover, the matrix is mainly composed of organic matter that has the least tendency or wettability for water. This section takes a close look at the coalbed methane and shale gas reservoirs from the reservoir structure point of view.

2.1. Coalbed Methane Gas Reservoirs

Coalbeds are characterized as naturally fractured, shallow, low pressure, and water saturated gas reservoirs. The natural fractures in the coalbed are called cleat. The word “cleat” is a mining term, which has been frequently used to describe a variety of fractures commonly found in the coal (Pattison et al. 1996). The natural fractures in the coal structure are divided into several categories. Figure 2.1 shows all of the major natural fractures and cleats encountered in a typical coal sample.

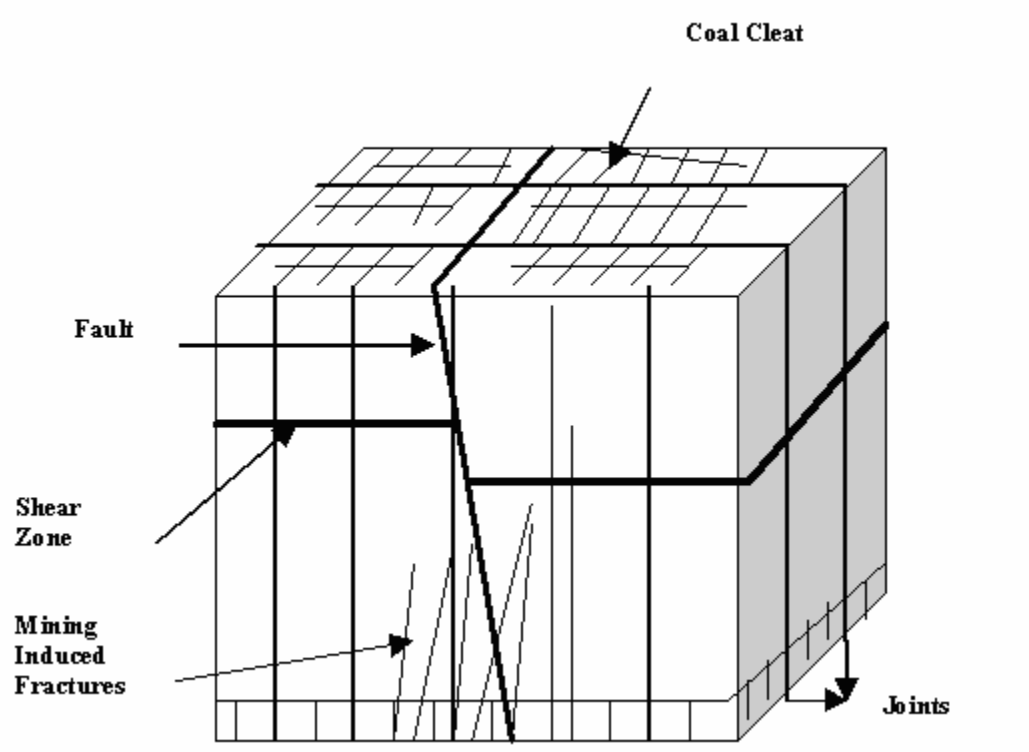

Figure 2. 1.Types of possible fractures in a typical coal structure (After Pattison et al., 1996).

1. Cleats. Cleat is an extensional fracture present in most coals that is confined to a particular lithology or microlithotype. The cleats themselves are divided into two major categories as butt and face cleats. Figure 2.2 shows that the face cleats are continuous natural fractures oriented in the horizontal direction. The butt cleats are discontinuous fractures oriented in the vertical direction.
2. Joints in coal. The definition of joint in coal refers to any extensional fractures other than cleats that are confined to or transect a coal seam. The coal joints are generally extended vertically. These are younger than cleats in the geological time formation sequences.
3. Mining-induced fractures. These fractures are induced during the mining operations due to the external stresses.

4. Faults and shear zones. The coalbed methane reservoir located in the fault or shear-zone areas. These fractures are usually large and have very high permeability in compared with cleats.

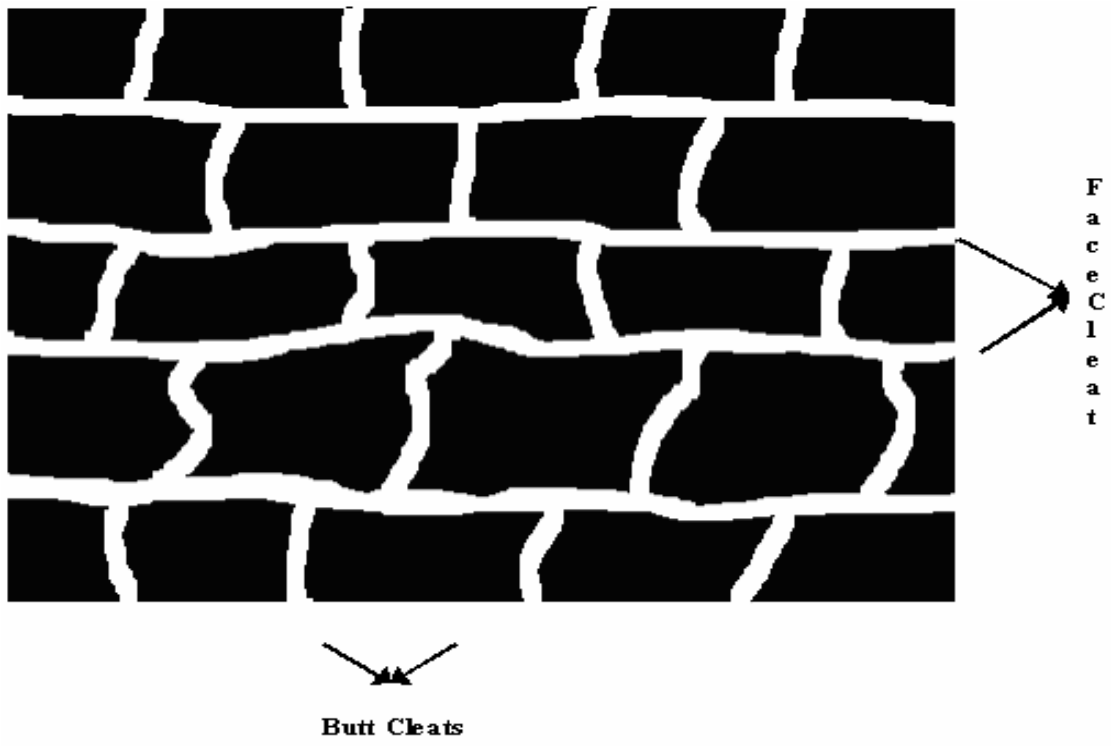

Figure 2. 2. Butt and face cleat distribution in a typical coal matrix.

The typical coal matrix permeability is around 10^{-5} to 10^{-9} md, whereas, the cleat permeability is around 1-50 md. The cleats, also known as micro-fractures, are themselves divided into five distinct groups. These groups are: (1) Vertical micro-cleats (5-20 μm wide and 50-500 μm long and spaced about 30-100 μm apart). (2) Horizontal micro-cleats (0.5-2 μm wide and 50-200 μm long and spaced about 5-10 μm apart). (3) Blocky fractures (1-15 μm wide and 50-200 μm long and spaced less than 100 μm apart). (4) Conchoidal fractures (no regularity in spacing). (5) Striae

fractures (0.1 μm wide and 10-100 μm long and spaced about 0.1-0.3 μm apart) (Gamson et al., 1996).

The coalbed methane reservoir properties, especially the matrix properties, are functions of the coal rank and composition as well as other geological conditions, such as the depositional environment, depth, and quality of the reservoir water. The high rank coals usually have tighter matrix pores, smaller matrix porosities, and higher capacity to adsorb and hold gas. In contrast, the low rank coals have larger pores, higher matrix permeability, and adsorb less gas. Therefore, the major hydrocarbon storage mechanism in high rank coals is through adsorption. The adsorbed gas in high rank coals accounts for approximately 98% of the stored gas in these reservoirs. Practically, the matrix porosity is too low that it cannot contain more than 1-5% of the gas reserves in high and very high rank coals.

On the other hand, the hydrocarbon storage mechanism in low rank coals is usually influenced by the free gas in place in the matrix structure. This gas may account for up to 70-80% of the total gas in-place of the low rank coalbed methane reservoir. For both low and high rank coals very minor percentage of the gas (usually less than 2%) exists as dissolved gas in water that is initially in the cleat system. Figure 2.3 shows that the solubility of methane in water at the typical coalbed methane reservoir condition is not significant.

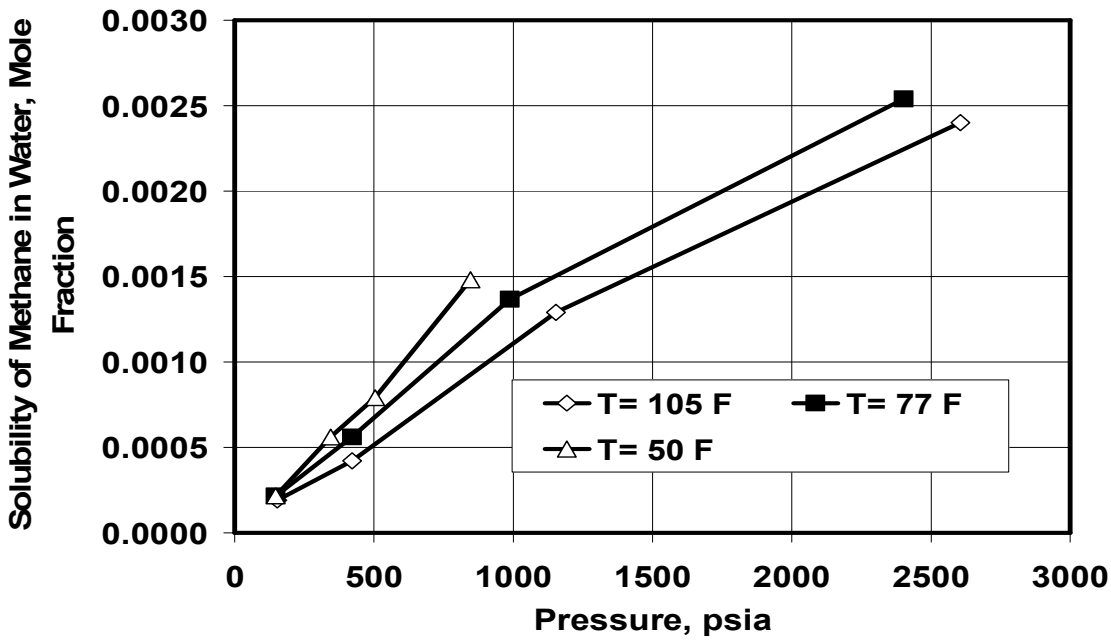

Figure 2. 3. Mole fraction of methane in water phase at various pressures and three different temperatures (Data after Chapoy et al., 2004).

2.2. Black Shale Gas Reservoirs

The black shale gas reservoirs are also naturally fractured reservoirs. The natural fracture system in shale is very similar to the low rank coal structure. The availability of several micro-fractures throughout the shale reservoir helps better and faster gas production and movement inside and from the reservoir. However, the gas storage mechanism in shale reservoirs is to some extent different than the coalbed methane reservoirs. Part of the gas is adsorbed on the internal shale surface in the carbonaceous sites and organic matter.

The shale itself is a combination of several minerals that may affect the ability of shale to adsorb and store methane and natural gases. The average composition of shale is 33% quartz, 47% illite, and 3% chlorite, with the remaining

17% being minerals such as amorphous clays, pyrite and albite (Schettler et al. 1991). The clay minerals themselves are good adsorbents and may be responsible for some of the adsorbed methane in shale structure. Measured matrix permeability for shales ranges from 10^{-3} to 10^{-9} md.

Like low rank coals, the shale reservoir gas content also consists of both adsorbed and free gas available in the shale matrix. The ratio of these two changes from one case to another. Lane et al. (1989) reported that for Devonian shale samples in low pressures up to 400 psia the adsorbed gas in the matrix structure accounts for almost all of the stored gas in shale samples. However, at high pressures, the free gas to adsorbed gas ratio available in matrix pore volume increases up to about 50%. The adsorption studies of Xiaco-Chun et al. (1995) on some Antrim Devonian shale samples also confirmed the Lane et al. results. Xiaco-Chun et al. (1995) found that the ratio of free gas to the adsorbed gas for some samples exceeded over 3.0 meaning that the matrix free gas is the major source of methane for these reservoirs. Furthermore, Xiaco-Chun et al. (1995) investigated the effects of other shale components on the adsorption capacity of the shale samples. The presence of illite in the shale can contribute significantly to the total gas storage in Devonian shales. They also examined the effect of total carbon matter on adsorption capacity. They concluded that the shale adsorption capacity is a linear function of the total organic carbon in the shale samples.

2.3. Fluid Transport Mechanisms in Shale and Coalbed Methane Reservoirs

From the reservoir engineering perspective, the coalbed methane and shale gas reservoirs are divided into two distinct segments, matrix and fractures. The fluid transportation mechanisms in coalbed/shale gas reservoirs are divided into three major categories: (1) Flow from the coal or shale internal surface to the matrix pore volume. (2) Flow through matrix pore volume to the natural fractures. (3) Flow from the natural fractures to the wellbore. Figure 2.4 shows the sequence of these three production stages throughout a CBM or shale gas reservoir.

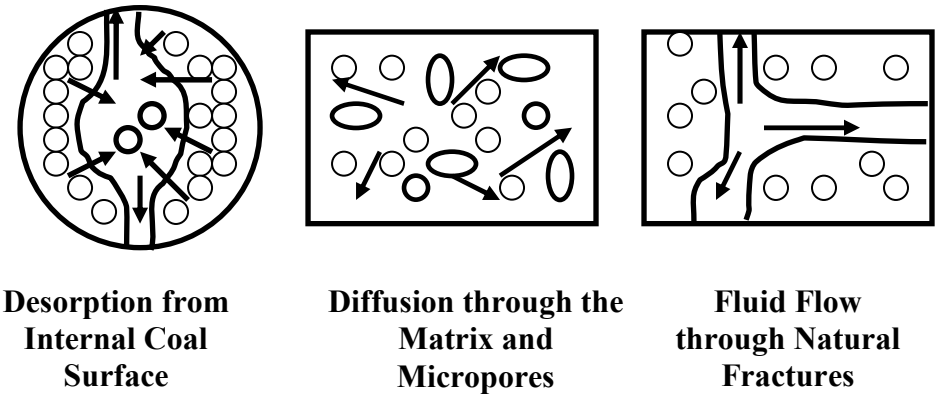

Figure 2. 4. Model of methane flow through the coal showing desorption, diffusion and Darcy flow (Idea After Gamson et al., 1996).

As described in Figure 2.4, the first gas transportation step is gas desorption from the coal or shale internal surfaces. As soon as the matrix pressure drops below the sorption pressure, the gas molecules start detaching from the coal/shale internal surface and entering the coal or shale matrix pore volumes. In high rank coals, where the matrix permeability is very low, the fluid movement in the matrix

structure occurs by diffusion. The detached molecules diffuse throughout the matrix and enter the natural fractures surrounding the matrix structure.

In low rank coals and shale gas reservoirs, the matrix permeability is relatively higher than the high rank coals. The major fraction of the gas is stored as the free gas in the pore volume of the matrix. The transport mechanism in the cleat system is governed by the Darcy flow. The third gas production stage is the same for all three cases. The fluid entering the natural fracture structure moves toward the wellbore based on the Darcy law. One of the differences between the high and low rank coals and shale is that the matrix structure in high rank coals is almost water free; whereas, in other two cases, the water can be stored in the matrix and therefore, the two phase flow of water and gas should be accounted for when modeling these reservoirs.

CHAPTER 3

REVIEW OF THE EQUILIBRIUM AND NON-EQUILIBRIUM ADSORPTION MODELS

The gas production procedures in the coalbed methane and shale gas reservoirs are different from other conventional gas reservoirs. The main difference is due to the adsorption process that takes place in the coal and shale internal surfaces. This is the primary reason for gas storage within the reservoir and is very important in studying these reservoirs. This chapter will discuss the fundamentals of the adsorption. The important equilibrium adsorption models and theories will be explained. The last section of this chapter reviews the most popular non-equilibrium adsorption theories, the recent developments, and the novel techniques available in the area of the non-equilibrium adsorption.

When certain amount of molecules continually approach a solid surface and stay there for a certain length of time by the influence of attraction forces without re-separating, the concentration and density of the gas molecules in the vicinity of the solid surface will increase. Under specific circumstances, the dense molecules form a liquid-like phase on the solid internal surface (Boer, 1899). The liquid-like "condensed" phase is called the adsorbed phase. The solid surface that holds the adsorbed phase is called the adsorbent. This phenomenon is called the adsorption phenomenon. The reverse of the adsorption phenomenon is named desorption; during which the adsorbed phase is released from the adsorbent surface.

In most of the industrial applications, both adsorption and desorption are referred to as the sorption phenomenon. The sorption phenomenon occurs every day and everywhere. This is a universal concept, used in many industries and sciences including, separation, polymer, surfactants, reaction, gas storage, hydrology, soil physics, biophysics, and chemistry.

In the petroleum industry, sorption is a very important concept in fluid flow through porous media, coalbed methane, shale gas reserve analysis and reservoir simulation, immiscible gas flooding and miscible solvent flooding in oil and especially heavy oil reservoirs to improve oil recovery, and studying heavy petroleum material depositions at the reservoir conditions.

The significance of sorption phenomenon for a specific gas and solid system depends on the gas phase pressure, temperature, size of gas molecules, solid contact area, and solid surface configurations. In gas adsorption, the number of molecules attracted to a solid surface depends on the conditions in the gas phase. For very low pressures, relatively few molecules are adsorbed, and only a fraction of the solid surface is covered. As the gas pressure increases at a given temperature, surface coverage increases. When the thickness of the adsorbed phase on solid surface is about equal to the adsorbed molecule diameter, the adsorption is said to form a monolayer. Further increase in pressure may result in multilayer adsorption. However, the complexity of the solid surface makes it possible for multilayer adsorption to occur on one part of a porous surface while vacant sites still remain on another part.

3.1. Equilibrium Adsorption Models and Theories

Several adsorption models and theories are available in the literature. These theories are divided into the single component and multi-component adsorption theories. These theories are developed under various assumptions and may be suitable for some specific cases. However, as the adsorption types differ, the theories to describe the adsorption models also vary. The most important adsorption theories can be divided into two separate groups as:

1. Layer-by-layer adsorption theory.
2. Theory of volume filling of micropores

The Langmuir and Brunauer-Emmett-Teller (BET) are examples of the layer-by-layer adsorption theories and the Dubinin–Radushkevich–Stoeckli theory is the best example of the volume filling theory. These theories are fully described in Appendix 1.

3.2. Non-Equilibrium Adsorption Models and Theories

The described models in Appendix 1 are based on the assumption that all the measurements are conducted under the equilibrium conditions. In another words, the expressions are given for equilibrium cases and do not represent the intermediate non-equilibrium stages. The kinetic of adsorption has also been a concern for many years. The researchers are still in the process of developing and improving the adsorption models to describe the kinetics of adsorption of several systems. The adsorption kinetics play very important role in several sciences

including polymer, separation, filtration, soil mechanics, material mechanics, quantum physics, biomaterials, chromatography, water purification, electrophoresis and even petroleum science. The following sections review the most important adsorption/desorption kinetic models. The description of each model and the improvements are also discussed in more details.

3.3.a. Absolute Rate Theory (ART)

The absolute rate theory was first introduced by (Glasstone et al., 1941). According to this theory, for any reaction, there is always an intermediate stage through which the reaction progresses. Therefore, for a simple reaction progress of A to B, the following paths are assumed:

$$A \longrightarrow AB \longrightarrow B$$

where AB is the form of A and B that represents the transient state and is neither A nor B. Theoretically, each material has a certain level of energy. The activation energy needed for conversion of A to AB is given by the following expression:

$$\Delta G^{*} = G^{AB} - G^{A} \qquad (3.1)$$

The assumption is made that the molecules transfer from the gas phase to the intermediate bulk phase on the solid surface and then from the bulk solid surface to the solid internal pore structures (Ward et al., 1982). The intermediate stage is called activated complex. The activated complex is at equilibrium with the gas phase and the gas molecules have to pass through the activated complex in

order to be adsorbed (Rudzinski and Panczyk, 2000). Figure 3.1 explains this process further.

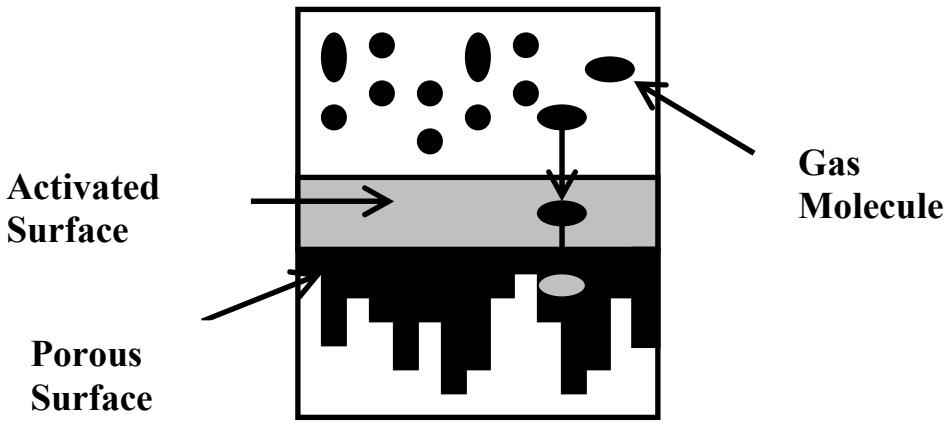

Figure 3. 1. The schematics of ART approach; the gas molecules pass through an activated surface to adsorb on the solid structure.

According to Equation 3.1, there is an energy difference between any molecule in the gas phase and the activated phase. This energy difference is called as activation energy and is the amount of energy that will be released by a molecule when it is adsorbed on the activated surface. The rate of the adsorption in such a case will be a function of the gas phase characteristics and the solid surface parameters. The combined form of these parameters can be expressed as:

$$R_a = \alpha \nu F(\theta) \exp\left(\frac{-\varepsilon_a}{kT}\right) \quad \text{.....(3.2)}$$

where $\nu = P/\sqrt{2\pi mkT}$ is the rate of collision of the gas molecule of mass m with the solid surface, F(θ) is the fraction of surface available for adsorbing molecules, P is the pressure, and k and T are the Boltzmann constant and absolute temperature, respectively.

The adsorbed molecules may desorb under favorable conditions and return to the gaseous phase. The rate of desorption of an adsorbed molecule from the activated surface to the gas phase is a function of the surface and gas properties. When an adsorbed molecule being released from the activated surface into the gas phase some energy is either released or consumed. This energy is called the activated energy for desorption. Therefore, desorption rate can be expressed as the following form:

$$R_d = \gamma G(\theta)\exp\left(\frac{-\varepsilon_d}{kT}\right) \quad \text{.....(3.3)}$$

where γ is constant, G(θ) is a function related to the surface coverage θ, and ε_d is the activated desorption energy. The overall non-equilibrium expression for any sorption process is written according to the following:

$$\frac{d\theta}{dt} = R_a - R_d \quad \text{.....(3.4)}$$

The ART approach by itself, as expressed by several authors, does not provide any explicit function for the surface coverage dependency parameters (Ward and Elmoselhi, 1986). To account for the coverage dependency of the variables several empirical functions are presented. One of the most popular empirical equations, that has frequently been used in the literature to describe the kinetics of a sorption process, is usually referred to as "Langmuir adsorption kinetics" (Ward and Elmoselhi, 1986). This equation is given as:

$$\frac{d\theta}{dt} = K_a P(1-\theta)^s e^{\frac{-\varepsilon_a}{kT}} - K_d \theta^s e^{\frac{-\varepsilon_d}{kT}} \quad \text{.....(3.5)}$$

where s is the number of adsorption sites. For the case of s = 1 and equilibrium Equation 3.5 yields the Langmuir isotherm. However, Nagai and Hirashima (1986) expressed that for localized particles the rate of desorption to be proportional to the $\theta/(\theta+1)$ instead of θ in Equation 3.5. This new innovation was the focus of several articles. Nevertheless, Nagai and coworkers proved that their new expression is able to explain the desorption process better than the previous ones.

Despite several modifications of the ART approach, the shortcomings of this approach in explaining the sorption kinetic phenomenon have been proven (Ward and Elmoselhi 1986). Therefore, after several years of relying on the ART approach, researchers introduced some other theories to improve the quality of the sorption kinetics modeling.

3.3.b. Statistical Rate Theory (SRT)

In contrast to the other theories, the SRT approach turns out to be very successful in predicting the rate of molecular or atomic transport across the interface between macroscopic phases in terms of experimentally controllable variables and material properties of the phases. The need to construct and build a rate equation, that can be used more generally as a universal sorption kinetics theory, has encouraged several researchers to find novel and more applicable rate functions.

In the SRT approach, a thermodynamically isolated system is considered and the transition probability concept is used to construct the expression for the rate of molecular transport. If this approach is successful, the material properties of a

particular pair of macroscopic phases could be tabulated and used in the governing equations for predicting the rate of molecular transport across the interface in any circumstance.

The statistical thermodynamic is one of the powerful tools to predict various thermodynamic properties of the materials in contact with each other. This tool is adopted to construct series of sorption rate equations. Despite the novel appearance of the SRT approach, the idea behind this approach goes back to de Boer (1956) who presented the relationship between chemical potential of any component in the adsorbed phase. Therefore, the rate of desorption could be described by the same procedure:

$$R_d = \xi \exp\left(\frac{\mu^s - \varepsilon_d}{kT}\right) \quad \text{.....(3.6)}$$

where μ^s is the chemical potential of the adsorbed molecules and ξ is a constant. Various correlations are considered in the literature to estimate the chemical potential of the adsorbed molecules. Similar expression can also be applied for the adsorption rate as described by Ward (1983), given by:

$$R_a = \xi \exp\left(\frac{\varepsilon_a - \mu^s}{kT}\right) \quad \text{.....(3.7)}$$

Ward (1983) and Ward et al. (1982) were the first to apply the SRT approach to model the sorption kinetics in the following format:

$$J_{gs} = K_{gs}\left(\delta_{gs} - \delta_{gs}^{-1}\right) \quad \text{.....(3.8)}$$

where K_{gs} is the equilibrium exchange rate for the molecules transferred between the adsorbed state and the gas phase. δ_{gs} can be related to the chemical potential of the adsorbed and gas phase expressed as:

$$\delta_{gs} = \exp\left(\frac{\mu^g - \mu^s}{kT}\right) \quad \text{.....(3.9)}$$

The equilibrium exchange rate is a function of the gas-solid equilibrium properties including equilibrium pressure, and equilibrium adsorbed volume. Therefore, the rate expression itself is limited by the conditions under which the system equilibrates.

The question is how to come up with an explicit expression for the net adsorption rate as a function of the surface coverage. The SRT claims to solve this problem. Ward and Elmoselhi (1986) examined this case for the adsorption of a diatomic molecule on a solid surface. They applied the Born-Openheimer approximation and Boltzmann statistics to estimate the diatomic component in the gas phase:

$$\mu^g = kT \ \ln(P\varphi) \quad \text{.....(3.10)}$$

where φ is expressed as following:

$$\varphi = \left[1 - \exp\left(-\frac{h\omega}{kT}\right)\right] \exp\left(-\frac{D_o}{kT}\right) \frac{h^5}{2m_1 m_2 r_e^2 (m_1 + m_2)^{1/2}} \left(\frac{1}{2\pi kT}\right)^{7/2} \quad \text{.....(3.11)}$$

where h is Planck's constant, m_1 and m_2 are the masses of the atoms in the molecule; D_o is the dissolution energy of the diatomic molecule at 0 K; ω is the fundamental frequency of the vibratory modes; and r_e is the distance of separation of the two nuclei at the lowest energy.

For the adsorbed phase on the solid internal surfaces, the following relationship for the chemical potential was applied:

$$\mu^s = kT \ln\left[\frac{N^s}{M - N^s}(q_1 q_2)^3\right] \quad \text{.....(3.12)}$$

where N^s is the number or moles of the adsorbed molecules, M is the available adsorption sites on the solid surface, and q_1 and q_2 are given by the following expression:

$$q_i = \frac{\exp\left(\frac{\varepsilon_{oi}}{kT}\right)}{1 - \exp\left(1 - \frac{h\omega_i}{kT}\right)} \quad \text{.....(3.13)}$$

and

$$\varepsilon_{oi} = \frac{U_o}{3}\frac{\omega_i}{\omega_1 + \omega_2} + \frac{h\omega_i}{2} \quad \text{.....(3.14)}$$

Using this approach, they could predict the time-dependency of the sorption process in the case of the CO adsorption on Ni. However, there are several parameters in their approach that makes the procedure very complicated. These parameters may not be easily obtained. Elliot and Ward (1997) modified the previous procedure and came up with the following general expression:

$$J = K_e\left[\exp\left(\frac{\mu^g - \mu^s}{kT}\right) - \exp\left(\frac{\mu^s - \mu^g}{kT}\right)\right] \quad \text{.....(3.15)}$$

Using Equations 3.28, and 3.30-3.33, they obtained the following expression for the adsorption kinetics:

$$\frac{d\theta}{dt} = \frac{P_e(\theta_M - \theta_e)}{\sqrt{2\pi mkT}}\left[\frac{(\theta_M - \theta)P\phi\psi \exp\left(\frac{b-\beta'}{kT}\right)}{\theta} - \frac{\theta}{(\theta_M - \theta)P\phi\psi \exp\left(\frac{b-\beta'}{kT}\right)}\right] \quad \text{....(3.16)}$$

Equation 3.16 is being represented as a function of the equilibrium properties. The equilibrium pressure and surface coverage are needed to predict the kinetics of the adsorption process. Moreover, like their previous approach, several unknown parameters present in Equation 3.16 complicate the solution. To further modify the SRT approach and in the continuation of the approach of Elliot and Ward (1997), Rudzinski and Panczyk (2000) adopted the Langmuir adsorption equation and expressed the adsorbed phase chemical potential with the following expression:

$$\mu^s = kT \ln\left(\frac{\theta}{1-\theta}\right) - kT \ln q^s \quad \text{.....(3.17)}$$

where q^s is the molecular partition function of the adsorbed molecules.

$$q^s = q_o^s \exp\left(\frac{\varepsilon}{kT}\right) \quad \text{.....(3.18)}$$

where q_o^s is the molecular partition function of the adsorbed molecules which include all internal degrees of freedom. Rudzinski et al. (2000) assumed three scenarios for the gas-solid cases. These scenarios are:

1. Volume dominated: the amount of the gas in gas phase above the surface dominates strongly over the adsorbed portion.

2. Solid dominated: the adsorbed amount prevails so strongly over the amount in the bulk gas phase that the surface coverage after equilibrating remains unchanged.

3. Equilibrium dominated: The process is carried out under such condition that throughout the process the surface coverage and pressure are the same as the equilibrium surface coverage and pressure.

Rudzinski and Panczyk (2000), obtained several mathematically complicated kinetic equations for each cases explained above. Their equations contain less parameter than Equation 3.34, nevertheless are more complicated to operate. They obtained good matches between experimental data and their approach for adsorption of benzene on activated carbon, CO_2 on Sc_2O_3, and CO_2 on polycrystalline tungsten.

The SRT approach has been able to fulfill its objectives of determining the explicit expressions for the adsorption and desorption rates. However, the expressions themselves are complicated and depend on several other parameters that make the prediction process very difficult.

3.3.c. The Statistical Rate Theory of Interfacial Transport (SRTIT)

The SRTIT approach is the most advanced form of the SRT approach considering a heterogeneous solid surface. The application of this approach in adsorption kinetic process was first introduced by Rudzinski and Aharoni (1995). They proposed a procedure for developing equations for adsorption kinetics and equilibria, corresponding to some model of a heterogeneous solid surface. They

examined the previous approaches and modified the available theories in a manner to transform the isotherm equation into a kinetic equation. For a heterogeneous surface, the adsorption will be a function of the surface heterogeneity and the activated energies described previously. Therefore, a more generalized form of the adsorption equation can be expressed with the following expression:

$$\frac{d\theta}{dt} = \int_{\Omega_a}\int_{\Omega_d}\left\{\left[K_a P(1-\theta)\exp\left(\frac{-\varepsilon_a}{kT}\right)\right] - \left[K_d\theta\exp\left(\frac{-\varepsilon_d}{kT}\right)\right]\right\}\chi(\varepsilon_a,\varepsilon_b)d\varepsilon_a d\varepsilon_d \quad \text{.....(3.19)}$$

where $\chi(\varepsilon_a,\varepsilon_d)$ is a two-dimensional differential distribution of the fraction of the surface sites among corresponding pairs of the values $\{\varepsilon_a,\varepsilon_d\}$. They claimed that using the SRTIT approach readily eliminates the problems due to the difficulties in determining the explicit relationships between the surface coverage and other parameters expressed in Equation 3.37. They introduced Equation 3.38 to describe the time-dependency of the adsorption process:

$$\theta_t^n = \left[1 + \frac{\left(\frac{\partial\theta}{\partial t}\right)}{K'_{gs}PK}\exp\left(\frac{-\varepsilon}{kT}\right)\right]^{-1} \quad \text{.....(3.20)}$$

where the superscript n refers to the nonequilibrium case. This equation is obtained for very low surface coverage (low pressure) range of adsorption process and does not cover the high pressure region. Furthermore, they modeled the sorption activation energy ε using the Freundlich adsorption isotherm in Equation 3.38 and the result of the integration over the surface coverage ranging from 0 to θ was the following expression:

$$\theta_t^n = \left[\left(1+\frac{c}{kT}\right)K_{gs}K_o Pt\right]^{1/(1+c/kT)} \quad \text{.....(3.21)}$$

where c and K_{gs} are constants related to the Freundlich isotherm and K_o is a temperature depended parameter defined as:

$$K_o = K\exp\left(\frac{\varepsilon_o}{kT}\right) \quad \text{.....(3.22)}$$

Practically, when time goes to the infinity, Equation 3.40 should approach to the Freundlich isotherm to represent the equilibrium conditions. However, due to several simplifications in driving Equation 3.40, it is not suitable for the equilibrium cases where the surface coverage is high.

Rudzinski and Panczyk (2000) introduced Equation 3.23 to further modify the adsorption kinetic equations for an energetic heterogeneous surface:

$$\frac{d\theta_t}{dt} = 4kT\chi(\varepsilon_c)\left[\frac{1}{2}K_a P^2\exp\left(\frac{\varepsilon_c}{kT}\right)-\frac{1}{2}K_d\exp\left(\frac{-\varepsilon_c}{kT}\right)\right] \quad \text{.....(3.23)}$$

They assumed that the surface sites are distributed according to the D-R equation. Therefore, the following relationship between the surface coverage and the probability function exists:

$$\chi_c(\theta_t) = \frac{r}{\delta}(-\ln\theta_t)^{(r-1)/r}\theta_t \quad \text{.....(3.24)}$$

where r and δ are the D-R equation parameters. By using Equations 3.23, 3.24 and the D-R isotherm and after integration over the range of 0 to θ coverage they obtained Equation 3.43 as:

$$\theta(t) = \exp\left\{-\left\{-D\ln\left[\frac{P}{P_o}\tanh\left(2PK_{gs}t\right)\right]\right\}^r\right\} \quad \text{.....(3.25)}$$

where D and r are the D-R isotherm parameters. It is applied as following for the equilibrium case, when $\lim \tanh\left(2Pk_{gsi}t\right)\Big|_{t\to\infty} = 1.0$

$$\theta = \exp\left\{-\left[-D\ln\left(\frac{P}{P_o}\right)\right]^r\right\} \quad \text{.....(3.26)}$$

Equation 3.25 has several advantages upon Equation 3.21 and the most important one is its applicability for higher pressure and surface coverage ranges. Equation 3.21 contains two parameters K_{gs} and c, whereas, Equation 3.25 contains four parameters K_{gs}, D, P, and r.

Equation 3.25 has been demonstrated to successfully predict the kinetics of adsorption of benzene in the carbon F4 (Rudzinski and Panczyk, 2000), propane and propylene adsorption on Chemviron and Wesvaco activated carbon in low pressures, and various gas adsorption on adsorption on carbon molecular sieves (Jahediesfanjani and Civan, 2005).

It will be demonstrated in the present study that this approach can be applied in the coalbed methane isotherm development, and also coalbed methane reservoir simulation and enhanced coal gas recovery procedures by CO_2 and N_2 adsorption. It

will also be established that a similar approach can be taken to model the gas dissolution in water and water adsorption on coal. Equations 3.25 and 3.26 will be modified for high pressure, multi-component and multi-phase gas-water adsorption on coal/shale surfaces. The further development in the SRTIT approach is to expand the approach for the multi-component gas adsorption/desorption kinetics prediction on the coal surface. The pressure term in Equations 3.25 and 3.26 is replaced by fugacity and several other modifications are also applied to further generalize Equations 3.25 and 3.26 for non-equilibrium and equilibrium adsorption isotherms, respectively.

CHAPTER 4

EXPERIMENTAL STUDIES FOR MEASUREMENT OF ADSORBED GAS VOLUME IN COAL WITH AND WITHOUT WATER UNDER NON-EQUILIBRIUM CONDITION

According to the Dubinin–Radushkevich (D-R) adsorption theory, the gas adsorption occurs on the macropores by the volume filling process. This process was explained and it was emphasized that the volume filling of the macropores is a slow process. The non-equilibrium relationship describing this process was derived by applying the non-equilibrium thermodynamics.

The gas transport in the coal/shale micropores is usually modeled applying Fick's second law. According to the Fick's second law, the gas molecules diffuse from one point to another because of the concentration difference between two points. Therefore, in the modeling and simulating the coalbed methane reservoirs, two separate time-dependent processes should be considered. The gas diffusivity coefficients in the micropores of various coals are reported in the literature. However, the amount of data available in the literature regarding the time-dependency of the volume filling of the macropores are scarce.

The purpose of the experimental procedure here is to obtain the kinetics of the gas, water, and coal interactions with each other. Series of three-phase non-equilibrium models were developed in the next chapter to model the experimental data.

4.1. Description of the Equipment

4.1.a. Adsorption/Desorption Test Equipment.

The experimental set-up shown in Figure 4.1 and used in this study is composed of the following segments:

1. PVT-cell: The PVT cell is a cylindrical container that contains coal, water, and gas. The mixture of gases and water in contact with coal were pressurized in the PVT cell under a constant temperature.
2. Gas reservoirs: Two gas reservoirs of N_2 and CO_2 were used in the experimental set-up. The maximum gas pressure in each reservoir was approximately 1000 psia. However, the gas pressure can be controlled by a high-pressure regulator that is connected to the gas reservoir.
3. Check-Valve: The check-valve was used between the gas reservoir and the PVT cell to allow for the PVT cell pressure changes with more flexibility.
4. Pressure transducer: A pressure transducer was placed to monitor the pressure changes inside the PVT cell.
5. Heating Jacket: The heating jacket covers the PVT cell to keep the cell temperature constant and minimize the effect of the room temperature variations on the PVT cell pressure.
6. Computer: A PC containing a data acquisition system was used to convert the electrical voltages induced from the pressure transducer to the pressure changes.

7. Various mesh size: The various mesh sizes were used to separate the coals with various grain sizes.

4.1.b. Water Content Measurements

Figure 4.2 shows the Thermo-Gravimetric Analyzer (TGA) set-up used in this study to determine the water content of the coal samples at various temperatures and the atmospheric pressure. The TGA constantly measured the amount and rate of weight change of material either as a function of temperature or isothermally as a function of time, in a controlled atmosphere. The TGA 50 operates on a null-balance principle. Physically attached to a taut-band meter movement, the balance beam is maintained in a horizontal reference position by an optically actuated servo loop. Attached to the control end of the balance beam is a light shutter; a constant intensity lamp is focused through an aperture slit in the shutter to strike two vertically mounted photodiodes.

When the balance beam is in a null position, the focused light strikes both photodiodes equally. As sample weight is lost or gained, the beam becomes unbalanced and moves from the null position, causing more light to strike one photodiode than other. The sample temperature is obtained from the sample thermocouple located close to the sample. During heating, the sample may undergo changes that liberate gases. To prevent these gases from back-diffusing and condensing on the meter movement, purge gas is admitted into the balance housing. This gas flows over the meter movement, fills the control chamber, and purges the

sample chamber by exiting through the end of the furnace tube. This device is used to estimate some of the coal parameters, such as the coal, water, and ash contents.

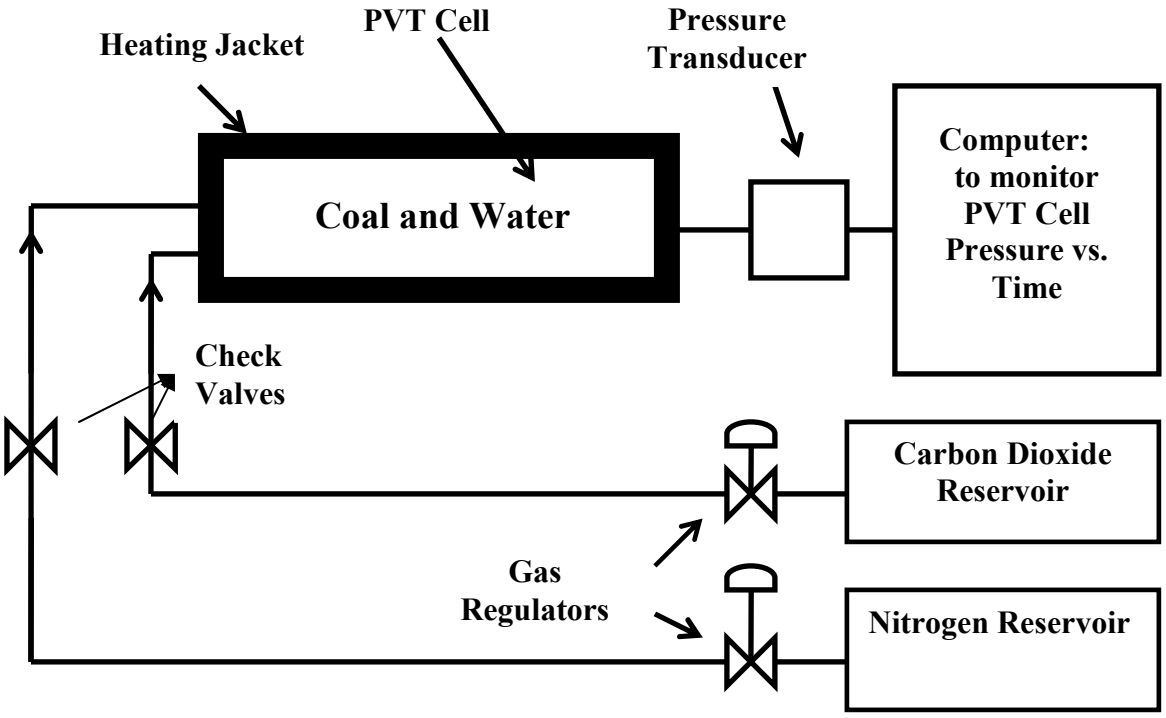

Figure 4. 1 The schematic of the designed volumetric adsorption apparatus composed of the PVT cell containing coal and water, gas reservoirs, and the computer.

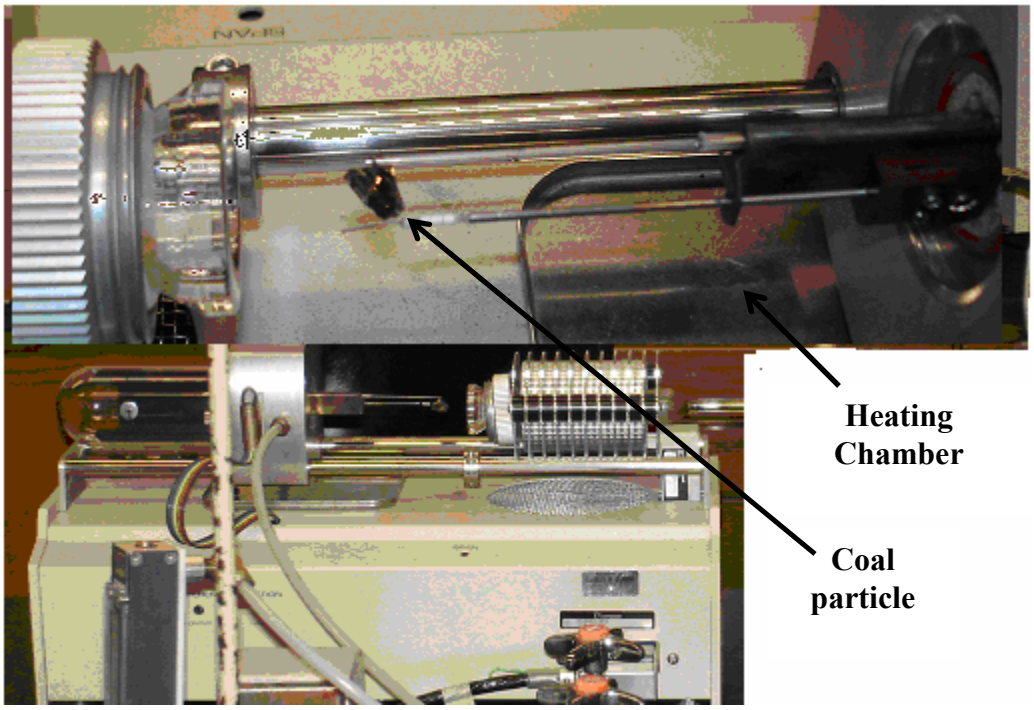

Figure 4. 2. The Termo-Gravimetric Analyzer (TGA) 50 device used to measure the coal water and ash content.

4.2. Description of the Materials

The following materials were used in the experimental study:

1. Coal: Two coal samples were obtained and grounded into six different size ranges. Figure 4.3 indicates the grounded coal samples in various meshes. The configuration of each coal including its rank and density were estimated.

2. Carbon dioxide, nitrogen, helium gases. These gases were used to conduct the sorption experiments and also to calibrate the system.

3. Distilled water: To avoid the presence of impurities that may influence the experimental results, the distilled water was used.

Figure 4. 3. Coal A is grounded into 6 different grain sizes indicated in Table 4.1.

4.3. Experimental procedure

The experimental set-up is designed, built, and tested for pressure sensitivity and fluid leakage. A certain load of weight was applied on the system and the pressure values corresponding to the certain load are monitored. To balance the system, some of the software variables relating the induced voltages from the pressure transducers to the system pressure were adjusted. This is repeated for five more loads to ensure the accuracy of the measurements. After adjusting the experimental equipment parameters, series of the experiments in the following order were performed.

Experiment 1. Gas-water system

The first step is to determine the kinetics of the solubility of CO_2 and N_2 gases in water. The equilibrium solubility of these gases in water at various pressures and temperatures are given in the literature (Evelein and Moore, 1979, Mohammadi et al., 2005, Dhima et al., 1999, and Chapoy et al., 2004). However, the literature data does not include the intermediate non-equilibrium gas-water interactions. When gas and water are in contact with each other, some of the gas may dissolve in water and some of the water will evaporate to the gas phase. Therefore, if the system temperature and volume are kept constant, the total system pressure variations will be a good indicator of the gas and water phase component changes versus time.

First step was to measure the PVT cell volume. The PVT cell was filled with water and the volume of the water was then measured. The measured PVT cell volume is 340.00 cc (cm^3) equal to 20.75 in^3. The PVT cell was loaded with 100 cc (6.10 in^3) water. The pressure regulator connected to the gas reservoir was adjusted at 50 psia. The gas reservoir valve opens. The check valve connecting the gas reservoir to the PVT cell opens and the gas was allowed to enter the PVT cell. When the PVT cell is charged with the gas the check valve was closed, the gas reservoir valve was also closed and therefore, a close system that contains gas and water under the constant ambient temperature, was provided. The pressure transducer shows the PVT cell pressure changes versus time. The recorded pressures versus time values indicate that the nitrogen and carbon dioxide dissolution in water are time-dependent phenomena. The pressure versus time

measurements for both gases at different applied pressures are indicated in Figures 4.4 and 4.5.

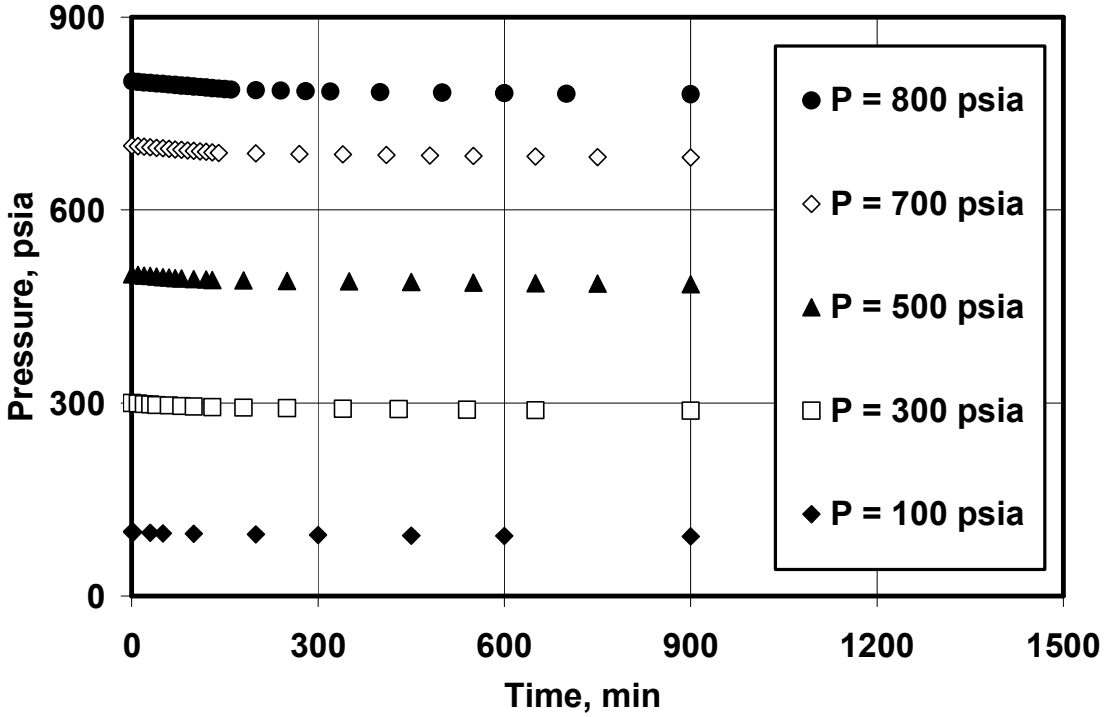

Figure 4. 4. The PVT cell total pressure versus time for the nitrogen-water system.

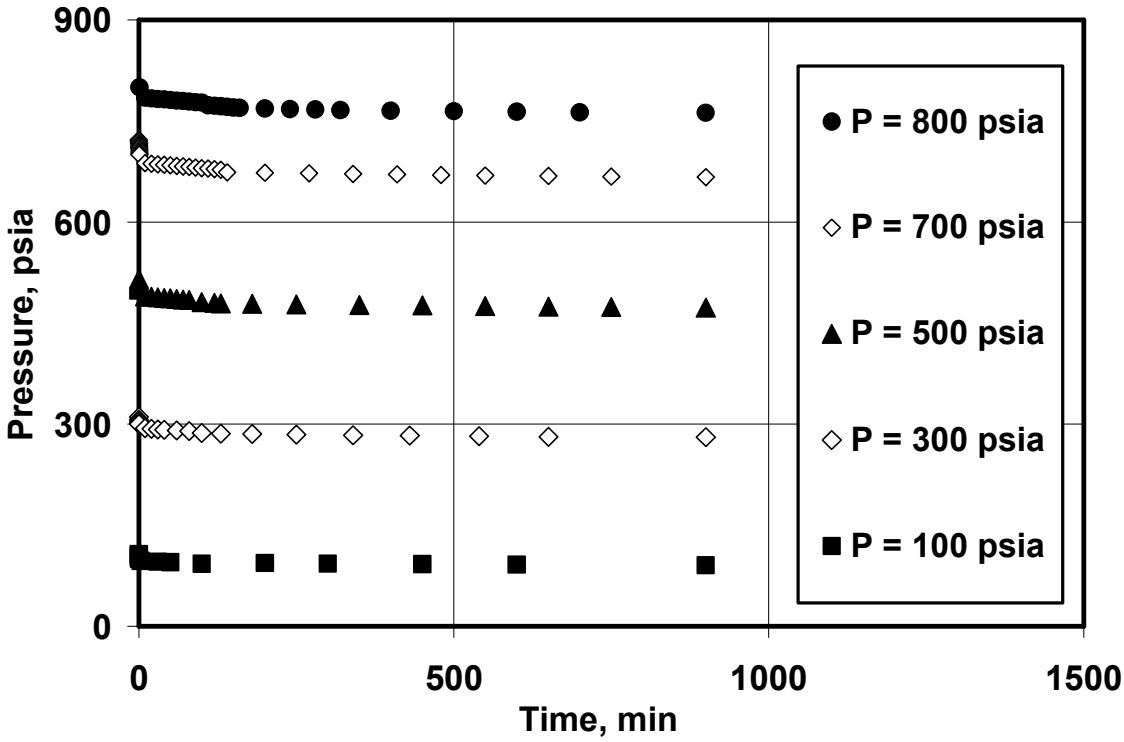

Figure 4. 5. The PVT cell total pressure versus time for the carbon dioxide-water system.

Coal-Gas Systems

Two coal samples available in the laboratory are considered in the coal-gas experiments.

Experiment 2. Coal Moisture and Ash Content Measurements

The first task was to determine the fixed carbon content, and hence the coal rank for both coal samples. The coal samples were first grounded using five mesh sizes. The grounded coal was separated using various mesh sizes and shaking sonic equipment. The sonic operates for approximately 30 minutes and separates the grounded coal particles into several particle ranges. Therefore, the coal particle

diameters were divided into seven different particle ranges in the following order: $d_g>0.131$, $0.131>d_g>0.0555$, $0.0555>d_g>0.0394$, $0.0394>d_g>0.0331$, $0.0331>d_g>0.0117$, $0.0117>d_g>0.0098$ and $d_g<0.0098$, where d_g is measured in inches.

One gram of each particle range was loaded into the heating chamber of the TGA device. The sample was heated up to the temperature of 220^o F (105^o C) for one hour. The mass reduction of coal sample was the indication of its moisture content. These coal samples have been kept in contact with the air for a long time and most of its volatile matter has already been evaporated. Therefore, it was not possible to predict the initial coal components and properties as they were in the reservoir conditions. However, some parameters like the current moisture content and coal ash content at 650^oC, were measured using the available devices. The obtained properties are summarized in Tables 4.1 and 4.2. The last column of each table indicates the estimated rank of the coal sample based on the measured ash content. Coals A and B contain 55 wt%, and 68 wt% ash content respectively. Therefore, coal A is composed of higher fixed carbons than coal B. It indicates that the coal A has higher rank than coal B.

Table 4. 1. Coal A characteristics (initial water and ash content).

Mesh size (inch)	Grain Diameter (inch)	Moisture Content, wt%	Ash, wt% ($650^{o}C$)	Coal Rank
d>0.131	0.15	0.63	55	high
0.131>d>0.0555	0.074	0.58	55	high
0.0555>d>0.0394	0.042	0.56	55	high
0.0394>d>0.0331	0.035	0.55	55	high
0.0331>d>0.0117	0.021	0.54	55	high
0.0117>d>0.0098	0.0105	0.54	55	high
d<0.0098	0.00090	0.54	55	high

Table 4. 2. Coal B characteristics (initial water and ash content).

Mesh size (inch)	Average grain Diameter (in.)	Moisture Content, wt%	Ash, wt% (650^{o}C)	Coal Rank
d>0.131	0.154	0.83	68	Medium-high
0.131>d>0.0555	0.079	0.78	68	Medium-high
0.0555>d>0.0394	0.045	0.76	68	Medium-high
0.0394>d>0.0331	0.0351	0.75	68	Medium-high
0.0331>d>0.0117	0.0270	0.74	68	Medium-high
0.0117>d>0.0098	0.0107	0.74	68	Medium-high
d<0.0098	0.0085	0.74	68	Medium-high

Experiment 3. Gas-Coal System

The third experimental procedure was to conduct the adsorption tests for the single component gas and coal samples without the presence of water. The PVT cell was loaded with 100 grams of the grounded coal. The pressure regulator connected to the nitrogen gas reservoir was adjusted at 50 psia. The nitrogen reservoir valve opens and the PVT cell was charged with nitrogen. When the computer connected to the cell indicates that the initial system pressure (P_{in}) is 50 psia, the check valve between the nitrogen reservoir and the PVT cell was closed and the PVT cell pressure versus time data are recorded until the system pressure change with time was negligible (less than 0.3 psia per hour).

The same procedure was repeated for other initial pressure levels such as 200, 400, 600, and 800 psia, for each particle size range and the nitrogen and carbon dioxide gases separately. The system pressure versus time data were obtained and indicated in Figures 4.6-4.7 for both nitrogen and carbon dioxide gases at Pin=50 psia for coal A. The similar figures for other initial pressure levels are indicated in Figures A2.1-A2.8 in the Appendix 2.

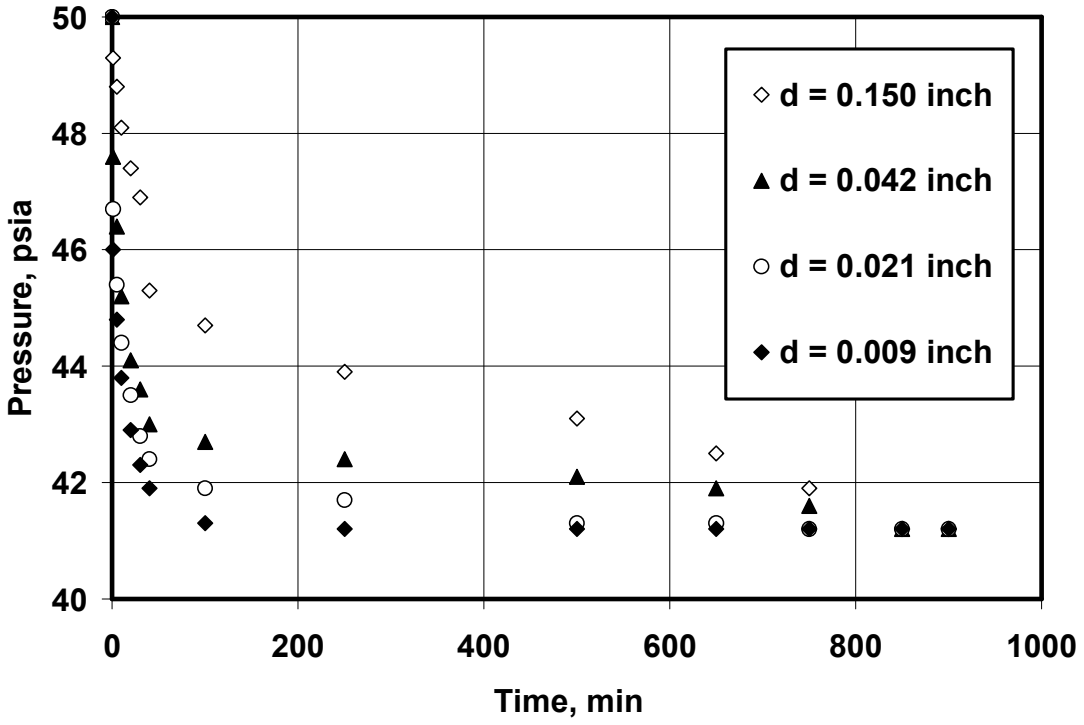

Figure 4. 6. Pressure versus time for various average coal A grain size and N_2 system (P_{in} = 50 psia).

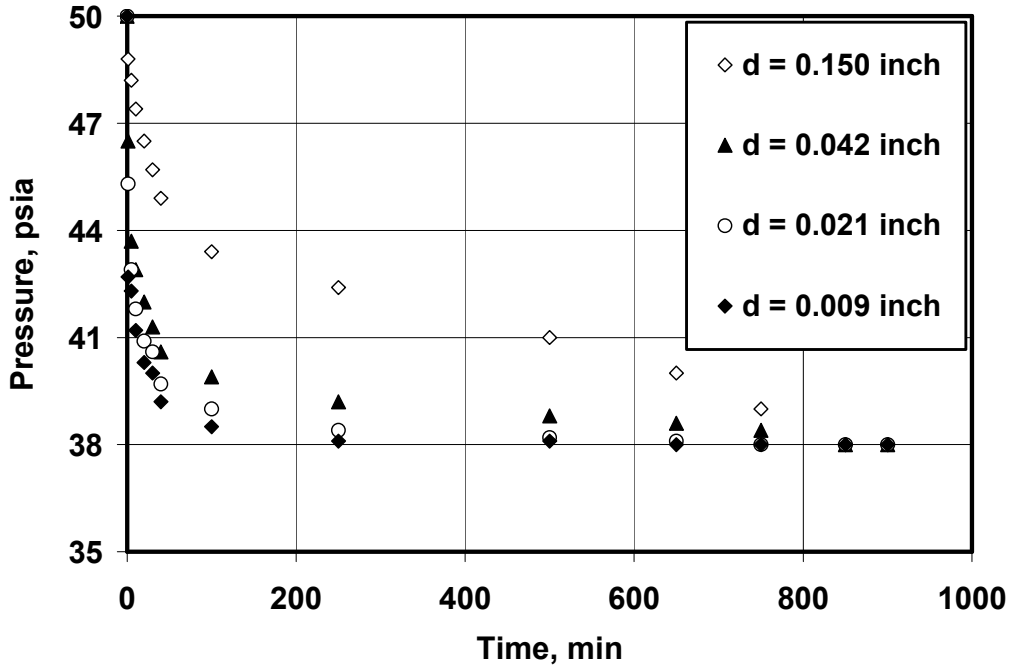

Figure 4. 7. Pressure versus time for various average coal A grain size and CO_2 system (P_{in} = 50 psia).

The similar experiments were conducted for coal B that has a lower rank that a coal A (indicated in Table 4.2). Figures 4.8-4.9 show the system pressure versus time for both nitrogen and carbon dioxide gases at P_{in} = 50 psia for coal B. The similar figures for other initial pressure levels are indicated in Figures A2.9-A2.16 in Appendix 2.

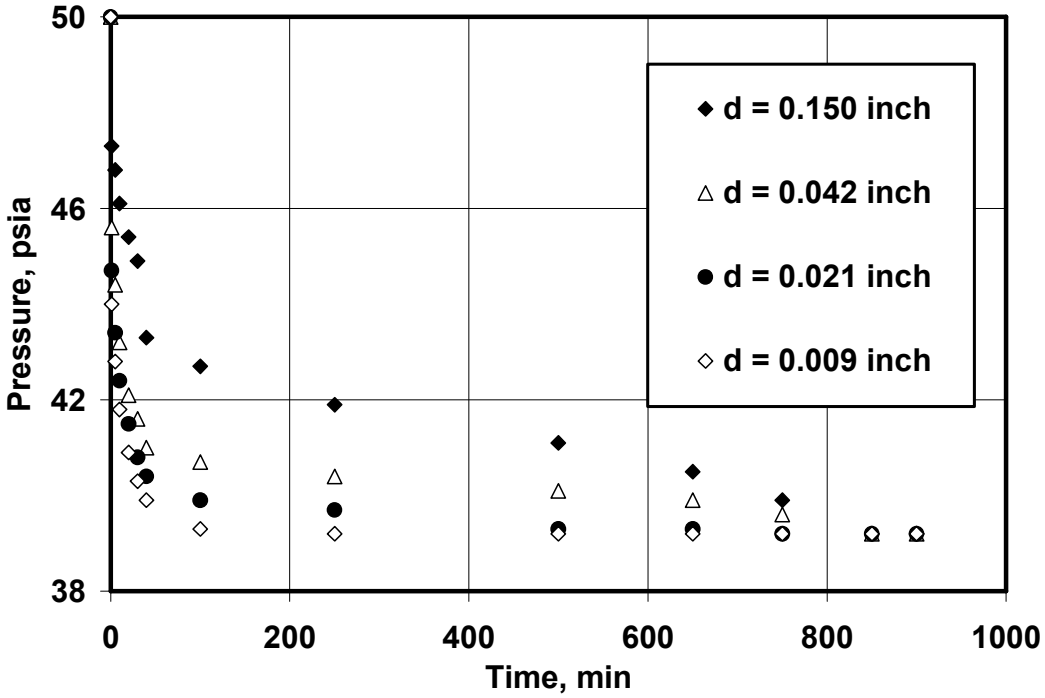

Figure 4. 8. Pressure versus time for various average coal B grain size and N_2 system (P_{in} = 50 psia).

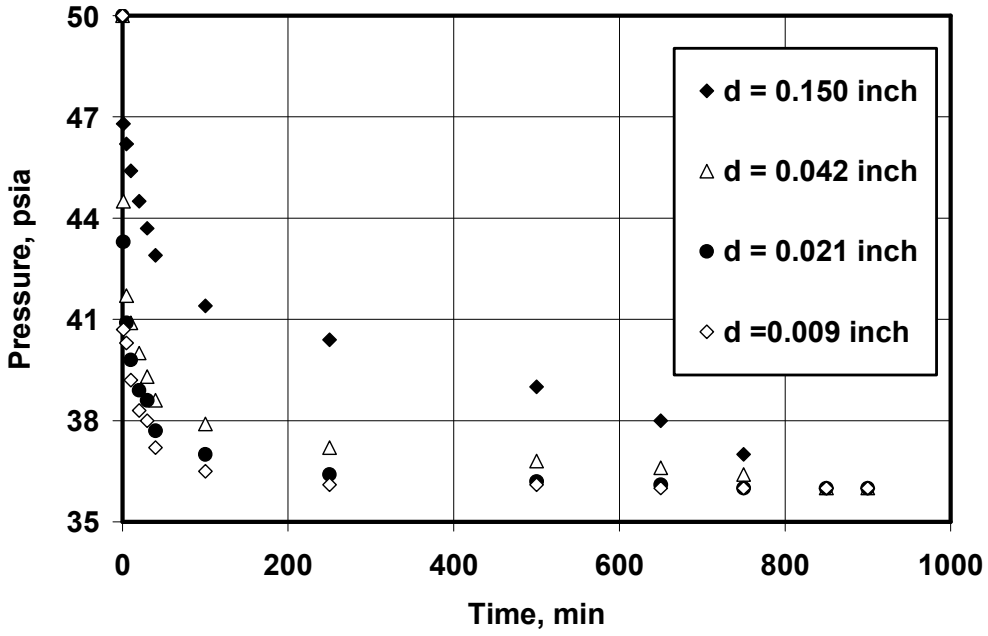

Figure 4. 9. Pressure versus time for various average coal B grain size and CO_2 system (P_{in} = 50 psia).

Experiment 4. Gas-Coal-Water

The forth experimental procedure was to conduct the adsorption tests for the single component gas and coal samples with the presence of water. The PVT cell was loaded with 100 grams of the grounded coal and 40 cc distilled water. The pressure regulator connected to the nitrogen gas reservoir is adjusted at 50 psia. The nitrogen reservoir valve opens and the PVT cell was charged with nitrogen.

When the computer connected to the cell indicates that the initial system pressure (P_{in}) is 50 psia, the check valve between the nitrogen reservoir and the PVT cell was closed and the PVT cell pressure versus time data were recorded until the system pressure change with time was negligible (less than 0.3 psia per hour). The same procedure was repeated for other initial pressure levels, such as 200, 400, 600, and 800 psia, for each particle size range for both nitrogen and carbon dioxide gases separately. The system pressure versus time data were obtained and indicated in Figures 4.10 and 4.11 for both nitrogen and carbon dioxide gases at Pin=50 psia for coal A. The similar figures for other initial pressure levels are indicated in Figures A2.17-A2.23 in Appendix 2.

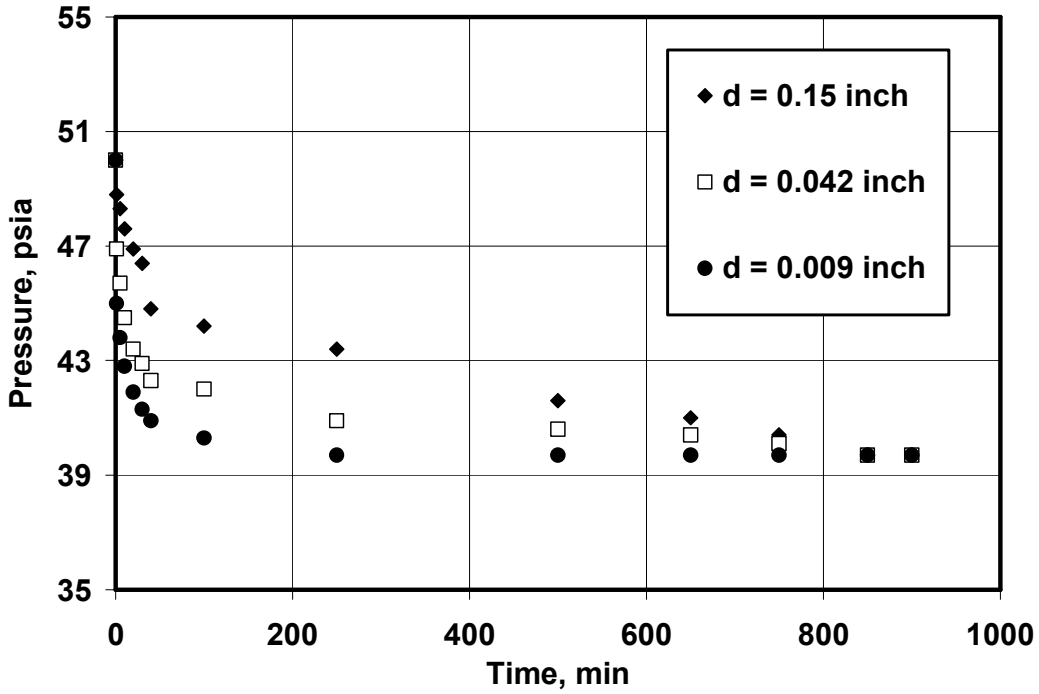

Figure 4. 10. Pressure versus time for coal A-N_2-Water, for different grain sizes (P_{in} = 50 psia).

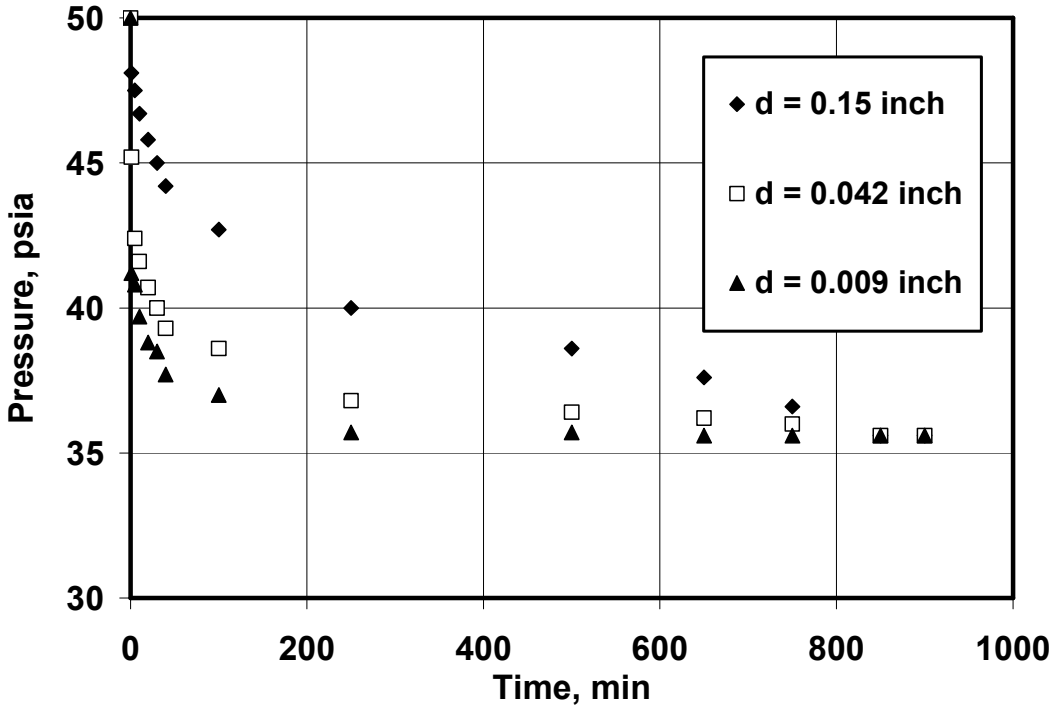

Figure 4. 11. Pressure versus time for coal A-CO_2-Water, for different grain sizes (P_{in} = 50 psia).

Experiment 5. CO_2-N_2 Mixture and Coal System

The fifth experimental procedure was to conduct the adsorption tests for the multi-component gas and coal samples without the presence of water. The PVT cell was loaded with 100 grams of the grounded coal. The pressure regulator connected to the nitrogen gas reservoir was fixed at 100 psia. The nitrogen reservoir valve opens and the PVT cell was charged with nitrogen. When the computer connected to the cell indicated that the initial nitrogen pressure (P_{N2}) was 100 psia, the check valve between the nitrogen reservoir and the PVT cell is closed. The pressure regulator connected to the carbon dioxide reservoir is fixed at 400 psia. The carbon dioxide reservoir valve was opened and the PVT cell was pressurized with carbon dioxide to the initial total pressure (P_{tin}) of 400 psia. Therefore, the initial PVT cell pressure was fixed at 400 psia and the initial nitrogen and carbon dioxide pressure in the PVT cell is 100 psia and 300 psia respectively. Hence, the term relative pressure is defined as:

$$P_r = \frac{P_{N_2}}{P_{CO_2}} \quad \text{.....(4.1)}$$

For this case the relative pressure becomes $P_r = 0.333$. When the computer connected to the PVT cell indicates that the initial system pressure was 400 psia, the check valve connecting the carbon dioxide reservoir to the PVT cell is closed. The pressure versus time data were recorded until the system pressure change with time is negligible (less than 0.3 psia per hour).

The same procedure was repeated for other initial total pressure levels, such as 200, 400, 600, and 800 psia, and different P_r values for each particle size range

for the mixture of the nitrogen and carbon dioxide gases. The system pressure versus time data were obtained and indicated in Figures 4.12 and 4.15 for various initial total pressure and relative pressure values.

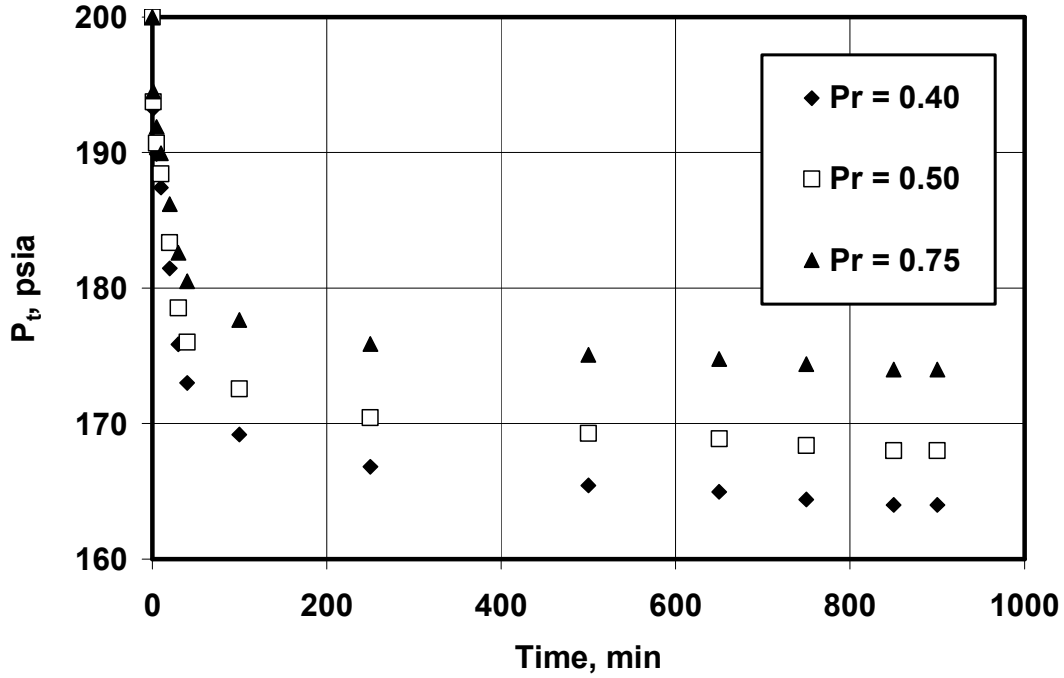

Figure 4. 12. Total pressure versus time for CO_2-N_2-Coal A system (P_{tin} = 200 psia).

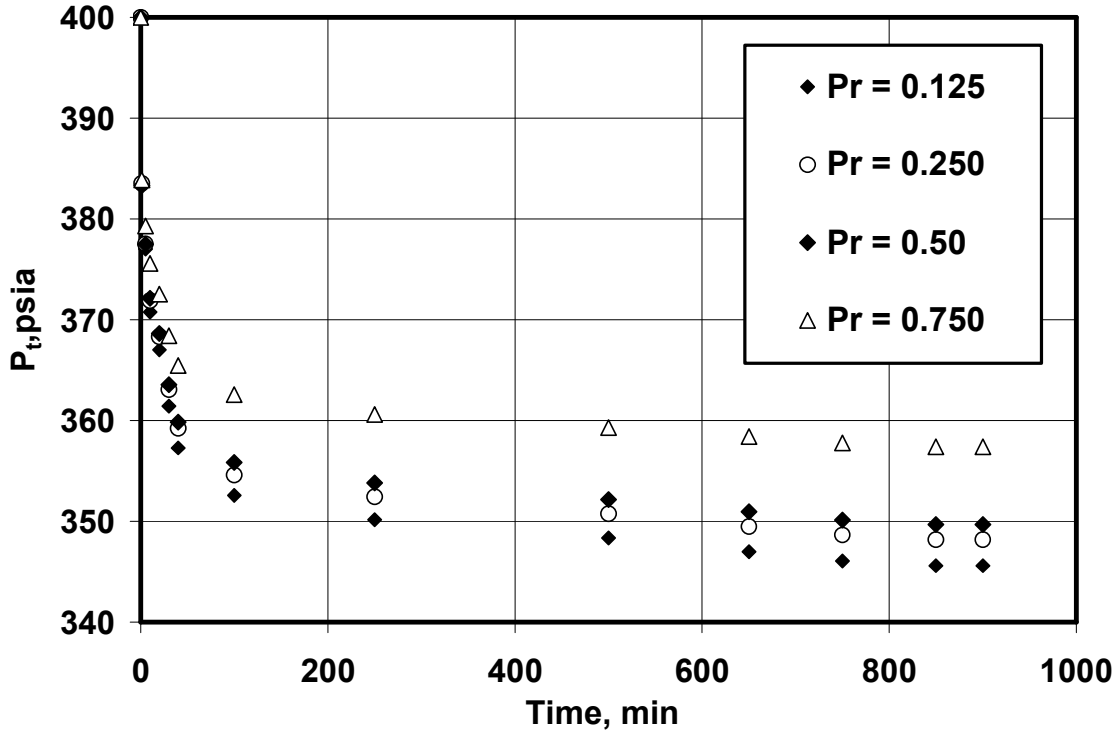

Figure 4. 13. Total pressure versus time for CO_2-N_2-Coal A system (P_{tin} = 400 psia).

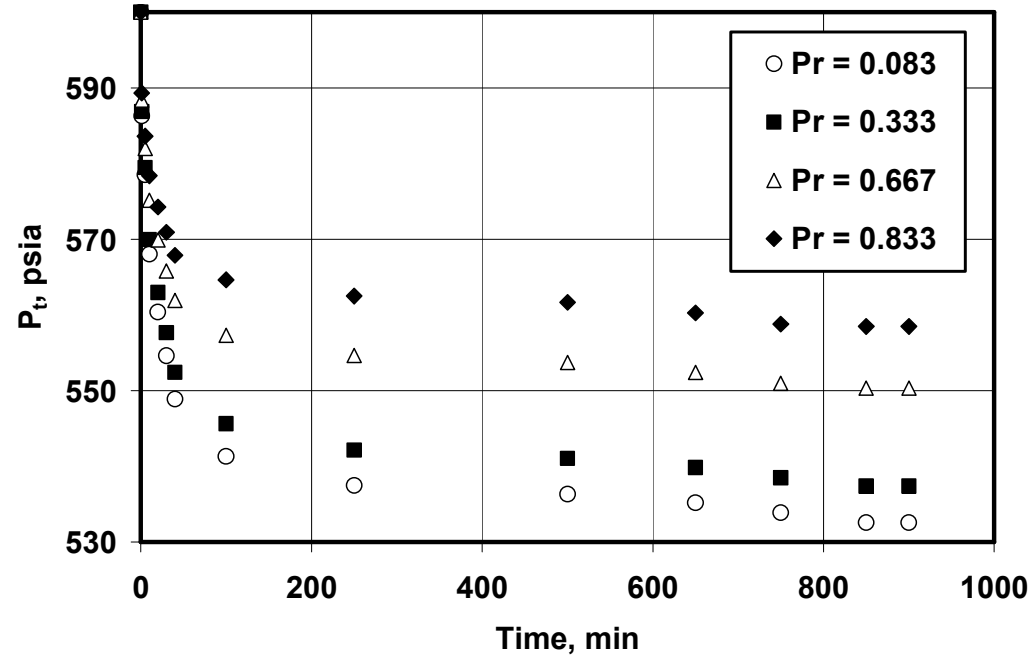

Figure 4. 14. Total pressure versus time for CO_2-N_2-Coal A system (P_{tin} = 600 psia).

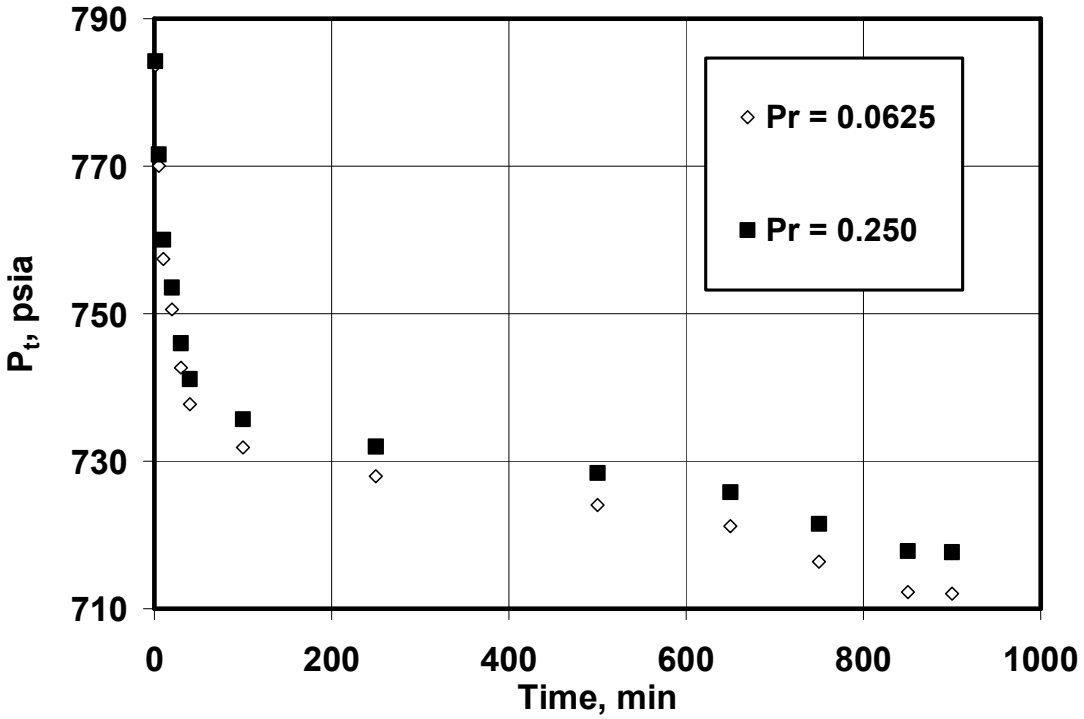

Figure 4. 15. Total pressure versus time for CO_2-N_2-Coal A system (P_{tin} = 800 psia).

Experiment 6. CO_2-N_2 Gas Mixture-Water-Coal B

The sixth experimental procedure was to conduct the adsorption tests for the multi-component gas and coal samples with the presence of water. The PVT cell was loaded with 100 grams of the grounded coal and 40 cc distilled water. The same procedure described in the previous section was followed to conduct these measurements for various initial total pressure levels, such as 200, 400, and 600 psia, and different P_r values for each coal B particle size range for the mixture of the nitrogen and carbon dioxide gases. The system pressure versus time data were obtained and indicated in Figures 4.12 and 4.15 for various initial total pressure and relative pressure values.

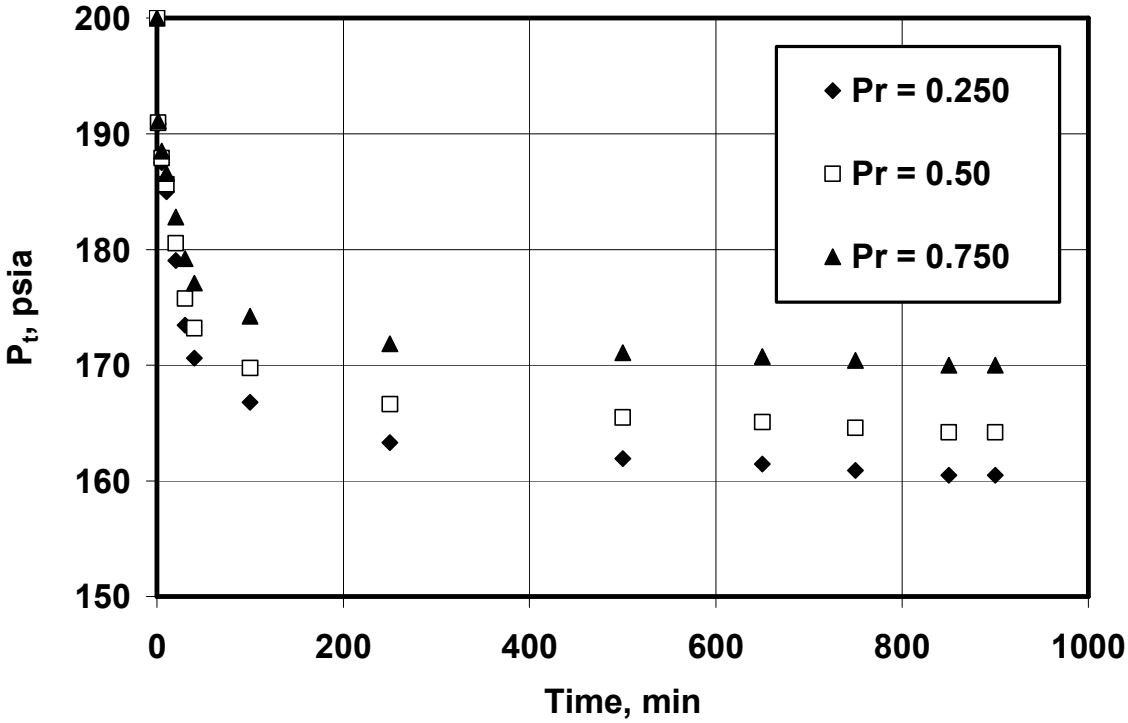

Figure 4. 16. Total pressure versus time for CO_2-N_2-water-Coal B system (P_{tin} = 200 psia)

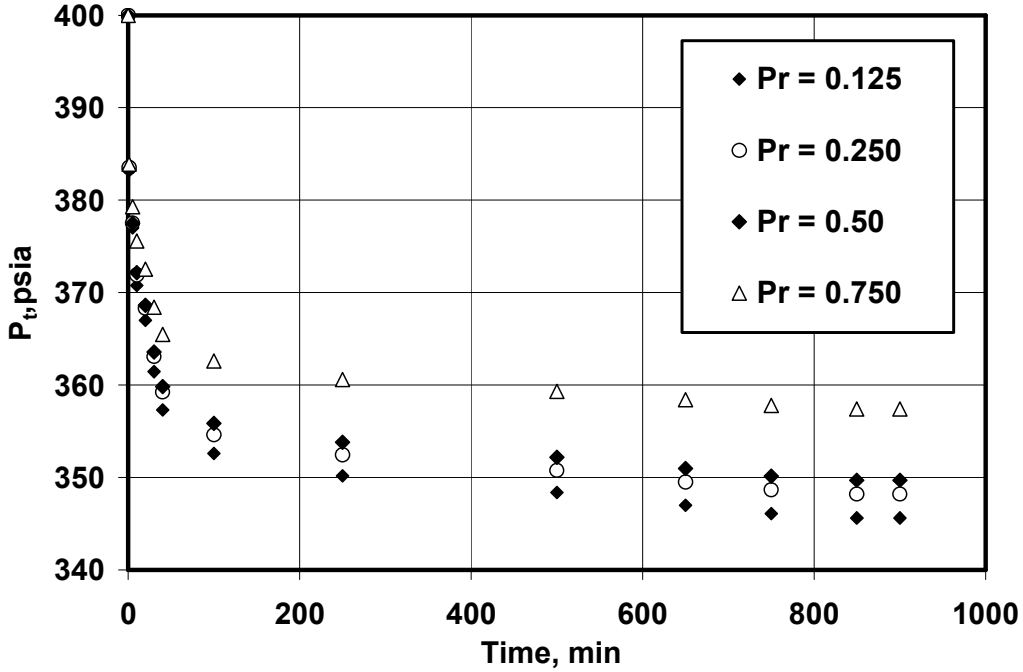

Figure 4. 17. Total pressure versus time for CO_2-N_2-water-Coal B system (P_{tin} = 400 psia).

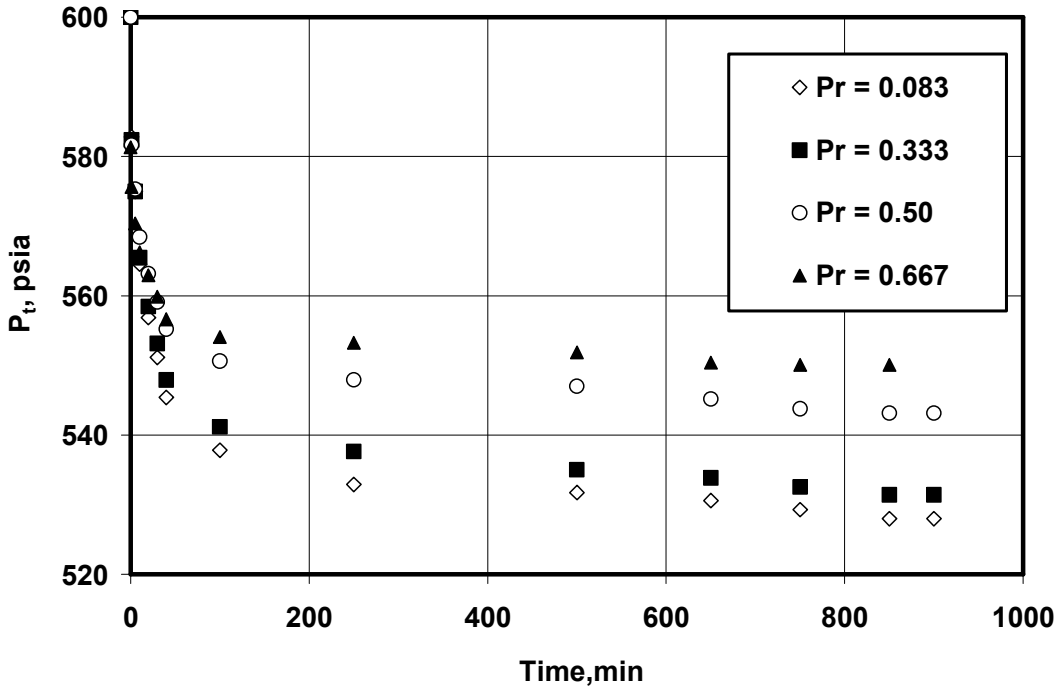

Figure 4. 18. Total pressure versus time for CO_2-N_2-water-Coal B system (P_{tin} = 600 psia).

CHAPTER 5

THEORETICAL STUDIES FOR DEVELOPMENT OF EQUILIBRIUM AND NON-EQUILIBRIUM ISOTHERMS WITH AND WITHOUT WATER PRESENT

The previous chapters explained that the coalbed methane and shale gas reservoirs are usually water saturated at the initial reservoir condition. The interaction of water, gas, and coal/shale phases in the reservoir complicates the study of the original gas in-place and also the isotherm development. The gas phase itself is usually a mixture of several gases including methane, ethane, propane, carbon dioxide, nitrogen, oxygen, water vapor and some other heavier hydrocarbons. The reservoir gas composition changes as the production time progresses. Three major concerns in studying the phase interactions in coalbed methane and shale gas reservoirs are: (1) Accurate estimation of the reservoir original gas in place. (2) Improvement of the reservoir fluid flow simulation quality. (3) Evaluation of the possible advanced coal/shale gas recovery methods with simultaneous CO_2/N_2 injection.

Studying the multi-component adsorption is essential due to the importance of the presence of the multi-component gas phase in coal/shale reservoirs in the presence of water. In this chapter first the non-equilibrium and equilibrium multi-component adsorption theories without the presence of water are developed and

discussed. Then, the development procedure of a non-equilibrium multi-component gas adsorption theory with the presence of water is explained.

5.1. Theoretical Studies for Development of Equilibrium and Non-Equilibrium Gas Isotherms without Water Present

This section develops and describes the equilibrium and non-equilibrium gas adsorption theories without the presence of water.

5.1.a. Equilibrium Adsorption Theory

Sutton and Davies (1935) developed an equilibrium-based isotherm to examine the adsorption of methane in the coal surface. Their data fit the Freundlich equation.

Choudhary and Mayadevi (1996) conducted several adsorption experiments to examine the adsorption of methane, ethane, ethylene, and carbon dioxide on silicalite-I. They observed that each of these gases can be fitted with various isotherms. The ethane adsorption was modeled by the Dubinin-Polany isotherms for low temperatures and Freundlich isotherm at high temperatures. Ethylene adsorption was modeled by Langmuir isotherm and carbon dioxide adsorption data could be fitted using the Langmuir and Freundlich equations.

Chaback et al. (1996) conducted several experiments of adsorption of carbon dioxide, methane, and nitrogen on the Fruitland and Mary Lee coals and observed good matches between the experimental data and the Langmuir isotherm.

Berlier and Frere (1997) conducted several sorption carbon dioxide experiments on activated carbons and silica gels. They did not attempt to fit their experimental data with any of the available isotherms.

Dreisbach et al. (1999) reported the single-component adsorption of methane, carbon dioxide and nitrogen gases on the activated carbons. They also did not fit their reported data with any correlations.

Karacan and Okandan (2001) conducted some single-component adsorption experiments. They successfully applied the Toth isotherm for adsorption of methane and carbon dioxide on the Acilik K-6 coal.

Ferer et al. (2002) conducted numerous numbers of experiments to evaluate the adsorption of nitrogen, methane, and propane on activated carbons. Their reported data covers pressures up to 800 psia and temperatures up to 200^{o} F. They did not fit their experimental data with any correlations.

Choi et al. (2003) obtained the equilibrium data for the adsorption of methane on activated carbon and fitted the data with the Langmuir-Freunlich equations.

Clarkson (2003) fitted the equilibrium adsorption data using the vacancy solution and Dubinin-Polany theories. This approach provided accurate results for binary gas/coal systems.

Other researchers including Reich et al. (1980), Ritter and Yang (1987), Talu and Zwiebel (1986), Wakasugi et al. (1981), Zhou (1994), and Zhou et al. (2000) have also reported numerous experimental data points of adsorption of various gases on activated carbon, zeolite, and coal.

As indicated above, the numerous equilibrium sorption data points are available in the literature. To investigate the applicability of the D-R isotherm in modeling the equilibrium sorption data points, the following procedure is applied. Equation 3.43 can be rewritten as:

$$V = V_m \exp\left\{-\left[-D\ln\left(\frac{P}{P_o}\right)\right]^r\right\} \quad \text{.....(5.1)}$$

where V is the adsorbed volume usually expressed in standard cubic feet of gas per tons of the solid. V_m is the theoretical maximum adsorbed volume of gas on the coal, usually expressed as the standard cubic feet of gas per tons of the solid. D and r are the Dubinin–Radushkevich coefficient and exponent. The value of *r* usually varies between 1.0 and 4.0 for carbons with large micropores (Apol et al., 1996). However, the values less than 1.0 also have been reported for adsorption of gases on activated carbons (Rudzinski W and Panczyk, 2001). P_o in Equation 5.1 is the saturation pressure at the specific temperature. A good estimation for P_o may be obtained using the correlation suggested by Kapoor et al. (1989):

$$P_o = P_C \exp\left[\frac{T_{nbp}}{T_C}\left(\frac{\ln P_C}{1-\frac{T_{nbp}}{T_C}}\right)\left(1-\frac{T_C}{T}\right)\right] \quad \text{.....(5.2)}$$

where P_c and T_c are the critical pressure and temperature of the gas component respectively and T_{nbp} is the boiling-point temperature of the gas component. Nevertheless, in some occasions, the values of P_o in Equation 5.1 may also be estimated by the curve fitting procedure in order to fit the experimental data with more accuracy.

The process of curve fitting for Equation V.1 is explained as the following:

1. Measure adsorbed volume versus the applied pressure.

2. Calculate P_o applying Equation 5.2.

3. Calculate $\ln V$ and $\ln\left(\frac{P}{P_o}\right)$.

4. Assume r = 0.0 and increase r values by increment of 0.1 until r = 4.0.

5. Calculate $\left[\ln\left(\frac{P}{P_o}\right)\right]^r$ for all the assumed values of r in step 4.

6. According to Equation 5.3, that is the convenient form of Equation 5.2, plot $\ln V$ versus $X = \left[-\ln\left(\frac{P}{P_o}\right)\right]^r$ for various values of r and fit a straight line for each series of data points.

$$\ln V = \ln V_m - D^r\left[-\ln\left(\frac{P}{P_o}\right)\right]^r \quad \text{.....(5.3)}$$

7. Obtain the straight line equations and also the fitting coefficient R^2.

8. Plot values of R^2 versus the corresponding r.

9. The maximum value of R^2 will correspond to the best fit and the best value of r. Read off the corresponding r and also the corresponding straight line equation.

10. The slope of the line will be equal to D^r and the intercept will be equal to $\ln V_m$

11. Calculate the D-R isotherm coefficient by D = $(\text{slope})^{(1/r)}$ and estimate theoretical maximum adsorbed volume corresponding to the specific temperature by V_m = exp(intercept).

Consequently, the D-R isotherm can be constructed applying steps 1 to 11

from the above procedure. Figures 5.1 and 5.2 show the best straight lines obtained by plotting $\ln V$ versus $X = \left[-\ln\left(\frac{P}{P_o}\right)\right]^r$ and different r values for the CO_2 and CH_4 adsorption in Takeda 3A CMS at 70°C, respectively.

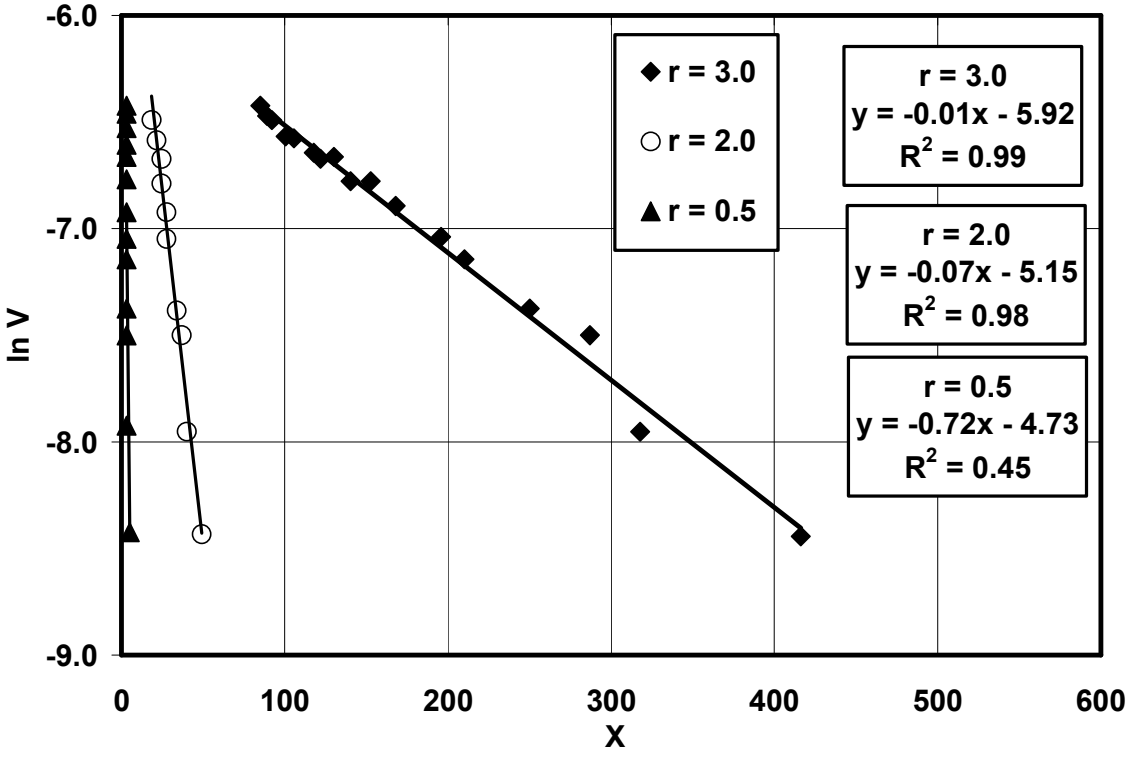

Figure 5. 1. Plot of $\ln V$ versus $X = \left[-\ln\left(\frac{P}{P_o}\right)\right]^r$ for three values of r (the maximum R^2 corresponds to r = 3.0) for CO_2 adsorption in Takeda 3A CMS at 20°C (Data from Rutherford and Coons, 2003).

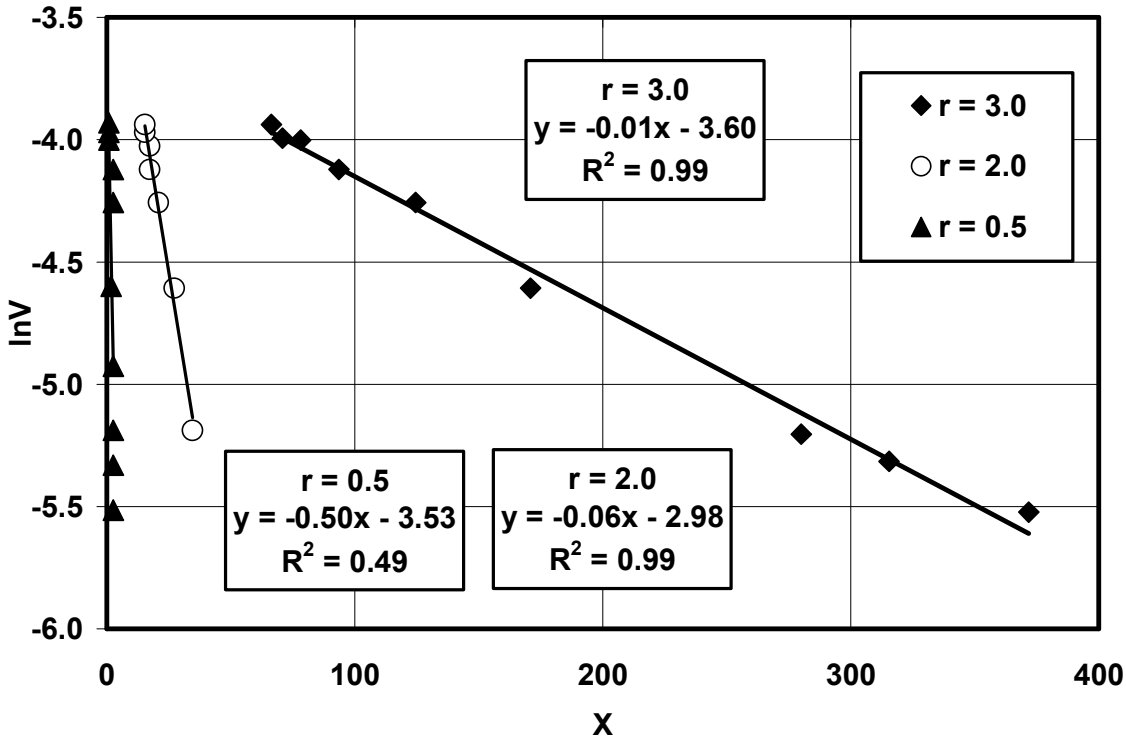

Figure 5. 2. Plot of $\ln V$ versus $X = \left[-\ln\left(\frac{P}{P_o}\right)\right]^r$ for three values of r (the maximum R^2 corresponds to r = 3.0) for CH_4 adsorption in Takeda 3A CMS at 20°C (Data from Rutherford and Coons, 2003).

In order to evaluate the D-R isotherm parameters and obtain good correlations between various data sources and isotherm parameters, series of single component literature data for various gases and adsorbents at different temperatures have been studied. The D-R isotherm parameters are obtained after the curve fitting for numerous available data points. The results of applying the D-R isotherm to fit the adsorption data are very satisfactory. A good match (R^2>0.99) was observed for all of the data points. Table A2.1 in Appendix 2 reports the fitting parameters and also the accuracy of the match for each data set.

Investigating Table A3.1 reveals that the value of the D-R isotherm exponent (r) usually varies between 1.0 and 3.0 for various carbonaceous materials.

It also shows that different adsorbents result in different r values for the same gas. Therefore, it can be concluded that the value of r is a function of the adsorbent properties rather than the gas properties.

More investigation in the obtained value of the D-R isotherm coefficient (D) shows that this value varies between 0.001 and 0.2 for different gaseous and carbonaceous materials. It has been indicated that the value of D is a function of temperature and adsorbent properties (Clarkson 2003). However, the relationship between D and gas type may also be a concern in this scenario.

The value of the theoretical maximum solid capacity V_m, is a function of the gas and solid properties, temperature, and pressure range.

The most important feature of Table A3.1 is the column related to the value of R^2. This value is always higher than 0.99 indicating that the D-R isotherm can successfully fit the experimental data points for various sorption systems.

5.1.b. Non-Equilibrium Adsorption Theories

In this section, the applicability and accuracy of the non-equilibrium form of the D-R isotherm is examined. Rudizinsky et al. (2000) developed this theory using the SRITIT method that was previously discussed in modeling the non-equilibrium sorption process. Equation 3.25 is used to model the non-equilibrium experimental sorption data. Equation 3.25 can be rewritten in the following form:

$$\ln V = \ln V_m - D^r \left\{ -\ln\left[\frac{P}{P_o} \tanh\left(2PK_{gsi}t\right) \right] \right\}^r \quad \text{.....(5.4)}$$

Similar to the previous cases, the unknown parameters can be obtained using the straight line curve fitting procedure. This procedure is described as the following:

1. Estimate value of P_o using Equation 5.2.

2. Assume a value for K_{gs} and calculate the term $\left\{-\ln\left[\frac{P}{P_o}\tanh\left(2PK_{gsi}t\right)\right]\right\}$.

3. For various values of r (r is usually between 0.0 and 4.0), plot $\ln V$ versus $X=\left\{-\ln\left[\frac{P}{P_o}\tanh\left(2PK_{gsi}t\right)\right]\right\}^r$.

4. Obtain the best fit using the least-squares error method and determine the optimum value of r yielding the best fit.

5. Adjust the value of K_{gs} so that the value of R^2 improves. For the best value of R^2, obtain the value of K_{gs}. If changing K_{gs} does not improve the value of R^2, take the best straight line with the maximum R^2 and obtain the corresponding K_{gs} value.

6. The slope of the best straight line passing through the data points is equal to D^r and is used to estimate D.

7. The intercept of the line is equal to $\ln V_m$ and is used to estimate the value of V_m.

Unlike the equilibrium sorption, the non-equilibrium sorption data available in the literature are scarce. Even though several researchers have contributed to model the non-equilibrium sorption phenomenon, the reported experimental data is of limited amount. However, to verify the applicability of Equation 3.43 to model the non-equilibrium sorption various adsorption experimental data sources are considered. Figures 5.1 and 5.2 show the best straight lines obtained by plotting

$\ln V$ versus $X = \left\{ -\ln\left[\frac{P}{P_o} \tanh\left(2PK_{gsi}t\right) \right] \right\}^r$ and different r values for the CO_2 and CH_4 adsorption on dry coal at 130 psia and 300 K, respectively.

The non-equilibrium D-R isotherm parameters can be obtained using the similar method described in Figures 5.3 and 5.4 by the trial-and-error method. Table AII.2 also summarizes the non-equilibrium D-R isotherm parameters for various gas and water adsorption on different adsorbents. The reported values of R^2 indicate that equation 3.43 is capable of covering a wide range of non-equilibrium sorption experimental data with very high accuracy.

The calculated values in Table A2.2 in Appendix 2 show that like the equilibrium cases, the value of D varies in the range of 0.001 to 0.9 and the value of r varies in the range of 0.5 to 3.5. The D value is a function of the pressure and temperature and also the gas and adsorbent characteristics; whereas, the value of K_{gs} is usually a small number and remains constant for the same system of gas and adsorbent.

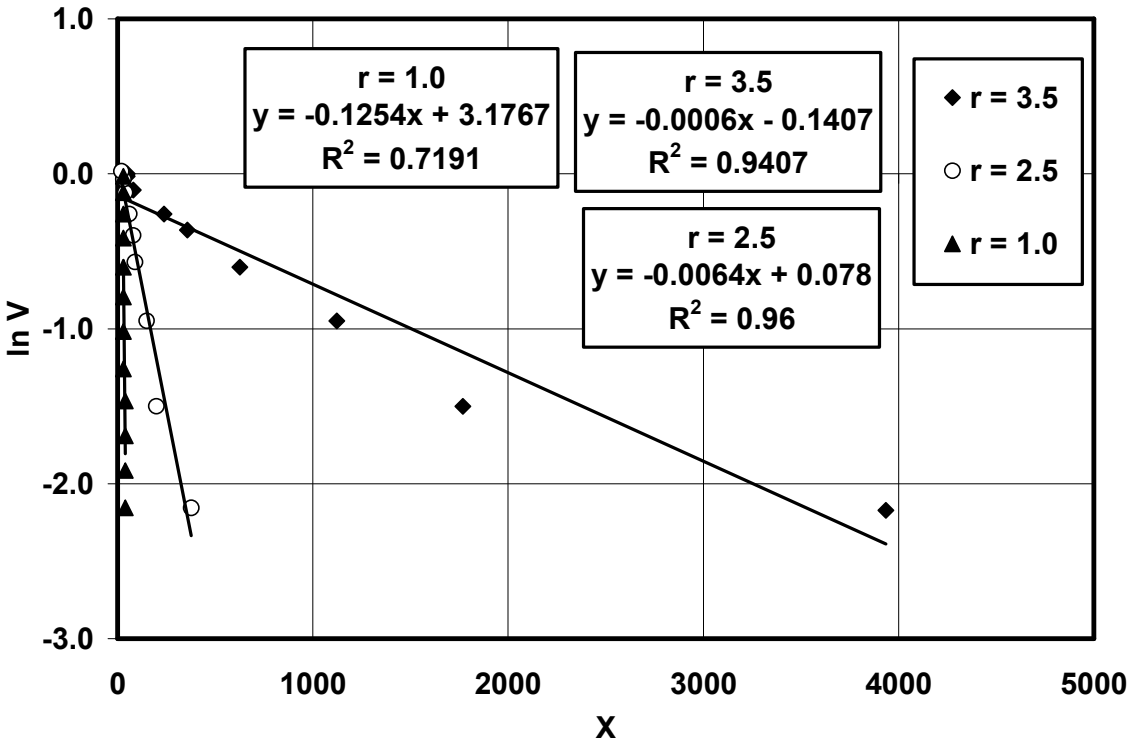

Figure 5. 3. Plot of $\ln V$ versus $X = \left\{ -\ln\left[\frac{P}{P_o} \tanh\left(2PK_{gsi}t\right) \right] \right\}^r$ for three values of r (the maximum R^2 corresponds to r = 2.5) for CO_2 adsorption in dry coal at 130 psia and 300 K (Data from Clarkson, 2003).

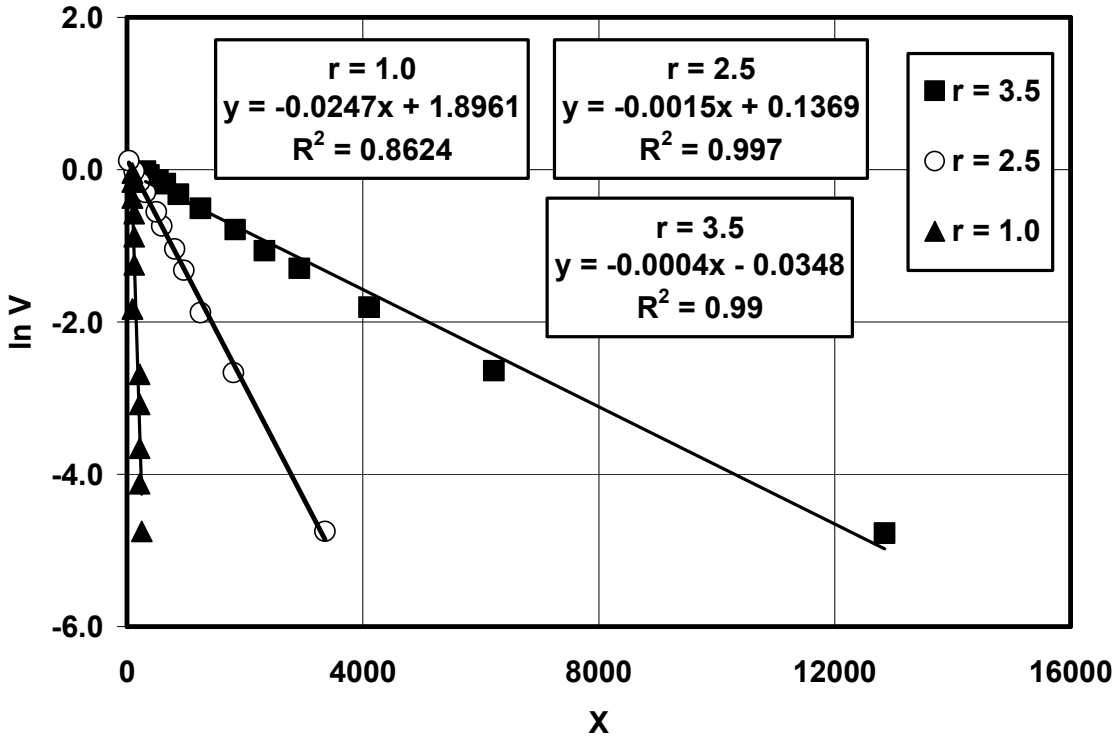

Figure 5. 4. Plot of $\ln V$ versus $X = \left\{ -\ln\left[\frac{P}{P_o} \tanh\left(2PK_{gsi}t\right) \right] \right\}^r$ for three values of r (the maximum R^2 corresponds to r = 2.5) for CH_4 adsorption in dry coal at 130 psia and 300 K (Data from Clarkson, 2003).

5.2. Equilibrium Multi-Component Gas Adsorption on Carbonaceous Materials

Single component adsorption is the most elementary adsorption case. In reality, we may deal with multi-component gas adsorption on various carbonaceous materials. Several modifications are made in the available single component models to extend them to represent the multi-component cases.

One of the earliest models for multi-component adsorption is the extended Langmuir model (Equation 5.2). The shortcomings of this theory in modeling the

experimental data especially at very low and very high pressure ranges brought the idea of applying other models, such as two and three dimensional EoSs, and extended BET and others, to formulate the multi-component adsorption.

Despite some successful applications, the available multi-component theories have several shortcomings and disadvantages such as: (1) They are the equilibrium based models, which do not describe the time-dependency of the sorption phenomenon. (2) They are usually composed of very complex equations that are difficult to operate. (3) They contain several parameters that are difficult to obtain.

In this study, the extended D-R isotherm is introduced. The extended D-R isotherm has the same parameters as the single component D-R isotherm with some modifications. The following expression represents the extended D-R isotherm:

$$V_i = V_{mi} \exp\left\{-\left[-D_i \ln\left(\frac{\hat{f}_{ga_i}}{P_{oi}}\right)\right]^r\right\} \quad \text{.....(5.5)}$$

where subscript i stands for component i and $\hat{f}_{ga_i}$ is the fugacity of the component i in the adsorbed phase. Equation 5.5 can be written in terms of gas component mole instead of volume. Therefore, we have:

$$n_{ga_i} = n_{m_i} \exp\left\{-\left[-D_i \ln\left(\frac{\hat{f}_{ga_i}}{P_{gao_i}}\right)\right]^{r_i}\right\} \quad \text{.....(5.6)}$$

where n_{ga_i} is the mole fraction of the adsorbed component i. The following relationship between the fugacity and pressure is applied:

$$\hat{f}_{ga_i} = \phi_{ga_i} P y_{ga_i} \quad \text{.....(5.7)}$$

$$n_{ga_i} = y_{ga_i} n_{gat} \quad \text{.....(5.8)}$$

where P is the total pressure, y_{ga_i} is the mole fraction of the component i in the adsorbed phase, ϕ_{ga_i} is the fugacity coefficient of the adsorbed component i, and n_{gat} is the total adsorbed gas moles. Substituting Equations 5.7 and 5.8 into Equation 5.6 we have:

$$y_{ga_i} n_{gat} = n_{m_i} \exp\left\{ -\left[-D_i \ln\left(\frac{\phi_{ga_i} P y_{ga_i}}{P_{gao_i}} \right) \right]^{r_i} \right\} \quad \text{.....(5.9)}$$

To simplify Equation 5.9, a new term is defined as:

$$\frac{P_{gao_i}}{\phi_{ga_i}} = \hat{P}_{gao_i} \quad \text{.....(5.10)}$$

where $\hat{P}_{gao_i}$ is the modified saturation pressure for the component i in the adsorbed phase. Substituting Equation 5.10 into Equation 5.9 we have:

$$y_{ga_i} n_{gat} = n_{m_i} \exp\left\{ -\left[-D_i \ln\left(\frac{P y_{ga_i}}{\hat{P}_{gao_i}} \right) \right]^{r_i} \right\} \quad \text{.....(5.11)}$$

To describe the application of Equation 5.11, a binary gas mixture of CO_2-CH_4 is assumed. The subscript 1 stands for CO_2 and 2 stand for CH_4. The applicability of Equation 5.11 to model the multi-component gas adsorption in solid surface is described using the following relationship:

1. Equation 5.11 is applied for CO_2 as:

$$\ln\left(y_{ga_1} n_{gat}\right) = \ln n_{m_1} - D_1^r \left[-\ln\left(\frac{P y_{ga_1}}{\hat{P}_{gao_1}} \right) \right]^{r_1} \quad \text{.....(5.12)}$$

2. Similarly for CH_4 we have:

$$\ln\left(y_{ga_2} n_{gat}\right) = \ln n_{m_2} - D_2^r \left[-\ln\left(\frac{P y_{ga_2}}{\hat{P}_{gao_2}} \right) \right]^{r_2} \quad \text{.....(5.13)}$$

3. To fit the experimental data, guess a value for $\hat{P}_{gao_i}$ and plot $\ln\left(y_{ga_1} n_{gat}\right)$ versus $\left[-\ln\left(\frac{P y_1}{\hat{P}_{gao_1}} \right) \right]^{r_1}$ for various values of r_1 (r_1 usually varies between 0.0 and 4.0). Fit the straight line for each of the obtained plots. Change the value of $\hat{P}_{gao_i}$ so that the obtained R^2 value improves. Choose the best straight line corresponding to the maximum R^2 and determine the corresponding r_1 and $\hat{P}_{gao_i}$ value to the obtained straight line.

4. Obtain the slope and intercept of the chosen straight line and calculate the D-R isotherm coefficient by D_1 = (slope)$^{(1/r_1)}$ and the theoretical maximum adsorbed moles corresponding to the specific temperature is estimated by V_{m1} = exp(intercept).

5. Repeat the same procedure for component 2. If the gas phase contains more than two components, the steps 1-4 should be repeated for each component separately.

Applying the mentioned procedure for various literature data, the model parameters are obtained. The multi-component sorption data are reported in various sources. We first review the available data and then apply the present methodology.

Reich et al. (1980) reported binary and ternary mixtures of methane, ethane, and ethylene gases sorption data on activated carbons. They applied the adsorption potential theory for gas mixtures to model the experimental sorption data points. DeGance (1992) reported several sets of binary and ternary sorption data for the

systems of CH_4/N_2, CH_4/CO_2, and $CH_4/CO_2/N_2$ for various initial mole fractions of each component in the gas phase. The reported data were correlated using the modified version of Erying EoS. Chaback et al. (1996) performed several binary and ternary component sorption experiments. They reported total adsorbed volume and also adsorbed volume fraction of each component for a binary test of CH_4/N_2 and ternary mixture of $CH_4/CO_2/N_2$. They correlated their experimental data with Lewis rule. The correlations show that the adsorbed volume of each component in the coal is a function of gas component mole fraction in the gas phase and also the total system pressure. Dreisbach et al. (1999) conducted several binary sorption experiments on activated carbons. They reported the CO_2/CH_4 mixture gas phase composition versus the adsorbed phase composition. They applied the Gibbs adsorption theory and extended Langmuir isotherms to fit their experimental data. Equation 5.11 and the above mentioned procedure is used to fit the reported experimental data. The results of applying Equation 5.11 are very satisfactory. The fitting coefficients of over 0.997 are obtained in most of the cases.

Figures 5.5, 5.6 and 5.7 show the curve fitting procedure for a ternary mixture of CO_2, CH_4 and N_2 experimental data reported by Chaback et al. (1996). The curve fitting process for multi-component sorption data is very similar to those of single components. The fugacity coefficients and other D-R isotherm parameters are obtained for each component separately by the curve fitting process.

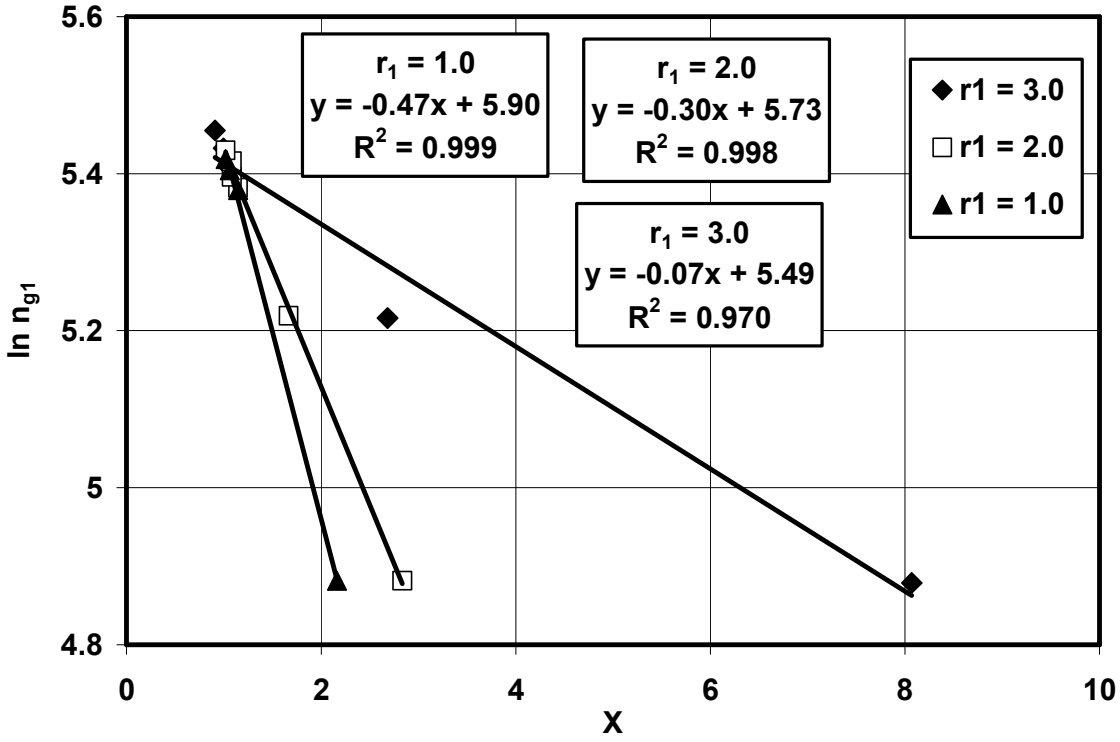

Figure 5. 5. Plot of $\ln n_{g_1}$ versus $X = \left[-\ln\left(\frac{Py_1}{\hat{P}_{gao_1}} \right) \right]^{r_1}$ for three values of r (the maximum R^2 corresponds to $r_1 = 1.0$) for N_2 adsorption from a ternary mixture (CH_4+N_2+CO_2) with initial gas mixture of (7%, 90%, 3%) (Date from Chaback et al., 1996).

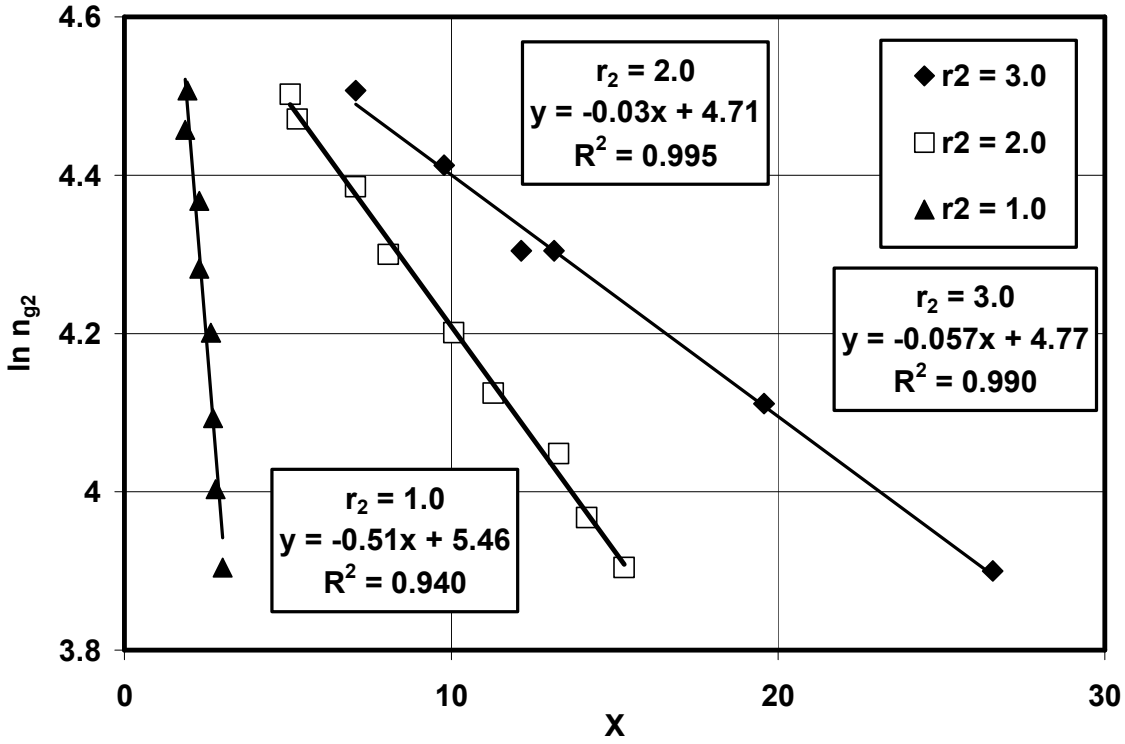

Figure 5. 6. Plot of $\ln n_{g_2}$ versus $X = \left[-\ln\left(\frac{Py_2}{\hat{P}_{gao_2}} \right) \right]^{r_2}$ for three values of r (the maximum R^2 corresponds to $r_2 = 2.0$) for CH_4 adsorption from a ternary mixture (CH_4+N_2+CO_2) with initial gas mixture of (7%, 90%, 3%) (Date from Chaback et al., 1996).

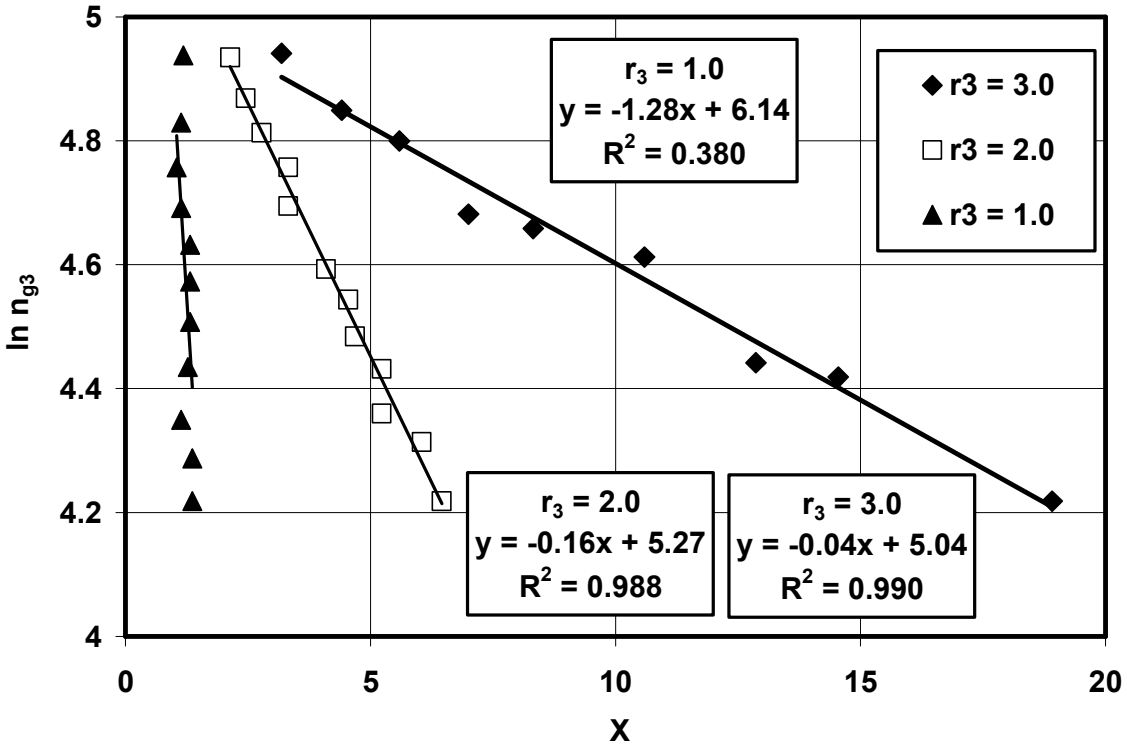

Figure 5. 7. Plot of $\ln n_{g3}$ versus $X = \left[-\ln\left(\frac{Py_3}{\hat{P}_{gao_3}} \right) \right]^{r_3}$ for three values of r (the maximum R^2 corresponds to $r_3 = 3.0$) for CO_2 adsorption from a ternary mixture (CH_4+N_2+CO_2) with initial gas mixture of (7%, 90%, 3%) (Date from Chaback et al., 1996).

Table A3.3 represents series of curve fitting parameters for various multi-component gas adsorptions on different solids. Unlike other multi-component adsorption models, Equation 5.13 is very convenient to operate and apply. The model parameters and the fugacity coefficient and hence the fugacity values of each component can be easily obtained using Equation 5.13.According to Table A2.3 of Appendix 2 for most of the reported data the accuracy of curve fitting (R^2) is over

0.999. It indicates that the above mentioned procedure can predict the multi-component sorption isotherm parameters with very high accuracy.

According to Equation 5.13 the fugacity coefficient is an indicator of the ideality of the component in the gas mixture. If the fugacity coefficient of any component is very close to 1.0, the behavior of that specific component in the gas mixture is close to the ideal behavior. However, as the fugacity coefficient for a component deviates from the unity, the component shows a non-ideal behavior in the gas mixture.

The last column of Table A3.3 indicates the estimated values of the fugacity coefficients for various components in different systems. The most common point in the evaluated data is that the fugacity coefficient of methane is very close to unity. The following order can be summarized from Table A3.3 for fugacity coefficients of the various components in the binary and ternary gas mixtures (fugacity coefficient decreases from left to right): CH_4>C_2H_6>C2H_4>CO_2>N_2

Similar to the single component adsorption parameters summarized in Table A3.2 the D-R isotherm coefficient (D) for the multi-component sorption isotherm is also between 0.0001-0.9. The values of r_i are also in the range of 0.5-3.5 for different gases and adsorbents. The similar conclusion is drawn for multi-component adsorption that the value of r_i is independent of the type of gas and is a characteristic of the adsorbent. However, the value of D_i is a function of both gas and adsorbent properties in contact with each other.

5.3. Theoretical Studies for Development of Equilibrium and Non-Equilibrium Gas Isotherms with Water Presence

The volumetric method is the most popular technique to construct an isotherm in the coalbed methane industry. Usually, seven to ten measurements at different pressures are needed to construct an isotherm using this technique (Owen et al., 1990). Chapter 4 described the volumetric experimental technique. The measured pressures versus time data were also reported for various scenarios.

In this chapter, a calculation procedure is developed to construct the equilibrium and non-equilibrium isotherms from the pressure versus time data points reported in Chapter 4. The applications of the non-equilibrium isotherm developed by Rudzinsky and Panczyk (2000) is extended for the multi-component gas and water adsorption on carbonaceous materials and coals by replacing the pressure with the equivalent fugacity and applying the modified relationships introduced by Ward and Elmoselhi (1997) to estimate the fugacity of the adsorbed phase in coal. The similar procedure is also used to model the time-dependency of the dissolution of various gases in water. The modified Peng-Robinson EoS, the modified UNIFAC-Lyngbe, and UNIFAC-Dortmund procedures are applied to predict the fugacity of the components in the gas and water phases. It is demonstrated that both equilibrium and non-equilibrium isotherms can be obtained by applying the computational procedure provided in this chapter from the volumetric sorption technique.

Formulation

A novel and rapid interpretation procedure is developed for obtaining the equilibrium and non-equilibrium isotherms from volumetric laboratory measurements. The formulation procedure is described in the following:

Overall Material Balance

Figure 4.1 shows the schematic of the experimental equipment composed of a constant volume PVT cell kept at a constant temperature during the measurement. First, a certain volume of gas is charged into the PVT cell initially loaded with a certain amount of coal and water. The system is allowed sufficient time to attain an equilibrium at the initial pressure. As the gas and water adsorb on the coal, the composition and total pressure of the gas, water, and coal change in the PVT cell change. The pressure variation in the PVT cell is recorded at various time steps until the equilibrium is reached.

The sum of the gas phase volume (V_g), water phase volume (V_w), and coal volume (V_c) is equal to the PVT-cell volume (V_{cell}) which remains constant while the volumes of the coal, water, and gas change with time. Hence, for a mixture below its critical pressure and temperature the following expression is true:

$$V_{cell} = V_g(t) + V_c(t) + V_w(t) \quad \text{.....(5.14)}$$

where:

$$V_w(t) = V_{Ww}(t) + V_{Gw}(t) \quad \text{.....(5.15)}$$

$$V_g(t) = V_{Gg}(t) + V_{Wg}(g) \quad \text{.....(5.16)}$$

The lower case subscript is a phase indicator and the upper case subscript represents the specific component contained in a phase. For instance, V_{Gw} refers to the volume of the gas component in the water phase.

The relationships between the volume of each phase and its moles can be defined by:

$$V_{Ww}(t) = \frac{n_{Ww}(t)\ Mw_w}{\rho_{Ww}} \quad \text{.....(5.17)}$$

$$V_{Gw}(t) = \frac{n_{Gw}(t)\ Mw_g}{\rho_{Gw}} \quad \text{.....(5.18)}$$

$$V_{Gc}(t) = \frac{n_{Gc}(t)\ Mw_g}{\rho_{Gc}} \quad \text{.....(5.19)}$$

$$V_{Wg}(t) = \frac{n_{Wg}(t)\ Mw_g}{\rho_{Wg}} \quad \text{.....(5.20)}$$

$$V_{Wc}(t) = \frac{n_{Wc}(t)\ Mw_w}{\rho_{Wc}} \quad \text{.....(5.21)}$$

The mass conservation equations of the water and gas components are expressed as the following:

$$n_W = n_{Winitial} = n_{Wg}(t) + n_{Wc}(t) + n_{Ww}(t) \quad \text{.....(5.22)}$$

$$n_G = n_{Ginitial} = n_{Gw}(t) + n_{Gc}(t) + n_{Gg}(t) \quad \text{.....(5.23)}$$

Assuming a single component gas and low pressure region (ideal mixture) the average density of the gas phase is given by:

$$\rho_{Gg}(t) = y_{Gg}\rho_{Gg}(t) + y_{Gw}\rho_{Gw}(t) \quad (5.24)$$

$$\rho_{Gg}(t) = \frac{n_{Gg}(t)}{n_{Gw}(t)+n_{Gg}(t)}\frac{Z_g RT}{P} + \frac{n_{Gw}(t)}{n_{Gw}(t)+n_{Ww}(t)}\frac{Z_w RT}{P} \quad (5.25)$$

$$\rho_{Gg}(t) = \rho_{Wg}(t) \quad (5.26)$$

$$\rho_{Ww}(t) = \frac{n_{Wg}(t)}{n_{Wg}(t)+n_{Ww}(t)}\frac{Z_g RT}{P} + \frac{n_{Ww}(t)}{n_{Wg}(t)+n_{Ww}(t)}\rho_w \quad (5.27)$$

The further step is to define the relationship necessary to calculate the density of the adsorbed phase inside the coal. The results of the analysis (Vyas et al., 1994) of some fluids tested on many different carbonaceous solids show that the adsorbed phase density is very close to that of the liquid phase density at high pressure. Thus, the following expression for the density of the adsorbed phase can be written:

$$\rho_{Gc}(t) = b'\rho_{gL}(t) = b\frac{Z_{gL}RT}{P} \quad (5.28)$$

$$\rho_{Wc}(t) = c'\rho_{Wc}(t) = c\rho_{Ww}(P,T) \quad (5.29)$$

where b' and c' are the ratio of the adsorbed phase densities to density of the corresponding liquid phase at the prescribed pressure and temperature. The subscript L refers to the liquid phase. However, in reality the gas and water phases act as non-ideal phases. It will be explained later that the density of such mixtures is estimated using an appropriate equation of state.

Coal Volume Alterations

Coal volume changes because of coal swelling due to gas adsorption and coal shrinkage due to the external gas pressure. Maggs (1946) assumed that the coal swelling is proportional to the heat of adsorption that is proportional to the system total pressure at a constant temperature. This assumption is approximately valid for gaseous hydrocarbon and nitrogen gas adsorption on coal (Larsen, 2004). Reucroft and Sethuraman (1987) reported the coal volume changes at various pressures and carbon content. Figure 5.8 confirms Maggs' assumption for CO_2 adsorption on coal. Karacan (2003) expressed the CO_2 swelling effects on coal very similarly to the water and liquid slurries. Thus, the coal swelling coefficient (c_s) can be used to estimate the coal volume change as:

$$V_c^{t+1}(t) = \left(1 + \sum_{i=1}^{n} c_{si} P_i^e - c_c P_{total}\right) V_c^t \quad \text{.....(5.30)}$$

where *i* refers to any adsorbed gas or water components, e refers to the equilibrium state between components i in gas and coal phases, and c_c refers to the coal compressibility due to the external pressures or the overburden pressure in the reservoir condition. Tables 5.1 and 5.2 report the coal swelling factors and coal compressibility factors for various coal-gas systems, respectively.

Table 5. 1. Coal swelling coefficients for various gas-coal systems.

Data source	Coal Type	Gas Type	Swelling Coefficient, psi^{-1}
Moffat and Weale (1995)	Low rank bituminous	methane	1.70E-6
Gunther (1978)	Anthracite	methane	2.76E-6
Wubben et al. (1986)	Anthracite	methane	1.4E-6
Reucroft and Patel (1986)	Appalachian Basin	carbon dioxide	6.55E-6
Gray (1987)	Japanese Coal	methane	8.62E-7
Harpalani and Chen (1995)	Piceance Basin	methane	6.2E-6
George and Barakat (2001)	New Zealand Coal	methane	8.33E-6
George and Barakat (2001)	New Zealand Coal	methane	3.61E-5
Harpalani and Chen (1995)	San Juan Basin	methane	1.59E-6
Harpalani and Chen (1995)	San Juan Basin	helium	3.4E-7

Table 5. 2. Coal compressibility factor for various coals, (Li, 1999).

Reference	Toda and Toyoac (1972)	Splizter (1981)	Yong et al. (1999)	Reeves and Pekot (2001)
c_c, psi^{-1}	4.85E-07-1.60E-06	1.73E-06-2.17E-06	1.19E-06-1.45E-06	2.0E-06

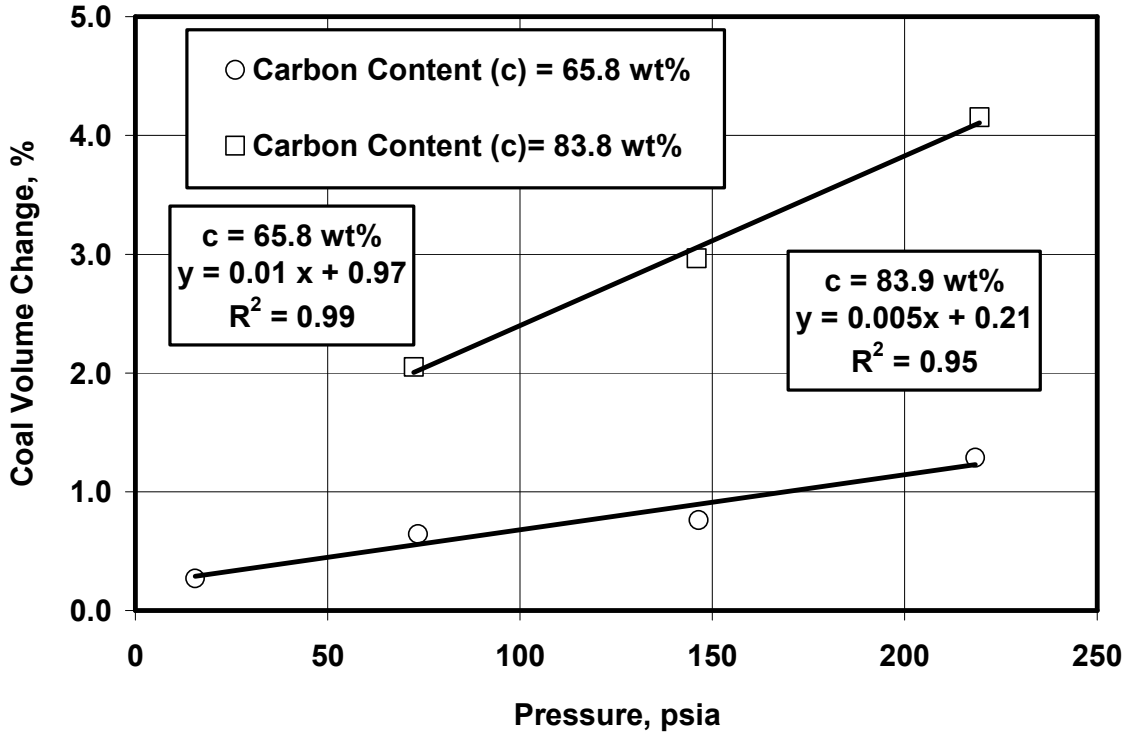

Figure 5. 8. Coal volume change due to the carbon dioxide adsorption versus the applied pressure (Data after Reucroft and Sethuraman, 1987).

Non-Equilibrium Gas Sorption Thermodynamics

The chemical potentials for the equilibrium gas, water, and coal system are equal at the initial reservoir condition. Thus,

$$\mu_{Gc} = \mu_{Wg} = \mu_{Gg} \quad \text{.....(5.31)}$$

$$\mu_{Wc} = \mu_{Wg} = \mu_{Ww} \quad \text{.....(5.32)}$$

Ward and Elmoselhi (1986) used the Born-Oppenheimier approximation (Equation 3.29) to estimate the chemical potential per molecule of an ideal, asymmetric, and diatomic gas for the gas phase behavior. We use the simplified form of their expression for the ideal solution given by:

$$\mu_{gg} = kT \ln\left(y_{gg} P\right) \quad (5.33)$$

Similarly for water vapor in gas phase, we have:

$$\mu_{wg} = kT \ln\left(y_{wg} P\right) \quad (5.34)$$

Rudzinsky and Panczyk (2000) described the net adsorption rate by the following kinetic equations.

$$J_{gc} = R_a - R_d \quad (5.35)$$

The adsorption and desorption rates are expressed by the SRIIT approach as:

$$R_a = K'_{gs} \exp\left(\frac{\mu_{Gc} - \mu_{Gg}}{kT}\right) \quad (5.36)$$

$$R_d = K'_{gs} \exp\left(\frac{\mu_{Gg} - \mu_{Gc}}{kT}\right) \quad (5.37)$$

where J_{gc} is the net gas exchange between the coal and gas phases.

Dubinin and Astakhov (D-A) (1971) developed an isotherm for adsorption of vapors on microporous adsorbents using Polany's theory of adsorption (1932) based on the physical and chemical concepts (Clarkson, 2003). The Dubinin and Radushkevich (D-R) and D-A isotherms are the semi-empirical relationships that describe the adsorption of various gases and water vapors on coal surfaces, expressed as:

$$\theta_i = \exp\left\{-\left[-D_i \ln\left(\frac{P_i}{P_o}\right)\right]^r\right\} \quad \text{.....(5.38)}$$

where r and D_i are the empirical values to be determined using the experimental data points. Equation 5.38 is called D-R isotherm for r = 2.0 and D-A isotherm for other values of r. Using the D-A isotherm and substituting equations 5.36, 5.37, and 5.38 into Equation 5.35 and integrating using the initial condition of θ (t = 0) = 0.0, yields:

$$\theta(t) = \exp\left\{-\left\{-D \ln\left[\frac{P}{P_o}\tanh\left(2PK_{gs}t\right)\right]\right\}^r\right\} \quad \text{.....(5.39)}$$

Non-Equilibrium Gas-Water Thermodynamics

The following equations similar to those given above can also be written for the gas-water system as:

$$J_{gw} = K_{gw}\exp\left(R_{ds} - R_s\right) \quad \text{.....(5.40)}$$

$$R_{ds} = K_{1gw}\exp\left(\frac{\mu_{Gg} - \mu_{Gw}}{kT}\right) \quad \text{.....(5.41)}$$

$$R_s = K_{2gw}\exp\left(\frac{\mu_{Gw} - \mu_{Gg}}{kT}\right) \quad \text{.....(5.42)}$$

$$\mu_{Gg} = kT\ \ln\left(Py_{Gg}\right) \quad \text{.....(5.43)}$$

$$\mu_{Gw} = kT\ \ln\left(H_{Gw}x_{Gw}\right) \quad \text{.....(5.44)}$$

Substituting Equations 5.41-5.44, into Equation 5.40 results:

$$\frac{dy_{Gg}}{dt} = -\frac{dy_{wg}}{dt} = K_{gw} \exp\left(K_{1gw} \frac{Py_{Gg}}{H_{Gw} x_{Gw}} - K_{2gw} \frac{H_{Gw} x_{Gw}}{Py_{Gg}} \right) \quad \text{.....(5.45)}$$

$$\frac{dx_{Ww}}{dt} = -\frac{dx_{Gw}}{dt} = K_{wg} \exp\left(K'_{1gw} \frac{H_{Gw} x_{Gw}}{Py_{Gg}} - K'_{2gw} \frac{Py_{Gg}}{H_{Gw} x_{Gw}} \right) \quad \text{.....(5.46)}$$

Equations 5.45 and 5.46 are subject to the following initial conditions and the auxiliary equations:

$$x_{Gw} = 0.0 \;\; and \;\; y_{Wg} = 0.0 \,, \; t = 0.0$$

$$\sum_{i=1}^{n} y_i = 1.0 \quad and \quad \sum_{i=1}^{n} x_i = 1.0$$

This procedure can be expanded for the multi-component gas and water adsorption on the coal surface. In multi-component adsorption, the gas phase is composed of more than one component. Therefore, the gas and adsorbed mixtures deviate from the ideal mixture state. To account for these deviations, the pressure (P) in Equations 5.33-5.46 is substituted by fugacity $\left(\hat{f}_{g_i g}\right)$. Therefore, the Equations 5.39, 5.45, and 5.46 become:

$$\theta_{G_i c}(t) = \exp\left\{ -\left\{ -D_{g_i} \ln\left[\frac{\hat{f}_{g_i g}}{P_o} \tanh\left(2 \hat{f}_{g_i g} K_{g s_i} t\right) \right] \right\}^{r_i} \right\} \quad \text{.....(5.47)}$$

$$\frac{dy_{Gg_i}}{dt} = -\frac{dy_{wg_i}}{dt} = K_{gw_i} \exp\left(K_{1g_iw} \frac{\hat{f}_{Gg_i}}{\hat{f}_{Gw_i}} - K_{2gw} \frac{\hat{f}_{Gw_i}}{\hat{f}_{Gg_i}} \right) \quad \text{.....(5.48)}$$

$$\frac{dx_{Ww}}{dt} = -\frac{dx_{Gw}}{dt} = K_{wg_i} \exp\left(K'_{1gw_i} \frac{\hat{f}_{Gw_i}}{\hat{f}_{Gg_i}} - K'_{2gw_i} \frac{\hat{f}_{Gg_i}}{\hat{f}_{Gw_i}} \right) \quad \text{.....(5.49)}$$

The coal volume change is also expressed with the following modified equation:

$$V_c^{t+1}(t) = \left(1 + \sum_{i=1}^{n} c_{si} \hat{f}_{G_ig}^{e} - c_c P_{total} \right) V_c^{t} \quad \text{.....(5.50)}$$

Fugacity Calculations

The fugacity of any component in the gas phase can be estimated using the Peng-Robinson (1976) equation of state:

$$\ln\left(\frac{\hat{f}_{G_ig}}{y_{G_ig} P} \right) = \frac{b_k}{b}(Z-1) - \ln(Z-B) - \frac{A}{2\sqrt{2}B} \left(\frac{2\sum_i y_{G_ig} a_{G_kg}}{a} - \frac{b_k}{b} \right) \ln\left(\frac{Z + 2.414B}{Z - 0.414B} \right) \quad \text{.....}$$

$$\text{.....(5.51)}$$

where, the value of Z is obtained from:

$$Z^3 - (1-B)Z^2 + (A - 3B^2 - 2B)Z - (AB - B^2 - B^3) = 0 \quad \text{.....(5.52)}$$

$$a = \sum_i \sum_j y_{G_ig} y_{G_jg} a_{ij} \quad \text{.....(5.53)}$$

$$b = \sum_i y_{G_ig} b_i \quad \text{.....(5.54)}$$

$$a_{ij} = \left(1 - \delta_{ij}\right) a_i^{1/2} a_j^{1/2} \quad \text{.....(5.55)}$$

$$a\left(T\right) = 0.45724 \frac{R^2 T_c^2}{P_c} \alpha\left(T_r\right) \quad \text{.....(5.56)}$$

$$b = 0.07780 \frac{RT_c}{P_c} \quad \text{.....(5.57)}$$

$$\alpha\left(T\right) = \begin{cases} \left[1 + C_1\left(1 - \sqrt{T_r}\right)\right]^2 & T_r > 1.0 \\ \left[1 + C_1\left(1 - \sqrt{T_r}\right) + C_2\left(1 - \sqrt{T_r}\right)^2 + C_3\left(1 - \sqrt{T_r}\right)^3\right]^2 & T_r < 1.0 \end{cases} \quad \text{.....(5.58)}$$

$$k\left(\omega\right) = 0.37464 + 1.54226\omega - 0.26992\omega^2 \quad \text{.....(5.59)}$$

$$A = \frac{aP}{R^2 T^2} \quad , \quad B = \frac{bP}{RT} \quad \text{.....(5.60)}$$

Tables 5.3 and 5.4 represent the values of binary interaction coefficients (δ_{ij}) and the gas eccentric factor (ω) for water, methane, carbon dioxide, and nitrogen, and their binary mixtures.

Table 5. 3. The binary interaction coefficients for Peng-Robinson EoS obtained from the literature (Peng and Robinson, 1976, Evelein and Moore, 1979, and Mohammadi et al., 2005).

Component	CH_4	C_2H_6	C_3H_8	C_4H_{10}	CO_2	N_2	H_2O
CH_4		0.0079	0.0153	0.0218	0.13	0.11	0.50
C_2H_6	0.0079		0.0013	0.0038	0.13	0.03	0.5
C_3H_8	0.0153	0.0013		0.007	0.1268	-0.06	0.52
C_4H_{10}	0.0218	0.0038	0.0007		0.1236		0.54
CO_2	0.13	0.13	0.1268	0.1236		-0.13	0.1896
N_2	0.11	0.03	-0.06	-0.10	-0.13		

Table 5. 4. Critical component parameters and acentric factors, obtained from the literature (Dhima et al., 1999 and Chapoy et al., 2004).

Component	T_c (K)	P_c (psia)	Zc	ω
CH_4	190.4	671.6	0.288	0.011
C_2H_6	305.4	712.5	0.285	0.099
C_3H_8	369.8	620.5	0.281	0.153
C_4H_{10}	304.1	1077.5	0.274	0.239
CO_2	647.3	3230	0.235	0.344
N_2	126.05	490.0	0.26	0.0403

The fugacity of the components in the water phase is calculated by Evelein and Moore (1979) and Mohammadi et al. (2005).

$$\ln\left(\frac{\hat{f}_{G_i w}}{x_{G_i w}}\right) = \ln\left(\gamma_{G_i w} H^{\circ}_{i,w}\right) + \frac{\bar{v}_{G_i w}}{RT}\left(P - P^{sat}_{w}\right) \quad \text{.....(5.61)}$$

$$\ln\left(\frac{\hat{f}_{Ww}}{x_{Ww}}\right) = \ln\left(\gamma_{Ww} \phi^{sat}_{Ww} P^{sat}_{Ww}\right) + \frac{v^{sat}_{Ww}}{RT}\left(P - P^{st}_{Ww}\right) \quad \text{.....(5.62)}$$

where $\gamma_{G_i w}$ is the activity of the gas component i in water phase and $\gamma_{W_i w}$ is activity coefficient of the water component in the water phase. The activity coefficients are calculated using the modified UNIFAC-Lyngby (Li et al., 1997, Larsen, 1987, and Weidlich and Gmehling, 1987) and UNIFAC-Dortmond (Larsen, 1987 and Weidlich and Gmehling, 1987) correlations. This correlation is described below.

In the modified UNIFAC model, the activity coefficient is expressed in the following form:

$$\ln \gamma_i = \ln \gamma_i^C + \ln \gamma_i^R \quad \text{.....(5.63)}$$

The first term on the right-hand side of Equation 5.63 represents the combinatorial part of the activity coefficient and the second term refers to the residual part. In the modified UNIFAC-Lyngby, Mohammadi et al., (2005) described the combinatorial part as:

$$\ln \gamma_i^C = 1 - \varphi_i + \ln \varphi_i \quad \text{.....(5.64)}$$

where:

$$\varphi_i = \frac{r_i^{2/3}}{\sum_j x_j r_j^{2/3}} \quad and \quad r_i = \sum \upsilon_k^{(i)} R_k \qquad (5.65)$$

In the modified UNIFAC-Dortmund, the combinatorial part is given by:

$$\ln \gamma_i^C = 1 - V_i' + \ln V_i' - 5q_i\left(1 - \frac{V_i}{F_i} + \ln \frac{V_i}{F_i}\right) \qquad (5.66)$$

where:

$$V_i' = \frac{r_i^{2/3}}{\sum_j x_j r_j^{3/4}} \quad , \quad V_i = \frac{r_i}{\sum_j x_j r_j} \quad , \quad F_i = \frac{q_i}{\sum_j x_j q_j} \quad , \quad and \quad q_i = \sum \upsilon_k^{(i)} Q_k \qquad (5.67)$$

The residual part of the activity coefficient is calculated:

$$\ln \gamma_i^R = \sum \upsilon_k^{(i)} \left(\ln \Gamma_k - \ln \Gamma_k^{(i)}\right) \qquad (5.68)$$

$$\ln \Gamma_k = Q_k \left[1 - \ln\left(\sum_m \Theta_m \Psi_{mk}\right) - \sum_m \frac{\Theta_m \Psi_{km}}{\sum_n \Theta_n \Psi_{nm}}\right] \qquad (5.69)$$

where:

$$\Theta_m = \frac{Q_m X_m}{\sum_n Q_n X_n} \quad and \quad X_m = \frac{\sum_j \upsilon_m^{(i)} x_j}{\sum_j \sum_n \upsilon_n^{(j)} x_j} \qquad (5.70)$$

$$\Psi_{mn} = \exp\left(-\frac{a_{mn} + b_{mn} T}{T}\right) \qquad (5.71)$$

where a_{mn} and b_{mn} are UNIFACT interaction parameters between the groups m and n and are estimated from experimental data. Tables 5.5 and 5.6 represent the constant values used in the above procedure.

The Henry coefficients for components methane, nitrogen, and carbon dioxide in water are presented in Table 5.7 (Mohammadi et al., 2005). Table 5.8 summarizes the molar volume values ($\overline{v}_{G_i w}$) reported by Dhima et al. (1999) for different pressure and temperature ranges.

Table 5. 5. The R and Q values used in the UNIFAC-Lyngby, UNIFAC-Dortmund methods for various group assignments (Data from Li et al., 1997 and Larsen, 1987).

Main Group	Subgroup	R	Q
N_2	N_2	1.8680	1.9700
CO_2	CO_2	2.5920	2.5220
CH_4	CH_4	2.2440	2.3120
C_2H_6	C_2H_6	3.6044	3.3920
C_3H_8	C_3H_8	4.9532	4.4720
H_2S	H_2S	2.3330	2.3260
H_2O	H_2O	0.9200	1.4000

Table 5. 6. Modified UNIFAC Group interaction parameters (Data from Li et al., 1997 and Larsen, 1987).

i	j	a_{ij}	a_{ji}	b_{ij}	b_{ji}

N_2	H_2O	2280	403.8	-3.607	0.5907
CO_2	H_2O	624	257.3	-0.320	0.01808
CH_4	H_2O	2435	477.3	-3.057	-0.03417
C_2H_6	H_2O	1478	324.9	-1.509	0.2567
C_3H_8	H_2O	2699	326.6	-3.559	0.1518
H_2S	H_2O	1019	349.5	-0.8687	-0.3832

Table 5. 7. The molar volume of various gaseous components in water, obtained from the literature (Evelein and Moore, 1979, Dhima et al., 1999, and Mohammadi et al., 2005).

Component	T, K	P, psia	$\bar{v}_{g_i g}, ft^3/mol \times 1000$
CH_4	298-344	>50	1.13-1.271
C_2H_6	300-344	>50	1.695-1.73
C_3H_8	300-344	>50	2.295-3.107
C_4H_{10}	285-330	>50	2.401-2.931
CO_2	285-348	>50	1.13-1.165
N_2	All	All	Mohammadi et al. (2005) Correlations

Table 5. 8. The correlations between Henry coefficients and temperature, obtained from the literature (Dhima et al., 1999 and Weidlich and Gmehling, 1987).

Component	Henry's constant, psia	Reference	Temperature Range, K
CH_4	H^o = 8401.4T-2.0E-6	Dhima et al. (1999)	273-330

C_2H_6	H^o = 1.08E4T-3.0E-6	Dhima et al. (1999)	273-325
C_3H_8	H^o = 2.21E4T-6.0E-6	Dhima et al. (1999)	273-345
C_4H_{10}	H^o = 1.32E3T-3.0E-6	Dhima et al. (1999)	273-344
CO_2	H^o = 650.0T-1.69E-5	Weidlich and Gmehling (1987)	273-340
N_2	H^o = 1.38E4T-3.0E-6	Weidlich and Gmehling (1987)	273-343

It was previously demonstrated that the adsorbed phase fugacity can be best estimated using Equation 5.7. Substituting Equation 5.7 into Equation 5.47 we have:

$$\theta_{G_i c}(t) = \exp\left\{-\left\{-D_{g_i}\ln\left[\frac{Py_{ga_i}}{\hat{P}_{gao}}\tanh\left(2Py_{ga_i}\phi_{ga_i}K_{gs_i}t\right)\right]\right\}^{r_i}\right\} \quad \text{.....(5.72)}$$

For further simplification, the following expression is defined:

$$\hat{K}_{ga_i} = K_{ga_i}\phi_{ga_i} \quad \text{.....(5.73)}$$

Therefore Equation 5.72 is rewritten in the following form:

$$\theta_{G_i c}(t) = \exp\left\{-\left\{-D_{g_i}\ln\left[\frac{Py_{ga_i}}{\hat{P}_{gao}}\tanh\left(2Py_{ga_i}\hat{K}_{gs_i}t\right)\right]\right\}^{r_i}\right\} \quad \text{.....(5.74)}$$

Determination of the Non-equilibrium Isotherms

A computer code was prepared in MATLAB to solve the above equations and calculate the amount of each gas component in the water, gas, and coal phases. The calculation procedure is as following:

1. Measure the initial coal, gas, water volumes, and their component mole fractions in the PVT cell.

2. Monitor the pressure changes as a function of time.

3. Calculate the values of P_o for various gas components using the method proposed with Kapoor et al. (1987) (Equation 5.2).

4. Guess new gas and water phase component mole fractions for both gas and water phases.

5. Estimate the gas phase components fugacity using Equations 5.51-5.60 and water phase activity coefficients using Equations 5.61-5.62.

6. Calculate the gas and water phase component mole fractions using Equation 5.75, (a convenient form of Equations 5.48 and 5.49).

$$m_{Gg}^{t+1} = \Delta t K_{gw} \exp\left(K_{1gw} \frac{\hat{f}_{Gg}}{\hat{f}_{Gw}} - K_{2gw} \frac{\hat{f}_{Gw}}{\hat{f}_{Gg}} \right) + m_{Gg}^{t} \quad \text{.....(5.75)}$$

where m represents y for gas phase and x for liquid phase and t represents the time step.

7. Compare the calculated x and y with the assumed values in step 4. If the difference is sufficiently small, then move to step 8, otherwise repeat steps 5-7 using the just calculated values of x and y.

8. Use the overall material balance equations (5.14-5.25) to calculate the volume of the adsorbed gas components and calculate the mole fraction of each component in the coal.

9. Estimate the fugacity of the adsorbed phase using Equation V.7.

10. Plot $\ln V$ versus $X = -\left\{ - D_{g_i} \ln\left[\frac{P y_{ga_i}}{\hat{P}_{gao_i}} \tanh\left(2 P y_{ga_i} \hat{K}_{gs_i} t\right) \right] \right\}^{r_{gi}}$ according to Equation 5.76 (a convenient form of Equation 5.47), and fit the best curve to the data points and determine the parameters of *D, r,* K_{gs} and V_m for each component.

$$\ln V_{gai} = \ln V_{m_{gai}} - \left\{ - D_{g_i} \ln\left[\frac{P y_{ga_i}}{\hat{P}_{gao_i}} \tanh\left(2 P y_{ga_i} \hat{K}_{gs_i} t\right) \right] \right\}^{r_{gi}} \quad \text{.....(5.76)}$$

Therefore, the non-equilibrium isotherm in the form of Equation 5.76 is constructed. However, the rate of adsorption/desorption and the parameters of Equation 5.76 may be functions of the total pressure, temperature, and grain size of the coal particles in a given system of gas, coal, and water. Therefore, Equation 5.76 can be rewritten in a general form as:

$$\ln V_i = \ln\left[G_{V_{mi}}\left(\hat{f}_{g_i c}, d, T\right)\right] - \left[G_{D_i}\left(\hat{f}_{g_i c}, d, T\right)\right]^{G_r\left(\hat{f}_{g_i c}, d, T\right)} \left\{ - \ln\left\{ \frac{\hat{f}_{g_i c}}{P_o} \tanh\left[2 \hat{f}_{g_i c} t G_{K_{gs_i}}\left(\hat{f}_{g_i c}, d, T\right)\right] \right\} \right\}^{G_r\left(\hat{f}_{gic}, d, T\right)} \quad \text{.....(5.77)}$$

where *G* represents a series of empirical relationships for the parameters of V_m, *D, r*, and K_{gsi} as functions of fugacity (pressure), grain size, and temperature. The dependency of the general function of G to the mentioned parameters will be discussed and obtained applying the experimental data points. When Equation 5.78

is constructed and all the empirical functions are determined, the equilibrium isotherm is also established by applying the following rule:

$$\lim_{t\to\infty}\left\{2\hat{f}_{Gic}G_{kgi}\left(\hat{f}_{Gic},d,T\right)t\right\}=0 \quad \text{.....(5.78)}$$

Therefore, Equation 5.78 becomes:

$$\ln V_i=\ln\left[G_{V_{mi}}\left(\hat{f}_{g_ic},d,T\right)\right]-\left[G_{D_i}\left(\hat{f}_{g_ic},d,T\right)\right]^{G_r\left(\hat{f}_{g_ic},d,T\right)}\left[-\ln\left(\frac{\hat{f}_{g_ic}}{P_o}\right)\right]^{G_r\left(\hat{f}_{gic},d,T\right)} \quad \text{.....(5.79)}$$

To analyze, confirm, and modify the applicability and accuracy of the above procedure in determining non-equilibrium, equilibrium gas-water-coal isotherms the literature and our experimental data are considered. The validation procedure will be described in Chapter 6.

CHAPTER 6

VALIDATION OF THE EQUILIBRIUM AND NON-EQUILIBRIUM GAS ISOTHERMS WITH AND WITHOUT WATER PRESENCE

This chapter validates the model developed in the previous chapter by applying the literature and in-house experimental data. The first section of this chapter validates the non-equilibrium gas adsorption in coal model without the presence of water applying the literature data. The available data in the literature are for the gas adsorption in coal without the presence of water. The gas adsorption model with the presence of water is validated applying the in-house experimental data. The last section of this chapter discusses the applications of the developed model in rapid determinations of coalbed methane and shale gas reservoir equilibrium and non-equilibrium isotherms applying the early time non-equilibrium measurements.

6.1. Validation of the Equilibrium and Non-Equilibrium Gas Isotherms without Water Using the Literature Data

Case I: Pure methane, carbon dioxide, and nitrogen adsorption in coal

Gasem et al. (2002) reported pure methane, carbon dioxide, and nitrogen adsorption rate data in the Tiffany coal. Figures 6.1-6.3 represents the time-dependency of methane, nitrogen and carbon dioxide adsorption on the Tiffany coal at various pressure ranges, respectively. As can be seen, the equilibrium establishes

if sufficient time is given to the system at each pressure. Thus, theoretically, the plots given in Figure 6.1 at different pressures provide one equilibrium data point on the equilibrium isotherm given in Figure 6.4.

Equation 5.77 is applied for the procedure of curve fitting of the data points to determine the model parameters. Tables 6.1-6.3 present the best-estimate values for r, k, D, P_o, and V_m for the system of methane, carbon dioxide, and nitrogen on coal at various pressures. As can be seen, the value of r and k are independent of pressure and are only functions of the gas and carbonaceous material properties. P_o is only a function of temperature and gas properties, D and V_m are both functions of pressure. The maximum theoretical gas adsorption volume (V_m) according to Figure 6.5 has a logarithmic relationship with pressure that can be described as:

$$G_{V_m}(P) = a_{V_m} \ln P + b_{V_m} \quad \text{.....(6.1)}$$

However, *D* (D-R coefficient) according to Figure 6.6 has a linear relationship with pressure, described as:

$$G_D(P) = a_D P + b_D \quad \text{.....(6.2)}$$

The value of D used in D-A and D-R equations is considered to be only a property of the adsorbent (coal) (Jahediesfanjani, and Civan, 2005). However, Figure 6.6 shows that pressure variation can affect the value of D. Therefore, the properties of the adsorbent (coal) itself change as the pressure and type of the gas in contact with the coal changes. In fact, Larsen (2004) concluded that gas solution in coal changes the coal properties to some extend depending upon the type of the gas and coal. Larsen points out that the dissolved carbon dioxide in coal acts as a

plasticizer enabling a structure rearrangement so that the second adsorption of CO_2 is subject to the same coal with different structure.

Figure 6.6 shows that the variations of the D with pressure for carbon dioxide is more than methane and nitrogen. Moreover, the rate of the change for carbon dioxide is faster than methane and nitrogen, because the carbon dioxide is adsorbed preferentially more on coal than other gases. Equation 5.77 can be rewritten as:

$$\ln V_i = a_{V_m} \ln \hat{f}_{g_i g} + b_{V_m} - \left(a_D \bar{f}_{g_i g} + b_D\right)^{r_i} \left\{ - \ln \left[\frac{\bar{f}_{g_i c}}{P_o} \tanh\left(2 \bar{f}_{g_i c} K_{gsi} t\right) \right] \right\}^{r_i} \quad \text{.....(6.3)}$$

This equation provides a non-equilibrium isotherm for adsorption of any gas on carbonaceous materials. The equilibrium isotherm can be obtained when time approaches the infinity. Therefore, a non-equilibrium equation can be transformed to equilibrium isotherm as:

$$\ln V_i = a_{V_m} \ln \hat{f}_{g_i g} + b_{V_m} - \left(a_D \bar{f}_{g_i g} + b_D\right)^{r_i} \left[- \ln \left(\frac{\hat{f}_{g_i c}}{P_o} \right) \right]^{r_i} \quad \text{.....(6.4)}$$

Equation 6.4 is the modified D-R isotherm for the case of high pressure and multi-component gas adsorption on the coal. This exercise illustrates that both non-equilibrium and equilibrium isotherms can be obtained from the same type of the measurements performed to obtain the equilibrium isotherms using this method.

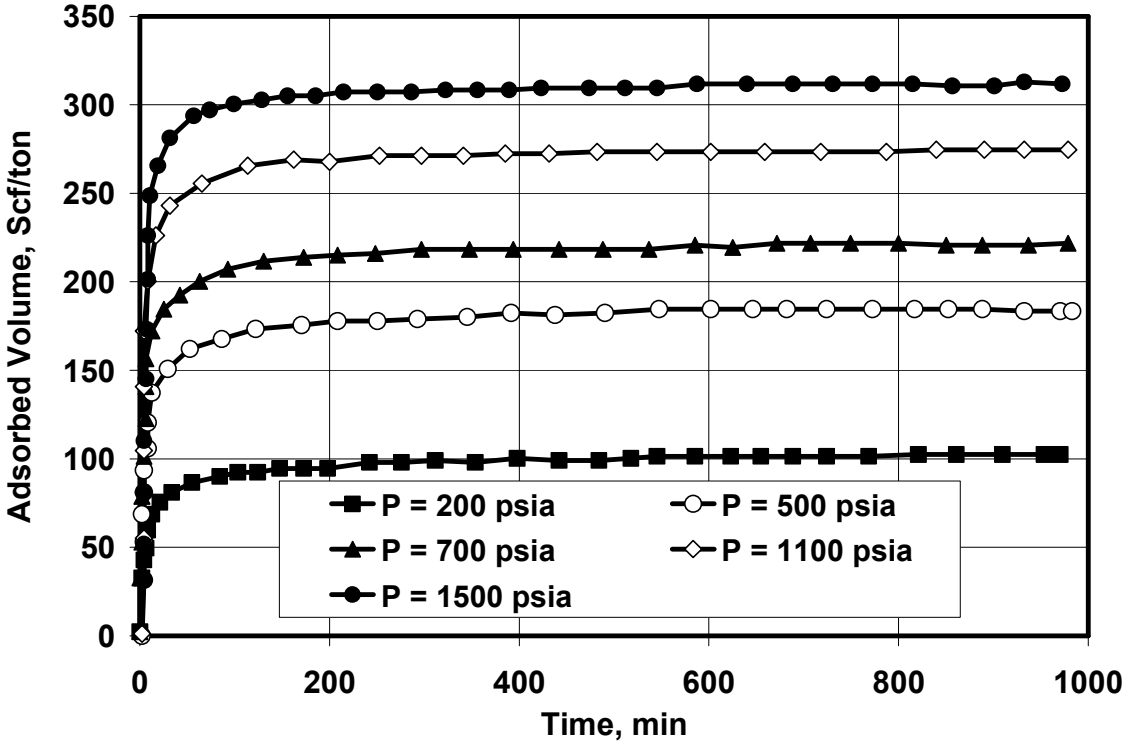

Figure 6. 1. Measured methane adsorbed volume on the Tiffany coal versus time of adsorption (Gasem et al., 2002).

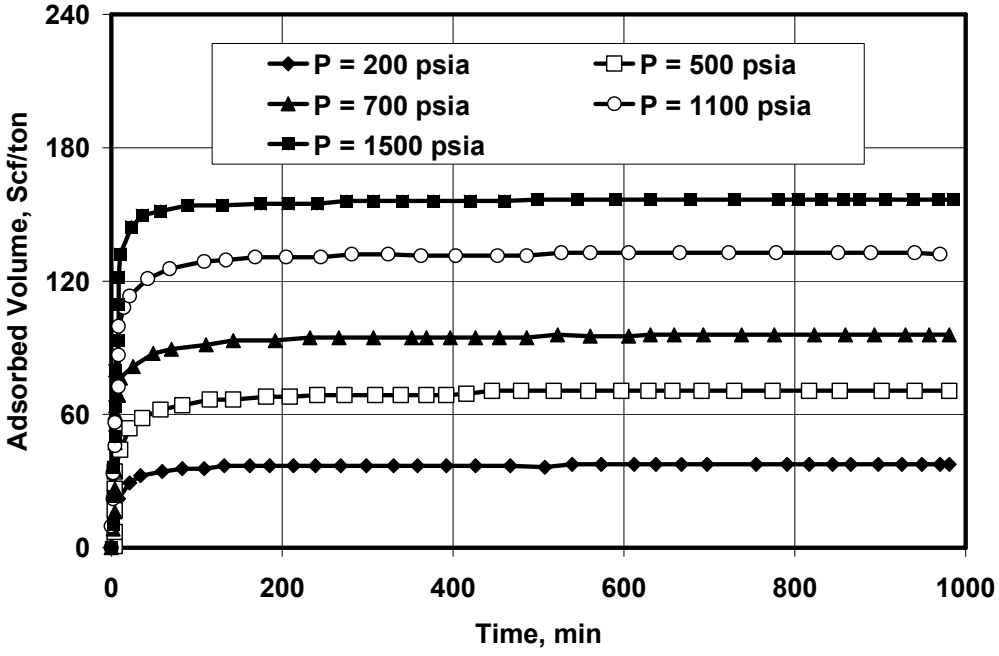

Figure 6. 2. Measured nitrogen adsorbed volume on the Tiffany coal versus time of adsorption (Gasem et al., 2002).

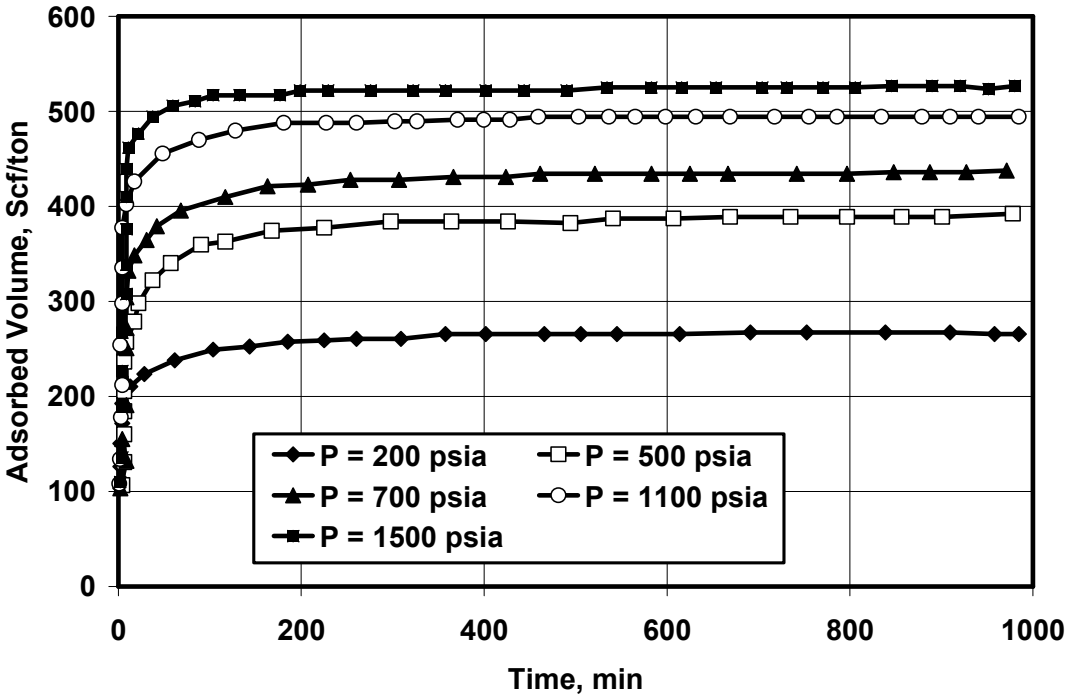

Figure 6. 3. Measured carbon dioxide adsorbed volume on the Tiffany coal versus time of adsorption (Gasem et al., 2002).

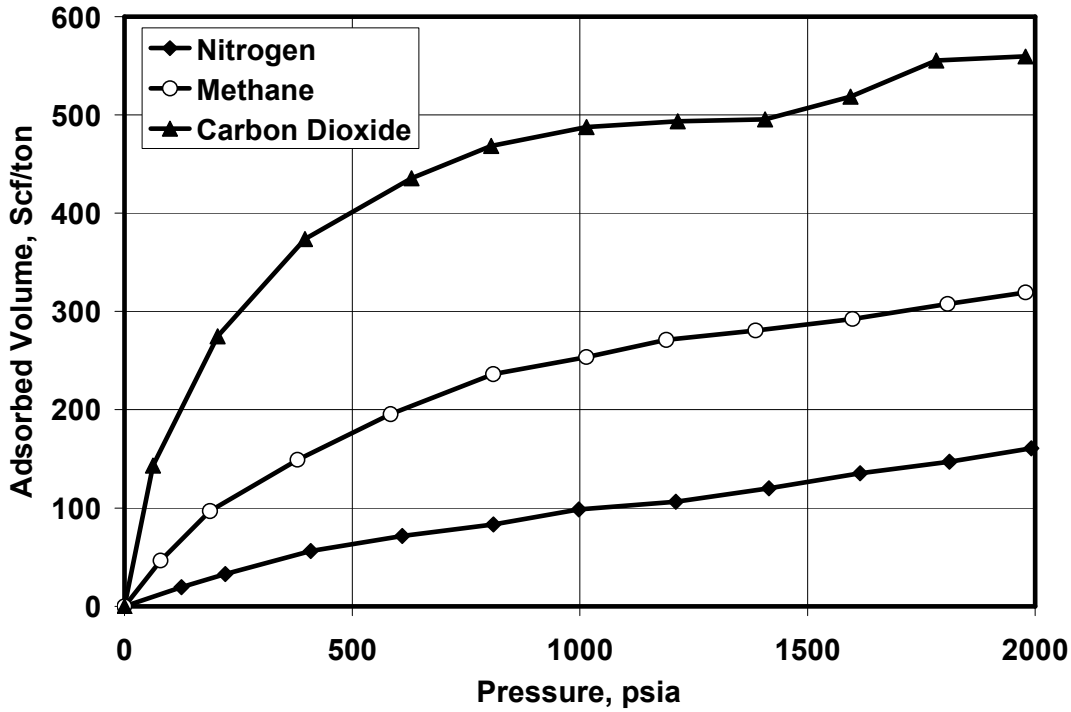

Figure 6. 4. Measured equilibrium isotherms for various gases adsorption on Tiffany coal (Gasem et al., 2002).

Table 6. 1. Best-estimate values of the parameters for CH_4 non-equilibrium isotherm on coal calculated in this study.

P,psia	r	P_o	K	ln V_m	D^r	V_m	D
200	1.75	6453	0.000016	4.873	0.029	130.66	0.132
500	1.75	6453	0.000016	5.436	0.046	229.52	0.171
700	1.75	6453	0.000016	5.603	0.054	271.29	0.189
900	1.75	6453	0.000016	5.7	0.057	298.93	0.194
1100	1.75	6453	0.000016	5.768	0.059	319.9	0.198
1300	1.75	6453	0.000016	5.855	0.077	349.04	0.23
1500	1.75	6453	0.000016	5.882	0.081	358.35	0.237

Table 6. 2. Best-estimate values of the parameters for CO_2 non-equilibrium isotherm on coal calculated in this study.

P	R	P_o	k	ln V_m	D^r	V_m	D
200	1.9	3000	0.000018	5.70	0.020	300.04	0.126
500	1.9	3000	0.000018	6.07	0.044	433.76	0.193
700	1.9	3000	0.000018	6.17	0.056	478.47	0.220
900	1.9	3000	0.000018	6.23	0.068	509.32	0.244
1100	1.9	3000	0.000018	6.27	0.081	529.32	0.266
1300	1.9	3000	0.000018	6.29	0.103	541.31	0.303
1500	1.9	3000	0.000018	6.31	0.105	549.72	0.306

Table 6. 3. Best-estimate values of the parameters for N_2 non-equilibrium isotherm on coal calculated in this study.

P	R	P_o	k	ln V_m	D^r	V_m	D
200	1.0	2300	0.000068	3.38	0.040	29.32	0.040
500	1.0	2300	0.000068	4.84	0.053	126.53	0.053
700	1.0	2300	0.000068	5.09	0.060	162.86	0.060
900	1.0	2300	0.000068	5.25	0.058	190.25	0.058
1100	1.0	2300	0.000068	5.36	0.062	212.32	0.062
1300	1.0	2300	0.000068	5.42	0.074	226.86	0.074
1500	1.0	2300	0.000068	5.48	0.071	240.89	0.071

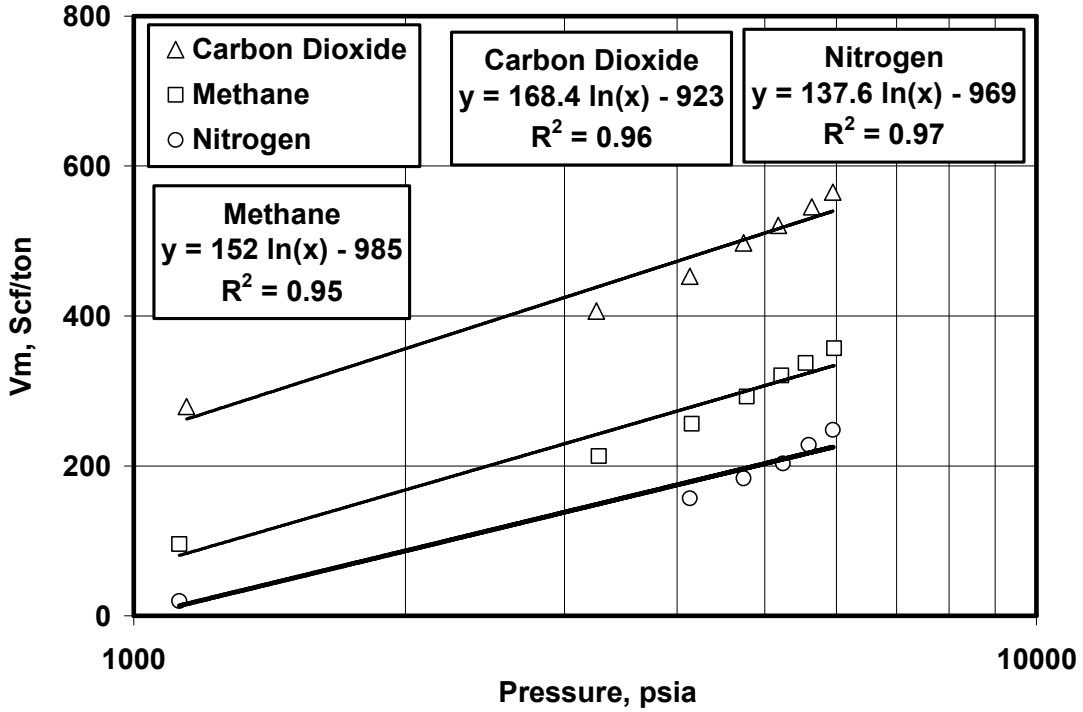

Figure 6. 5. Plot of the estimated values of V_m versus system pressure on a semi-logarithmic scale for methane, carbon dioxide and nitrogen adsorption on coal.

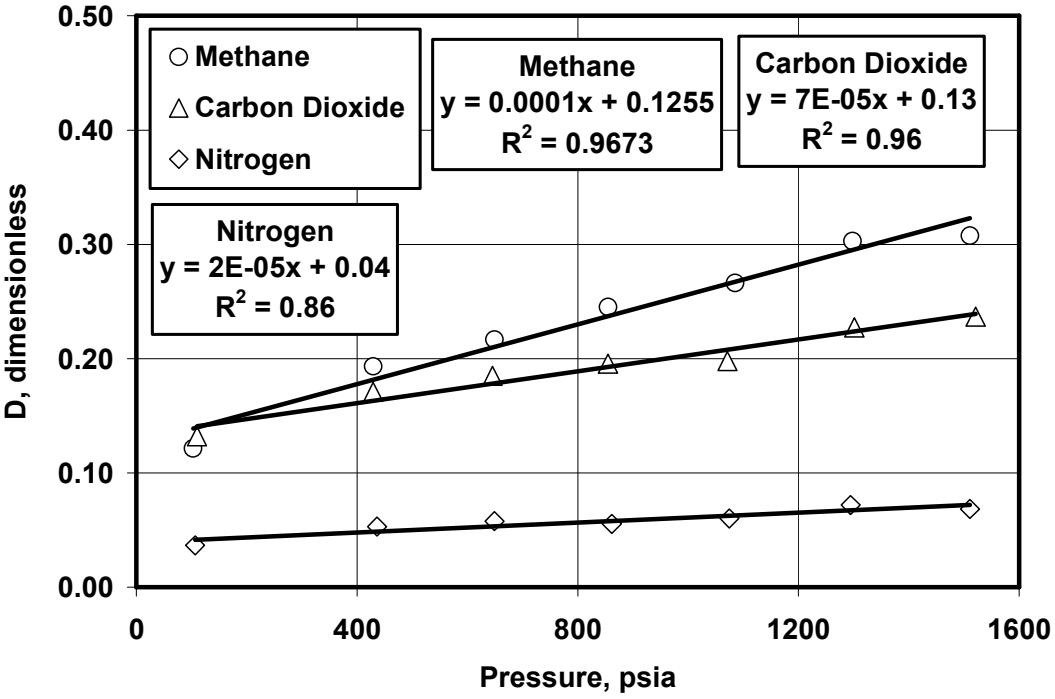

Figure 6. 6. Plot of the estimated values of D versus system pressure for methane, carbon dioxide and nitrogen adsorption on coal.

Case 2. Correlating of the D-R isotherm parameters with Coal Particle Sizes

Busch et al., (2002) reported several experimental rate data on the adsorption of methane and carbon dioxide in Silesia 315 coal for different grain sizes ranging from grain diameters less than 1.73 to higher than 9.73 inches. Their data indicate different times to reach equilibrium for different grain sizes. The rate of adsorption is faster for smaller particles than the bigger ones. Therefore, it appears that the particle size may influence the non-equilibrium isotherm parameters.

Tables 6.4 and 6.5 show the best estimate values of the parameters obtained by matching Equation 6.3 with Busch et al.(2002), adsorption kinetic data. As can be seen, the values of D and V_m decrease as the particles size increases. Figures 6.7 and 6.8 show that V_m has a logarithmic relationship with the grain size; whereas, *D* varies linearly with the grain size. In coalbed reservoirs, the coal matrix is composed of the grains in different sizes and combinations. Given the grain size distribution, the effect of the grain size on non-equilibrium isotherm and adsorption/desorption rates in the real reservoir condition can be considered in construction of the correct non-equilibrium and equilibrium isotherms using:

$$G_{\overline{D}_A}(d) = \frac{\int_0^A [a_{dD} f(d) + b_{dD}]dA}{\int_0^A dA} \quad \text{.....(6.5)}$$

$$G_{\overline{V}_{mA}}(d) = \frac{\int_0^A \{a_{dV_m} \ln[f(d)] + b_{dV_m}\}dA}{\int_0^A dA} \quad \text{.....(6.6)}$$

Equations 6.5 and 6.6 indicate the overall average values of parameters D and V_m over a coalbed methane cross-section area A with grain size distribution of $f(d)$.

Table 6. 4. Best-estimate values of the parameters for CH_4 non-equilibrium isotherm on Sileca coal for various grain sizes.

Grain Size (inch)	r	P_o, psia	k	ln V_m	D^r	V_m, Scf/ton	D
<1.73	3.0	6200	0.000006	7.83	0.0032	2518	0.147
1.73-4.86	3.0	6200	0.000006	7.50	0.003	1808	0.144
4.86-9.73	3.0	6200	0.000006	7.32	0.0029	1504	0.1426
>9.73	3.0	6200	0.000006	7.27	0.0023	1436	0.132

Table 6. 5. Best-estimate values of the parameters for CO_2 non-equilibrium isotherm on Sileca coal for various grain sizes.

Grain Size(inch)	r	P_o	k	ln V_m	D^r	V_m Scf/ton	D
<1.73	1.0	3000	0.001	8.92	1.52	7480	1.52
1.73-4.86	1.0	3000	0.001	8.55	1.41	5166	1.46
4.86-9.73	1.0	3000	0.001	8.12	1.37	3361	1.39
>9.73	1.0	3000	0.001	7.65	1.301	2038	1.15

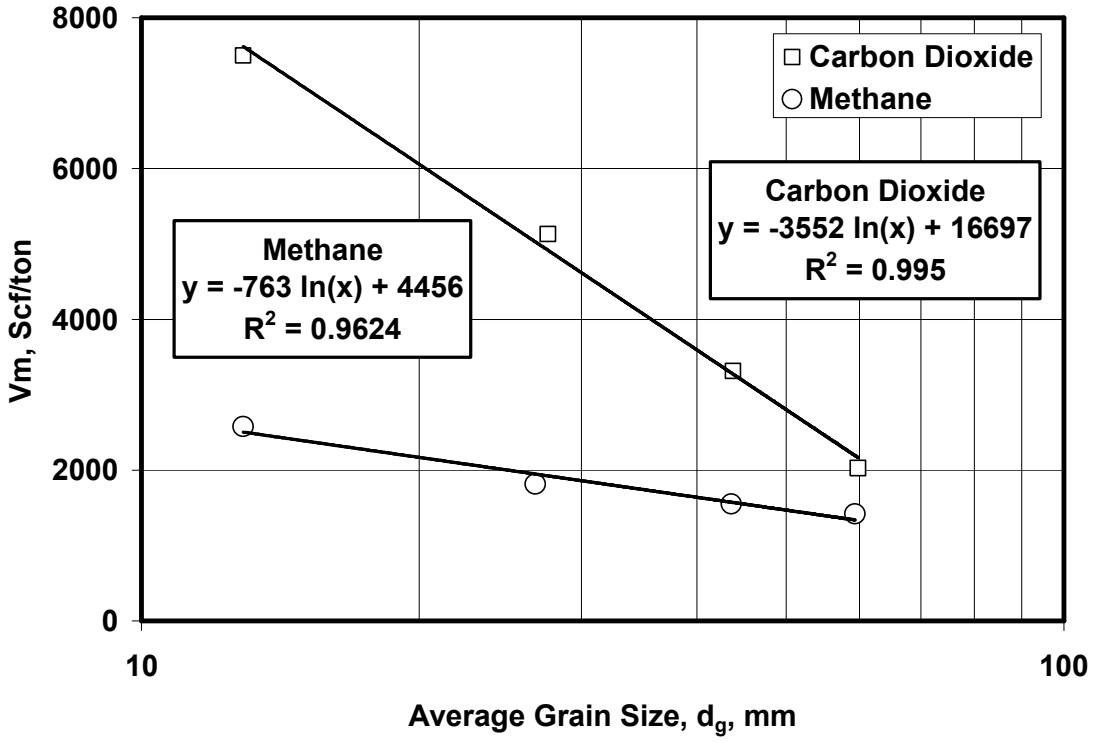

Figure 6. 7. Plot of the estimated V_m parameter (the theoretical maximum adsorption capacity of coal) values versus coal grain size on a semi-logarithmic scale.

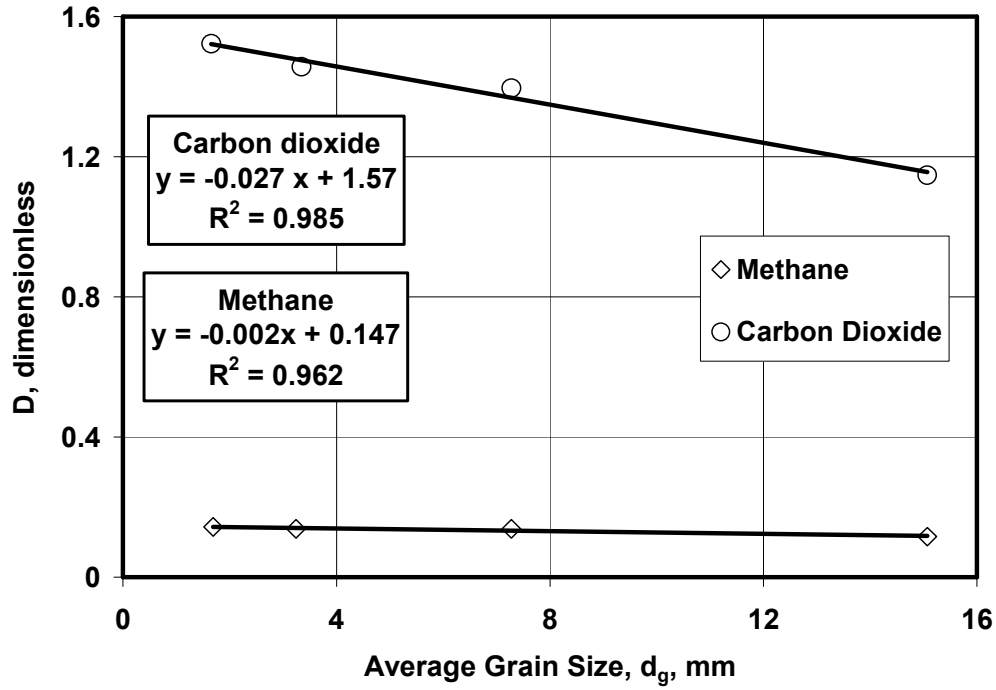

Figure 6. 8. Plot of the estimated D (D-R coefficient) values versus the average coal grain sizes.

6.2. Validation of the Equilibrium and Non-Equilibrium Gas Isotherms with and without Water Present Using the In-House Experimental Data

6.2.a. Gas-Water System

To investigate the time dependency of N_2 and CO_2 dissolution in water series of experiments at various pressures and a constant room temperature (average room temperature = 28°C= 82°F) are conducted. The PVT cell pressure versus time plots are already presented in Chapter 4. Appendix 4.1 contains an example to fully describe the interpretation procedure used for gas-water system. Figures 6.9 and 6.10 show the kinetics of nitrogen absorption in water at 100 psia and 301.3 K. To fit the non-equilibrium experimental data for gas-water system equations 5.48 and 5.49 are rewritten in the following form:

$$\frac{y_{N_2-N_2}^{t+1} - y_{N_2-N_2}^{t}}{\Delta t} = K_{N_2-w} \exp\left(K_{1N_2-w} \frac{\hat{f}_{N_2-N_2}}{\hat{f}_{N_2-w}} - K_{2N_2-w} \frac{\hat{f}_{N_2-w}}{\hat{f}_{N_2-N_2}} \right) \quad \text{.....(6.17)}$$

$$\frac{x_{W-w}^{t+1} - x_{W-w}^{t}}{\Delta t} = K_{w-N_2} \exp\left(K_{1w-N_2} \frac{\hat{f}_{w-W}}{\hat{f}_{w-N_2}} - K_{2w-N_2} \frac{\hat{f}_{w-N_2}}{\hat{f}_{w-W}} \right) \quad \text{.....(6.18)}$$

The right hand side of the above equations inside the exponential function is indicated with the parameter Y. Figures 6.8 and 6.9 show the curve fitting procedure using Equations 5.48 and 5.49. The best fit is obtained by adjusting the parameters K_{1N_2-w}, K_{2N_2-w}, K_{1w-N_2}, and K_{2w-N_2} so that the best straight line passing through the data will pass through the origin as well. The slope of the straight lines are equal to K_{N_2-w} and K_{w-N_2}.

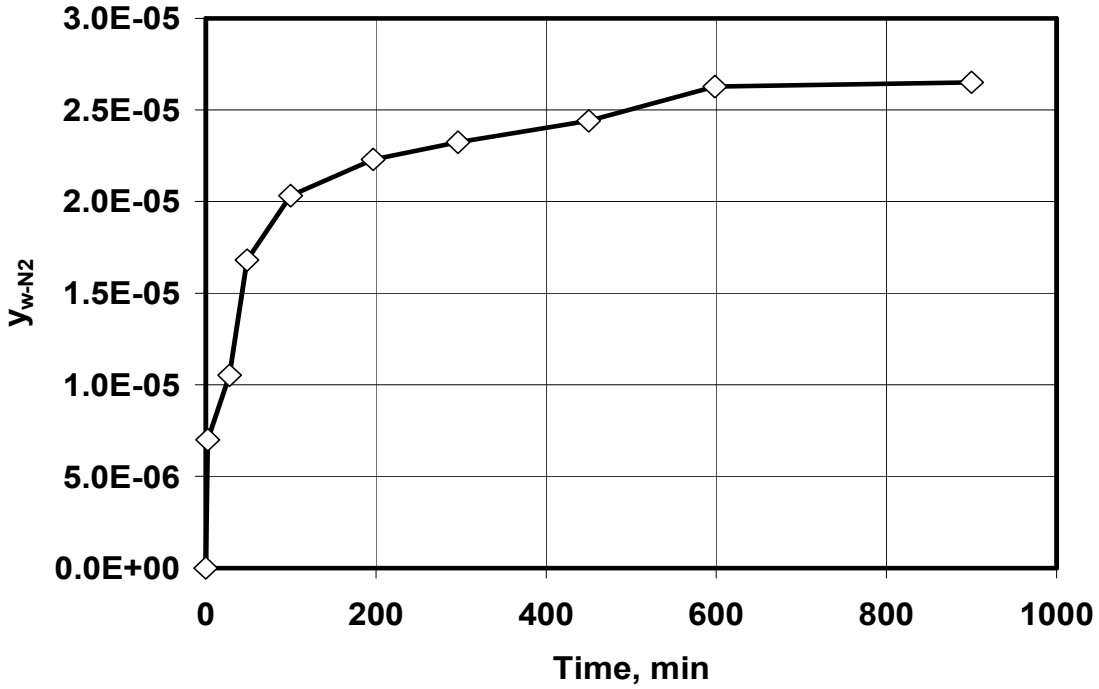

Figure 6. 9. The mole fractions of water component in the nitrogen phase versus time of absorption (100 psia, 301.3K).

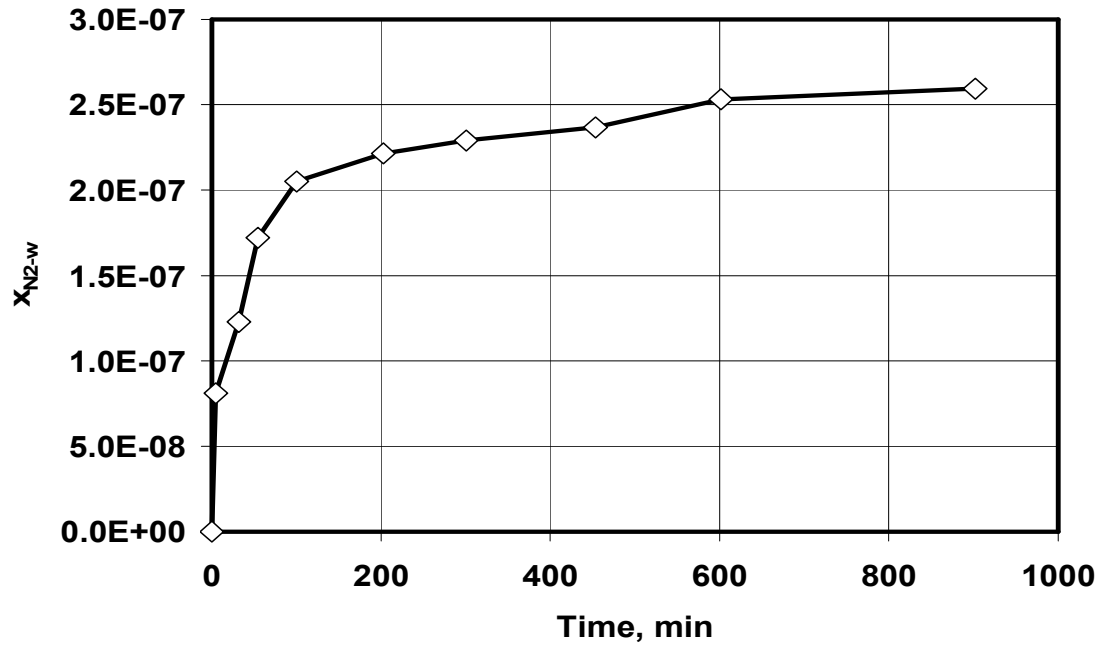

Figure 6. 10. The mole fraction of the nitrogen component in the water phase versus the absorption time (100 psia, 301.3K).

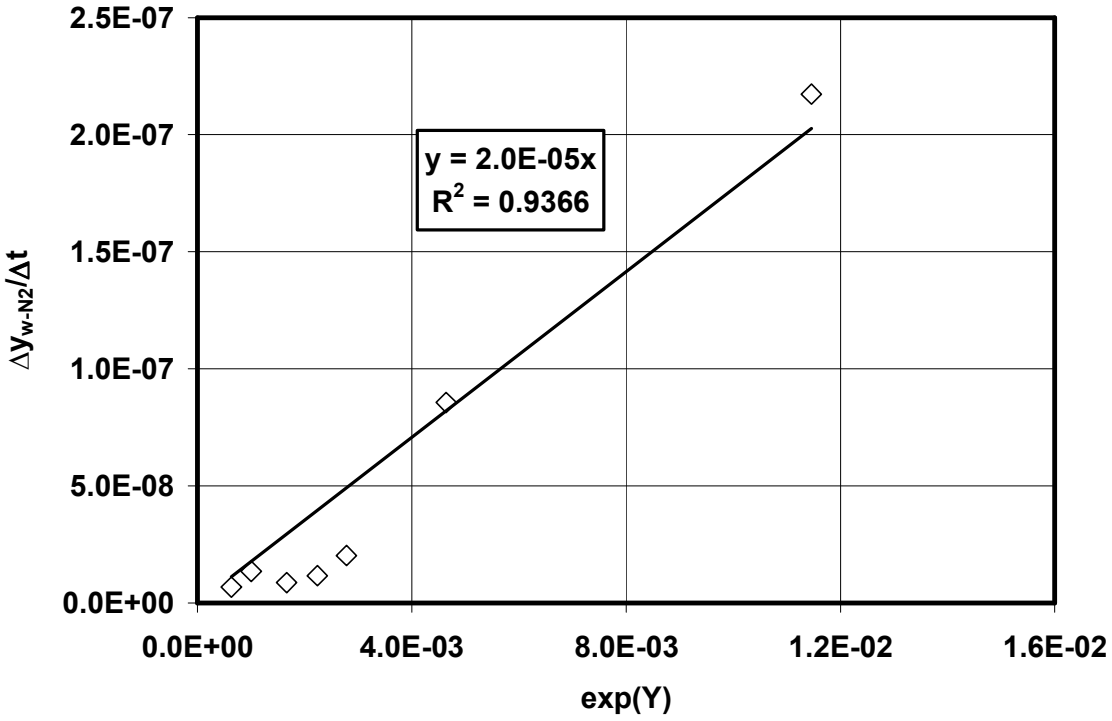

Figure 6. 11. Plot of $\frac{y_{N_2-N_2}^{t+1} - y_{N_2-N_2}^{t}}{\Delta t}$ versus $Y = K_{1N_2-w}\frac{\hat{f}_{N_2-N_2}}{\hat{f}_{N_2-w}} - K_{2N_2-w}\frac{\hat{f}_{N_2-w}}{\hat{f}_{N_2-N_2}}$ to fit the best straight line using Equation 6.17 (K_{1N_2-w} = 1.4E-06, K_{2N_2-w} = 1800) at 100 psia and 301.3K.

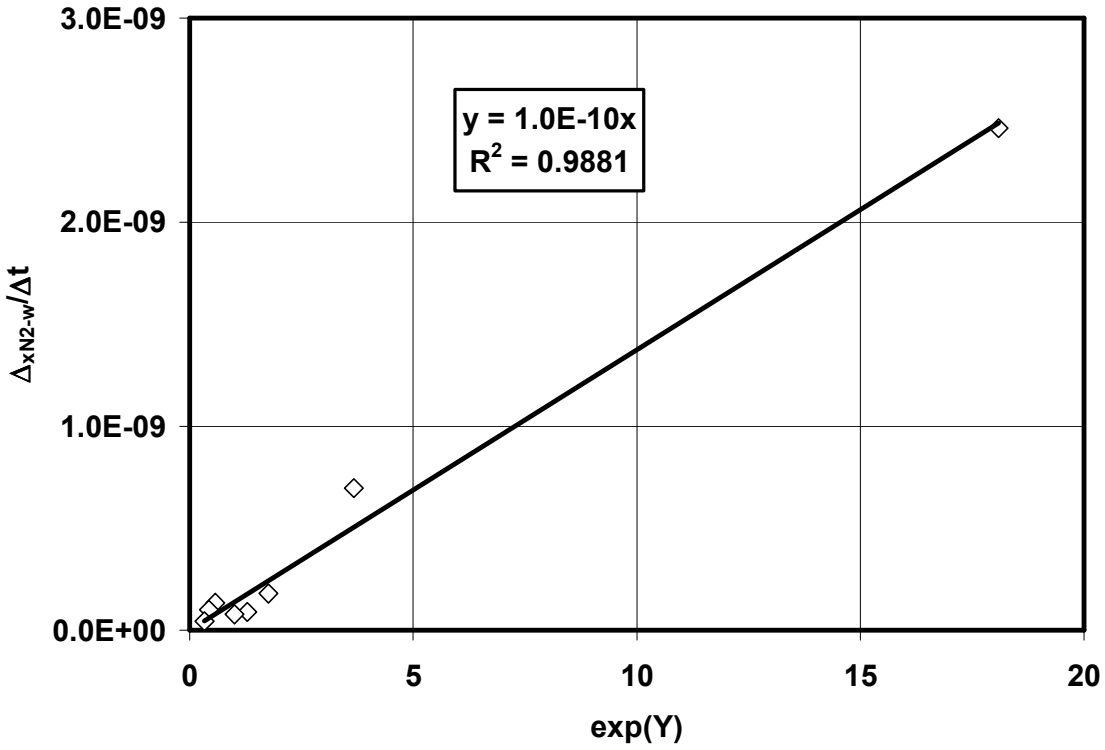

Figure 6. 12. Plot of $\frac{x_{W-w}^{t+1} - x_{W-w}^{t}}{\Delta t}$ versus $Y = K_{1w-N_2} \frac{\hat{f}_{w-W}}{\hat{f}_{w-N_2}} - K_{2w-N_2} \frac{\hat{f}_{w-N_2}}{\hat{f}_{w-W}}$ using Equation 6.18 ($K_{1w-N_2} = 0.001,\ K_{2w-N_2} = 20000$) at 100 psia and 301.3K.

The parameters $K_{N2\text{-}w}$ and $K_{w\text{-}N2}$ are obtained by the curve fitting procedure. Even though these equations are derived based on the kinetics of the thermodynamic relationships between the water and gas phases, the concept is very similar to that of the diffusivity of gases in water. Therefore, the parameters $K_{N2\text{-}w}$ and $K_{w\text{-}N2}$ can be recognized as the apparent diffusivity factors (D_a) and are obtained from the slope of the best fit according to Figures 6.11 and 6.12. These values for the nitrogen-water system at 100 psia and 301.3K are as following:

$K_{w-N_2} = 2.00 \times 10^{-05} / \min$ and $K_{N_2-w} = 1.00 \times 10^{-10} / \min$.

The same process (described in Appendix 4.1) is repeated for other pressure levels (200-900 psia) and the values for nitrogen apparent diffusivity in water and other parameters are obtained. These values are summarized in Table 6.6.

Table 6. 6. The calculated parameters of Equations 6.17 and 6.18 for the nitrogen-water system.

P, psia	K_{1N2-w}	K_{2N2-w}	K_{w-N2}, min^{-1}	K_{1w-N2}	K_{2w-N2}	K_{N2-w}, min^{-1}
100	1.4E-06	1800	2.00E-05	0.0010	20000	1.00E-10
200	5.2E-06	2000	4.00E-05	0.0025	19000	6.50E-10
300	8.9E-06	2150	7.00E-05	0.003	18200	9.2E-10
400	1.2E-05	2300	8.1E-05	0.0035	17300	2.1E-09
500	2.3E-05	2410	9.00E-05	0.0041	16700	2.5E-09
600	3.1E-05	2500	9.9E-05	0.0050	1600	3.1E-09
700	4.0E-5	2590	1.1E-04	0.0056	15200	3.2E-09
800	4.9E-5	2700	1.24E-04	0.0065	14600	3.27E-09
900	5.4E-05	2850	1.35E-04	0.0072	14000	3.35E-09

The next set of the experimental data is for the water-carbon dioxide system. The same procedure described in Appendix 4.1 is repeated for the water-carbon dioxide system. Figures 6.13 and 6.14 show the carbon dioxide mole fraction in

water phase versus the absorption time and water mole fraction in the gas phase versus the absorption time, respectively.

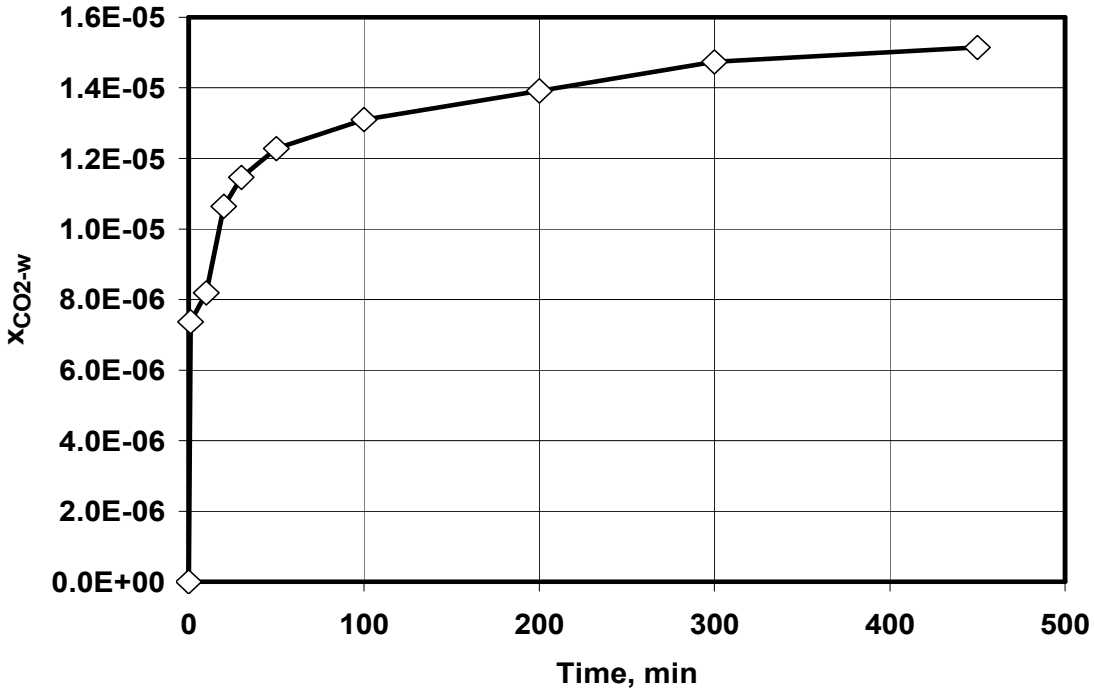

Figure 6. 13. The mole fractions of water component in the carbon dioxide phase versus time of absorption (100 psia, 301.3K).

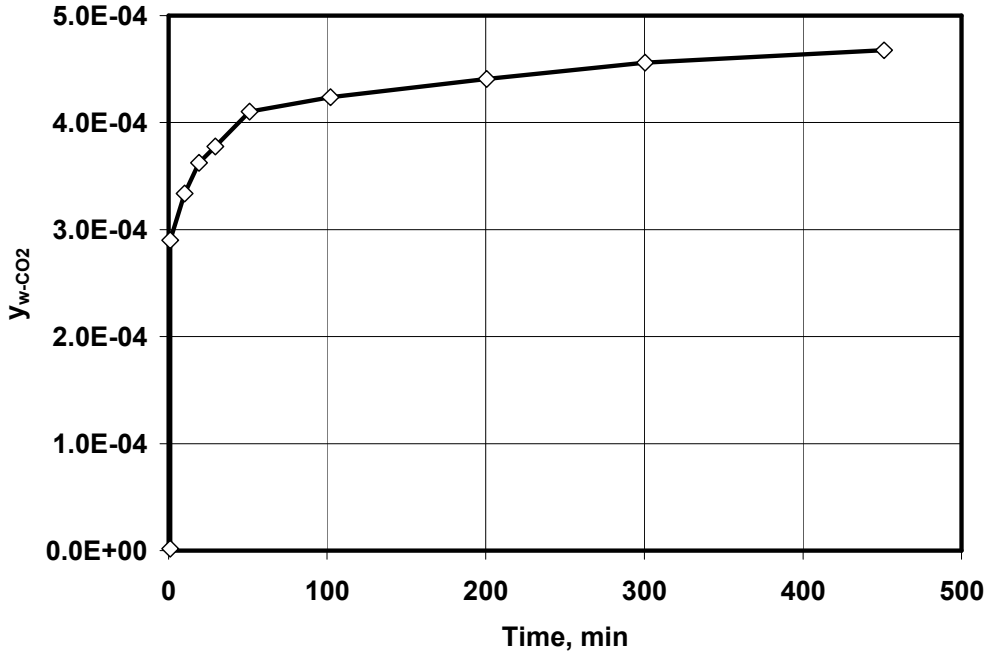

Figure 6. 14. The mole fraction of the carbon dioxide component in the water phase versus the absorption time (100 psia, 301.3K).

Figures 6.15 and 6.16 show the curve fitting process for the system of carbon dioxide and water at 400 psia and 301.3 K. The apparent diffusivity of water in carbon dioxide and carbon dioxide in water are also obtained. However, these values are pressure dependent. Table 6.7 summarizes these values for the system of carbon dioxide and water at various pressure levels.

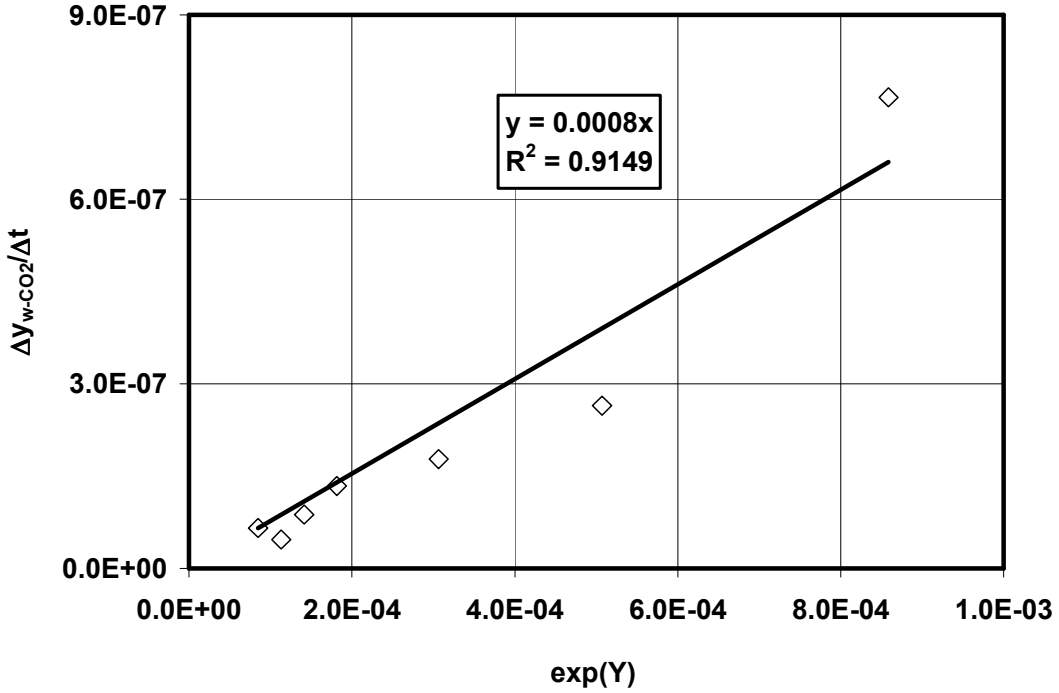

Figure 6. 15. Plot of $\frac{y_{CO_2-CO_2}^{t+1} - y_{CO_2-CO_2}^{t}}{\Delta t}$ versus $Y = K_{1CO_2-w}\frac{\hat{f}_{CO_2-CO_2}}{\hat{f}_{CO_2-w}} - K_{2CO_2-w}\frac{\hat{f}_{CO_2-w}}{\hat{f}_{CO_2-CO_2}}$ to fit the best straight line using Equation 6.18 ($K_{1CO2-w} = 0.03$, $K_{2CO2-w} = 96.0$) at 400 psia and 301.3K.

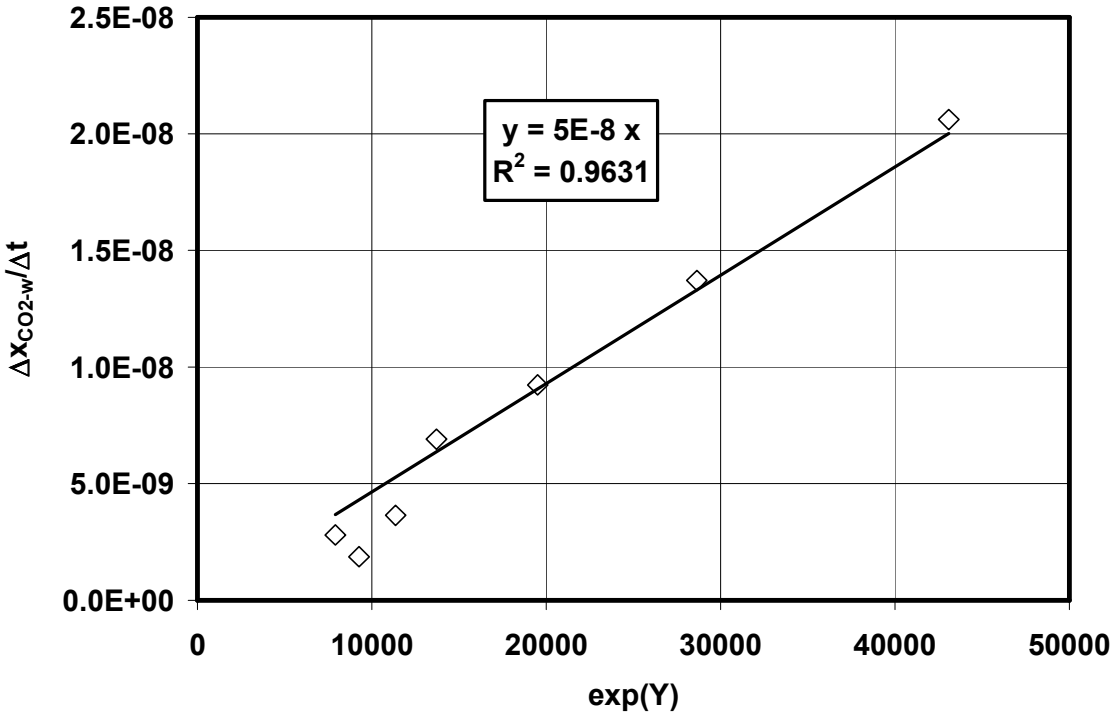

Figure 6. 16. Plot of $\frac{x_{W-w}^{t+1} - x_{W-w}^{t}}{\Delta t}$ versus $Y = K_{1w-CO_2} \frac{\hat{f}_{w-W}}{\hat{f}_{w-CO_2}} - K_{2w-CO_2} \frac{\hat{f}_{w-CO_2}}{\hat{f}_{w-W}}$ using Equation 6.18 ($K_{1w\text{-}CO2} = 0.099$ and $K_{2w\text{-}CO2} = 21.0$) at 400 psia and 301.3K.

Table 6. 7. The calculated parameters of Equations 6.17 and 6.18 for the carbon dioxide-water system.

P, psia	K_{1CO-w}	K_{2CO2-w}	K_{w-CO2}, min^{-1}	K_{1w-CO2}	K_{2w-CO2}	K_{CO2-w}, min^{-1}
100	2.6E-02	86	5.2E-04	0.075	35.0	1.00E-08
200	2.74E-02	90	6.5E-04	0.085	32.0	2.70E-08
300	2.82E-02	93	7.4E-04	0.092	27.0	3.80E-08
400	3.00E-02	96	8.0E-04	0.099	21.0	5.00E-08
500	3.10E-02	100	9.00E-04	0.110	19.0	6.50E-08
600	3.25E-02	105	9.5E-04	0.130	18.0	8.10E-08
700	3.32E-04	109	1.06E-03	0.150	16.0	9.80E-08
800	3.43E-04	113	1.14E-03	0.160	15.0	1.10E-07
900	3.50E-04	117	1.21E-03	0.170	14.0	3.35E-07

6.2.b. Coal –Gas System

The process of evaluation of the coal-gas system is very similar to that of the water-gas system. In both cases there are two phases interacting with each other. The gas component is present in both gas and coal phases. However, the coal component is only present in the coal phase. The procedure described in Appendix 4.2 step by step calculates the adsorbed gas volume in coal using pressure versus time curves obtained from the experiment and reported in Chapter 4.

Figure 6.17 shows the constructed non-equilibrium isotherm for nitrogen-coal A at an initial pressure of 200 psia for various coal grain sizes. Figure 6.17 indicates the time required reaching the equilibrium increases as the grain size increases. However, if enough time is given to the system, the final adsorbed gas by each coal is equal. Therefore, the net adsorbed gas volume by coal is independent of the coal particle size.

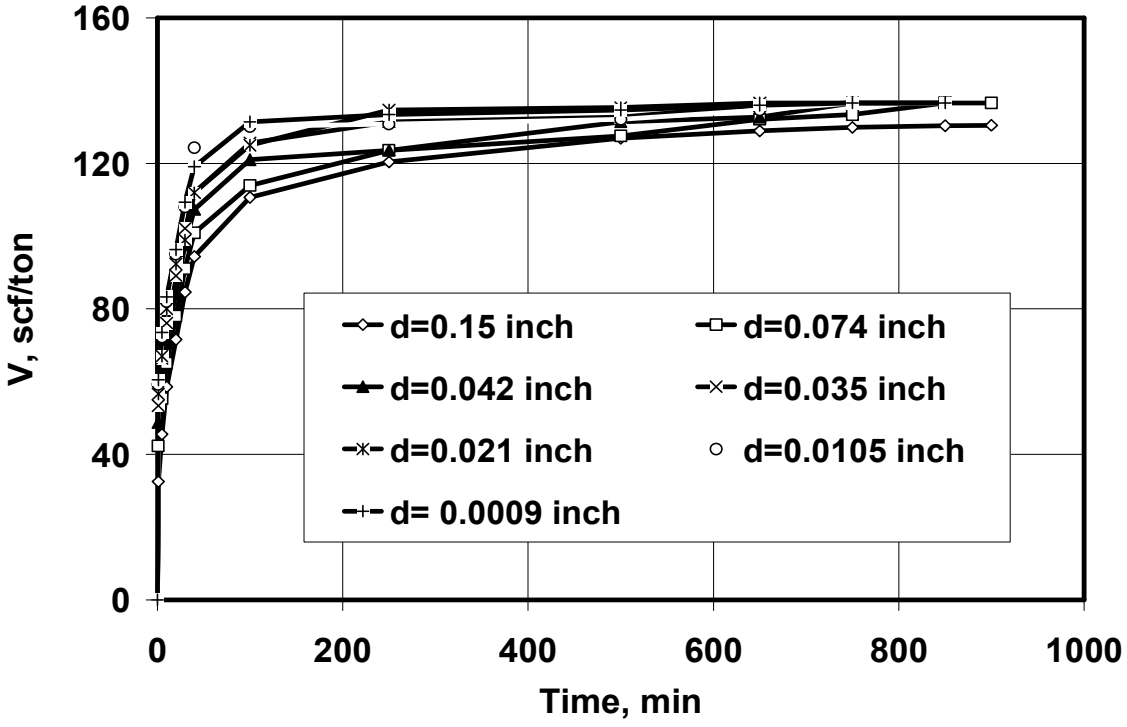

Figure 6. 17. Pure nitrogen adsorbed volume versus time for P_{in} = 200 psia and P_e = 182 psia for different grain sizes.

The similar procedure is applied at other pressure levels and similar plots are generated for pressure levels of 50, 400, 600, and 800 psia as shown in Figures 6.18 and 6.19.

To obtain the non-equilibrium isotherm parameters, the curve fitting procedure described earlier in Chapter 5 is followed. Figures 6.18 and 6.19 show the obtained non-equilibrium and equilibrium isotherms for both nitrogen and carbon dioxide gases at various grain size and pressure ranges respectively.

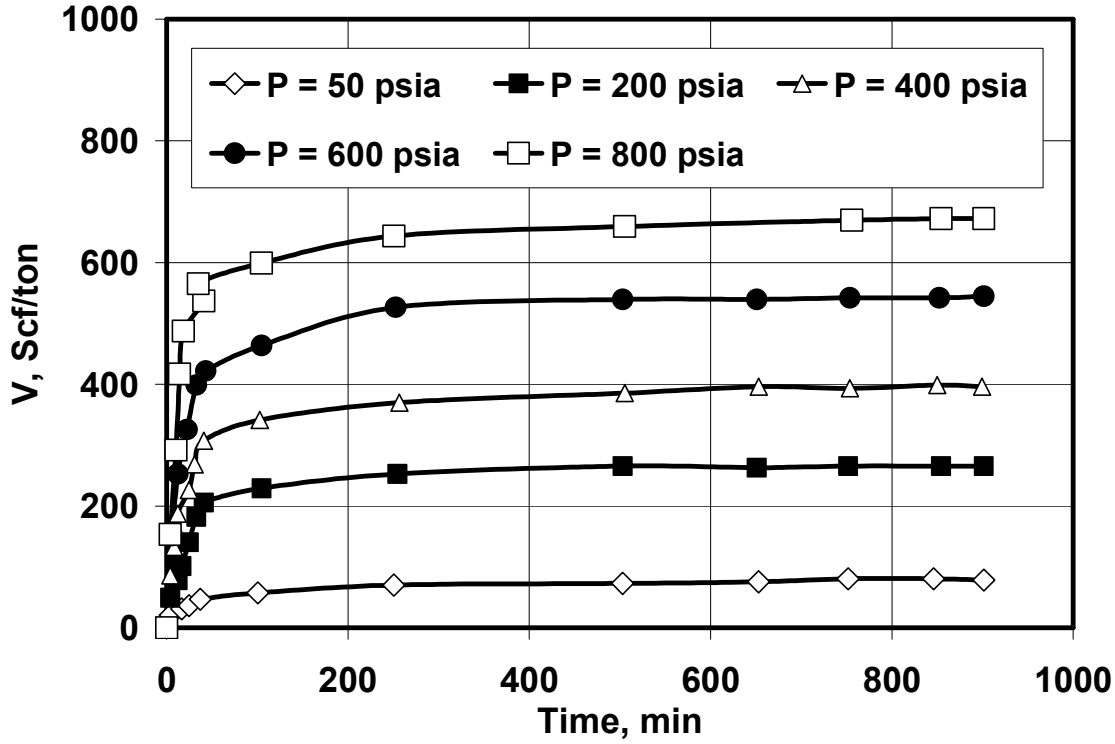

Figure 6. 18. Adsorbed carbon dioxide volume on coal A versus the adsorption time (d_g = 0.15 inch).

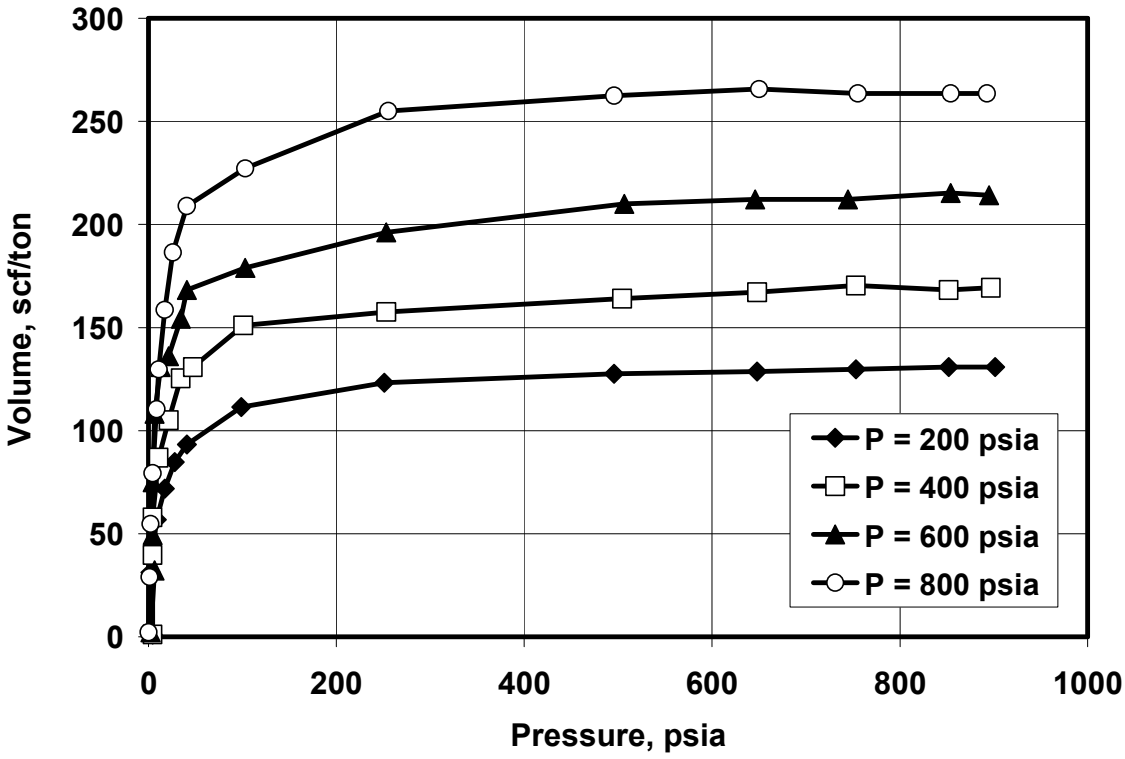

Figure 6. 19. Adsorbed nitrogen volume on coal A versus the adsorption time (d_g = 0.15 inch).

The curve fitting results show that the value of D-R exponent r, and the coal-gas kinetic parameter, K_{gs} remain constant for all range of grain size and pressure range; while the D-R coefficient, D, and the maximum theoretical adsorbed volume, V_m, change with particle size and pressure. Table 6.8 summarizes the values of r and K_{gs} for systems of nitrogen-coal A, nitrogen-coal B, carbon dioxide-coal A, and carbon dioxide-coal B. As indicated in Table 6.14 the values of r, and K_{gs} are functions of only gas and solid type in contact with each other. The results also indicate that the D-R coefficient, D, has a linear relationship with grain size and pressure. The parameter V_m has a logarithmic relationship with the pressure and grain size.

Table 6. 8. Experimental parameters r and K_{gs} for systems of nitrogen and carbon dioxide, coal A and coal B.

Coal Type	Nitrogen (N_2)		Carbon Dioxide (CO_2)	
	r	K_{gs}	r	K_{gs}
A	2.60	4.0×10^{-07}	0.095	1.00×10^{-06}
B	3.1	9.0×10^{-07}	0.120	4.50×10^{-06}

Figures 6.20 and 6.22 show the relationship between the theoretical maximum adsorbed volume (V_m) and the coal particle size for nitrogen-coal A and carbon dioxide-coal B systems at a semi-logarithmic plot respectively. As can be seen V_m has a logarithmic relationship with the coal particle size. The obtained R^2 value for each straight line improves as pressure increases.

Figures 6.21 and 6.22 show plots of the D-R coefficient value and the coal particle size for nitrogen-coal A and carbon dioxide-coal B systems in a Cartesian scale for three pressure levels. As can be seen the coefficient D has a linear relationship with the coal grain size. As pressure and particle size increase the value of D increases correspondingly.

Figures 6.24 and 6.26 show the relationship between V_m and the system pressure for both nitrogen-coal B and carbon dioxide-coal B systems at three different coal particle sizes, respectively. The value of V_m increases as the system

pressure increases. It is because the coal adsorbs more gas as pressure increases and hence the maximum theoretical adsorbed volume increases correspondingly.

Figures 6.25 and 6.27 show plots of the D-R coefficient value and the system pressure for nitrogen-coal A and carbon dioxide-coal B in a Cartesian scale for three different coal particle sizes, respectively. The D-R coefficient (D) value exhibits a linear relationship with the system pressure. The value of D increases as the system pressure increases.

The obtained empirical relationships for V_m and D relationships between the coal particle sizes and the system pressure confirm the previous results obtained from the literature data for the single-component gas adsorption on coal. The next step is to test the validity of the obtained empirical relationships for the multi-component gas adsorption on coal.

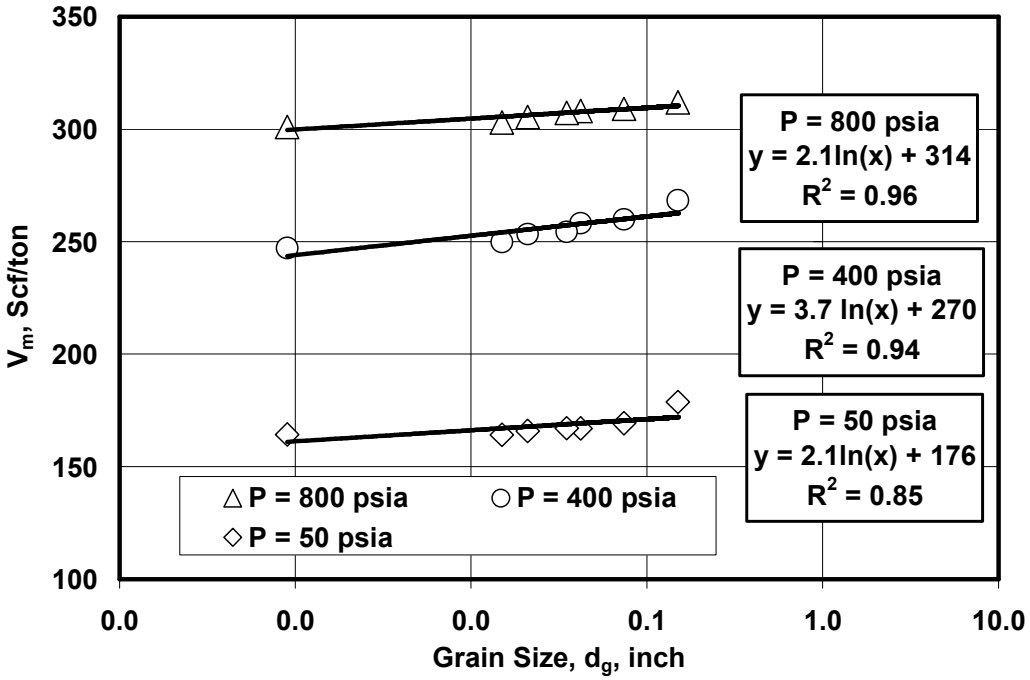

Figure 6. 20. The estimated V_m values versus the average grain size for the system of N_2-Coal A and various pressure levels (logarithmic relationship between V_m and grain size, d_g)

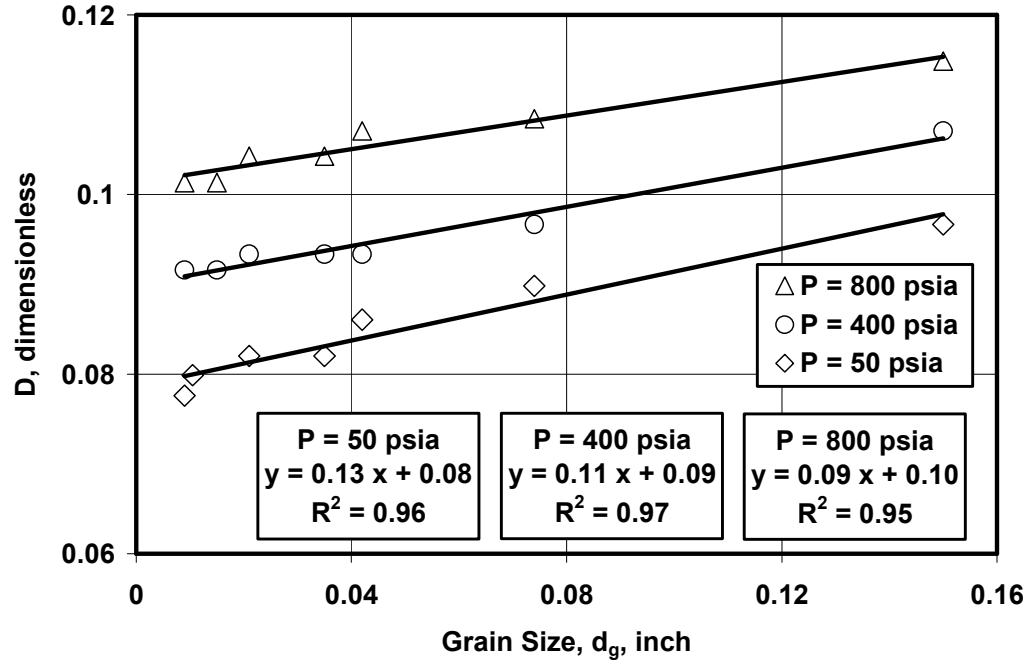

Figure 6. 21. The estimated D values versus the average grain size for the system of N_2-Coal A and various pressure levels (linear relationship between D and grain size, d_g)

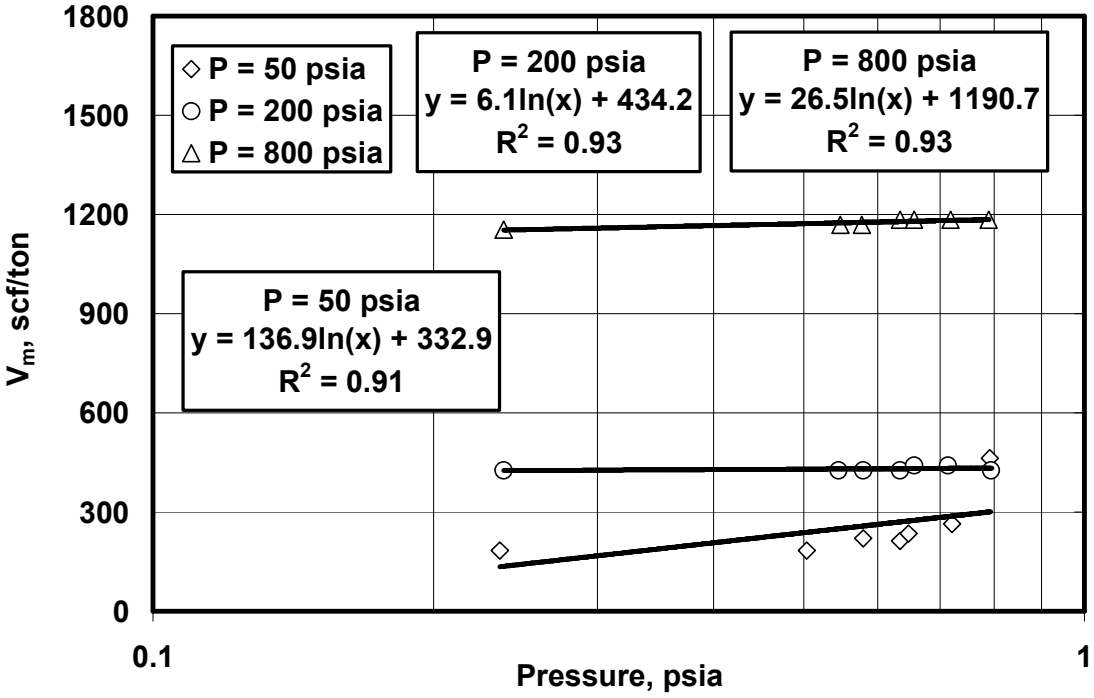

Figure 6. 22. The estimated V_m values versus the average grain size for the system of CO_2-Coal A and various pressure levels.

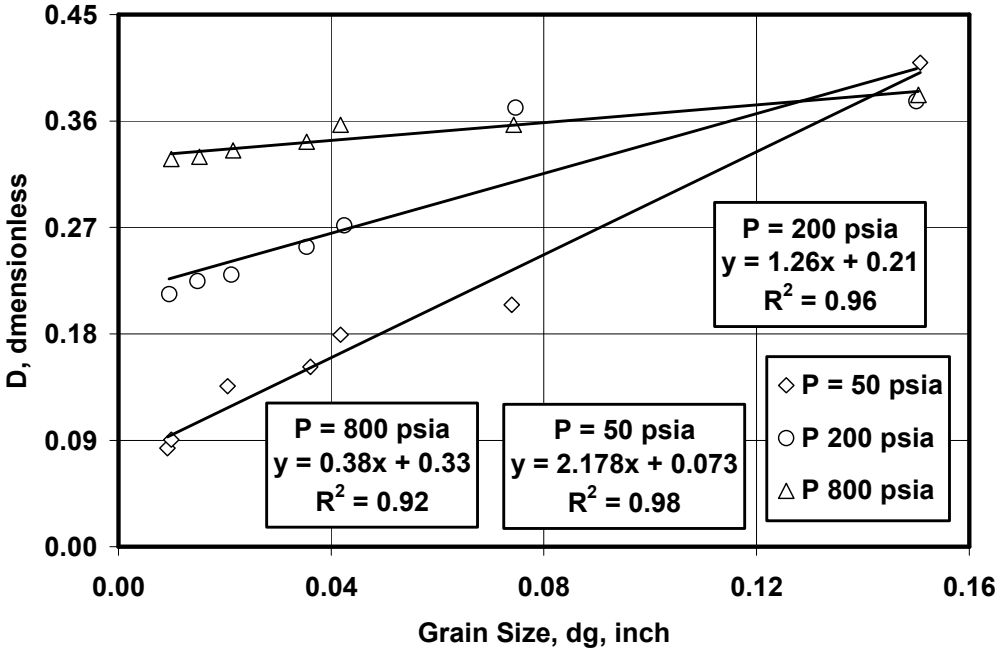

Figure 6. 23. The estimated D values versus the average grain size for the system of CO_2-Coal A and various pressure levels.

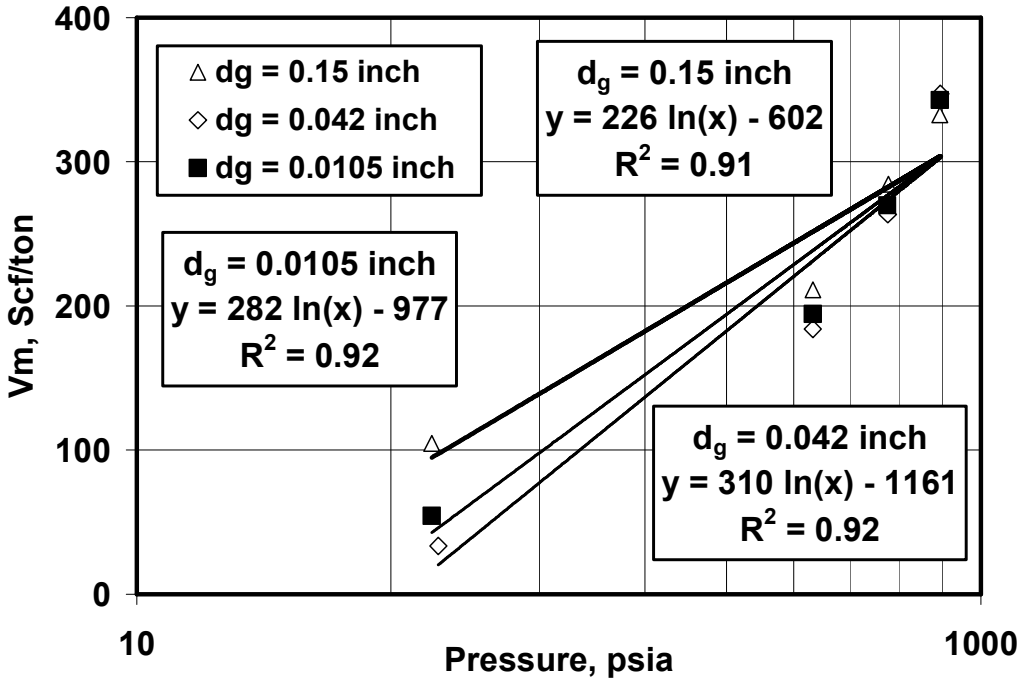

Figure 6. 24. The estimated V_m values versus the system pressure for the system of N_2-Coal B and various pressure levels.

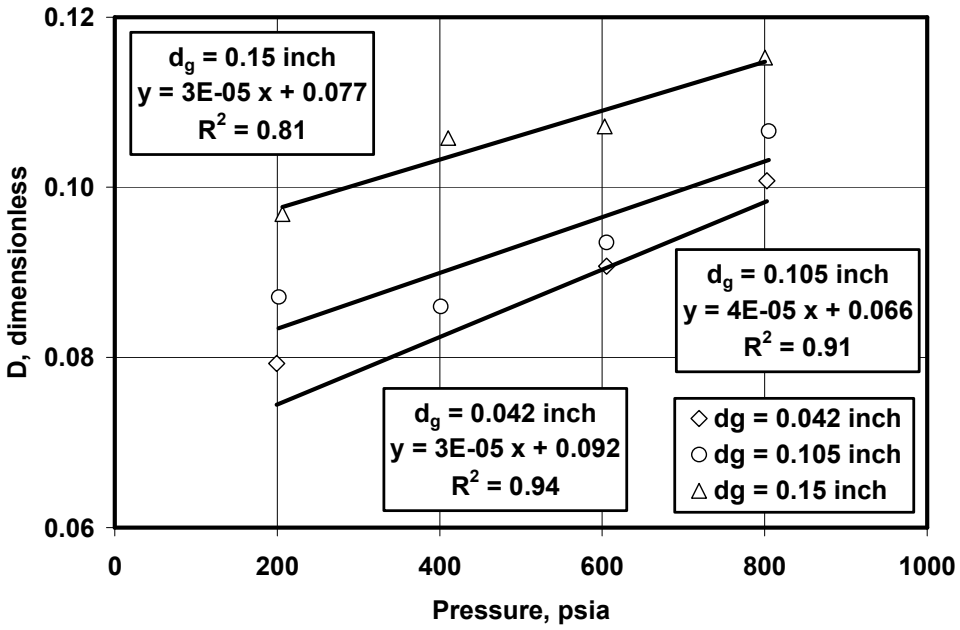

Figure 6. 25. The estimated D values versus the system pressure for the system of N_2-Coal B and various pressure levels.

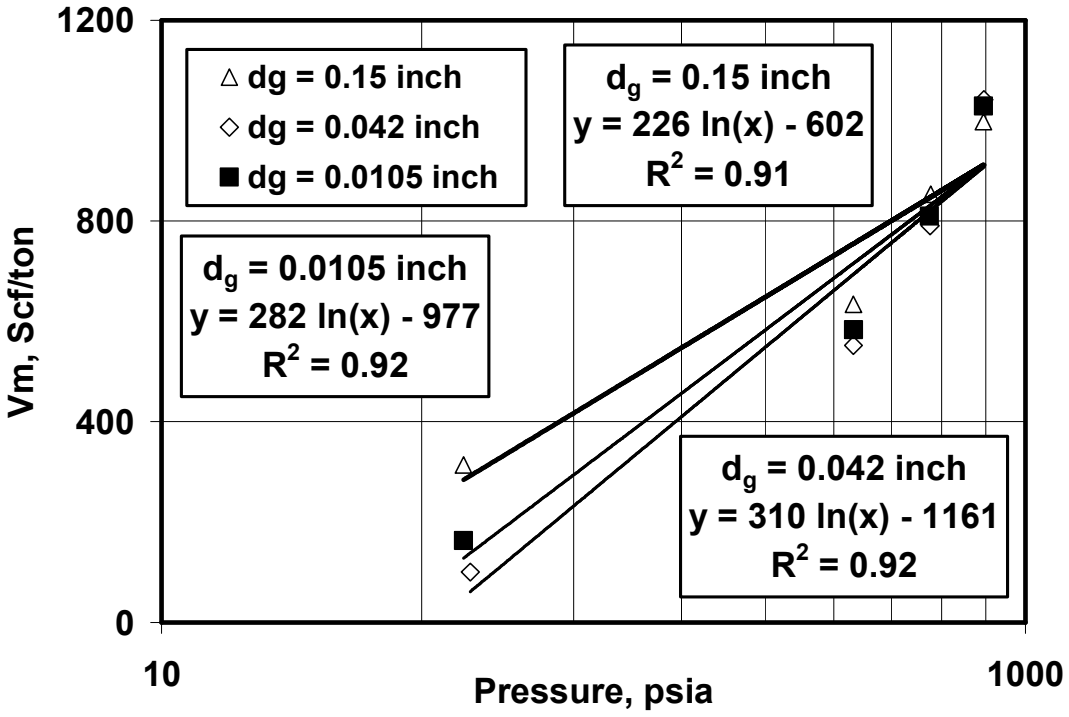

Figure 6. 26. The estimated V_m values versus the system pressure for the system of CO_2-Coal B and various pressure levels.

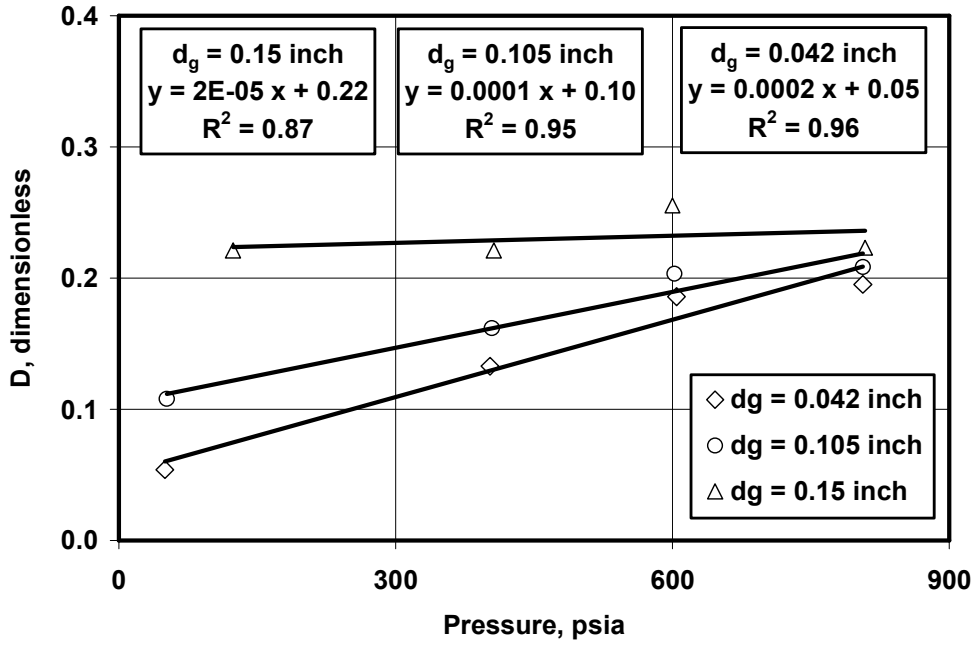

Figure 6. 27. The estimated D values versus the system pressure for the system of CO_2-Coal B and various pressure levels.

Coal-Water-Single Component Gas Isotherms

It was explained in Chapter 4 that to conduct the coal-water-single component gas adsorption experiments 40 cc water is added to 100 gram coal inside the PVT cell. The cell is pressurized by N_2 or CO_2 gas to the specified pressure. The system pressure changes as a function of time due to the interactions among the phases and components.

The process of obtaining gas-water, water-coal, and gas-coal non-equilibrium and equilibrium isotherms from the measured pressure versus time values is explained through an example is Appendix 4.3. Figures 6.28 and 6.29 show the calculated adsorbed nitrogen and carbon dioxide volumes on coal versus the adsorption time for the average grain size of 0.15 inch at five different pressure levels, respectively. As can be seen the adsorbed volume of both gases increases by increasing the pressure. The adsorbed volume of carbon dioxide in coal is preferentially 3-6 times higher than the carbon dioxide.

Comparing the calculated adsorbed volume of carbon dioxide in this case (three-phase) with the previous case (two-phase) reveals that the presence of water in the system reduces the gas adsorption. For instance, for the system of CO_2-coal at 193 psia and 301.3 K the adsorbed gas reduces from 60 scf/ton to 43.4 scf/ton for the system of CO_2-coal-water at 193 psia and 301.3 K. This shows approximately 30% reduction in the CO_2 volume adsorbed by coal. The main reason is that some of the adsorption sites are covered with water at the initial condition. Some gas may directly contact with the coal and some other parts are in contact with water.

Therefore, some gas diffuses through water and adsorbs on the coal and some other adsorbs directly on the coal surface.

The amount of the initial water added to the system may affect the adsorption capacity of the coal. However, in this study, only one ratio of coal to water (100gm/40cc) is used. Further investigations may be necessary to evaluate the effects of this ratio on coal gas and water adsorption results. Repeating the same procedure for each time step and also various pressure levels, the non-equilibrium and equilibrium isotherms for water, nitrogen, and carbon dioxide for various coal particle sizes are obtained.

Figure 6.30 and 6.31 show the calculated adsorbed coal water content (wt %) versus the adsorption time at various pressure levels and average grain size of 0.15 inch. As can be seen, the coal water content increases as the system pressure increases. However, the coal is almost saturated with water and does not adsorb water at approximately 400 psia any more. Practically, at 400 psia the bigger coal internal macropores are either filled or plugged with water. This pressure is called the water saturation pressure and the corresponding water content of the coal at the saturation pressure is called the saturation water content. These values can be obtained for various systems and depending on the coal type, and the system gas components may be different for different adsorption systems.

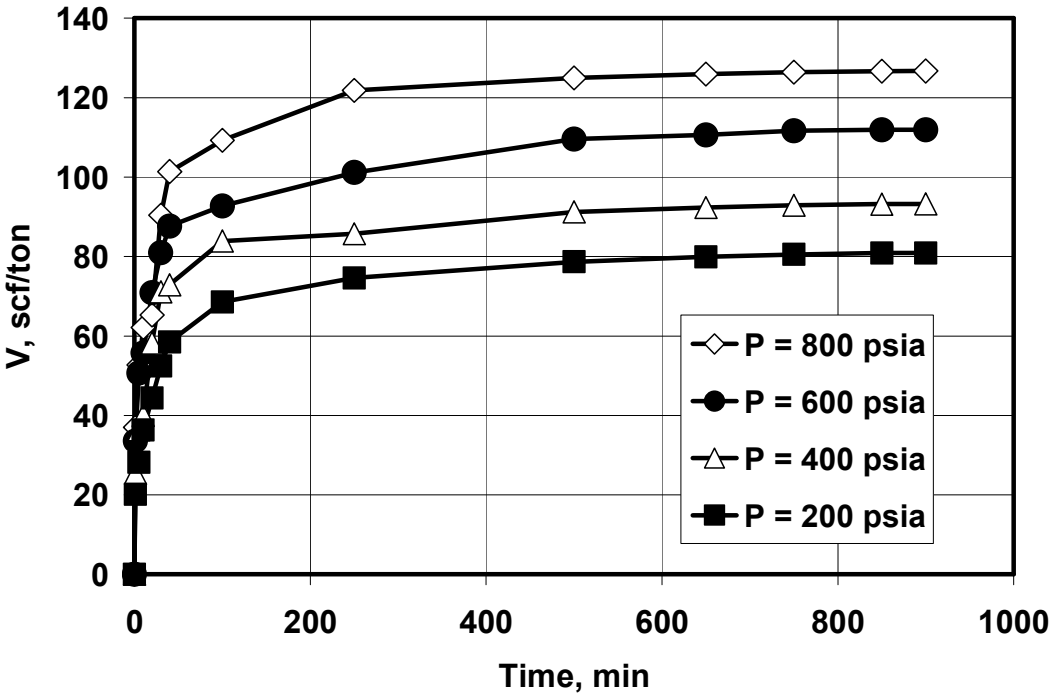

Figure 6. 28. Adsorbed volume of nitrogen in coal A versus the adsorption time from the system of water- N_2-coal (d_g = 0.15 inch).

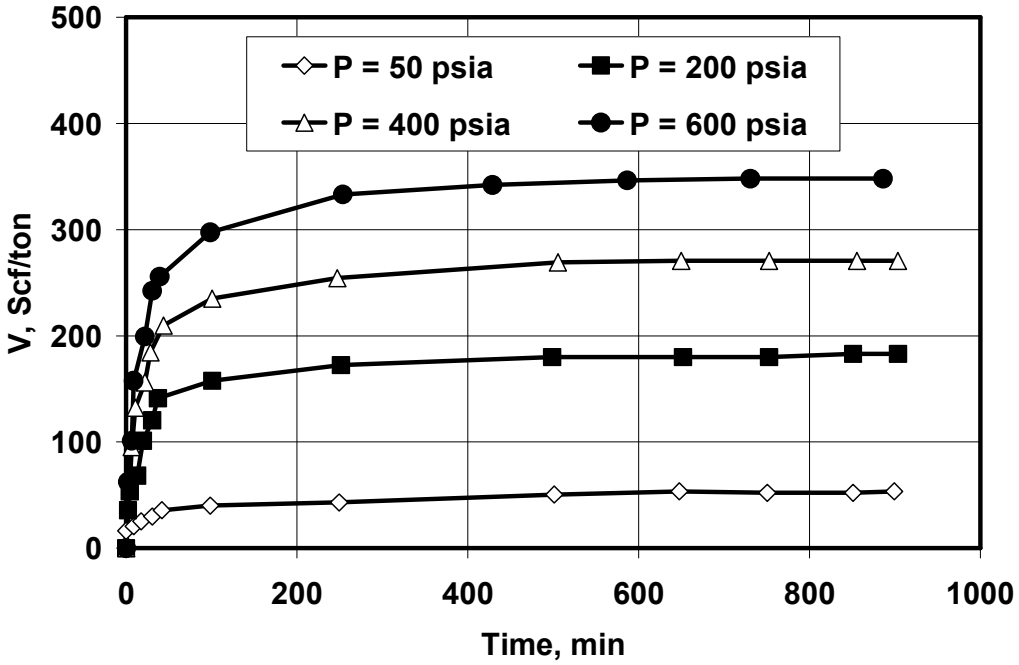

Figure 6. 29. Adsorbed volume of the carbon dioxide gas in coal A versus the adsorption time for the system of water-CO_2-coal (d_g = 0.15 inch).

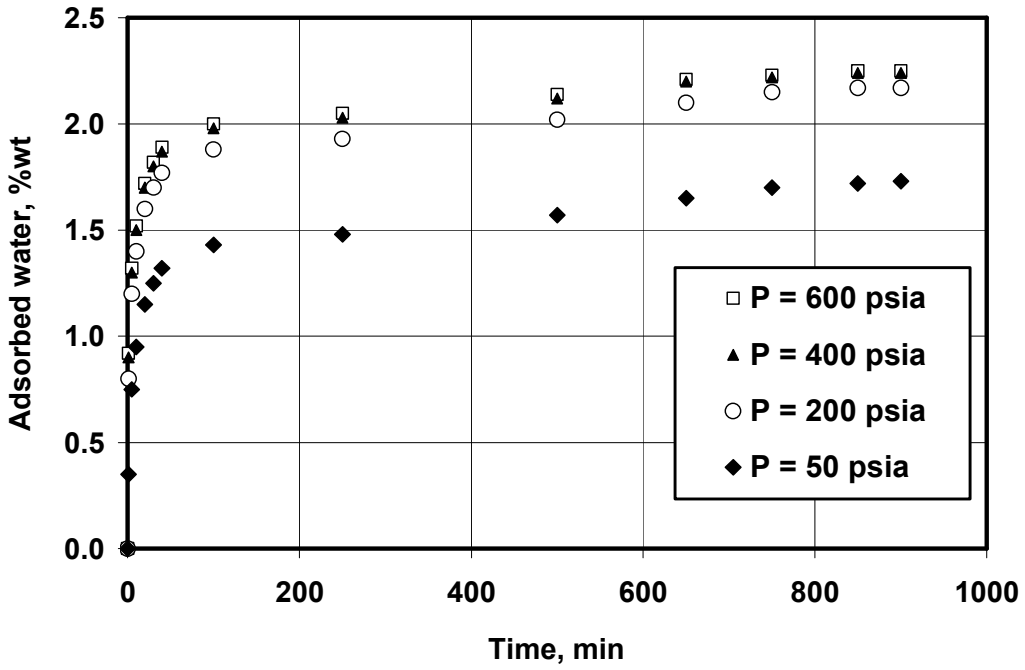

Figure 6. 30. Adsorbed wt% of water in coal A versus the adsorption time for the system of CO_2-water-coal ($d_g = 0.15$).

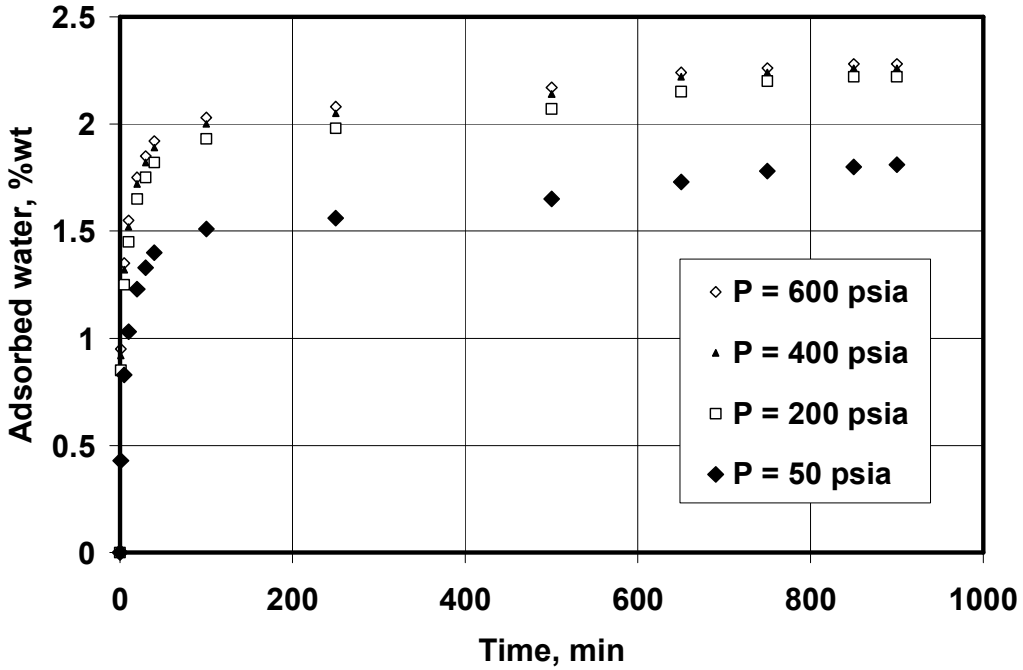

Figure 6. 31. Adsorbed wt% of water in coal A versus the adsorption time for the system of N_2-water-coal A ($d_g = 0.15$).

The similar plots are obtained for other grain sizes. To fit the parameters of the non-equilibrium isotherm, the following form of the multi-component non-equilibrium isotherm (Equation 5.76) is used.

$$\ln V_{G_i c} = \ln V_{mG_i c} - \left\{ - D_{g_i} \ln \left[\frac{P_e \vec{y}_{G_i c}}{\hat{P}_{G_i co}} \tanh\left(2 P_e \vec{y}_{G_i c} \hat{K}_{gs_i} t\right) \right] \right\}^{r_{G_i}} \quad \text{.....(6.14)}$$

where the mole fraction of the adsorbed phases in coal ($\vec{y}_{G_i c}$) is defined as:

$$\vec{y}_{G_i c} = \frac{n_{G_i c}}{n_{G_i c} + n_{Wc}} \quad \text{.....(6.15)}$$

The results of evaluation of the obtained data show that the parameters of the obtained non-equilibrium isotherms follow the same trends of the observed in the previous case.

Figures 6.32 and 6.33 indicate that the D-R coefficient has linear relationship with the grain size and pressure and the D-R maximum theoretical adsorbed volume, V_m, has logarithmic relationship with coal particle grain size and pressure levels. The liquid-like adsorbed fluid fugacity coefficients are also obtained for various cases. This value is independent of the coal particle size and increases linearly with pressure. The following figures indicate these relationships for both nitrogen and carbon dioxide non-equilibrium isotherms.

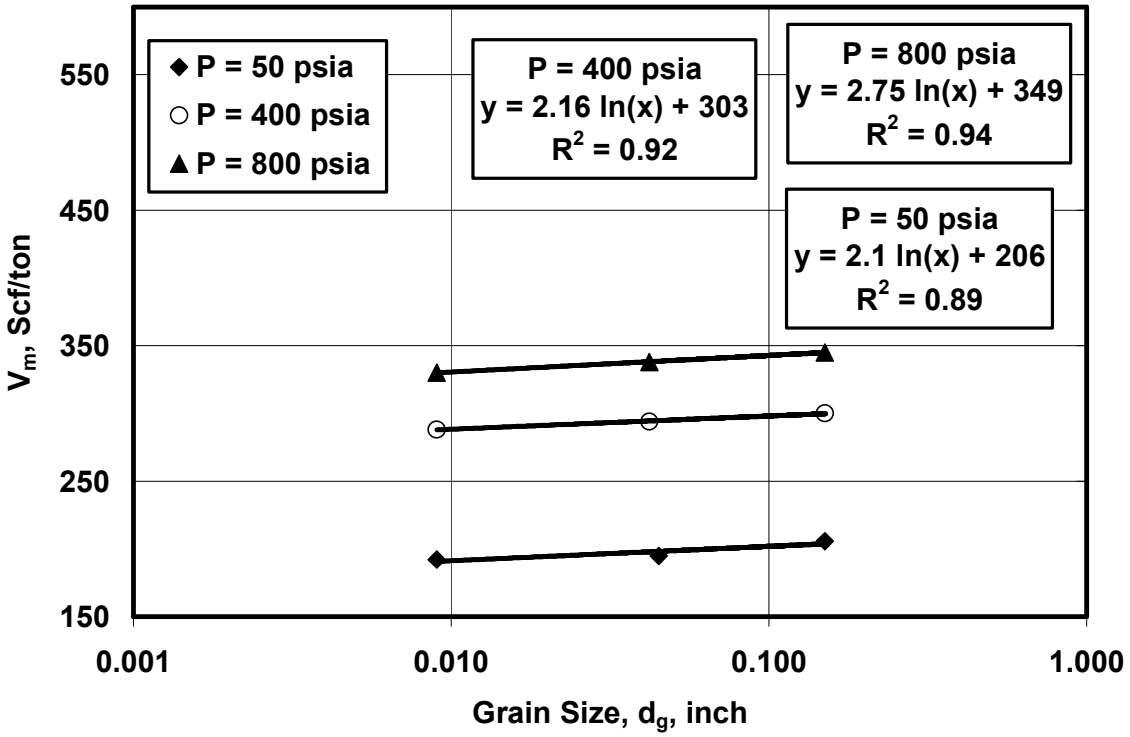

Figure 6. 32. The estimated V_m values versus the average coal grain sizes for the system of N_2-Water-Coal A and various pressure levels.

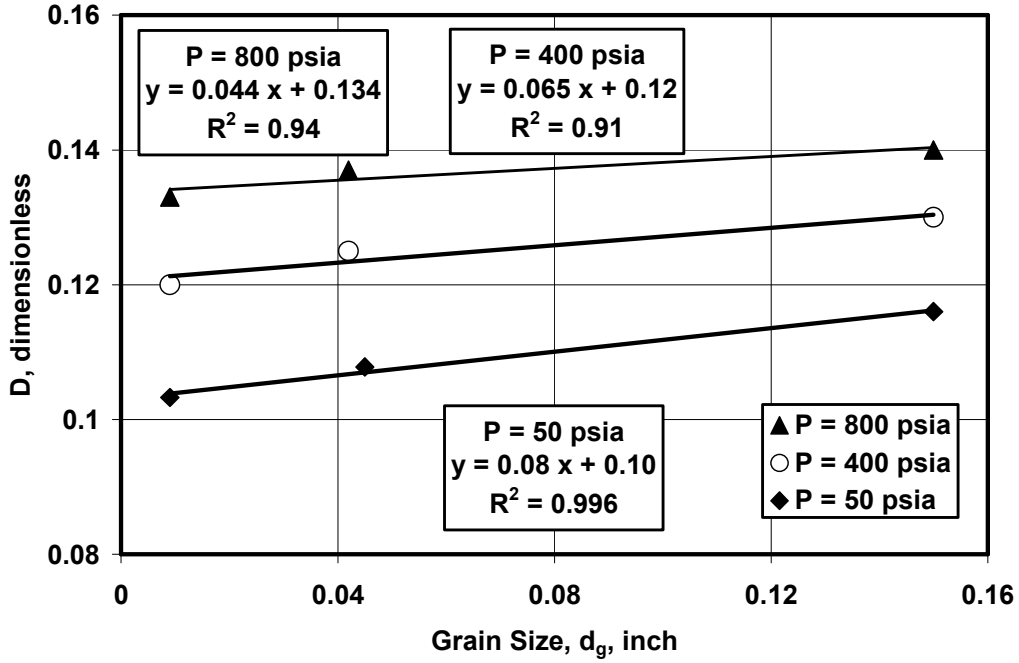

Figure 6. 33. The estimated D values versus the average coal grain sizes for the system of N_2-Water-Coal A and various pressure levels.

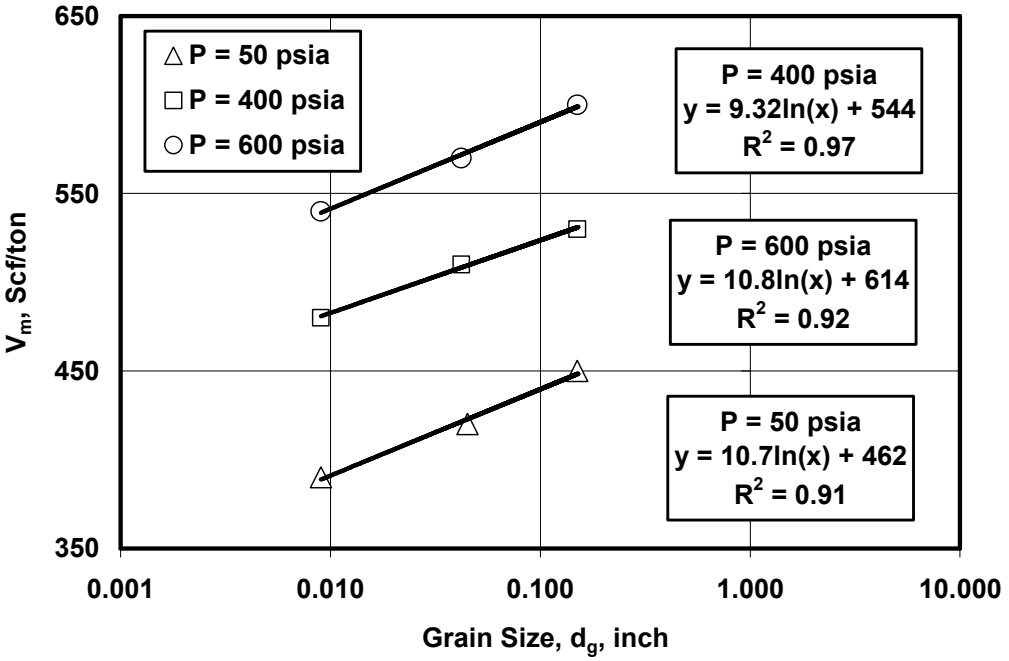

Figure 6. 34. The estimated V_m values versus the average coal grain sizes for the system of CO_2-Water-Coal A and various pressure levels.

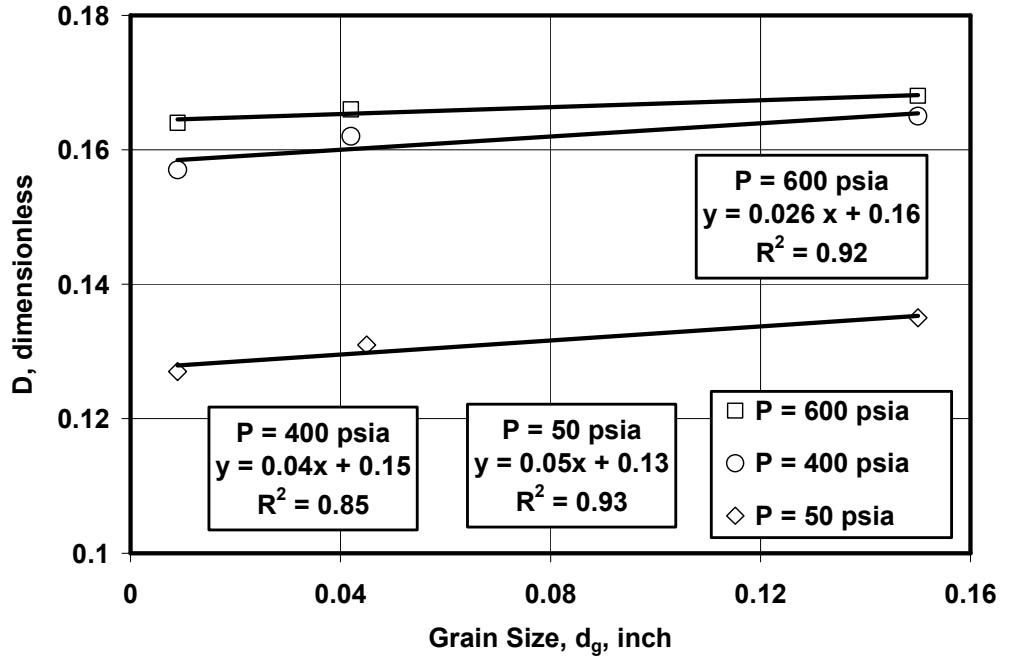

Figure 6. 35. The estimated D values versus the average coal grain sizes for the system of CO_2-Water-Coal A and various pressure levels.

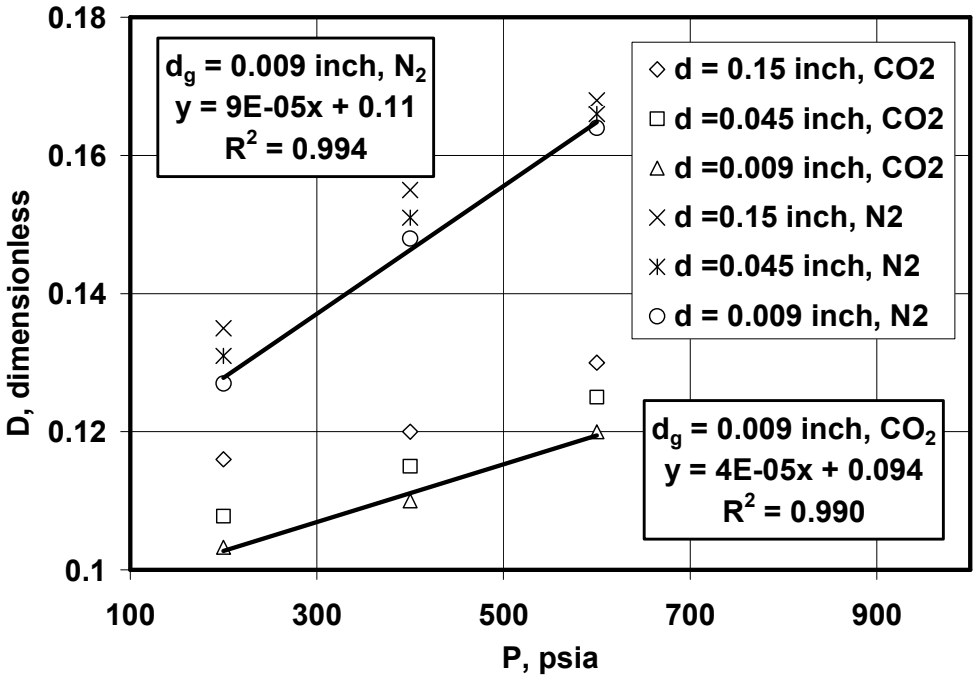

Figure 6. 36. The estimated D values versus the adsorption pressure for N_2-water-coal A and CO_2-Water-Coal B systems.

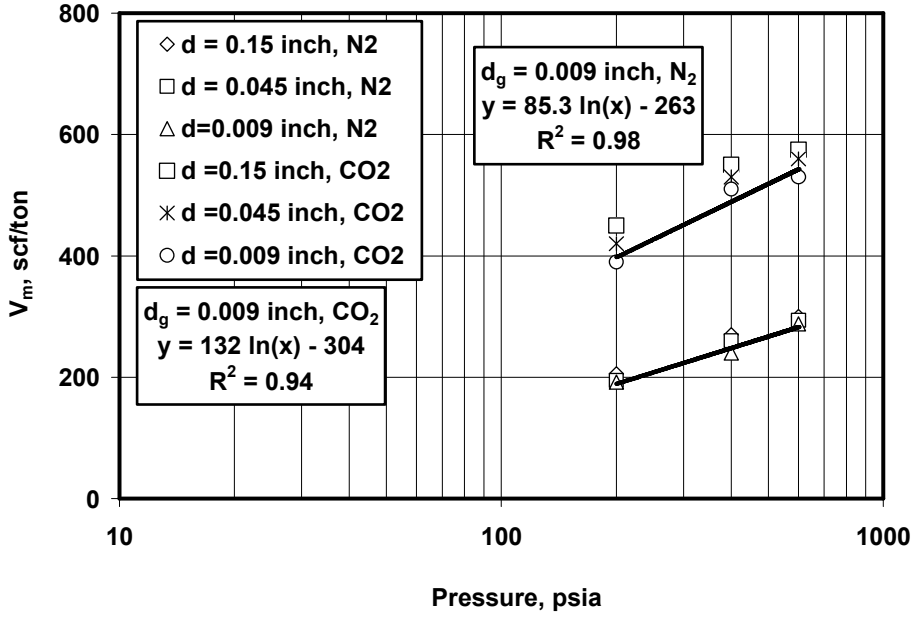

Figure 6. 37. The estimated V_m values versus the adsorption pressure for N_2-water-coal A and CO_2-Water-Coal B systems.

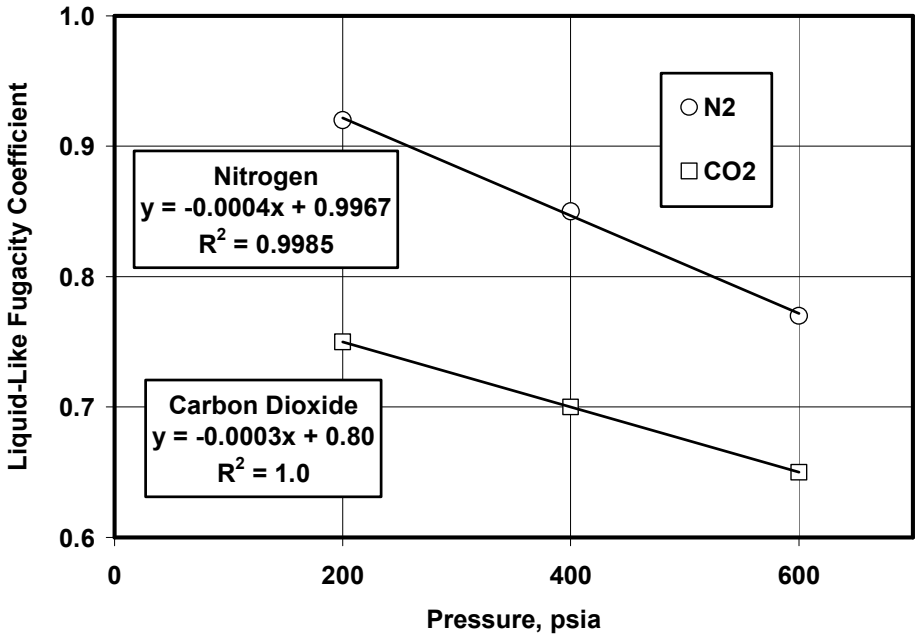

Figure 6. 38. Liquid-like fugacity coefficient values for nitrogen and carbon dioxide versus pressure.

The similar procedure is applied for the kinetics of water adsorption in coal. For the adsorbed water in coal the following equation is applied.

$$\ln W_{W_c} = \ln W_{mWc} - \left\{ - D_W \ln\left[\frac{P_e \vec{y}_{Wc}}{\hat{P}_{Wco}} \tanh\left(2 P_e \vec{y}_{Wc} \hat{K}_{gs_i} t\right) \right] \right\}^{r_W} \quad \text{.....(6.16)}$$

where W_{Wc} represents the weight percentage of the adsorbed water in coal. W_{mWc} is the theoretical maximum weight percentage of the adsorbed water in coal. The obtained parameters show similar trends. These parameters are plotted versus grain sizes and pressures. Figures 6.39 and 6.40 show the relationships between obtained parameters and the coal particle sizes and the applied pressure.

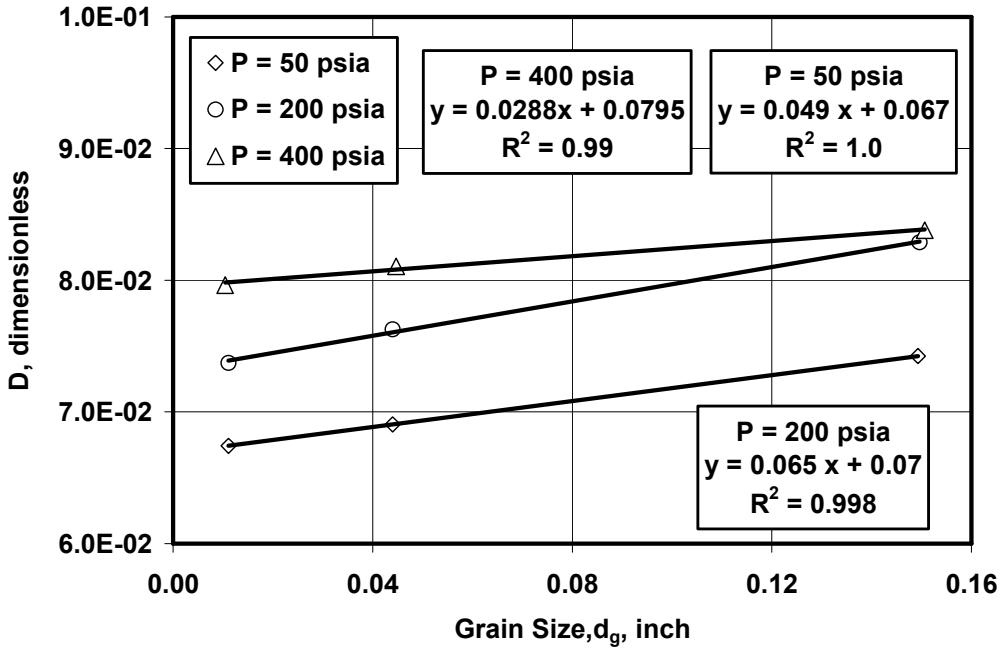

Figure 6. 39. The estimated D values versus the average coal grain sizes for the water component in the system of CO_2-Water-Coal A and various pressure levels.

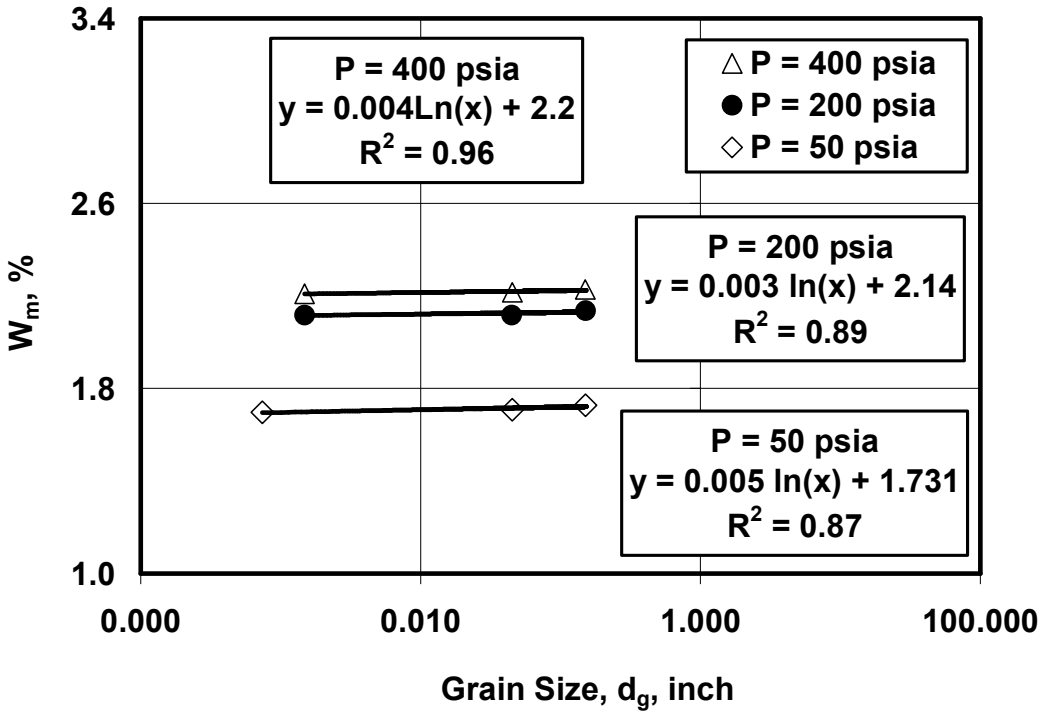

Figure 6. 40. The estimated V_m values versus the adsorption pressure for water component in the system of N_2-water-coal A.

Coal-Water-Multi-Component Gas Isotherms

Various mole fractions of N_2/CO_2 are injected into the PVT cell containing coal and water mixture and coal only in different experiments. The experimental process was previously explained. The total system pressure versus time plots are reported in Chapter 4 for various initial N_2/CO_2 ratios. The data interpretation method is similar to that already presented in the previous cases. The only difference here is that the gas phase is composed of more than one component.

The Extended Non-Equilibrium D-R (ENDR) theory that is already derived and introduced in this study is the only model available in the literature to model the kinetics of the adsorption of multi-component gases in any carbonaceous material and especially coals.

The example given in Appendix 4.4 further explains the application of the ENDR theory in modeling the multi-component gas adsorption in coal. Investigating the obtained values show that injecting mixture of CO_2/N_2 increases CO_2 adsorption on coal. For the case of the example described in Appendix 4.4, the presence of nitrogen increases the carbon dioxide adsorption rate by approximately 1.5%. This is very important in enhanced coalbed methane gas production by CO_2/N_2 injection. This will be discussed in more details in the next chapter. Figure 6.41 shows the relationship between the adsorbed volume of both nitrogen and carbon dioxide versus time for various initial CO_2/N_2 ratio.

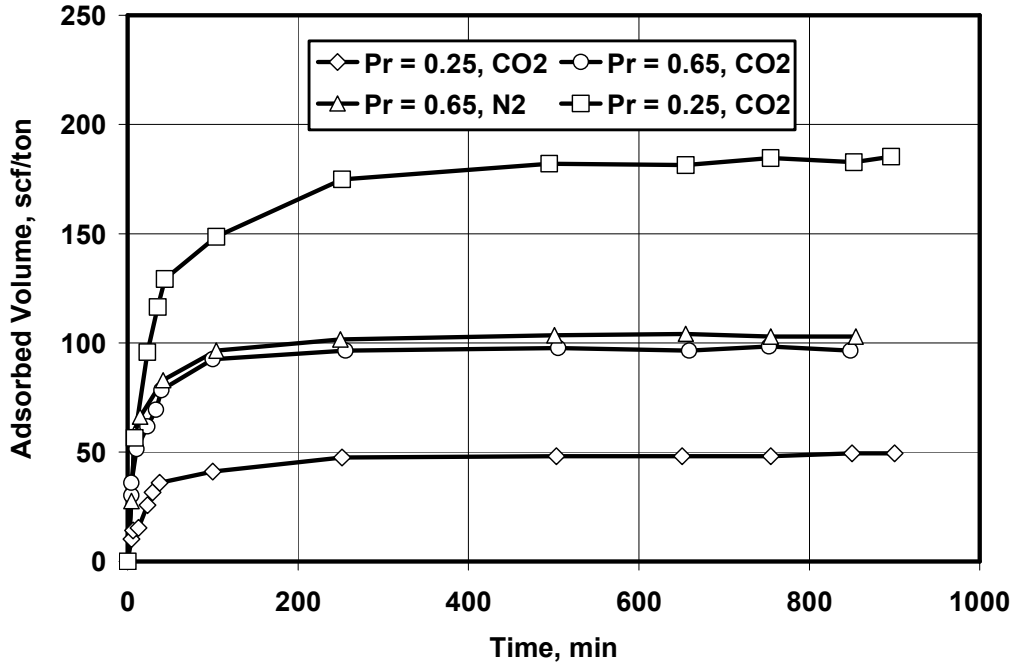

Figure 6. 41. Calculated adsorbed volume of nitrogen and carbon dioxide versus time for the system of CO_2/N_2 mixture adsorption in coal A at two different P_r values and P_{tin} = 200 psia.

The process described in Appendix 4.4 is repeated for other initial pressure levels. The non-equilibrium isotherms are fitted using Equation 6.14. The obtained parameters of the multi-component non-equilibrium isotherm have similar relationship with the initial pressure as previously explained.

The last series of the experiments are the non-equilibrium multi-component and three-phase adsorption on coal. The data interpretation process is similar to the previous cases. Therefore, the calculation details are not included here.

Rapid Determination of the Isotherms from Non-Equilibrium Adsorption Data with and without water Present

1. Without the presence of water

In general, the equilibrium isotherms expressing the amount of the adsorbed gas present in coal at various pressures are used to estimate the gas reserves and predict the gas production rate. An equilibrium isotherm is constructed by measuring several equilibrium data points at a constant temperature. This approach requires a long time, in the order of several days to weeks.

The volumetric method is the most popular technique in the coalbed methane industry. Typically seven to ten measurements at different pressures are needed to construct an isotherm using this technique. Sufficient time has to be allowed for each data points of the system to achieve equilibrium after each pressure reduction. Then, an appropriate isotherm is fitted to the data points. However, the constructed isotherm is based on the equilibrium measurements and does not represent the intermediate non-equilibrium conditions required for prediction of the gas production rates in actual coalbed/shale gas production. Thus, a rapid interpretation method is introduced to reduce the time required to construct the isotherms using the non-equilibrium sorption data points and applying the non-equilibrium isotherm developed in this study.

The general form of the multi-component non-equilibrium isotherm is given as:

$$\ln V_{G_i c} = G_{V_{mG_{ic}}}\left(d, \hat{f}_{G_i c}\right) - \left\{ - G_{D_{g_i}}\left(\hat{f}_{G_i c}, d_g\right) \ln\left[\frac{P_e \vec{y}_{G_i c}}{\hat{P}_{G_i co}} t \tanh\left(2 P_e \vec{y}_{G_i c} \hat{K}_{gs_i}\right) \right] \right\}^{r_{g_i}} \quad \text{.....(6.17)}$$

By examining several literature data and our experimental data sets, it was previously demonstrated that G_{Vm} and G_D are functions presenting the dependency

of the V_m and D parameters on the gas component fugacity and also coal particle grain size distribution. It was also obtained that the G_{Vm} has logarithmic relationship with pressure and grain size and G_D has linear relationship with pressure and grain size. Therefore, the following relationships are applied for various terms in Equation 6.17 for high pressure ranges (pressures more than 150 psia):

$$G_{V_{mi}} = a_{V_{mi},d} + \ln\left(b_{V_{mi},d} d_g\right) \quad \text{at a fixed pressure} \quad (6.18)$$

$$G_{V_{mi}} = a_{V_{mi},\hat{f}_{Gic}} + \ln\left(b_{V_{mi},\hat{f}_{Gic}} \hat{f}_{G_i c}\right) \quad \text{at a fixed coal particle size} \quad (6.19)$$

$$G_{D_{G_i}} = a_{D_{Gi},d} + b_{D_{Gic}} d_g \quad \text{at a fixed pressure} \quad (6.20)$$

$$G_{D_{Gi}} = a_{D_{Gi},\hat{f}_{Gic}} + b_{D_{Gic},\hat{f}_{Gic}} \hat{f}_{G_i c} \quad \text{at a fixed coal particle size} \quad (6.21)$$

$$\hat{K}_{ga_i} = K_{ga_i} \phi_{ga_i} \quad (6.22)$$

$$\hat{P}_{G_i co} = \frac{P_{G_i co}}{\phi_{ga_i}} \quad (6.23)$$

where ϕ_{ga_i} is the fugacity coefficient of the liquid-like adsorbed phase. This value is independent of the coal particle grain size and has a linear relationship with the system total pressure described as:

$$\phi_{ga_i} = a_{\phi_i} + b_{\phi_i} P \quad (6.24)$$

The non-equilibrium isotherm (Equation 6.17) can be constructed according to Equations 6.18-6.24 for pressures more than 150 psia if only two non-equilibrium data isotherms at two different pressure levels are determined. For low pressure ranges (less than 150 psia), only one non-equilibrium isotherm at one

pressure level is required. Because the isotherm (Equation 6.17) parameters do not change with pressure at low pressure ranges.

To demonstrate the applicability of the non-equilibrium isotherm (Equation 6.17) to significantly reduce the time required to construct both equilibrium and non-equilibrium isotherms several scenarios are presented for different reported literature and in-house experimental data for various gaseous and carbonaceous.

Case 1. Propane and propylene adsorption on Chemviron LAC and Westvaco BAX activated carbon at low pressures

The first scenario considers the reported data by Mofarahi et al. (2003) for adsorption of propane and propylene on two types of activated carbons at very low pressure ranges. Figure 6.42 shows a set of measured non-equilibrium adsorption data points for adsorption of propane and propylene on commercial activated carbons (Mofarahi et al., 2003). The present computer code uses one set of the non-equilibrium isotherm at 0.14 psia, and regenerates the equilibrium adsorption isotherms for each component. Figure 6.43 exhibits the comparison between measured and predicted isotherms. As can be seen, the average error is less than 2%.

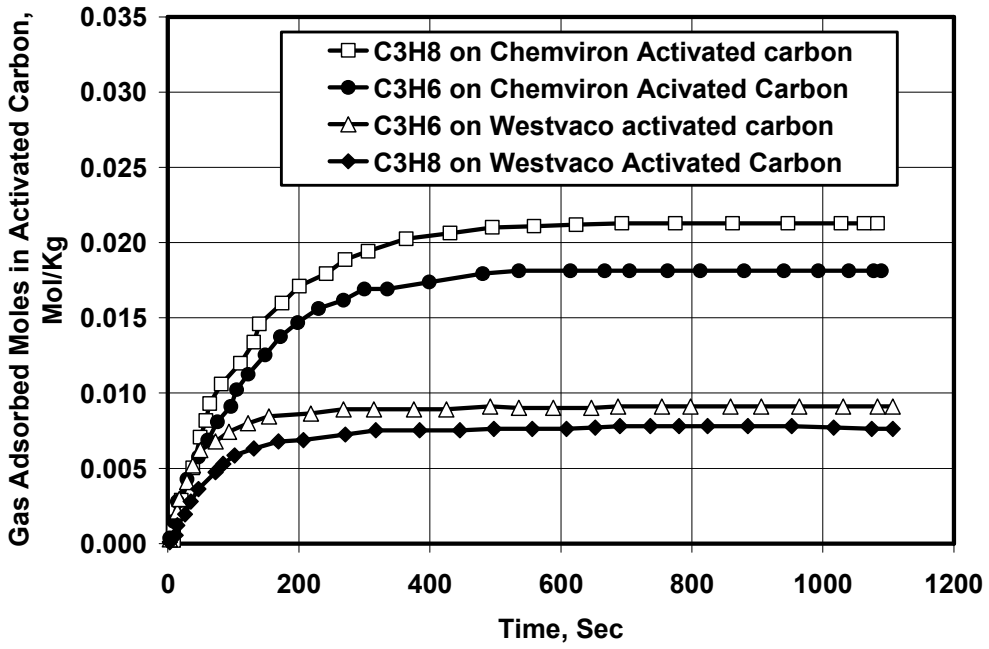

Figure 6. 42. Propane and propylene adsorbed volume in Chemviron LAC and Westvaco activated carbon versus the adsorption time at 0.14 psia (Mofarahi et al., 2003).

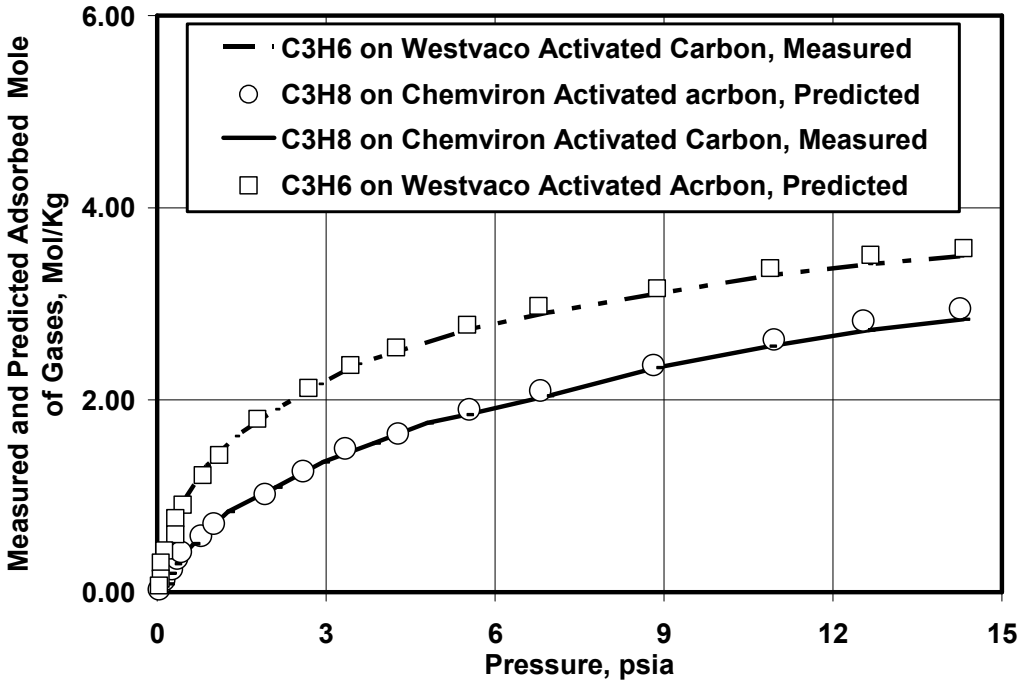

Figure 6. 43. Propylene adsorbed volume in Chemviron LAC and Westvaco activated carbon versus the system pressure (Mofarahi et al., 2003).

Case 2. Pure methane adsorption on carbon molecular sieves

The second scenario deals with the methane and other gas adsorption data on carbon molecular sieves, reported in the literature (Vyas, et al., 1994). Figure 6.44 shows the equilibrium adsorption isotherms for various gases in the carbon molecular sieve surface. Figure 6.45 exhibits a set of the non-equilibrium adsorption data points for the same gas and molecular sieve system at pressure of 2.32 psia.

Following the curve fitting procedure explained in Chapter 3, the equilibrium and non-equilibrium isotherm parameters are determined for each gas component. Table 6.15 summarizes the model parameters obtained by the curve fitting procedure. Figure 6.46 shows a plot of Equation 5.76 required to predict the mentioned parameters for methane. Similarly, the same set of plots can be developed for other gases. This figure is constructed for different values of r in a fixed value of K_{gs}. To determine the value of r we take into account that this value is usually between 0.1-4.0 for adsorption of different gases on carbonaceous materials. Therefore, the best value of r in this range that results in a better straight line fit (higher R^2 value) can be obtained by the least-square curve fitting method. To improve the value of R^2, parameter K_{gs} is varied until the best possible fit is obtained for the reported data. The slope of the straight line is equal to D^r that is used to estimate the value of D. The intercept is equal to $ln\ V_m$ that is used to estimate the value of V_m.

Now that the non-equilibrium isotherm is established, the corresponding equilibrium isotherm can also be established by substituting the obtained

parameters in Equation 5.1. Figure 5.47 shows the measured and predicted non-equilibrium methane adsorption isotherms in the carbon molecular sieves at different pressure levels. The measured non-equilibrium isotherm is given for 2.32 psia. Based on the curve fitting procedure explained above the non-equilibrium isotherm parameters are obtained. These parameters are substituted in the equilibrium isotherm and used to predict the equilibrium methane adsorbed volumes versus pressure. Figure 6.48 compares the predicted and measured equilibrium data points. According to this figure, the points are very close to each other and the error is less than 4%.

Table 6. 9. Best-estimated non-equilibrium isotherm parameters for various gases (applying non-equilibrium data of Vyas et al., 1994).

Parameter Gas Comp.	r	D	V_m, Scf/ton	A	B
CH_4	0.3	0.025	682	2.60	24.14
C_2H_6	0.3	0.020	906	1.747	10.171
CO_2	1.3	0.017	3719	4.14	5.51
C_3H_8	0.2	0.019	1630	1.21	4.34
N_2	0.2	0.024	7380	4.6	3.23

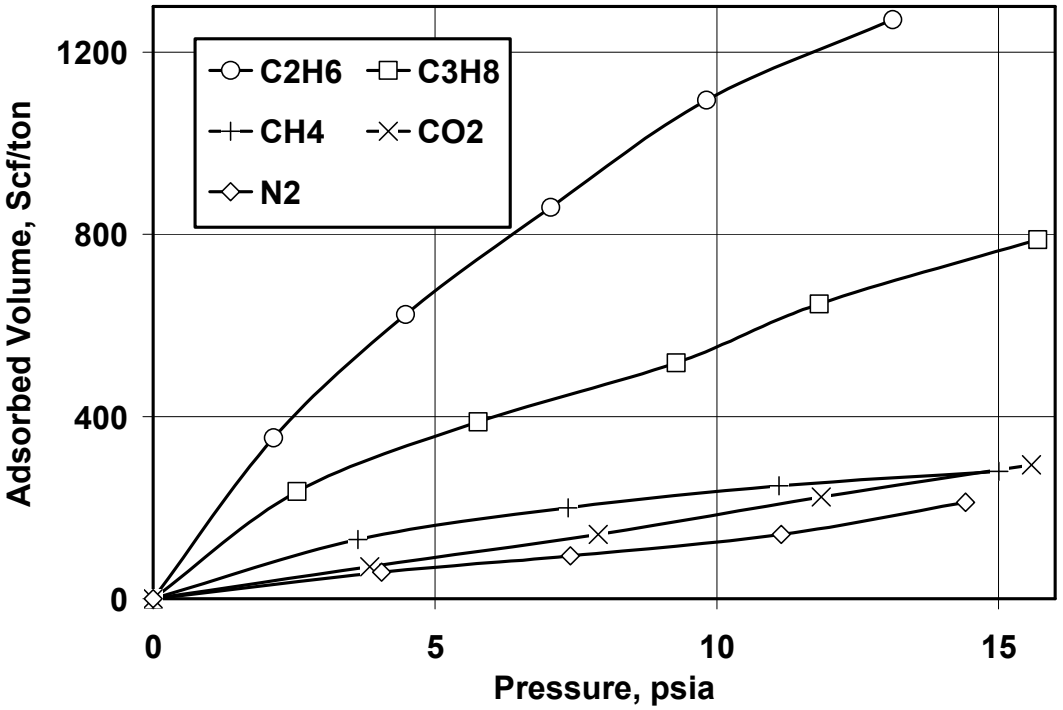

Figure 6. 44. Measured equilibrium adsorbed volume of various gases in the molecular sieve surface versus pressure sorption isotherm of methane (Vyas et al., 1994).

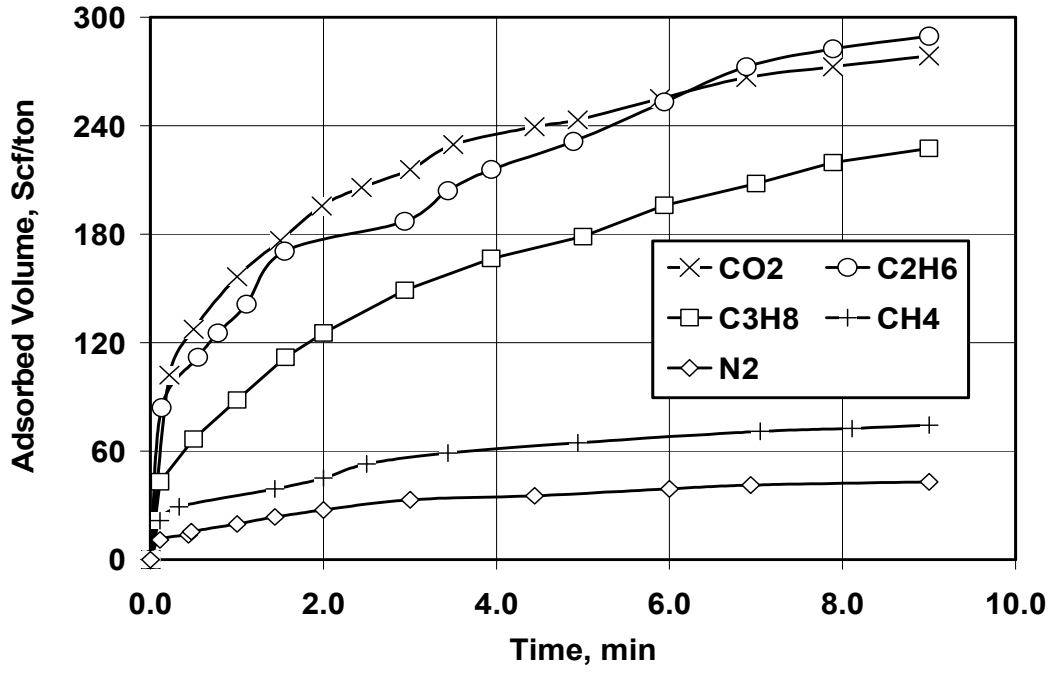

Figure 6. 45. Measured non-equilibrium adsorbed volume of various gases in the molecular sieve surface versus the adsorption time at 2.3 psia (Vyas et al., 1994).

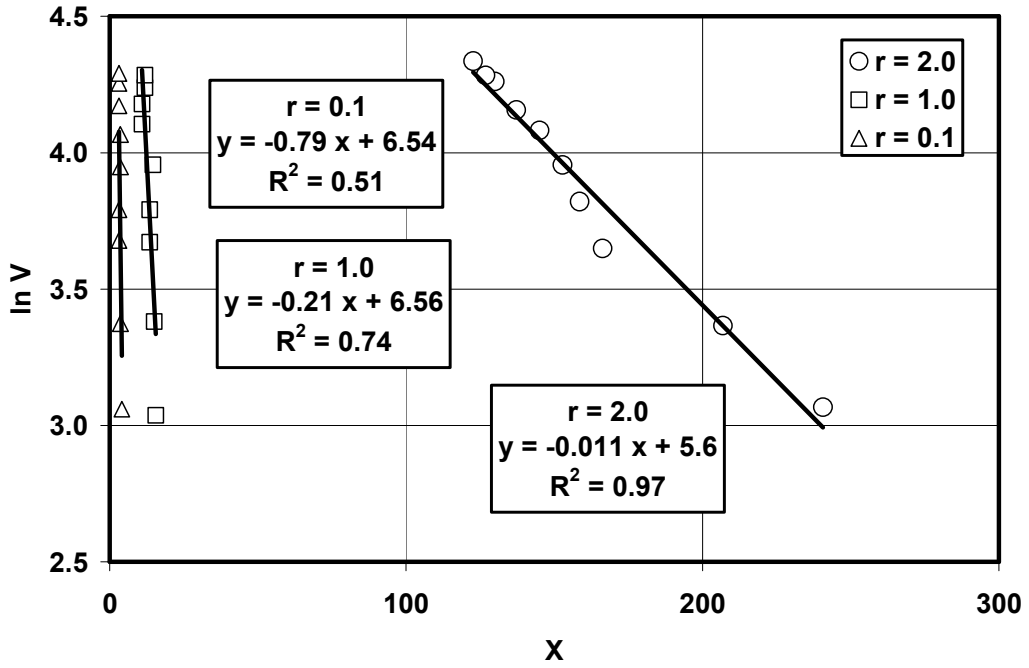

Figure 6. 46. Plot of $\ln V$ versus $X = \left\{ -\ln\left[\frac{P}{P_o} \tanh\left(2PK_{gsi}t\right) \right] \right\}^r$ for three values of r (the maximum R^2 corresponds to r = 2.0) Adsorbed methane volume vs. X explained in step 10.

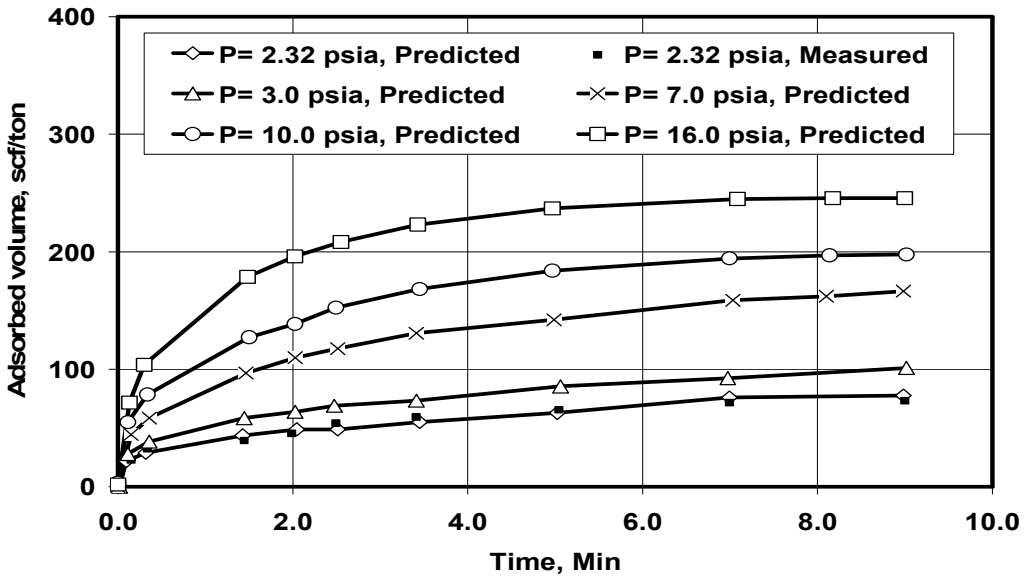

Figure 6. 47. Non-equilibrium adsorbed volume of methane in molecular sieve surface at various pressures, measured adsorption data points at 2.32 psia (Vyas et

al., 1994) and predicted adsorption curves at various pressures non-equilibrium isotherms.

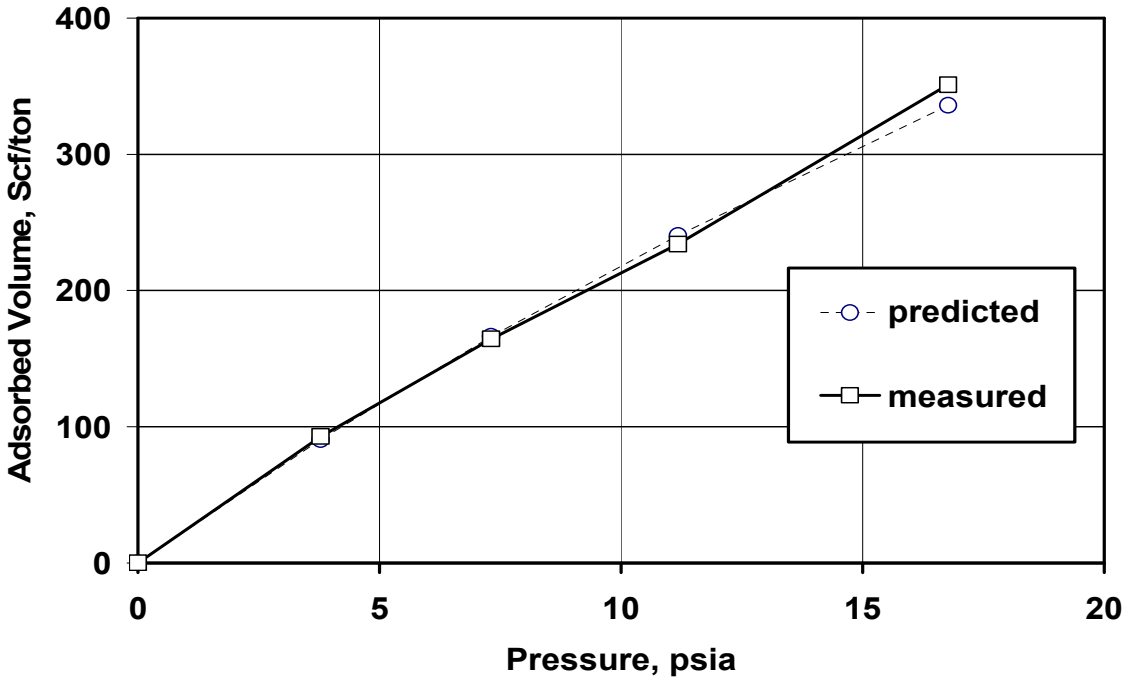

Figure 6. 48. Comparison of the measured and predicted equilibrium data with the estimated values using the non-equilibrium isotherm parameters.

Case 3. Mixture of methane, ethane and carbon dioxide adsorption on carbon molecular sieves.

The gas mixture contains 95% CH_4, 3% CO_2, and 2% C_2H_6. Reported data (Chapoy 2004) for equilibrium and non-equilibrium adsorption of each individual gas are presented in Figures 6.44 and 6.45**.** A volume of 130 cc gas mixtures is injected into a PVT-cell of 160 cc size at the initial condition of 75 $^{\circ}$ F and 14.6 psia.

The developed model enables to construct the equilibrium and non-equilibrium isotherms for various pressures using the estimated parameters reported in Table 6.16 and the compressibility values for various gases (Arnaud et al., 1993). Figures 6.49 and 6.50 show the non-equilibrium isotherms for the projected high

pressures using the reported low-pressure values for carbon dioxide, and ethane, respectively. Figure 6.51 shows the relationship between methane, carbon dioxide, and ethane mole fractions in the gas phase and the gas adsorbed volume on the coal phase. Ethane is adsorbed faster than carbon dioxide and methane.

Figure 6.52 compares the adsorbed mole fraction of each component at different pressures. Even though the adsorption of carbon dioxide on carbon molecular sieves is higher than methane, because the product of activity to mole fraction of methane in the gaseous phase is higher than that of the carbon dioxide, the adsorbed mole fraction of methane is higher than the other components. Figure 6.53 shows the relationship between the amount of adsorbed moles and pressure. The adsorbed moles of methane are significantly higher than carbon dioxide. Moreover, as pressure increases the difference between the adsorbed moles increases.

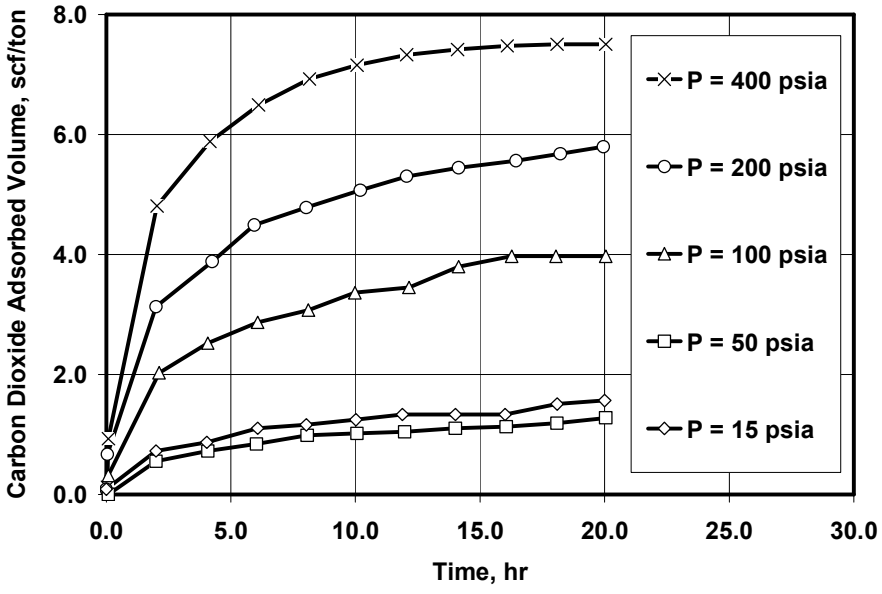

Figure 6. 49. Predicted adsorbed volumes of carbon dioxide in the carbon molecular sieve versus the adsorption time for the higher pressures.

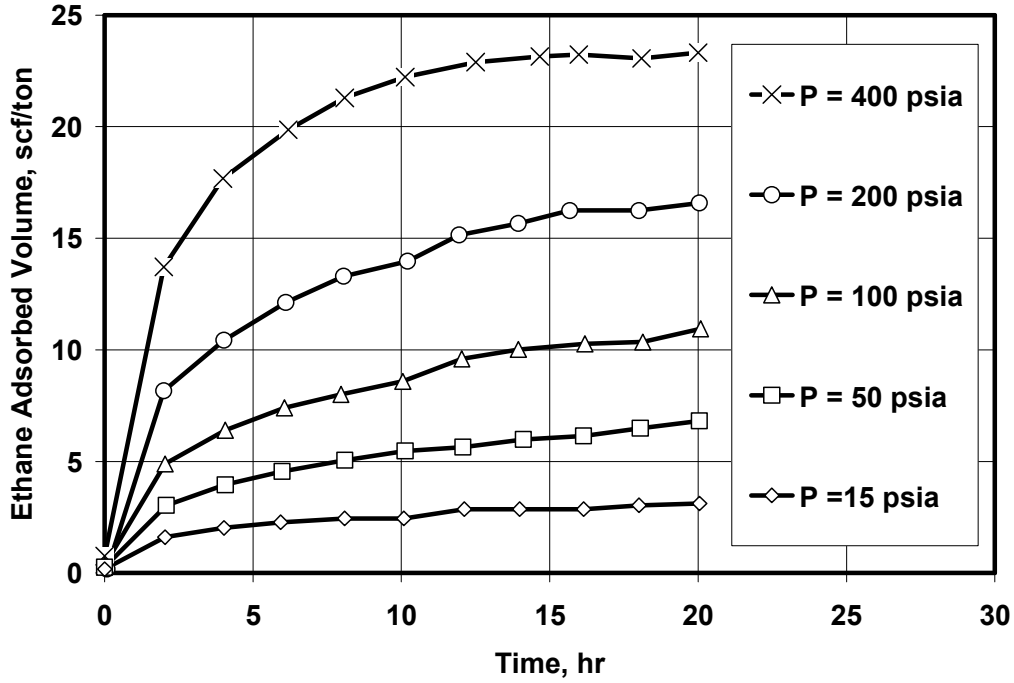

Figure 6. 50. Predicted adsorbed volume of the C_2H_6 in the carbon molecular sieve versus the adsorption time for the higher pressures.

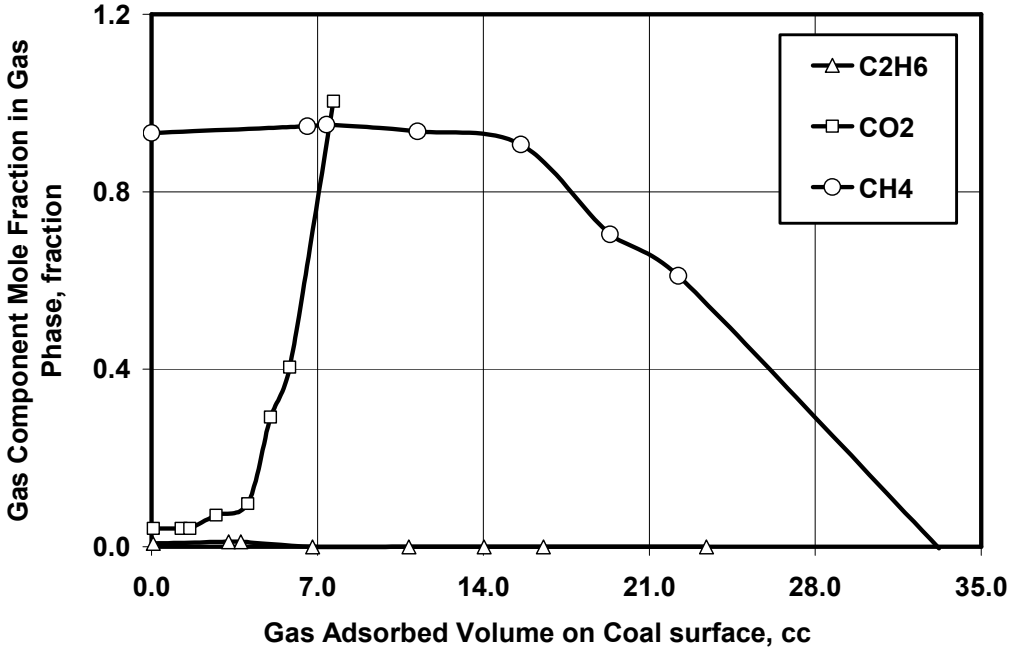

Figure 6. 51. Predicted gas mole fractions in gas phase versus the adsorbed gas volume in coal.

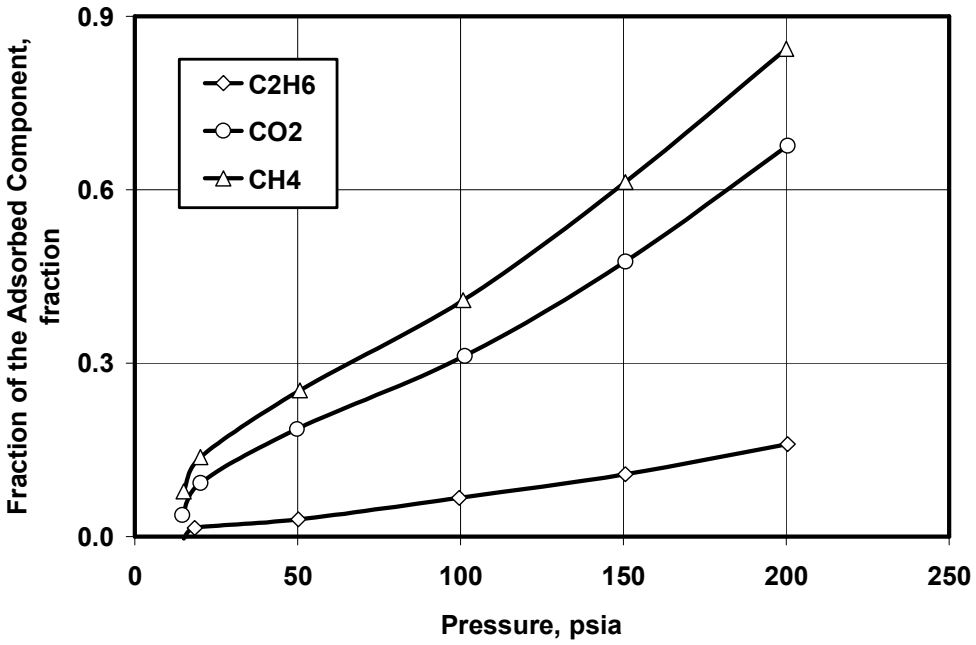

Figure 6. 52. Predicted fraction of the adsorbed methane, ethane, and carbon dioxide from a ternary mixture of 95% CH_4, 3% CO_2, and 2% C_2H_6 versus various equilibrium pressures.

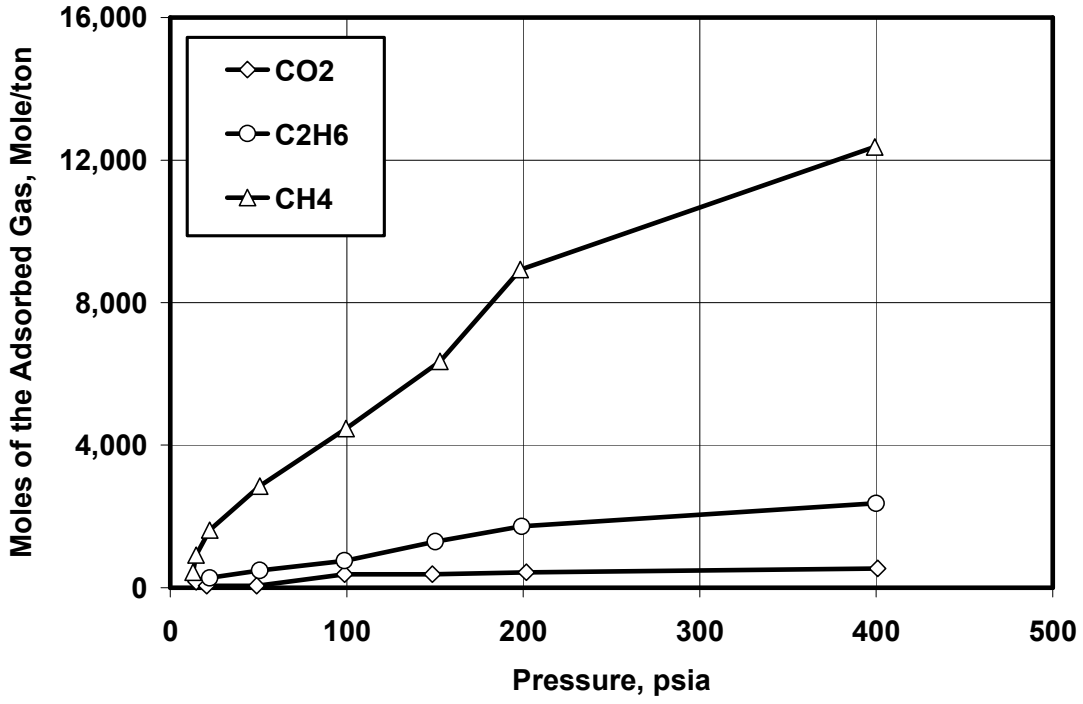

Figure 6. 53. Predicted moles of the adsorbed methane, ethane, and carbon dioxide from a ternary mixture of 95% CH_4, 3% CO_2, and 2% C_2H_6 versus various equilibrium pressures.

Case 4. Carbon dioxide adsorption in coal

The experimental results of nitrogen adsorption in coal are shown in Figure 4.18 as the adsorbed carbon dioxide volume versus time at various pressure levels. The time required to reach equilibrium for these curves is approximately 900 minutes for each pressure level. Therefore, if ten different measurements at various pressure levels are required to construct an equilibrium isotherm, approximately 9000 minutes (about seven days) of laboratory work has to be dedicated for constructing only one equilibrium isotherm. However, applying the method developed in this study reduces this time to only 1800 minutes (about 1.25 days) of the laboratory work by taking only two sets of the non-equilibrium adsorption isotherms for two different pressure levels and projecting the obtained results to other pressure levels. Figure 6.54 indicates that the calculated errors between the long time predictions using the full set of data (9000 minutes) and only two sets of data (1800 minutes) is less than 5%. Therefore, the equilibrium and non-equilibrium isotherms can be obtained using the model developed in this study in shorter time period and with good accuracy.

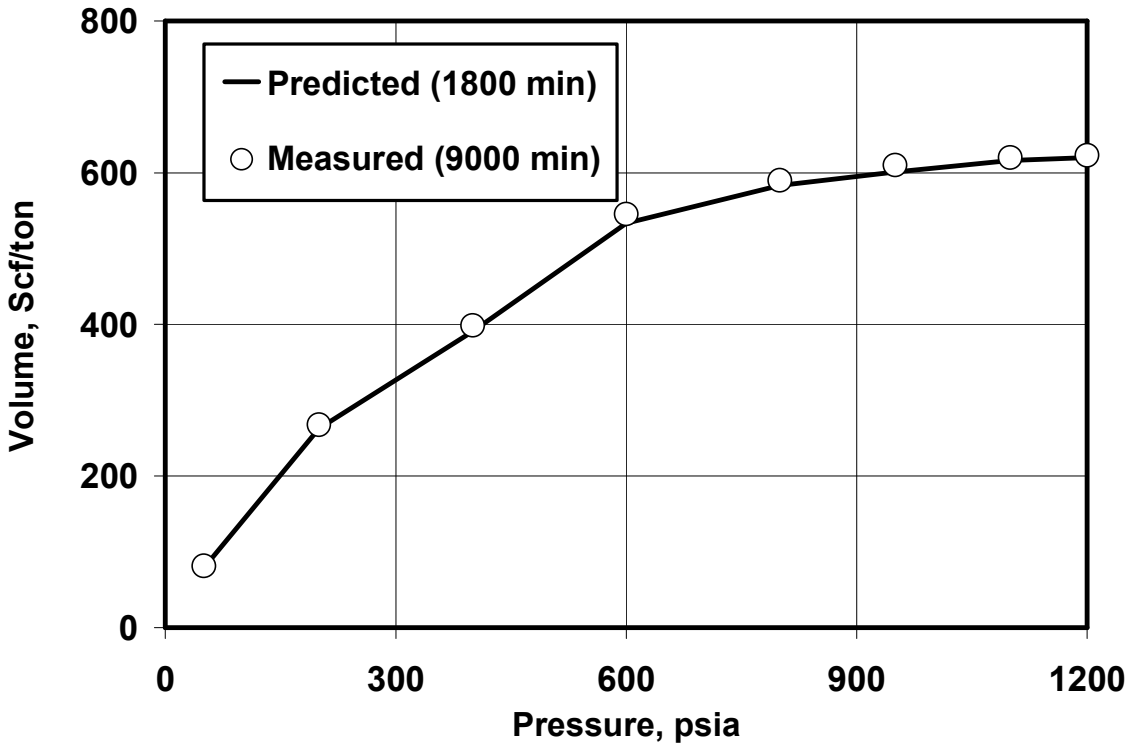

Figure 6. 54. The measured (9000 minutes) and the predicted (1800 minutes) carbon dioxide adsorbed volume in the coal A versus the equilibrium pressure levels.

It was demonstrated that two sets of the non-equilibrium isotherms at two different pressure levels are required to construct an equilibrium isotherm. Figure 6.57 indicates that the non-equilibrium isotherm at any pressure can be predicted using only the early portion of the sorption data. The magnitude of the early portion required to obtain the equilibrium data is different from case to case. Figure 6.58 shows that collection of data up to $1/20^{th}$ of the equilibrium time is sufficient to construct a non-equilibrium isotherm at 50 psia. Therefore, taking the data up to only 45 minutes instead of performing the experiment for 900 minutes will result in the same non-equilibrium isotherm for this example.

The data measured at each time step is fed to a computer program implementing the present theory. The computer code fits the data with the appropriate equations and calculates the system parameters using the least-squares method. The obtained parameters for each time step are compared with the previous time step. If the difference between the present and the previous values are relatively small, the experiment can be stopped and the next pressure can be applied. Figure 6.56 shows the same procedure for pressure level of 800 psia. The time required to build the non-equilibrium isotherm at 800 psia is approximately $1/10^{th}$ of the equilibrium time (around 81 minutes). Therefore, using the data obtained in Figures 6.57 and 6.58 the equilibrium and non-equilibrium isotherm can be constructed in almost 130 minutes that is 70 times less than the required time using the equilibrium techniques.

Figure 6.59 compares the equilibrium isotherm obtained using 9000 minutes, 1800 minutes, and 130 minutes. The comparison indicates that the prediction error using early time measurement and projecting them to the long time equilibrium state is less than 5%. However, the time required to construct the same isotherm is reduced from 9000 minutes to 130 minutes.

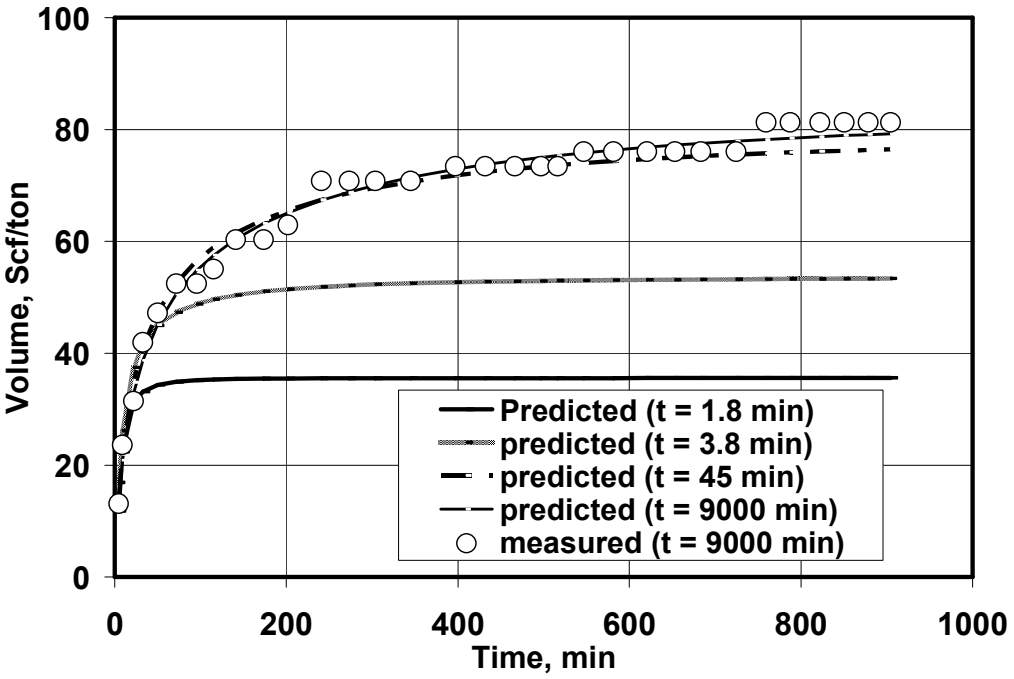

Figure 6. 55. The adsorbed carbon dioxide versus the adsorption time for the system of the carbon dioxide-coal A at 50 psia at different time steps (fitting the 9000 minutes measured using only the early portion of the data).

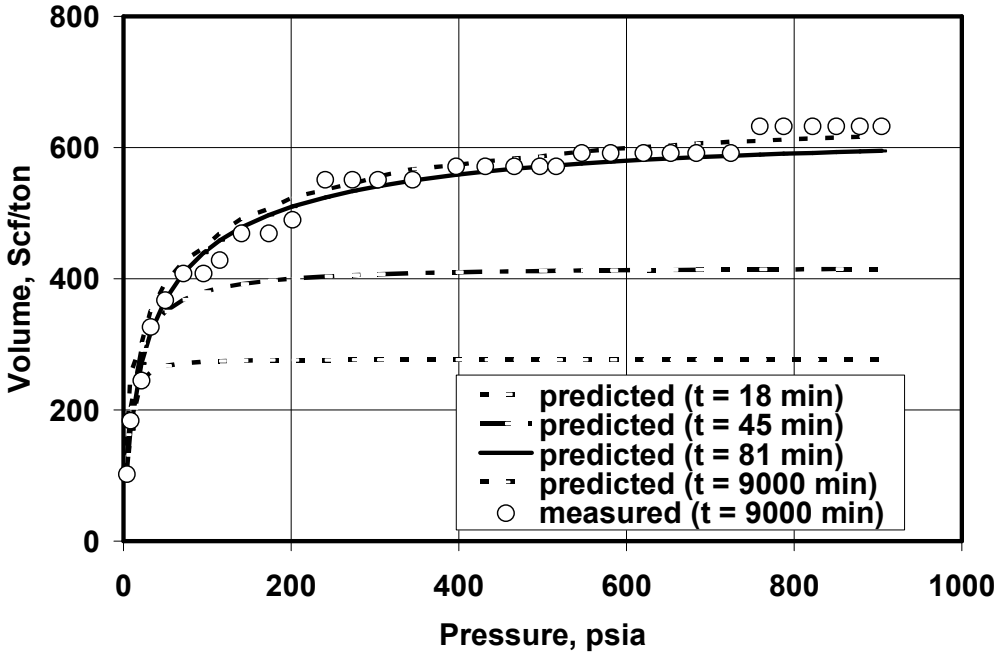

Figure 6. 56. The adsorbed carbon dioxide volume versus the adsorption time for the system of the carbon dioxide-coal A at 800 psia at different time steps (fitting the 9000 minutes measured using only the early portion of the data).

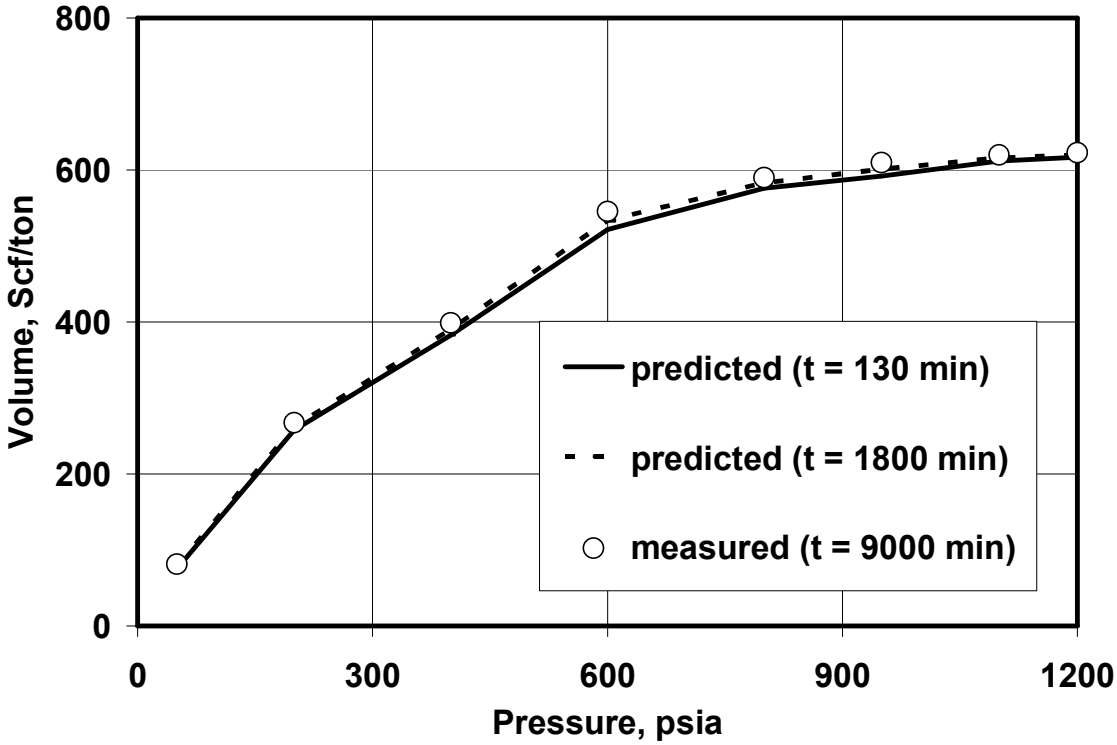

Figure 6. 57. The measured and predicted equilibrium adsorbed carbon dioxide volume versus the equilibrium pressure for the system of carbon dioxide-coal A.

Case 5. N_2-CO_2 Mixture Adsorption in Coal and Water

For illustration purposes the experimental data obtained from the N_2-CO_2-water-coal B adsorption tests are evaluated. The two sets of data at 200 and 600 psia are used and the parameters D and V_m for both nitrogen and carbon dioxide gases are obtained. The values of $a_{Vm,P}$, $b_{Vm,P}$, $b_{D,P}$, and $a_{D,P}$, are obtained by fitting these data using Equations 6.17-6.21.

Figures 6.60-6.63 show the curve fitting process for the mentioned equations. Using these parameters and Equation 6.17 the kinetics of the gas mixture adsorption on coal in the presence of water in 600 psia is estimated. The estimated

and measured values are compared in Figure 6.63. The comparison indicates that the estimation error is less than 4%.

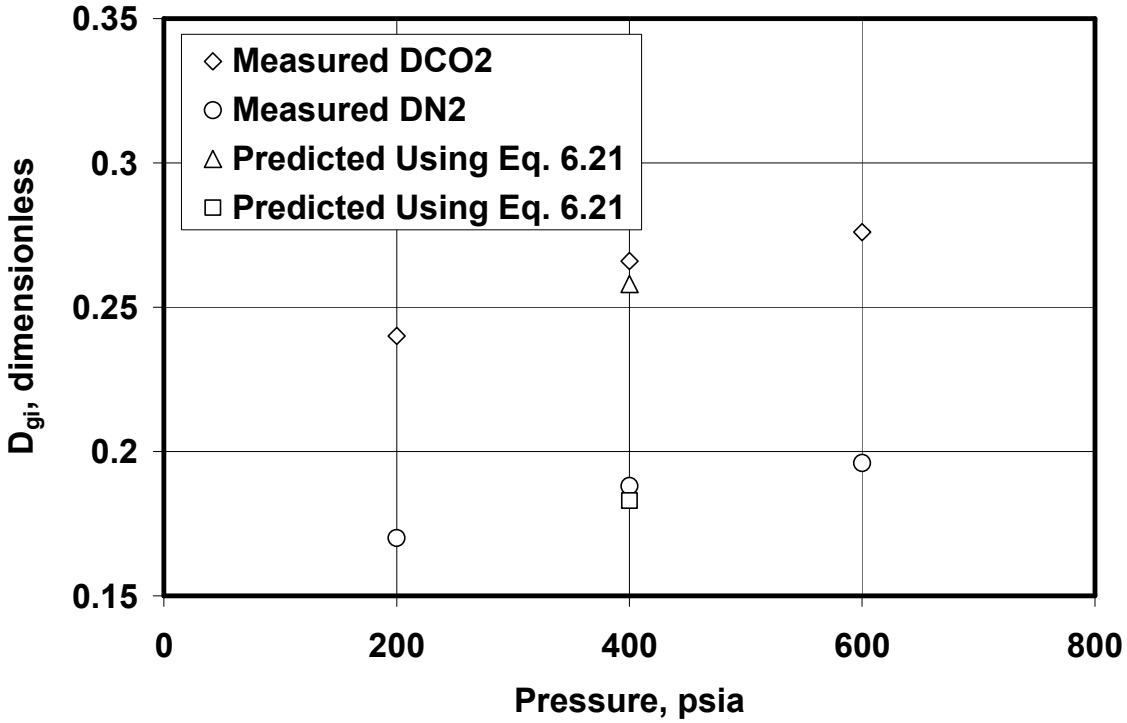

Figure 6. 58. The estimated D-R isotherm coefficient (D) versus the equilibrium pressure (prove of applicability of Equation 6.21) for CO_2/N_2 adsorption in coal A.

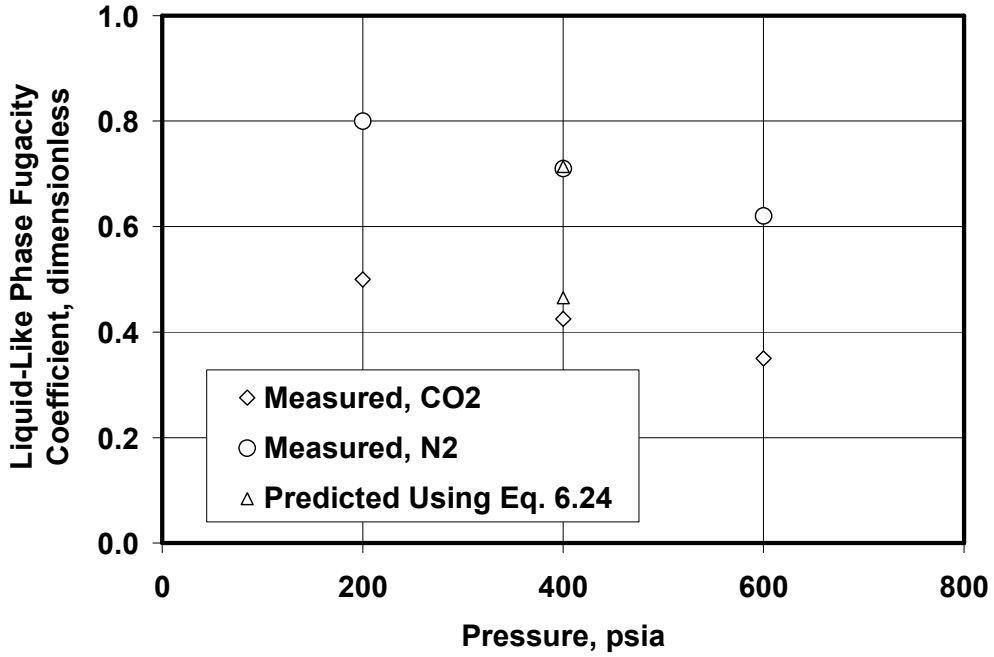

Figure 6. 59. The estimated liquid-like phase fugacity coefficient (ϕ_i) versus the equilibrium pressure (prove of applicability of Equation 6.24) for CO_2/N_2 adsorption in coal A.

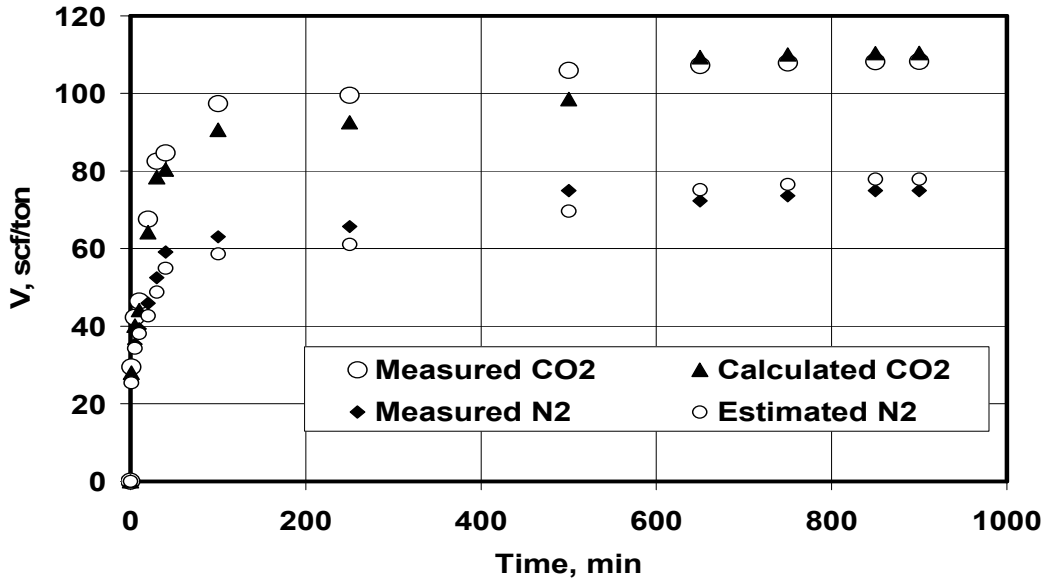

Figure 6. 60. Measured and predicted adsorbed CO_2 and N_2 volumes in coal B versus the adsorption time from a CO_2/N_2 mixture (50% CO_2, 50% N_2).

The above examples demonstrate that the developed procedure in this study is applicable to predict the single and multi-component two and three phase non-equilibrium and equilibrium isotherms from the early measurements. The calculated prediction error is less than 8% for the worst case scenario. In most of the cases the prediction error is less than 2%.

It can be observed from the in-house and literature experimental data that the time required to attend the equilibrium for one pressure level is usually between 8-18 hours. Seven to twelve data points are usually required to establish any equilibrium isotherm. Therefore, the total time required to construct one equilibrium isotherm is usually between 72 to 220 hours (3-10 days). However, applying the method developed in this study reduces this time to less than 3 hours. This is a significant reduction in time that can save considerable amount of cost and laboratory work to construct an equilibrium isotherm. Moreover, applying the method developed in this study, both equilibrium and non-equilibrium isotherms can be obtained from the same type of the adsorption experiments. In contrast, the other methods are based on the equilibrium measurements and only allow the construction of the equilibrium isotherms.

2. With the Presence of Water

Case 1. Reported literature data

Nordon and Bainbridge (1983), and Monazam (1998) reported some data sets of the kinetics of water adsorption in various coals. Their experimental system was composed of only water and coal phases in contact with each other. Equation

6.16 is applied to model their experimental data. Figures 6.63 and 6.64 show the curve fitting procedure of the water adsorption kinetic data using the present model. The data fitting error is about 1%-5%. This is considered a good match between the predicted and the measured values.

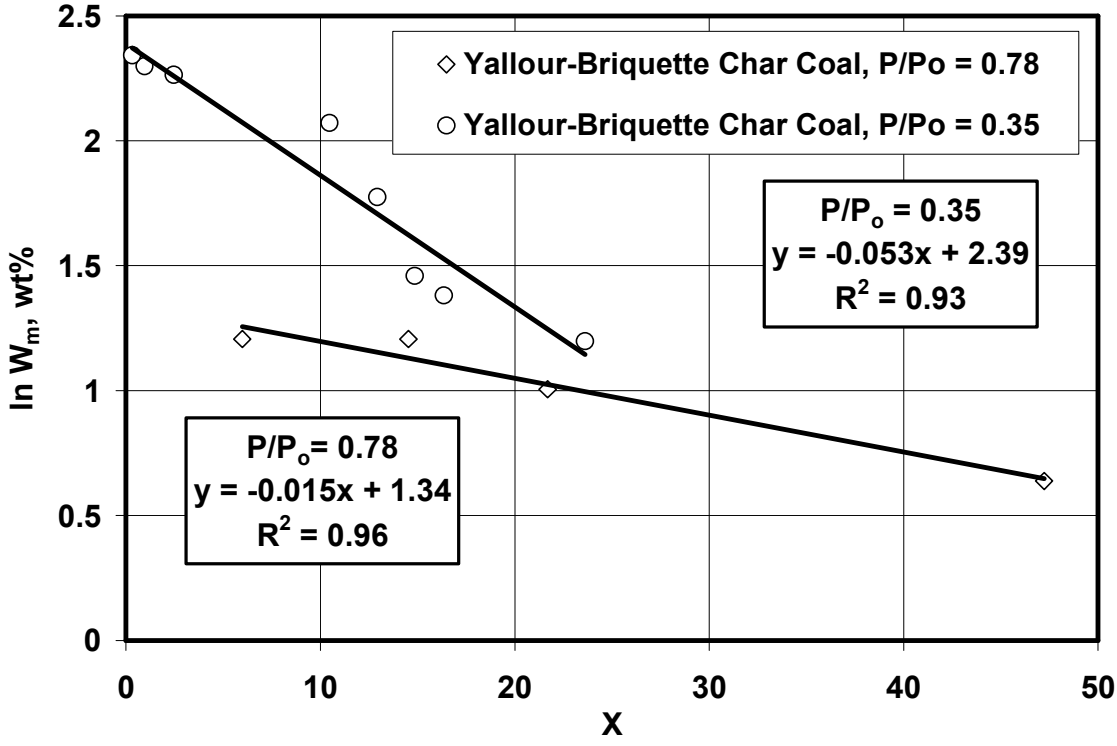

Figure 6. 61. Plot of $\ln W_{Wc}$ versus $X = \left\{ -\ln\left[\frac{P}{P_{Wco}} \tanh\left(2PK_{gs_i} t\right) \right] \right\}^{r_i}$ for r = 1.0, for the system of water-Yallour-Briquette char coal and various relative pressure ratios (good value of R^2 indicates the applicability of Equation 6.16 in modeling the water adsorption on coal).

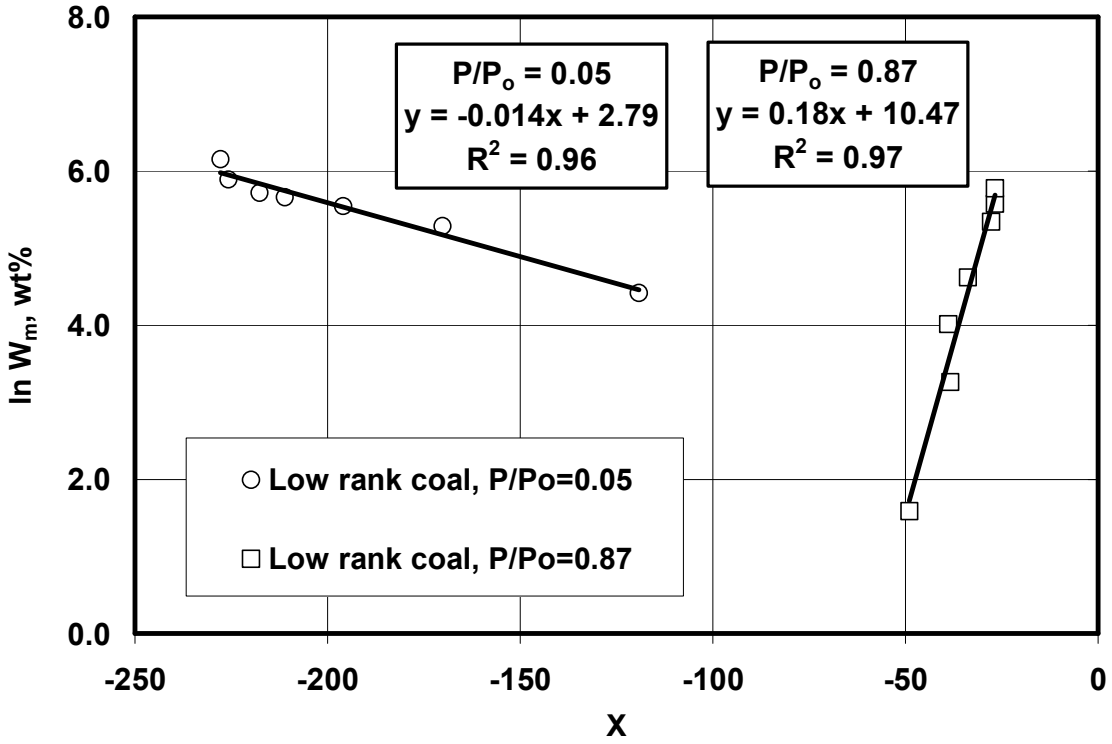

Figure 6. 62. Plot of $\ln W_{Wc}$ versus $X = \left\{ -\ln\left[\frac{P}{P_{Wco}} \tanh\left(2PK_{gs_i} t\right) \right] \right\}^{r_i}$ for r = 1.0, for the system of water-low rank coal with various relative pressure ratios (good value of R^2 indicates the applicability of Equation 6.16 in modeling the water adsorption on coal).

Case 2. CO_2/N_2 Gas Mixture and Water Adsorption in Coal

The experimental data and the data interpretation procedure for the system of CO_2/N_2 gas mixture and water adsorption in coal were already discussed and explained in the previous chapters. Figures 6.30 and 6.31 show the obtained gas and water isotherms. The results show that presence of water decreases coal ability to adsorb carbon dioxide and nitrogen. It is because some of the adsorption sites are occupied by water prior to the gas adsorption. During the experiment the coal water

content increases. This is due to the water adsorption from the water phase, water adsorption from the gas phase, water capillary rise into the coal capillary tubes, and water diffusion in the coal internal structure. Regardless of the prevailing mechanism that increases coal water content, the non-equilibrium trend can be modeled with the developed model in this study.

Figures 6.65 and 6.66 show the quality of the data fitting procedure for the non-equilibrium water adsorption on the coal A. The R^2 values obtained from the curve fitting procedure are higher than 0.94 indicating that the developed model can predict the adsorbed water content of the coal with high accuracy.

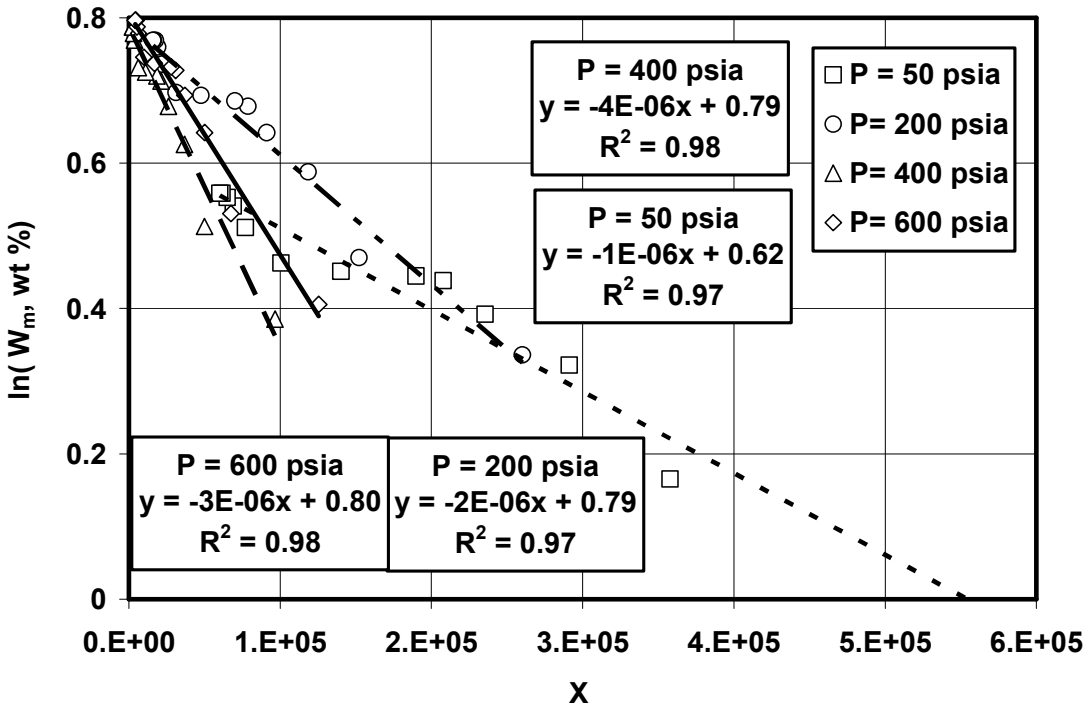

Figure 6. 63. Plot of $\ln W_{Wc}$ versus $X = \left\{ -\ln\left[\frac{P}{P_{Wco}} \tanh\left(2PK_{gs_i} t\right) \right] \right\}^{r_i}$ for r = 1.5, for the system of water adsorption in coal A from the N_2-water-coal A (good value of R^2 indicates the applicability of Equation 6.16 in modeling the water adsorption on coal).

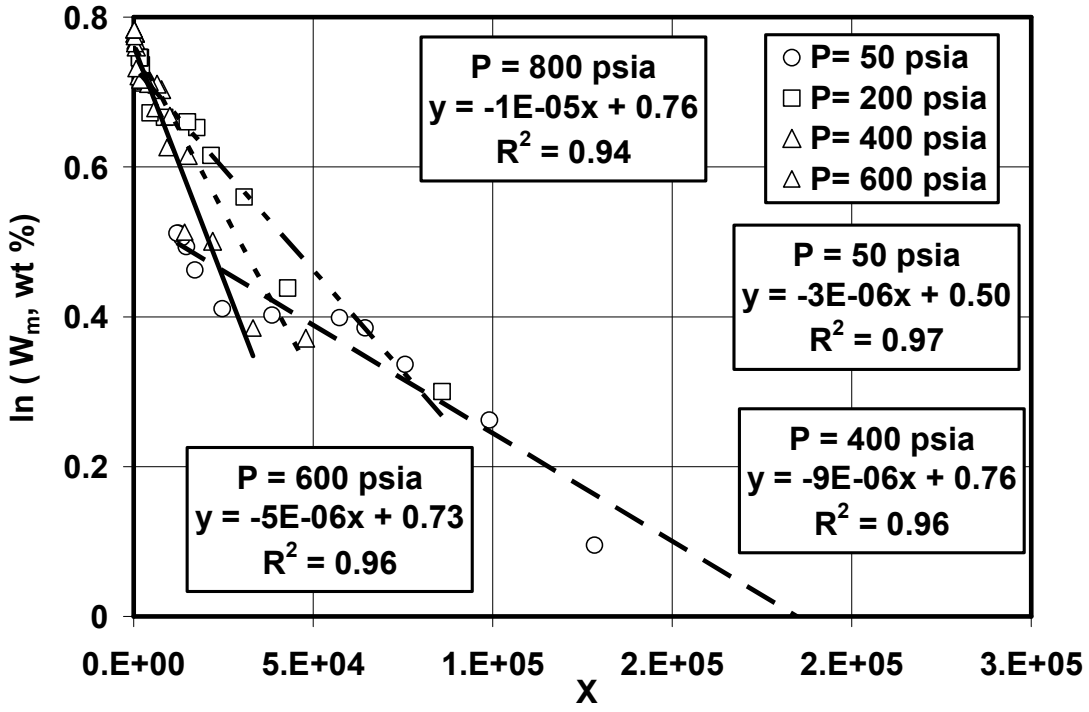

Figure 6. 64. Plot of $\ln W_{Wc}$ versus $X = \left\{ -\ln\left[\frac{P}{P_{Wco}} \tanh\left(2PK_{gs_i} t\right) \right] \right\}^{r_i}$ for r = 2.0, for the system of water adsorption in coal A from the CO_2-water-coal (good value of R^2 indicates the applicability of Equation 6.16 in modeling the water adsorption in coal).

Effect of the Resident Water in Simultaneous CO_2/N_2 Injection in Coalbed Methane Reservoirs

The presence of water in wet coal is a result of the chemical and physical bonding of coal and water, and influence of the properties of the coal (Snyder et al. 2003). Gosiewska et al. (2002) expresses that the mineralogical nature of the coal largely influences the wettability of the coal surface with water. At macroscopic scale, carbon surface is hydrophilic resulting in little water adsorption. However, if

H-bonding sites are present at the surface, forming strong bonds between the water and the coal surface may change the wettability and enhance water adsorption.

Nordon and Bainbridge (1982) reported that the self-heating phenomenon may cause the releasing of some heat when water is adsorbed on the coal, particularly in lower rank of bituminous coals. Kross et al. (2002) reported that moisture-equilibrated coals showed lower methane adsorption capacity by 20-25% with respect to the dry coal. They also indicated that the moisture content of the coal reduces the coal sorption capacity for carbon dioxide. Practically, the adsorbed water occupies some of the sorption sites and reduces the available surface for gas molecule adsorption on the coal internal surfaces. Some of the adsorbed water may block the gas path to the micropore system. However, there is a specific coal water content beyond which the coal sorption gas content does not reduce by increasing the coal water content. At this water content, all possible adsorption sites for water are occupied and hence the maximum water adsorption occurred.

Allardice and Evans (1971) modified the BET equation to fit the obtained equilibrium mono-layer water adsorption data on the Yallourn brown coals. They concluded that the number of the functional groups present on the coal surface affect the water sorption capacity of the coal. Most of the functional groups contain large amount of oxygen atoms that may make strong bonds with the hydrogen atoms available in water. Therefore, some of the adsorbed water in coal is due to the presence of these bonds. It is also presented that the capillary raise can be another major factor affecting the water adsorption on the coal internal surface.

Stamm (1956) used the steady-state diffusion measurements to represent the diffusion of water into uncoated cellophane. Stamm measured the liquid and vapor water adsorption on cellophane with time. The results show that the frequency of the impact of the surface by water molecules controls the take-up of the water in the solid surface by vapor adsorption. The frequency of the impact of the surface by water molecules is however a function of the vapor pressure. Stamm concluded that the same phenomenon must occur for the adsorption of water from the liquid phase. In solids with very tight structure like coals, where the void capillaries are of the molecular size, the penetration of the solid surface must be due to more energetic water vapor leaving the liquid phase as it happens in the vaporization process.

Muster et al. (2001) studied water adsorption kinetics on silica particles. They concluded that the amount and rate of water adsorption on silica samples depend on the frequency of the surface hydroxyl groups and also the water condensation rate to form multilayers. It was observed that the water adsorption rate is relatively high at the beginning of the adsorption process due to the hydroxylation-state of the silica particle surface. However, the adsorption rate decreased due to condensation and resulted in multilayer water coverage.

Monazam et al. (1998) presented a model to predict the coal moisture content at any time after exposing the coal to the moist air. They developed a model based on the Fick's law and material balance concept. Their model was applied to predict the time-dependency of water adsorption in coal and showed very satisfying results.

Clarkson and Bustin examined (2000) the effect of the moisture on binary gas adsorption/desorption isotherms. They concluded that the Dubinin and Astakhov (D-A) and Dubinin-Radushkevich (D-R) isotherms better fit the equilibrium adsorption data for both dry and moisture-equilibrated coals.

Despite the general understanding in the coalbed methane industry that presence of water in coal will alter its ability to adsorb, hold, and desorb gas, due to the complexity of evaluating three phases of coal-gas-water system simultaneously, most of the researchers have either ignored the water effects or considered it separately. However, one of the most important advantages of the technique developed in this study, as illustrated earlier in this chapter, is its ability to develop both gas and water adsorption isotherms simultaneously from one experiment and with very high accuracy and better quality.

The comparison of Figures 6.19 and 6.30 for nitrogen adsorption in coal A with and without the presence of water indicates that the presence of water reduces nitrogen adsorption by 25%-35% for higher rank coal A. Similar investigation for lower rank coal B shows that the presence of water in the sorption system reduces nitrogen adsorption rate by 30%-50%. High rank coals have tight structure and very tiny pore volume. Therefore, the water molecules cannot diffuse and adsorb on the coal internal structure as freely as low rank coals. This is why the presence of water can have a higher impact on the adsorption ability of low rank coals.

Likewise, comparison of Figures 6.18 and 6.29 for carbon dioxide adsorption in coal A with and without the presence of water reveals that presence of water in the system reduces the carbon dioxide adsorption rates by 30%-45% for

high rank coal A. Similar investigation of the experimental results for the lower rank coal B indicates that the presence of water in the sorption system reduces carbon dioxide adsorption rates by 40%-55%.

The presence of water in the sorption system affects carbon dioxide adsorption in coal more than nitrogen adsorption. The affinity of the coal to adsorb carbon dioxide is 2-10 times more than nitrogen gas. The earlier experimental results also indicated that the solubility of carbon dioxide in water is approximately 5-10 times higher than the solubility of the nitrogen in water. Therefore, presence of water in the sorption system has more effects on the ability of the coal to adsorb carbon dioxide than nitrogen.

It was demonstrated earlier that one of the methods to increase the carbon dioxide adsorption rate in the wet coals is to inject carbon dioxide and nitrogen gases simultaneously. In the reservoir condition, carbon dioxide dissolves and reacts with the resident water. Presence of nitrogen in the injected carbon dioxide will decrease the effect of water on carbon dioxide and also will alter the gas mixture critical pressure and temperature. An optimum CO_2/N_2 injection ratio can be found at which the carbon dioxide sequestration and methane production rates are the maximum, and the effects of the resident water in the CO_2 sequestration process is the minimum. Investigating the experimental results indicates that changing the initial CO_2/N_2 injection ratio will affect the shape of the developed non-equilibrium and equilibrium isotherms.

Comparing the sequestration results for the case of pure carbon dioxide and the mixture of nitrogen and carbon dioxide shows that for the case of total initial

pressure of 200 psia and the P_r = 0.25 the carbon dioxide sequestration rate is increased by 1.5% when a mixture of carbon dioxide and nitrogen is injected. The similar phenomenon was observed at the other pressure levels. Figure 6.67 exhibits the effects of changing the initial CO_2/N_2 injection ratio on enhancing the coal carbon dioxide sequestration rate for both high and low rank coals. Figure 6.67 indicates that P_r = 0.5 and P_r = 0.7 result in the maximum CO_2 sequestration rate beyond which increasing the initial injected N_2/CO_2 ratio in the CO_2-N_2 mixture does not affect the carbon dioxide sequestration rate further for coals A and B respectively.

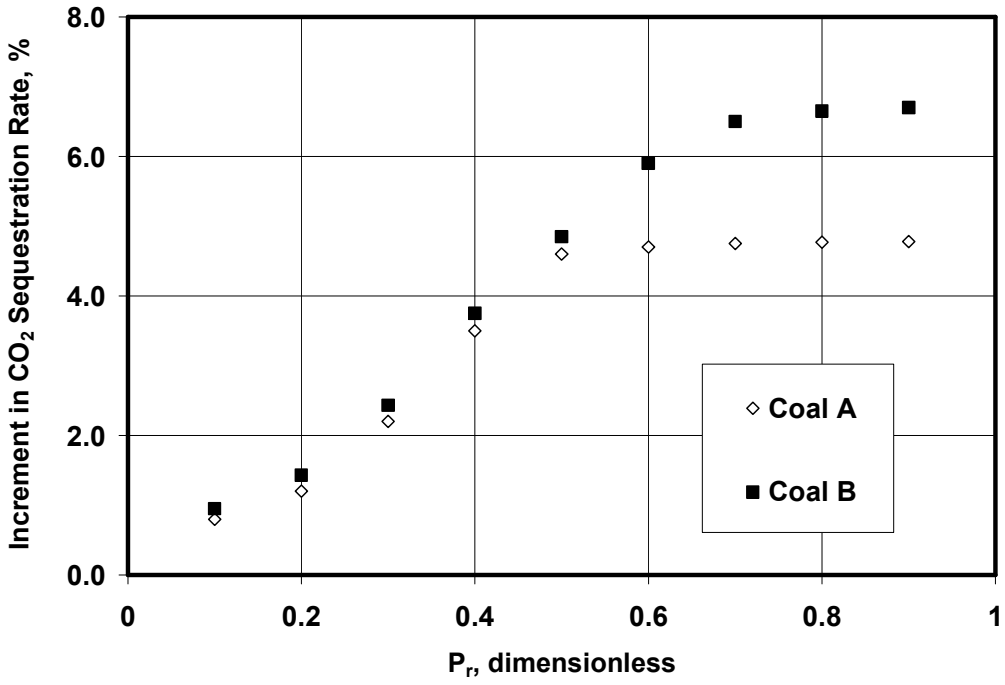

Figure 6. 65. Increment in CO_2 sequestration rate versus the initial $P_r = \frac{P_{N_2}}{P_{CO_2}}$ for P_{tin} = 200 psia.

CHAPTER 7

IMPROVING THE COALBED METHANE AND SHALE GAS RESERVOIR SIMULATION BY REPLACING THE EQUILIBRIUM WITH NON-EQUILIBRIUM ISOTHERMS

The three stages of the fluid (gas and water) transfer were described in Chapter 2. The matrix structure in the coalbed methane/shale gas reservoir contains several adsorption sites in various sizes and dimensions. The adsorbed phase that may contain several components desorbs from these particles and enters the surrounding matrix micropores due to the pressure difference between the adsorption sites and the micropores. The desorbed phase diffuses through the micropores towards the cleats due to the concentration difference between the micropores and the surrounding cleats.

In the following, series of the primary and enhanced coalbed methane and shale gas production scenarios under CO_2/N_2 injection are considered. The results of incorporating the non-equilibrium sorption model, and cleat porosity and permeability alterations due to the gas injection/production scenarios are discussed.

General Formulation

Desorption process over the specified area of the radius r indicated in Figure 7.1 is expressed as following:

$$\ln\left[V_{G_ic}(t)\right] = \ln\left[\overline{V}_{mi}\left(\hat{f}_{G_ic}\right)\right] - \left\{-\overline{D}_i\left(\hat{f}_{G_ic}\right)\ln\left[\frac{P_e\vec{y}_{G_ic}(t)}{\hat{P}_{G_ico}}\tanh\left(2P_e\vec{y}_{G_ic}(t)K_{gs_i}t\right)\right]\right\}^{r_i} \quad \text{.....(7.1)}$$

where:

$$\overline{D}_i\left(\hat{f}_{G_i c}\right)=\frac{\int_0^A\left[a_{dD}f(d)+b_{dD}\right]dA}{\int_0^A dA} \quad \text{.....(7.2)}$$

$$\overline{V}_{mi}\left(\hat{f}_{G_i c}\right)=\frac{\int_0^A\left\{a_{dV_m}\ln\left[f(d)\right]+b_{dV_m}\right\}dA}{\int_0^A dA} \quad \text{.....(7.3)}$$

where f(d) is the sorption particles size distribution function over the specified area.

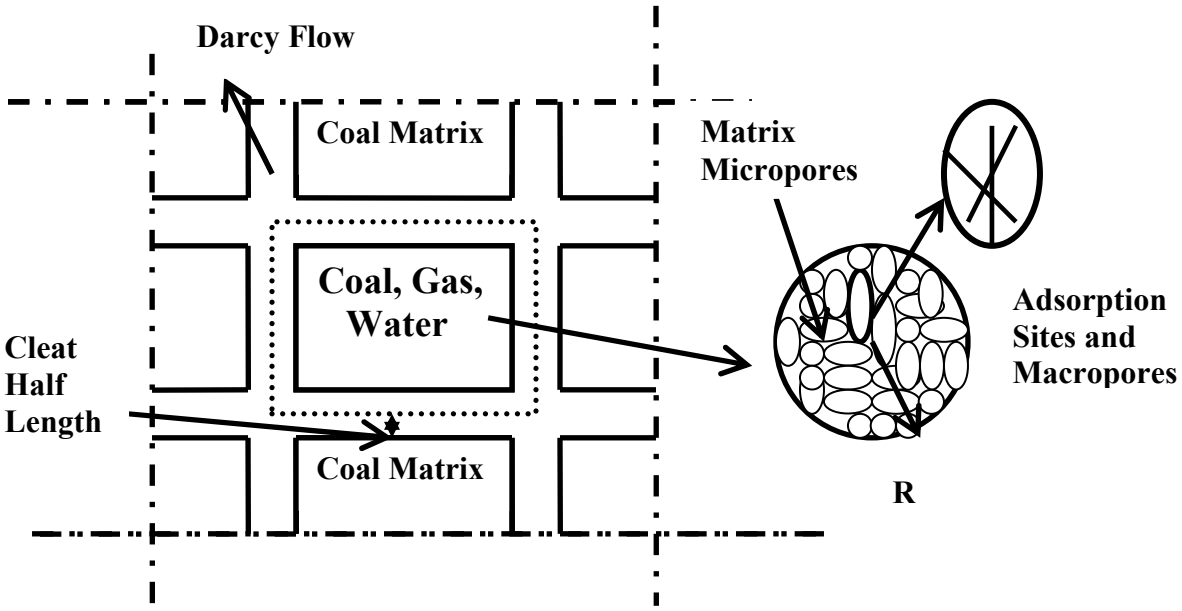

Figure 7. 1. Schematics of macropores and micropores in a specified coalbed surface.

Figure 7.1 considers a matrix block with an average bulk volume of $\overline{V}_b$ and an average micropore porosity of $\overline{\phi}_m$ containing y_i and x_i as the initial mole fractions of component i in both gas and water phases has an average pressure of $\overline{P}$. The total bulk mass is calculated using the coal bulk density. If the average bulk

pressure $\overline{P}$ is less than the adsorption pressure the adsorbed gas starts desorbing. Therefore, the net standard volume of the desorbed component i after time t is calculated according to Equation 7.1. This volume is then converted to the form of the net moles of component i in the gas phase using the ideal gas law and water phase using the liquid phase density. The new average mole fractions of the component i in both liquid and gas phases in the micropore structure are calculated using the following relationships:

$$\overline{y}_i^{new} = \frac{\overline{n}_i^{desorbed,g} + \overline{n}_i^{old,gas}}{\overline{n}_{total}^{old,gas} + \sum_j \overline{n}_{total}^{desorbed,gas}} \quad \text{.....(7.4)}$$

$$\overline{x}_i^{new} = \frac{\overline{n}_i^{desorbed,w} + \overline{n}_i^{old,w}}{\overline{n}_{total}^{old,w} + \sum_j \overline{n}_{total}^{desorbed,w}} \quad \text{.....(7.5)}$$

The average concentration of component i in both gas and water phases are calculated using the following expressions:

$$\overline{C}_i^{mac,gas} = \frac{\overline{n}_i^{new,gas}}{\overline{V}_b \overline{\phi}_{mac}} \frac{\overline{V}_{water}}{\overline{V}_{gas}} \quad \text{.....(7.6)}$$

$$\overline{C}_i^{mac,water} = \frac{\overline{n}_i^{new,w}}{\overline{V}_b \overline{\phi}_{mac}} \frac{\overline{V}_{gas}}{\overline{V}_{water}} \quad \text{.....(7.7)}$$

where $\overline{V}_{water}^{mac}$ and $\overline{V}_{gas}^{mac}$ are the average water and gas phases volume in the macropores of the matrix structure.

Similarly the average concentration of the component i in the most nearby cleat is calculated using the following relationships:

$$\overline{C}_i^{cleat,gas} = \overline{S}_{gi}^{cleat} \frac{\overline{P}_g^{cleat}}{\overline{Z}_i^{cleat} RT} \quad \text{.....(7.8)}$$

$$\overline{C}_i^{cleat,water} = \overline{S}_{wi}^{cleat} \rho_{wi}^{cleat} \left(\overline{P}_w\right) \frac{1}{Mw_{wi}} \quad \text{.....(7.9)}$$

where $\overline{S}_{gi}^{cleat}$ and $\overline{S}_{wi}^{cleat}$ are the average saturation of component i in both gas and water phases, respectively. $\overline{P}_g^{cleat}$ and $\overline{P}_w^{cleat}$ are the gas and water phases average pressures in the cleat system, respectively. The following relationship exists between the gas and water phases pressures in the cleat:

$$\overline{P}_c^{cleat} = \overline{P}_w^{cleat} - \overline{P}_g^{cleat} \quad \text{.....(7.10)}$$

where $\overline{P}_c^{cleat}$ is the average capillary pressure between the water and gas phases in the cleat system.

The non-equilibrium gas desorption rate is described using Equation 7.1. However, the gas diffusion rate in the matrix structure is described using the Fick's second law. The average concentration difference of component i between the fluid in the cleat and the macropores of the matrix is the driving force for the component i to diffuse through the matrix towards the nearby cleats. The transient-state gas diffusion is described by:

$$\frac{\partial C_i}{\partial t} = -\nabla.\left(\vec{D}_{mi}.\nabla C_i\right) \quad \text{.....(7.11)}$$

where C_i is the concentration of the component i in the micropores of the matrix, and $\vec{D}_{mi}$ is the diffusivity coefficient of the component i in the micropores of the matrix. The diffusivity coefficient, of component i in the macropores of the matrix does not remain constant. This value changes as the concentration of the component i changes. To account for the effects of the concentration on the diffusivity coefficient, the modified Darken's equation is adopted. While studying binary

alloys, Darken (1948) derived the following equation as the approximate relationship between the self-diffusivities and the transport-diffusivities of two component gas in an isothermal system:

$$D = \left(\frac{\partial \ln a_\alpha}{\partial \ln x_\alpha} \right)_{T,P} \left(x_\alpha D_{self,\beta} + x_\beta D_{self,\alpha} \right) \quad (7.12)$$

where a_α is the activity of component α. The diffusivity coefficient of component i is modified for the effect of the concentration using Equation 7.13. However, for the gas phase the following approximation is used:

$$\left(\frac{\partial \ln a_\alpha}{\partial \ln x_\alpha} \right)_{T,P} = \frac{x_\alpha}{k_B T} \left(\frac{\partial \ln \mu_\alpha}{\partial x_\alpha} \right)_{T,P} \quad (7.13)$$

where k_B is the Boltzman constant, and μ_α is the chemical potential of the component α in the gas phase. Therefore, for the component i in the gas phase of the macropores of the coal matrix:

$$\vec{D}_i^{mac} = \frac{y_{i,g}^{mac}}{k_B T} \left(\frac{\partial \ln \mu_{i,g}^{mac}}{\partial \ln y_{i,g}^{mac}} \right)_{T,P} \left(y_{i,g}^{mac} D_{self,j}^{mac} + y_{j,g}^{mac} D_{self,i}^{mac} \right) \quad (7.14)$$

The chemical potential of the component i in the gas phase is calculated using:

$$\mu_{i,g}^{mac} = k_B T \ \ln\left(y_{i,g}^{mac} P_g^{mac} \phi_{i,g}^{mac} \right) \quad (7.15)$$

where $\vec{D}_g$ in Equation 7.14 is the gas diffusivity tensor in the coal matrix. C is the gas concentration in the matrix blocks.

The presence and amount of the any gas or water component in the coal structure influence the final coal matrix swelling or shrinkage ratio. It was explained in Chapter 5 that the coal matrix swelling and shrinkage rate is a function

of the adsorbed gas and the overburden pressure. The coal matrix volume change affects the surrounding cleat permeability and porosity. The following relationship is given to describe the cleat permeability and porosity changes due to the gas adsorption/desorption processes (Syahrial 2005):

$$\sigma - \sigma_o = \frac{\nu}{1-\nu}(P - P_o) + \frac{E}{3(1-\nu)}\left[\sum_{i=1}^{n}\alpha_i V_i - \sum_{i=1}^{n} V_{io}\right] \quad \text{.....(7.16)}$$

where υ is the poison ratio, E is the Young's modulus, V_i is the adsorbed volume of component i, and α is the coal matrix volume swelling coefficient. $P\text{-}P_o$ is the pressure difference in the cleat structure. Hence the cleat new permeability is calculated using the following expression:

$$k = k_o e^{-c_f(\sigma - \sigma_o)} \quad \text{.....(7.17)}$$

where c_f ($psia^{-1}$) is the cleat volume compressibility with respect to changes in the effective horizontal stress $(\sigma - \sigma_o)$. This value is calculated using the following relationship:

$$c_f = (1-\phi)c_{cleat\ grain} + S_w c_w + (\phi - S_w)c_{gas} \quad \text{.....(7.18)}$$

where $c_{cleat\ grain}$, c_w, and c_{gas} are cleat grain, cleat water, and cleat gas compressibility factor (psi^{-1}).

Applying the permeability-porosity relationships the following expression is obtained to calculate the new cleat porosity:

$$\frac{\phi}{1-\phi} = \exp(-c_P \Delta\sigma) \quad \text{.....(7.19)}$$

The coalbed methane and shale gas reservoir simulation procedure is very similar with some minor differences. The following sections review the differences

between high rank, low rank, and shale gas reservoir characteristics and production simulation procedures.

High Rank Coals

High rank coals have very high carbon contents. The matrix structure in these coals is composed of very tight pores with very low permeability and very low affinity for water. The adsorbed methane in the matrix is the major source of gas, and the cleats are saturated with water at the initial reservoir condition. These reservoirs can be simulated using the dual porosity model expressed as a matrix structure surrounded by a series of cleats and natural fractures. The matrix is influenced by both gas desorption rate from the adsorption sites and gas diffusion rate through the matrix structure.

Low Rank Coals

Low rank coals are found in the Powder River basin and some other basins in the United States. These coals are young and hence adsorb less methane than high rank coals due to their low carbon content. Unlike the high rank coals, the matrix structure contains larger pores allowing for higher matrix porosity that results in more free gas storage in the matrix. Therefore, the gas and water flow throughout the matrix can be described with Darcy's law rather than Fick's law.

Shale Gas Reservoirs

Shale gas reservoirs are accounted for as one of the important natural gas reserves in the United States. The gas storage and gas flow mechanisms are very

similar to that of low-rank coalbed methane reservoirs. The studies show that the major gas storage mechanism in shale reservoirs at high pressures is the free gas storage in the pore volume of the matrix structure, whereas, at low pressures the adsorbed gas plays an important role. The matrix permeability in shale basins is extremely low (10^{-9} to 10^{-5} md). Therefore, for all practical purposes, the flow in the matrix is assumed to be only one-phase gas flow. However, most of the natural fractures in shaly basins are water saturated at the reservoir initial life.

CO_2/N_2 Sequestration Simulation, Case Studies, Results and Discussions

In this section, various coalbed/shale gas production scenarios will illustrate the results of applying the developed non-equilibrium sorption isotherm, matrix swelling/shrinkage equations due to the gas injection, and temperature difference between the injected gas and the matrix structure in effectively simulating both coalbed/shale gas reservoirs under the primary and enhanced gas production and simultaneous CO_2/N_2 sequestration processes.

Prior to the review of the field applications of the non-equilibrium sorption model the importance of the time-dependency of the sorption phenomenon is investigated using the following examples.

Example 1. Figures 7.2 and 7.3 investigate the time dependency of the desorption process. The normalized time (t_N) is the ratio of time over the equilibrium time at that specific pressure. As can be seen, neglecting the time dependency of desorption process may result in about 30-40% error in reservoir

simulation. This fact has been overlooked in coalbed methane and shale gas reservoir simulators where the equilibrium isotherms are usually used to describe the methane desorption from internal coal seams.

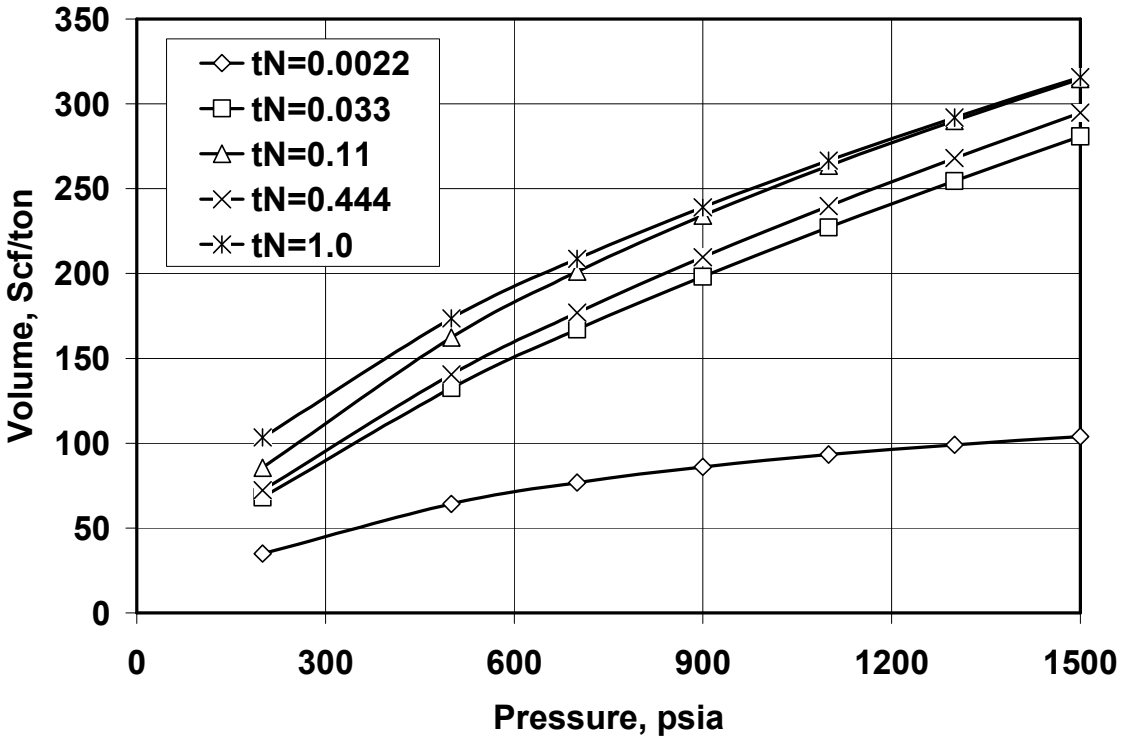

Figure 7. 2. Predicted adsorbed methane volume in Tiffany coal versus the system pressure for various normalized times (t_N).

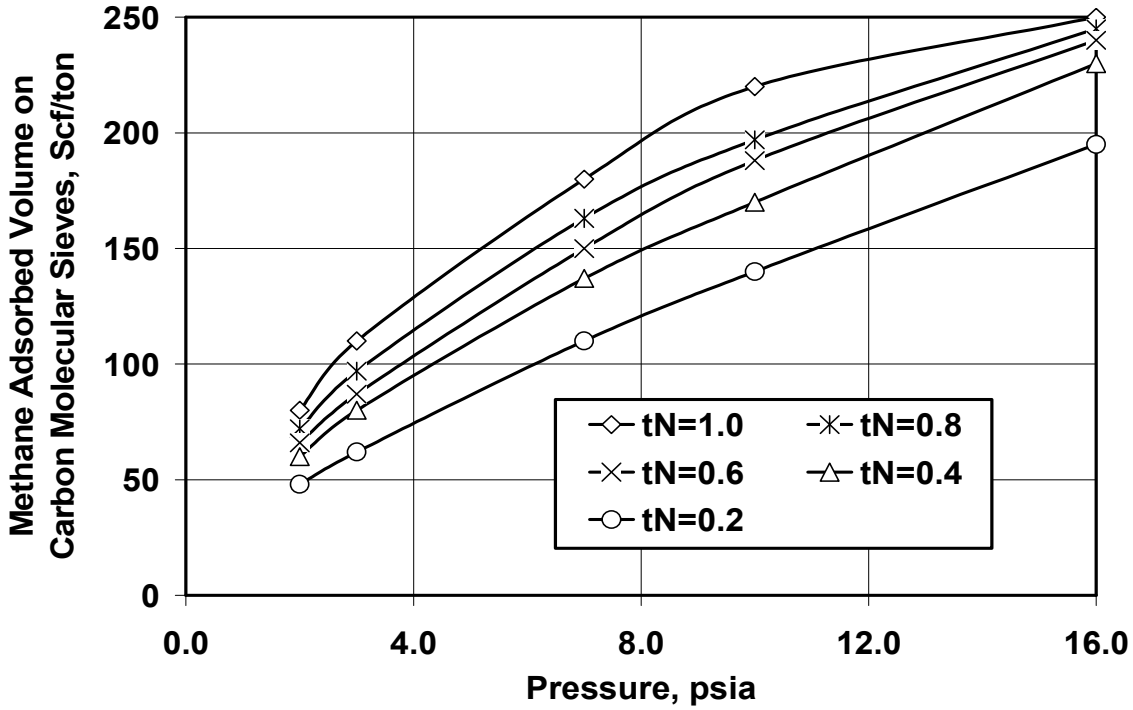

Figure 7. 3. Predicted adsorbed methane volume on carbon molecular sieves versus the system pressure for various normalized times (t_N).

Example 2. To illustrate the importance of the time-dependency of the sorption phenomenon in the CO_2/N_2 injection and CH_4 production consider a 120 cc vessel containing 20 cc coal and adsorbed methane and 100 cc free methane at 150 psia and 130^o F. The system is at equilibrium and the methane content of the coal is 83 Scf/ton (10 cc methane) according to Figure 7.2. If the total pressure increases from 150 psia to 300 psia by injecting a CO_2 and N_2 mixture of 90% CO_2 and 10% N_2, the free gas mixture composition inside the vessel will change to 74% CO_2, 17% CH_4, and 7% N_2. Therefore, the partial pressures of the CO_2, CH_4, and N_2 components in the gas phase will be 222, 51, and 21 psia, respectively. As a result, the coal adsorbs CO_2 and releases extra methane to reach the thermodynamic

equilibrium. As coal adsorbs CO_2 and releases CH_4, the mole fractions of the various components in the gas and coal phases change.

The kinetics of this phenomenon can be modeled using the model developed in this study. Figure 7.4 shows that the adsorbed volume of carbon dioxide and nitrogen in coal increases while methane is being released from the coal until a thermodynamic equilibrium is established at the prescribed pressure. Figure 7.5 presents the mole fraction of each component in the gas phase. The mole fraction of the methane in the gas phase increases as methane is being desorbed from the coal while the mole fraction of CO_2 decreases until the thermodynamic equilibrium is obtained. This approach is very useful in studying the enhanced coal gas recovery methods by different gas injections, including CO_2 and N_2.

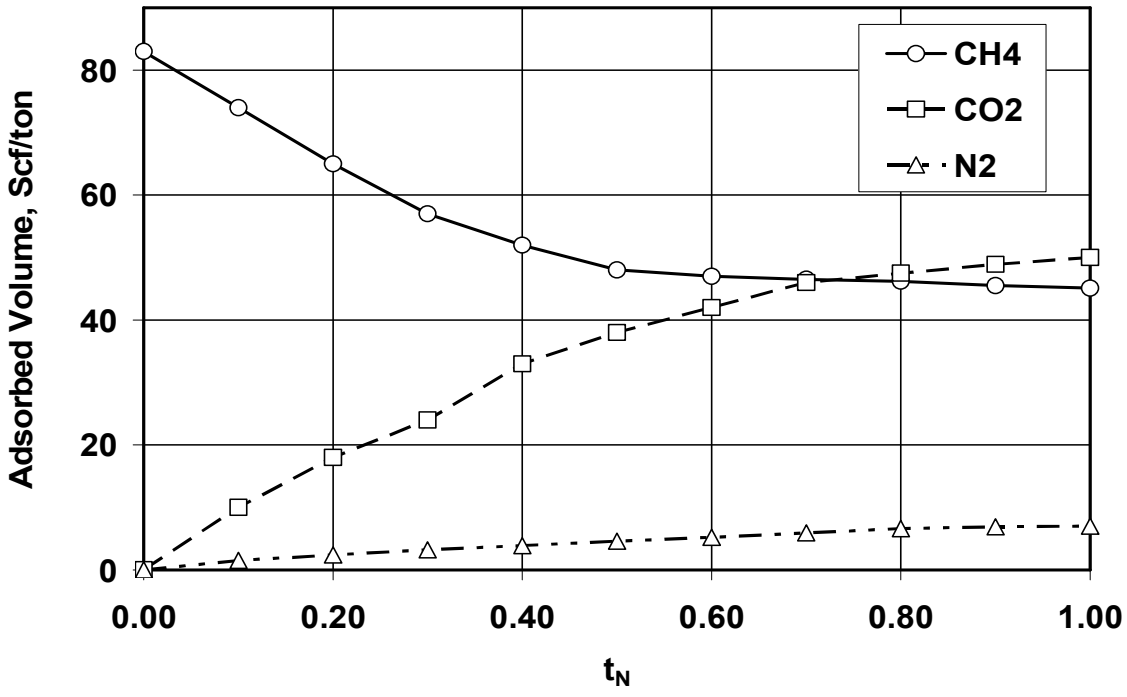

Figure 7. 4. Prediction of adsorbed volume of gas components on the coal versus the normalized time.

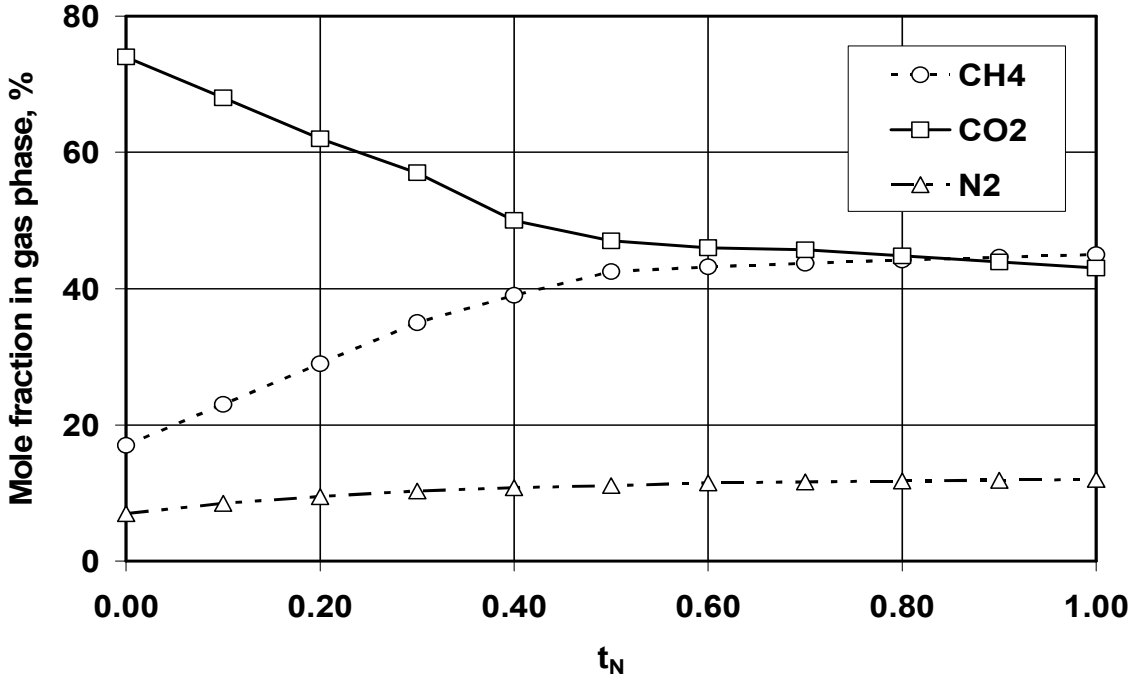

Figure 7. 5. Prediction of mole fractions of each component in gas phase versus the normalized time.

Now that the importance and significance of the time-dependency of the sorption phenomenon in the laboratory condition has been demonstrated, typical scenarios are discussed to illustrate the field applications of the technique developed in the previous chapters.

Case I. Single component gas, single phase flow in a rectangular reservoir

The gas transfer through the matrix structure in coal and shale gas reservoirs is described using the following approach (Figure 7.6):

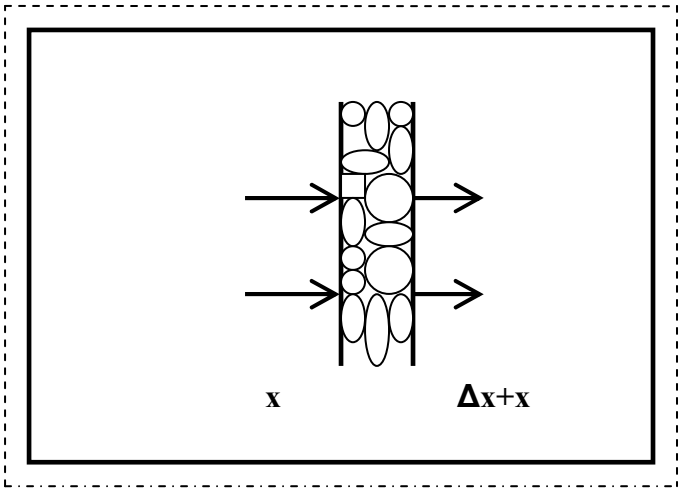

Figure 7. 6. A representative element within a CBM matrix block.

$$\left(\rho uA\Big|_{x+\Delta x} - \rho uA\Big|_{x}\right)\Delta t - \overline{\overline{m}}\Big|^{t+\Delta t} - \overline{\overline{m}}\Big|^{t} + \overline{\overline{\tau}}\Big|^{t+\Delta t} - \overline{\overline{\tau}}\Big|^{t} = \rho V_{bm}\phi\Big|^{t+\Delta t} - \rho V_{bm}\phi\Big|^{t} \quad \text{.....(7.20)}$$

where $\overline{\overline{m}}$ is the desorbed gas mass, and $\overline{\overline{\tau}}$ is the mass of the gas entered to the surrounding cleats from the matrix structure. The gas velocity in the matrix structure is estimated from the Fick's law according to the following relationships:

$$u = -\frac{D_{gm} ZRT}{P_{gas}^{matrix}} \frac{dc}{dx} \quad \text{.....(7.21)}$$

$$\rho_{gas} = \frac{P_{gas}^{matrix} Mw}{ZRT} \quad \text{.....(7.22)}$$

Substituting Equations 7.21 and 7.22 in Equation 7.20 and after some rearrangement we have:

$$\vec{\nabla} \bullet \left(\vec{D}_{gm} \bullet \vec{\nabla} c\right) + \frac{1}{V_b Mw} \frac{d\overline{\overline{m}}}{dt} - \frac{1}{V_b Mw} \frac{d\overline{\overline{\tau}}}{dt} = -\frac{1}{RT} \frac{d}{dt}\left(\frac{P_{gas}^{matrix}}{Z}\phi\right) \quad \text{.....(7.23)}$$

For one dimensional matrix-cleat system Equation 7.23 becomes:

$$\frac{\overline{D}_{gm} F_S V_b}{S_f^2}(\Delta c) = -\frac{1}{V_b Mw}\frac{d\overline{\overline{\tau}}}{dt} = \frac{1}{RT}\frac{d}{dt}\left(\frac{P_{gas}^{matrix}}{Z}\phi\right) + \frac{1}{V_b Mw}\frac{d\overline{\overline{m}}}{dt} \quad \text{.....(7.24)}$$

1.a. High Rank Coal with Extremely Low Matrix Porosity (Close to Zero)

The simplest case to model a coalbed methane reservoir is a single component gas (methane) and single phase gas flow. The simulation procedure is described in Appendix 5.1.

Equation A5.15 is applied for two different scenarios. First scenario involves the gas diffusion through the matrix structure as the limiting process. Therefore, the gas diffusivity in the matrix micropores is relatively small. The product of this small value and the concentration gradient results in even a smaller value. The second scenario involves the desorption process as the limiting process. Therefore, even if the gas diffusivity coefficient has a large value, the product of this value and the concentration difference will be moderately small. For illustration purposes, a portion of a CBM reservoir with drainage area of 2,500 ft^2, height of 15 ft, temperature of 100 ^oF, and initial pressure of 1,300 psia is considered. The methane isotherm properties are given as: a_{Vm}= 120, b_{Vm}=434, a_D=0.0009, b_D=0.131, Po= 6430 psia.

Scenario 1. The gas diffusivity throughout the matrix macropores is considered as the limiting process. The gas desorption rate is so slow that the whole desorbed gas is immediately produced. However, the gas micropore diffusion mechanism would have been able to transfer more gas, had there been more

desorbed gas available. Figure 7.7 shows the cumulative gas production due to micropore and macropore diffusion mechanisms. The cumulative gas production curve is same as the cumulative desorbed gas, because desorption is the limiting process. Figure 7.8 shows the average reservoir pressure decline versus time. The decline rate is very slow because the gas production rate is small. Figure 7.9 shows the same phenomenon for the gas production rate.

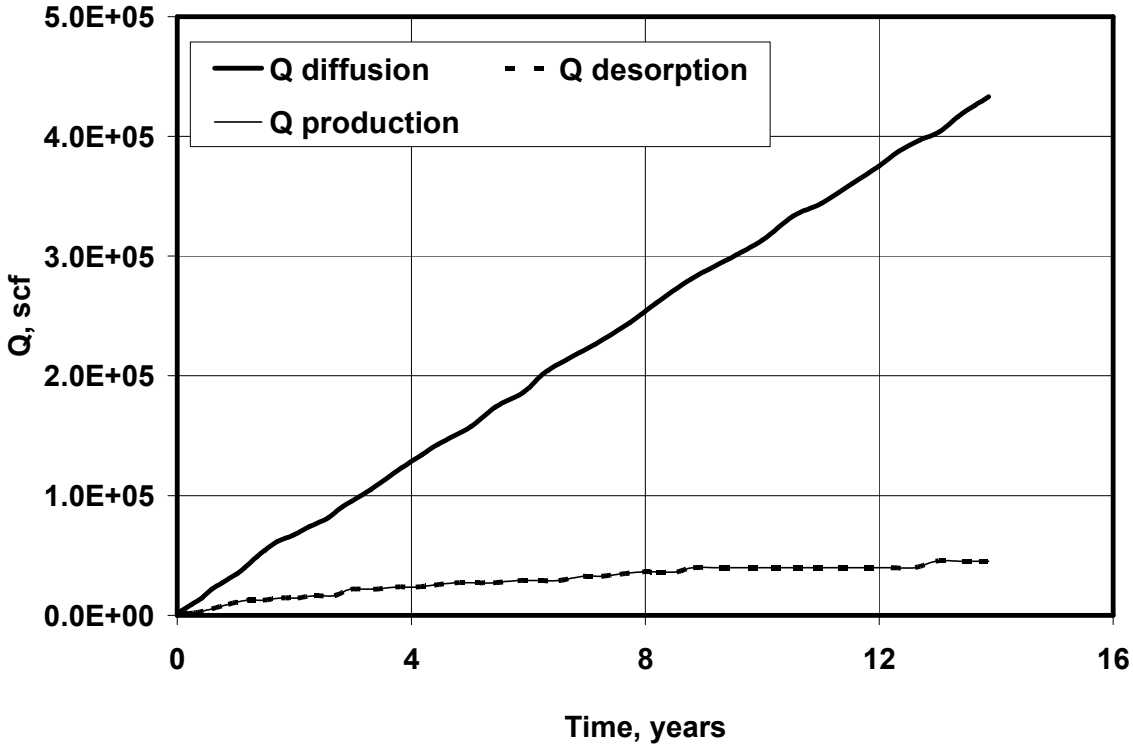

Figure 7. 7. Cumulative gas production versus the production time, the gas diffusion in the matrix macropores is the limiting process (K_{mic} = 1.05E-4 Day^{-1}, K_{mac} = 0.4 Day^{-1}).

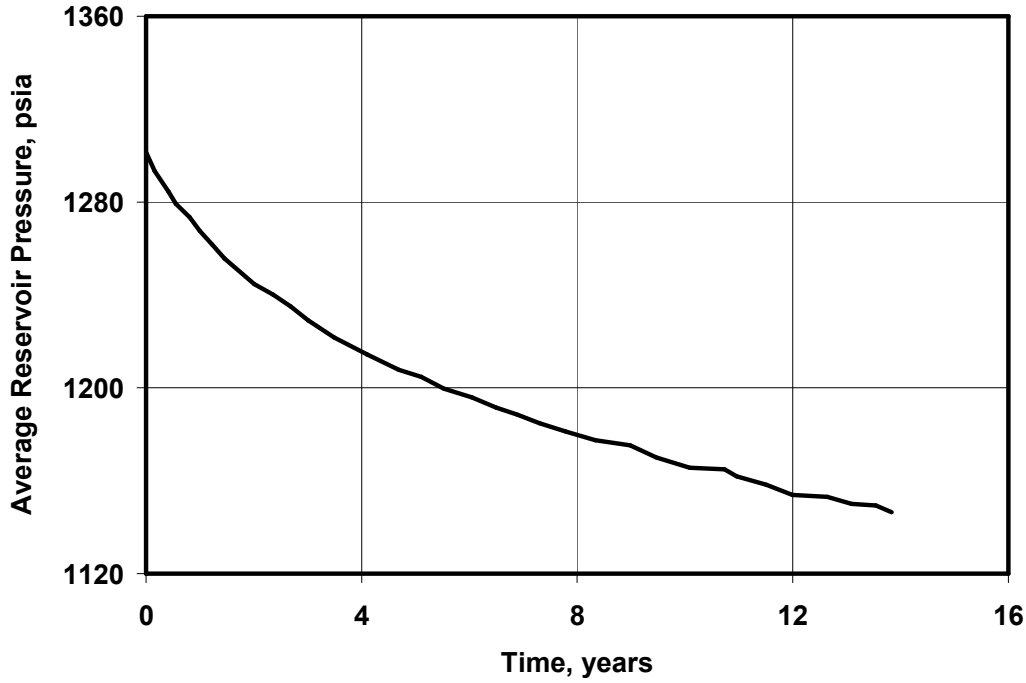

Figure 7. 8. Average reservoir pressure versus time the gas diffusion in the matrix macropores is the limiting process (K_{mic} = 1.05E-4 Day^{-1}, K_{mac} = 0.4 Day^{-1}).

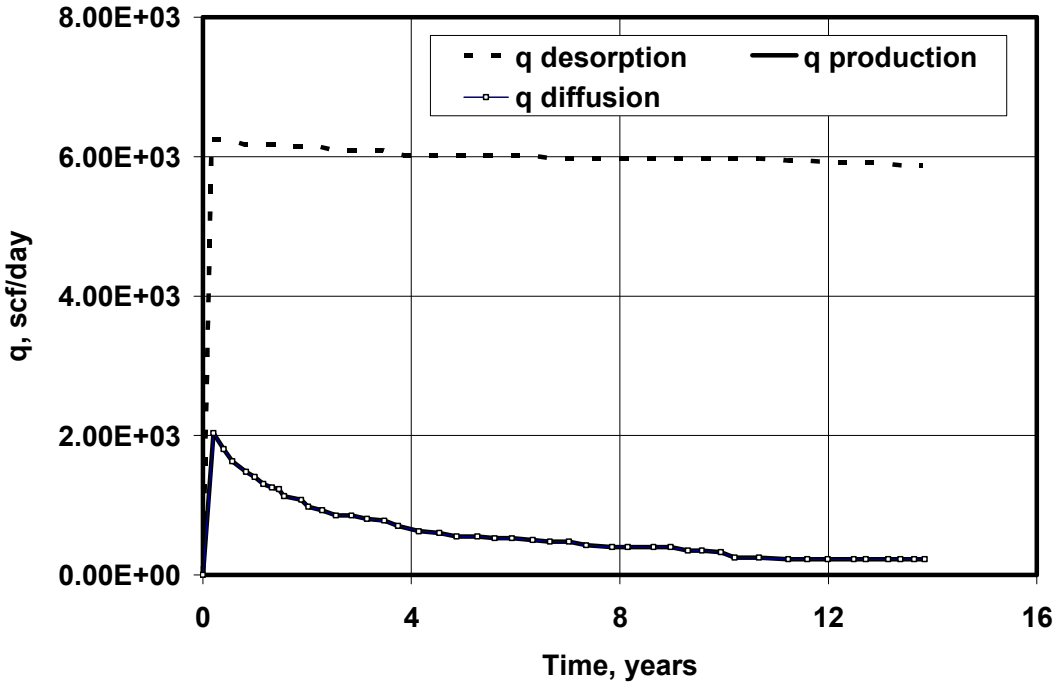

Figure 7. 9. Gas production rate versus time the gas diffusion in the matrix macropores is the limiting process (K_{mic} = 1.05E-4 Day^{-1}, K_{mac} = 0.4 Day^{-1}).

Scenario 2. The gas diffusion through the matrix micrpores is the limiting process. In this scenario, the gas desorption rate is high, but the rate to transfer the desorbed gas to the surrounding cleats is slow. Figure 7.10 shows the cumulative gas production due to micropore and macropore diffusion mechanisms. The cumulative gas production curve is same as the cumulative diffused gas, because the gas diffusion throughout the matrix micropores is the limiting process. Figure 7.11 shows the average reservoir pressure decline versus time. The decline rate is relatively high because the gas production rate is higher than the previous case. Figure 7.12 shows the same phenomenon for the gas production rate.

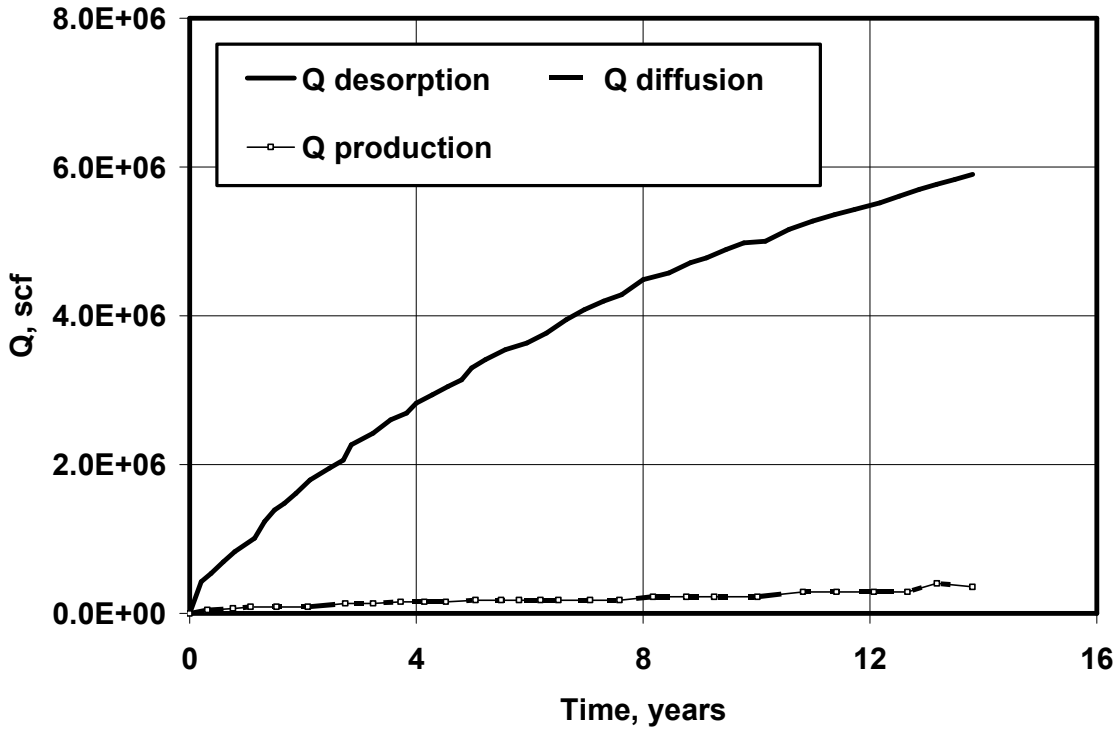

Figure 7. 10. Cumulative gas production versus the production time, the gas diffusion in the matrix micropores is the limiting process (K_{mic} = 1.05E-4 Day^{-1}, K_{mac} = 0.02 Day^{-1}).

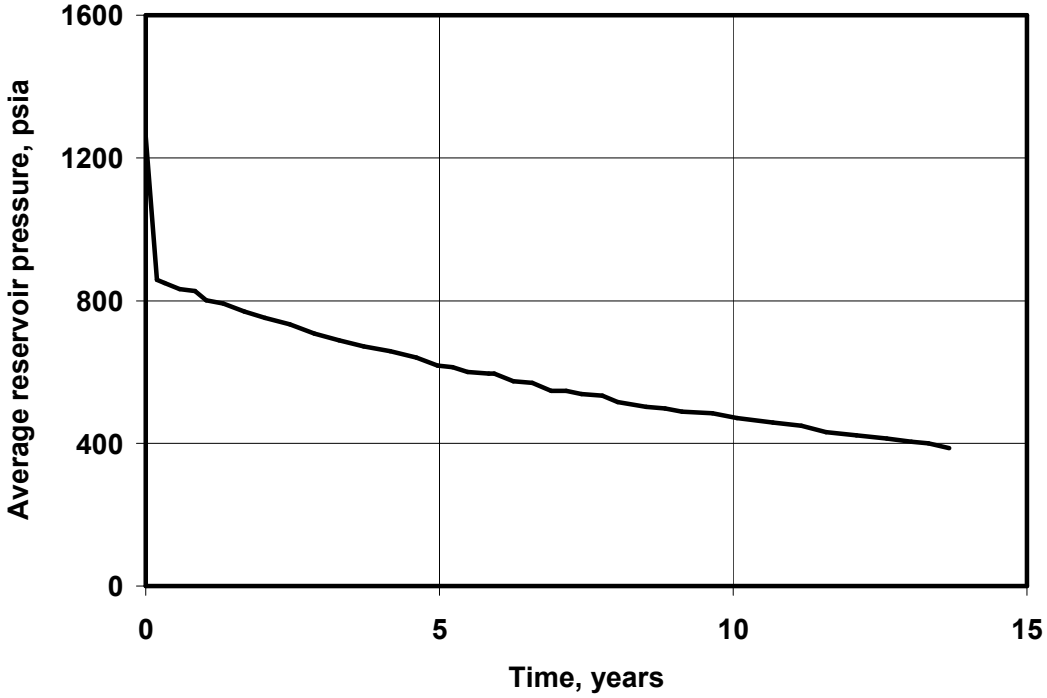

Figure 7. 11. Average reservoir pressure versus time, the gas diffusion in the matrix micropores is the limiting process (K_{mic} = 1.05E-4 Day^{-1}, K_{mac} = 0.02 Day^{-1}).

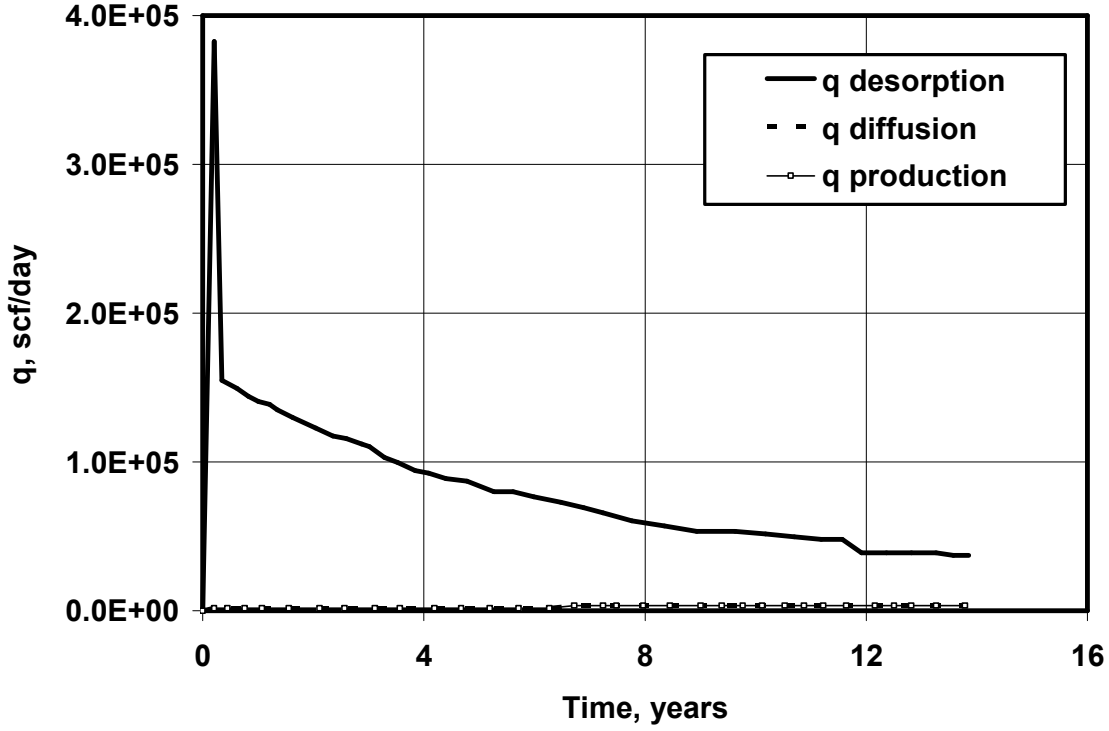

Figure 7. 12. Gas production rate versus time the gas diffusion in the matrix micropores is the limiting process (K_{mic} = 1.05E-4 Day^{-1}, K_{mac} = 0.02 Day^{-1}).

Scenario 3. The gas diffusion through both the matrix micropores and macropores is the limiting process. In this scenario it is assumed that for sometime gas production is limited by gas desorption and at other times by gas diffusion. Figure 7.13 indicates that in the early time of the reservoir gas production life the gas diffusion through the matrix micropores is the limiting process. However, the time dependencies of the gas desorption becomes the limiting process after 2.4 years. Figure 7.14 shows the average reservoir pressure changes with the production time for both the desorption and diffusion dominant regions. Figure 7.15 indicates two distinct regions for the gas production rate for the desorption and diffusion dominant processes. This is the case mainly when reservoir matrix properties change due to the gas production and formation damage mechanisms.

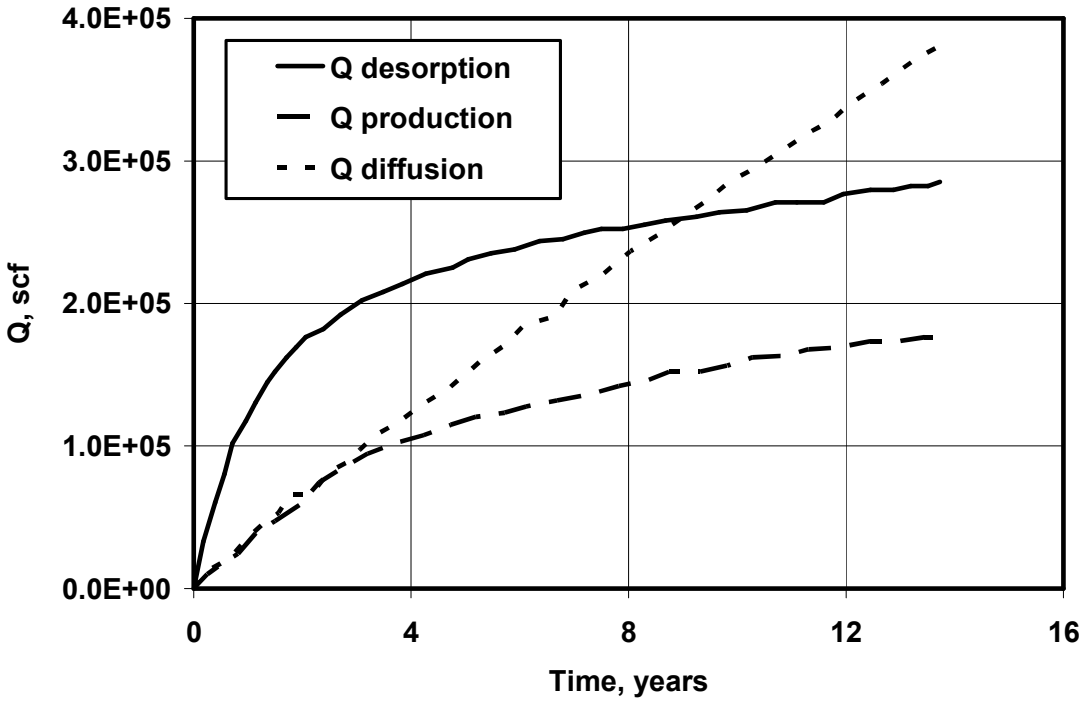

Figure 7. 13. Cumulative gas production versus the production time, the gas diffusion in the both matrix micropores and macropores is the limiting process (Kmic = 1.05E-4 Day^{-1}, K_{mac} = 0.2 Day^{-1}).

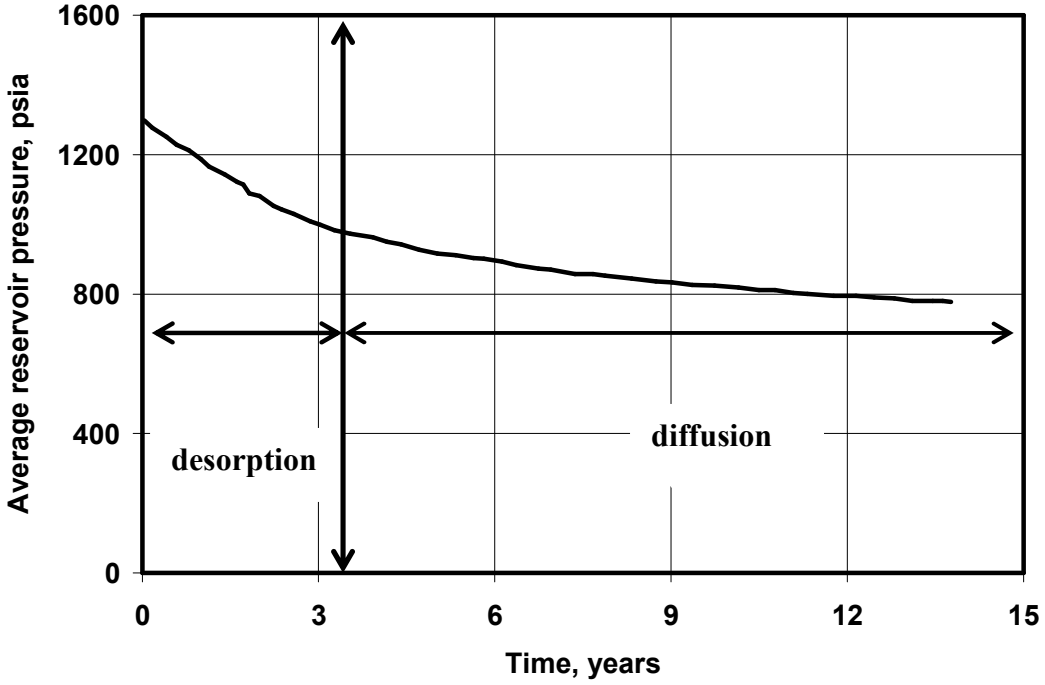

Figure 7. 14. Average reservoir pressure versus time the gas diffusion in the both matrix micropores and macropores is the limiting process (K_{mic} = 1.05E-4 Day^{-1}, K_{mac} = 0.2 Day^{-1}).

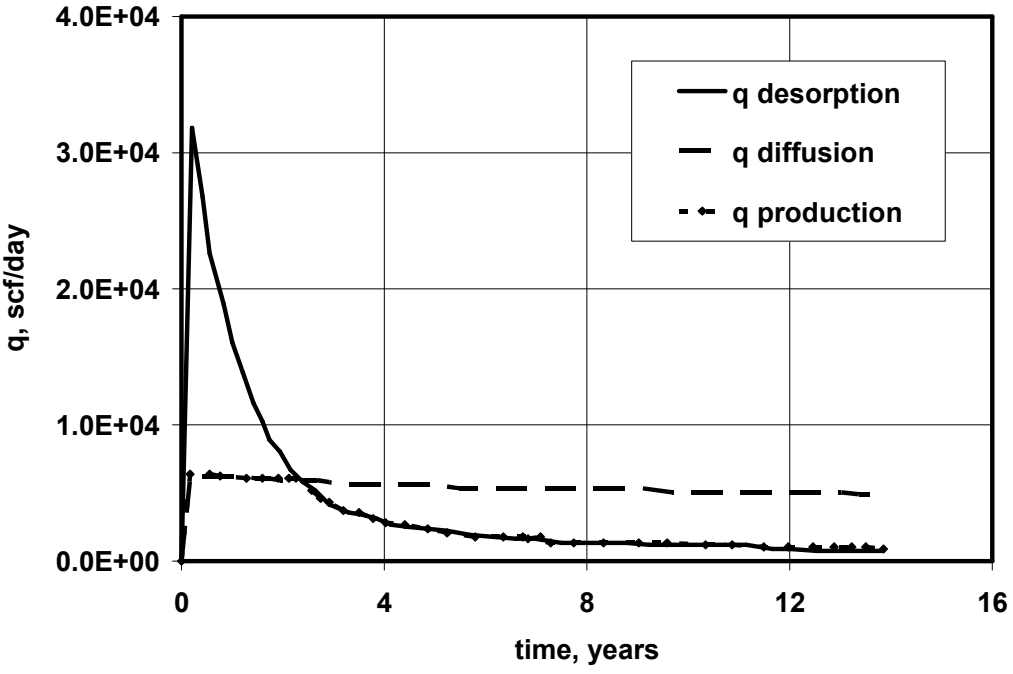

Figure 7. 15. Gas production rate versus time the gas diffusion in the both matrix micropores and macropores is the limiting process (K_{mic} = 1.05E-4 Day^{-1}, K_{mac} = 0.2 Day^{-1}).

1.b. Low rank Coals and Shale with Relatively Higher Matrix Porosity

The low rank coals and shale reservoirs contain higher matrix porosity and therefore, the free methane stored in the matrix pore spaces is comparable with the adsorbed methane in the matrix coal internal surfaces. The governing equations for this case are explained in Appendix 5.2. For the case of low rank coals and shale with higher matrix porosity various scenarios can be considered. These scenarios help studying and history matching different behaviors of coalbed methane and shale gas reservoirs under different conditions as illustrated in the following.

Scenario 1. The matrix porosity is so high that the available free gas in the matrix structure is the limiting process. Therefore, the coalbed or shale gas production is dominated by the produced gas from the matrix pore structure. In this case, usually the gas diffusion and gas desorption rates are very low. All the diffused gas is contributed by the free gas in the matrix structure. However, when the free gas is totally produced, the desorbed gas will contribute for the rest of the reservoir life. These type of reservoirs are usually non economical to produce. Because, the production rate is very slow. The matrix stimulation and somehow increasing the methane diffusivity throughout the matrix may increase the reservoir productivity.

Figure 7.16 shows the cumulative production of a coalbed methane reservoir with the characteristics indicated in the previous section. The main difference between this case and the previous case is the higher matrix porosity. The matrix porosity in this case is assumed to be 5%. According to Figure 7.17, the complete reservoir production comes from the free gas stored in the matrix pore structure because the diffusion rate is very low. Figure 7.17 shows the gas production rate for this

reservoir. Figure 7.18 shows the average reservoir pressure versus the production time. The reservoir average pressure does not drop appreciably over 15 years of the reservoir life.

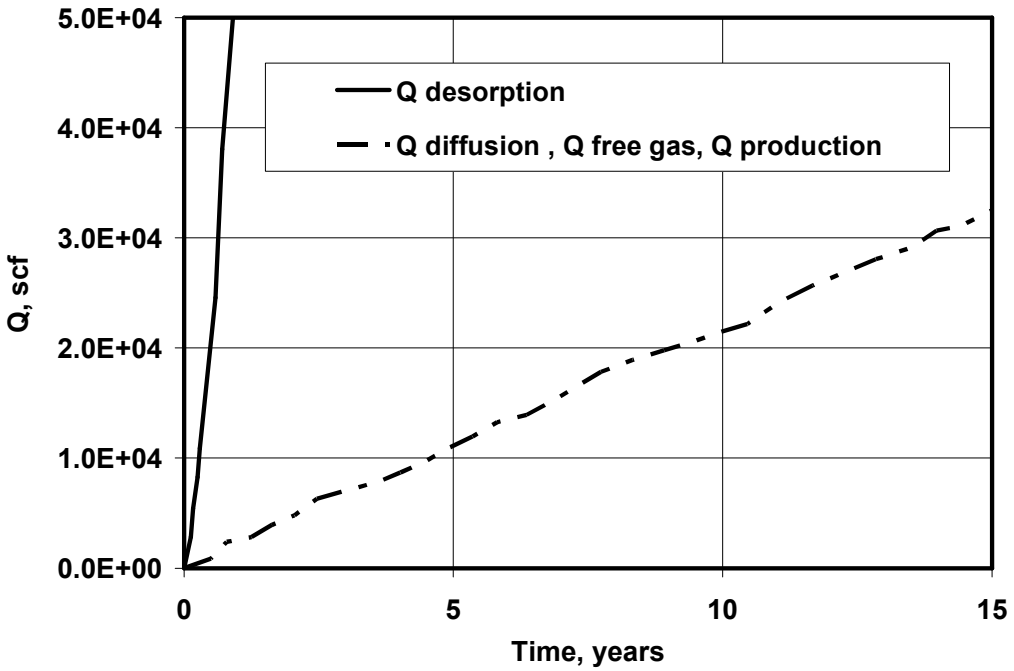

Figure 7. 16. Cumulative gas production versus the production time, the gas production from the matrix pore structure is the limiting process. ϕ_{matrix} = 0.05, K_{mic} = 2.1E-5 Day^{-1}, K_{mac} = 1.0E-5 Day^{-1}.

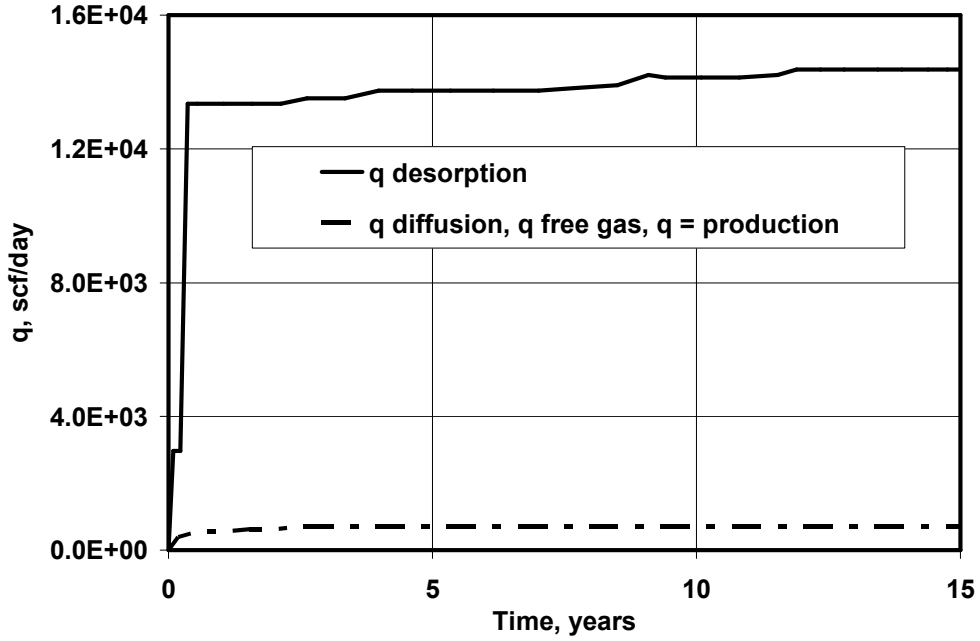

Figure 7. 17. Gas production rate versus time the gas production from the matrix pore structure is the limiting process. ϕ_{matrix} = 0.05, K_{mic} = 2.1E-5 Day^{-1}, K_{mac} = 1.0E-5 Day^{-1}.

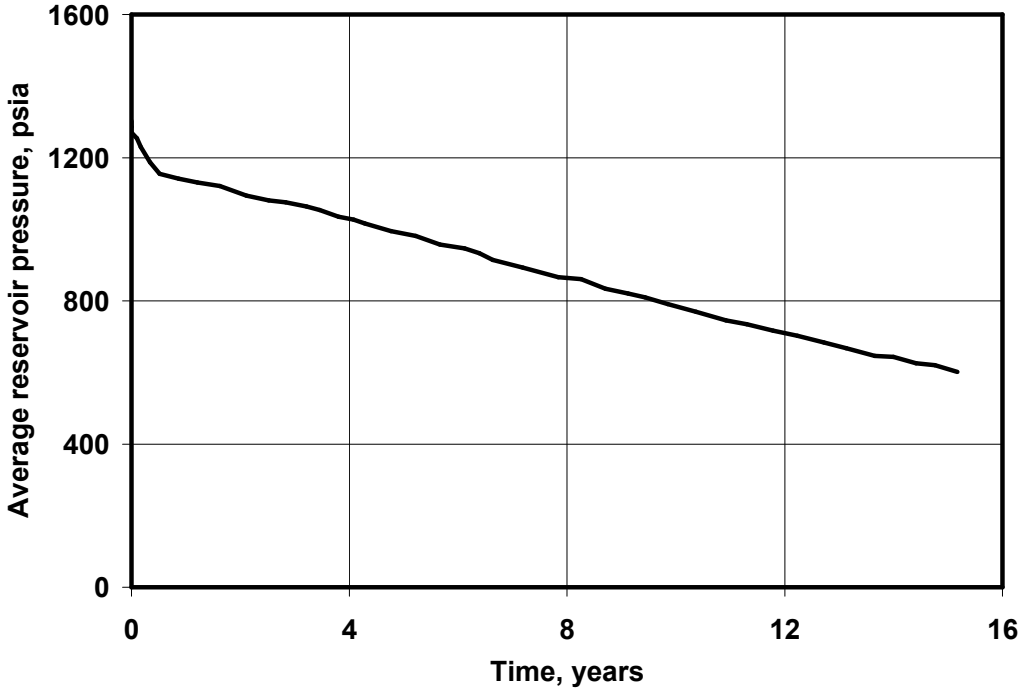

Figure 7. 18. Average reservoir pressure versus time the gas production from the matrix pore structure is the limiting process. ϕ_{matrix} = 0.05, K_{mic} = 2.1E-5 Day^{-1}, K_{mac} = 1.0E-5 Day^{-1}.

Scenario 2. The second scenario involves the case that the matrix free gas and the gas diffusion through the matrix macropores act together as the limiting processes. Therefore, the free gas is completely produced after sometime of the reservoir life and then the desorbed gas is being produced. However, the matrix macropore diffusion rate is slower than the gas desorption rate. Figures 7.19, 7.20, and 7.21 show the cumulative production, production rate, and reservoir average pressure versus the production time. The average reservoir pressure drops faster than the previous case. The gas production rate is also higher than the previous case. However, if there was any method available to increase the gas matrix diffusivity in the matrix macropores, the gas production rate would have been increased.

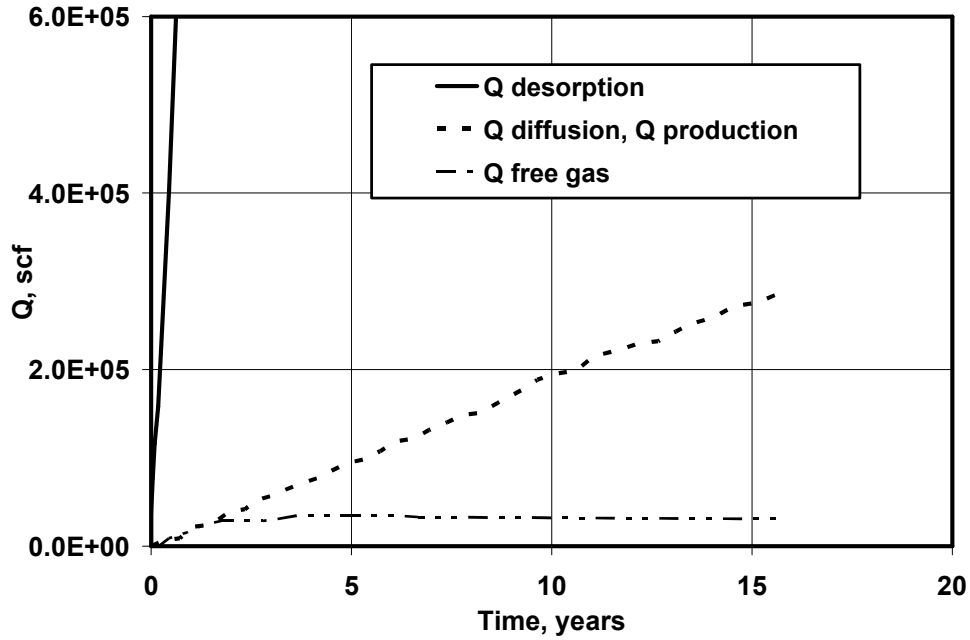

Figure 7. 19. Cumulative gas production versus the production time, the gas production from the matrix pore structure is the dominant process (ϕ_{matrix} = 0.05, K_{mic} = 2.1E-4 Day^{-1}, K_{mac} = 1.0E-3 Day^{-1}).

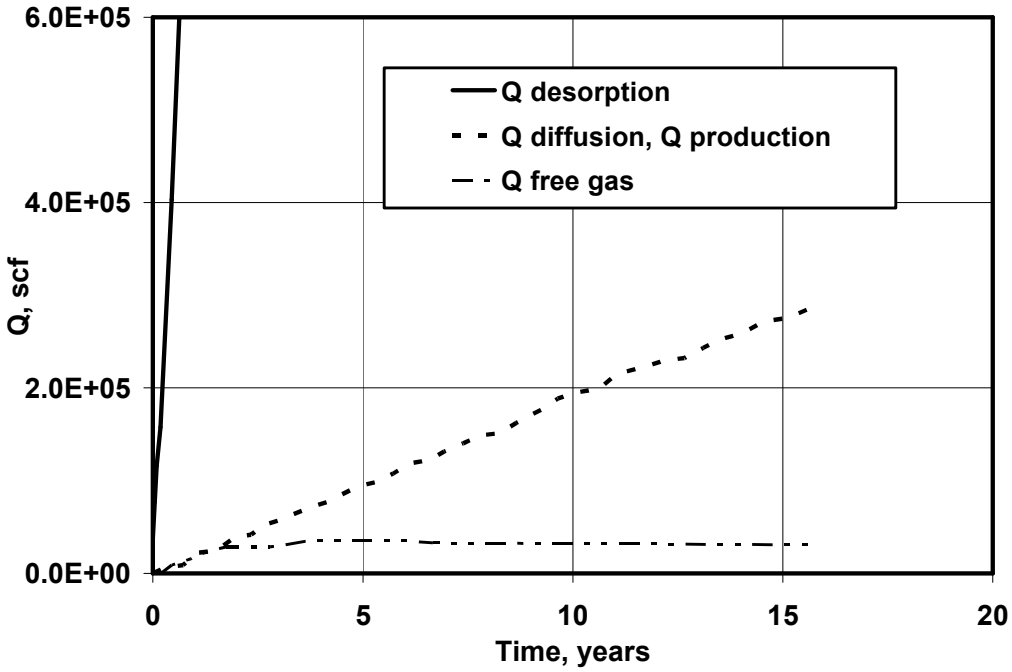

Figure 7. 20. Gas production rate versus time the gas production from the matrix pore structure is the dominant process (ϕ_{matrix} = 0.05, K_{mic} = 2.1E-4 Day^{-1}, K_{mac} = 1.0E-3 Day^{-1}).

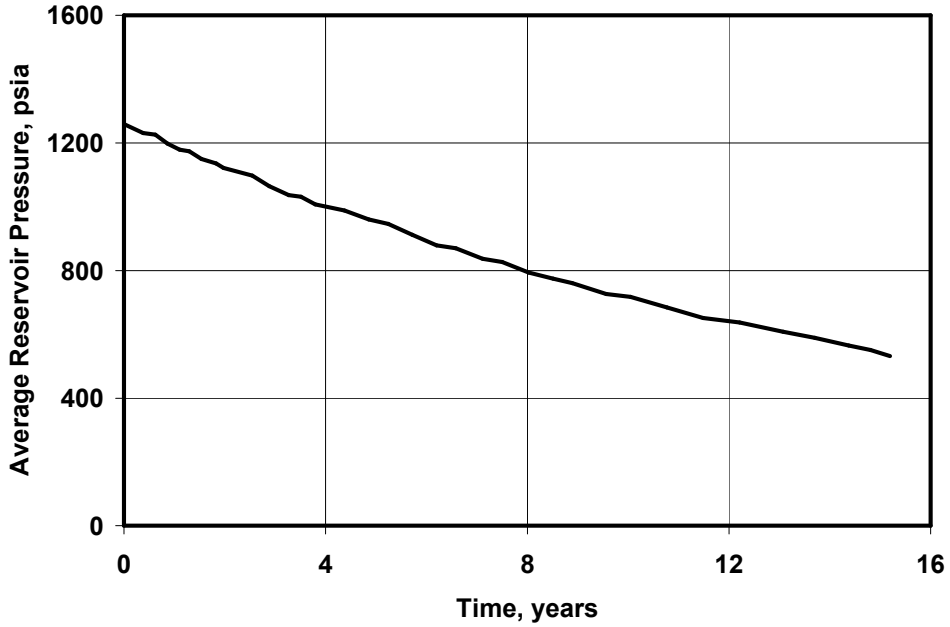

Figure 7. 21. Average reservoir pressure versus time the gas production from the matrix pore structure is the dominant process (ϕ_{matrix} = 0.05, K_{mic} = 2.1E-4 Day^{-1}, K_{mac} = 1.0E-3 Day^{-1}).

Scenario 3. The third scenario involves the case that the free matrix gas and the gas desorption through the matrix micropores are together acting as the limiting processes. Therefore, the free gas is totally produced after sometime of the reservoir gas production life and then the desorbed gas is produced. However, the matrix micropore desorption rate is slower than the gas matrix macropores diffusion rate. Figures 7.22, 7.23, and 7.24 show the cumulative production, production rate, and reservoir average pressure versus the production time. The first section of each plot is due to the free gas production from the pores of the matrix structure. The second section is due to the desorbed gas production. Increasing the productivity of these reservoirs is a difficult task.

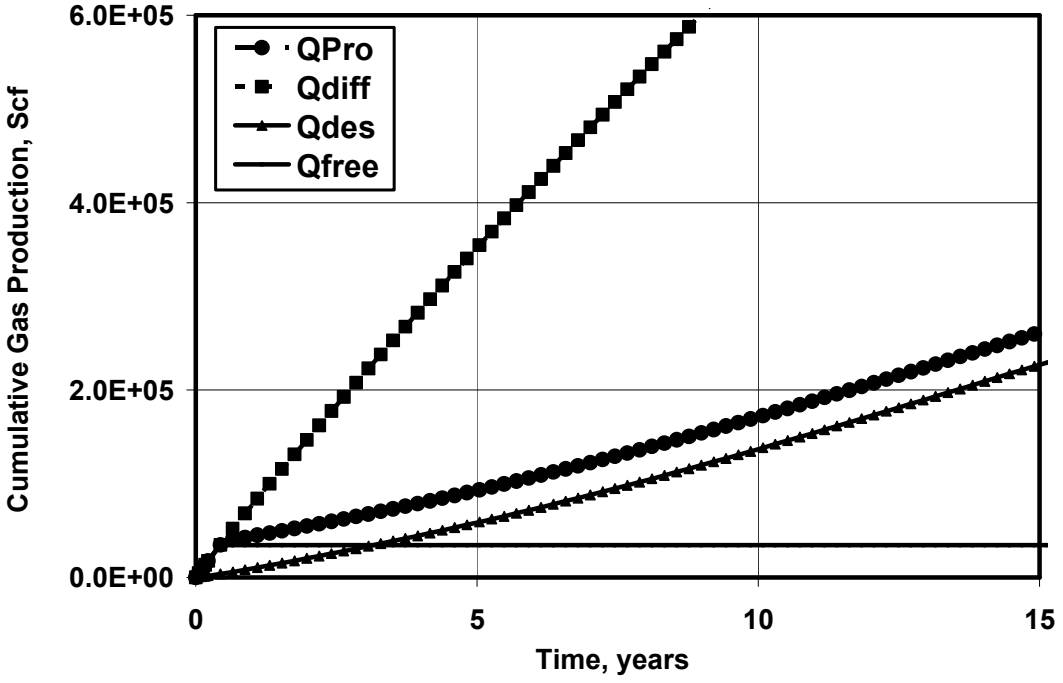

Figure 7. 22. Cumulative gas production versus the production time, the gas production from the matrix pore structure is the dominant process (ϕ_{matrix} = 0.05, K_{mic} = 9.96E-3 Day^{-1}, K_{mac} = 1.0E-6 Day^{-1}).

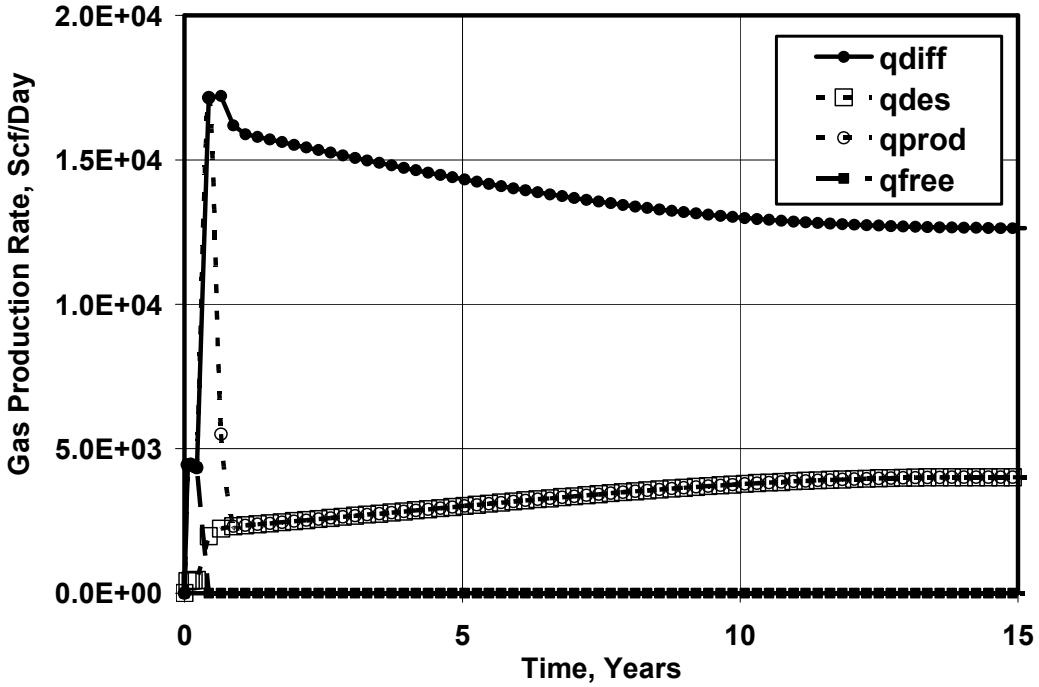

Figure 7. 23. Gas production rate versus production time (the gas production from the matrix pore structure is the limiting process) (ϕ_{matrix} = 0.05, K_{mic} = 9.96E-3 Day^{-1}, K_{mac} = 1.0E-6 Day^{-1}).

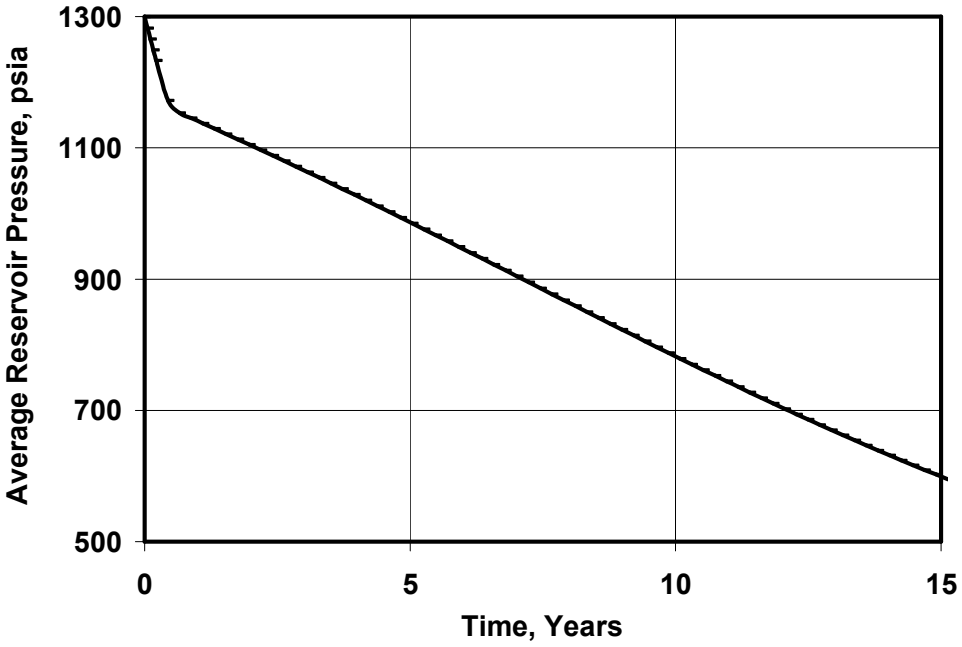

Figure 7. 24. Average reservoir pressure versus time the gas production from the matrix pore structure is the dominant process (ϕ_{matrix} = 0.05, K_{mic} = 9.96E-3 Day^{-1}, K_{mac} = 1.0E-6 Day^{-1}).

There are other scenarios that are combinations of the previously mentioned cases. Each combination may be used to model a specific case of the CBM and shale gas reservoirs.

Case 2. Pure Carbon Dioxide Injection and Methane Production

It was previously mentioned that the coal and shale adsorb carbon dioxide more than methane. Therefore, coal adsorbs carbon dioxide and desorbs the previously adsorbed methane. The adsorption/desorption process in the reservoir scale is described by the following expression. Equation 7.25 is a combination of Equations A5.21 and A5.22.

$$q_{m\,\mathrm{csc}\,i}(t) = -\frac{(K_{mic})_i V_{matrix} RT_{sc}}{P_{sc}} \begin{Bmatrix} \dfrac{P_{sc}\overline{\rho}_{matrix}}{RT_{sc}} \overline{V}_{mi} \exp\left\{-\left[-\overline{D}_i \ln(\mathrm{X})\right]^{r_i}\right\} \\ -\left(\overline{S}_{gasi}^{cleat} - S_{wc}\right) \dfrac{\overline{P}_i^{cleat}}{\overline{Z}_{gasi}^{cleat} R\overline{T}_{cleat}} \end{Bmatrix} \quad \text{.....(7.25)}$$

where the subscribe i refers to the carbon dioxide and methane component. X is defined as:

$$\mathrm{X} = \frac{\overline{P}^{matrix} y_i^{matrix} \phi_i^{matrix}}{P_{oi}} \tanh\left\{2\frac{\overline{P}^{matrix} y_i^{matrix} \phi_i^{matrix}}{P_o}(K_{mac})_i t\right\} \quad \text{.....(7.26)}$$

For the illustration purposes the following cases are considered:

2.a. High rank Coal with extremely low matrix porosity (Close to zero)

For the case of extremely small or zero matrix porosity, the gas component mole fraction in the matrix structure is estimated using the following relationship:

$$y_{CH_4} = \frac{V_{adCH_4}}{V_{adCH_4} + V_{adCO_2}} \quad (7.27)$$

$$y_{CO_2} = 1 - y_{CH_4} \quad (7.28)$$

The carbon dioxide is injected into the coal seam at high pressures. Therefore, the injected carbon dioxide temperature may be much lower than the reservoir temperature. The mixing of the injected carbon dioxide and the original reservoir fluids (water and methane) may alter the coalbed methane cleat properties including cleat permeability and porosity. The following equations are applied to describe the coal cleat properties alterations as a result of the injected fluid temperature changes.

$$\Delta\sigma_T = -\frac{E(1-\nu)}{3(1-2\nu)(1+\nu)} a_S \Delta T \delta_{ij} \quad (7.29)$$

$$a_S = 1 - \frac{K}{K_S} \quad (7.30)$$

where, $\Delta\sigma_T$ is the effective stress tensor due to the temperature difference (psi), a_S is the coefficient of thermal expansion of solid (K^{-1}), T is the temperature (Kelvin), k is the drained bulk modulus of rock, k_s is the of the mineral constituent, δ_{ij} is kroneker delta. The term ΔT refers to the temperature difference between injected carbon dioxide and coal matrix. The coal matrix temperature variations are estimated applying energy conservation law:

$$\rho C_P \left(\frac{\partial T}{\partial t} + \vec{V} \bullet \vec{\nabla} T \right) = -\vec{\nabla} \bullet q + A \quad (7.31)$$

$$\vec{q} = -k \bullet \vec{\nabla} T \quad (7.32)$$

$$\frac{\partial T}{\partial t} + \vec{V} \bullet \vec{\nabla} T = \frac{K}{\rho C_P} \nabla^2 T + \frac{A}{\rho C_P} \quad \text{.....(7.33)}$$

where, $a^2 = \frac{K}{\rho C_P}$ is the thermal diffusivity coefficient, ρ is the density of the fluid, C_P is the fluid heat capacity, T is the temperature, t is time, V is the velocity of the fluid, K is thermal conductivity, A is the energy generated per volume, and q is heat flux. The fluid velocity in the cleat structure is estimated using the Darcy's law as following:

$$\vec{V} = -\frac{k}{\mu} \vec{\nabla} \left(p \pm \rho g z \right) \quad \text{.....(7.34)}$$

For illustration purposes the same reservoir explained in the previous section is subjected to the CO_2 injection with the following information:

CO_2 injection rate: 1 Mscf/day, E : 4.21E+5 psi, υ: 0.35, α_{CH4}: 1.0E-7 ft^3/scf, α_{CO2} : 1.0E-7 ft^3/scf, k_o: 10 md, φ_o: 0.004, c_f: 9.6E-4psi^{-1} δ_{ij} : 1.0, a_S : 1.0E-6 $^oK^{-1}$, T_{in}: 323 K.

The coal matrix swelling/shrinkage due to the coal shrinkage/swelling will affect coal cleat porosity and permeability. These alterations are expressed using Equations 7.16 and 7.17. In the reservoir condition, several parameters may affect the CO_2 sequestration and methane production processes. The reservoir temperature, mechanical properties, and methane and carbon dioxide macropore and micropore apparent diffusivity coefficients are some of the most important parameters.

Figure 7.25 indicates that the under given conditions, for 5 Scf adsorbed carbon dioxide 1 Scf methane is desorbed. Figure 7.26 shows that the carbon dioxide injection increases methane production almost 2 times as the case without injection. Figure 7.27 shows that the carbon dioxide pressure in the coal matrix slowly increases, whereas, the methane pressure and system total pressures decrease. Figure 7.28 shows the similar trend for the mole fraction of the adsorbed carbon dioxide and desorbed methane for a given system of coal. Figures 7.29 and 7.30 show the coal cleat porosity and permeability alteration with respect to the production time. Because, the cleat gas pressure, the methane production makes the coal shrink. However, the carbon dioxide injection makes the coal matrix swell. The difference between these two phenomena will result either in coal matrix net swelling or shrinkage. The coal matrix swelling and shrinkage will affect the coal cleat properties. Figures 7.31 and 7.32 indicate that the matrix permeability and porosity start declining after 2 years because the carbon dioxide imbibitions rate is higher than the methane production rate. The other parameter that may affect coal cleat properties is the temperature difference between the coal and injected carbon dioxide. Figure 7.33 shows that after a rapid reduction in the coal cleat permeability in the beginning of the injection operation, the cleat permeability and porosity declines smoothly over the injection time. This phenomenon may be important in the beginning of the carbon dioxide injection. However, after some time, the reduction or incremental rate will be insignificant when the temperature difference between the coal and matrix is small.

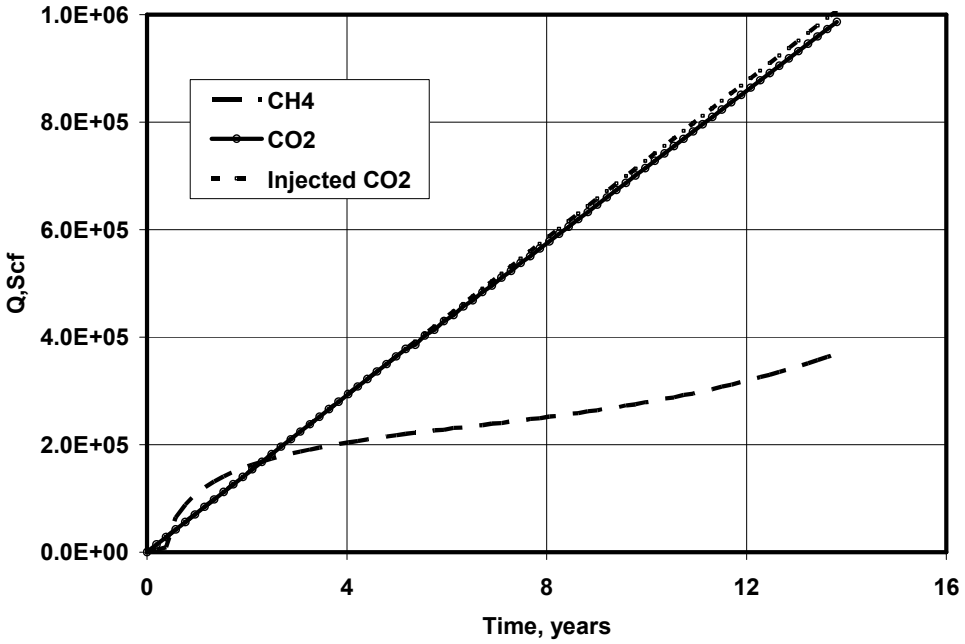

Figure 7. 25. Methane production and carbon dioxide injected rates versus time, $(K_{mic})_{CH4}$ = 1.05E-4 Day^{-1}, $(K_{mac})_{CH4}$ = 1.0E-2 Day^{-1}, $(K_{mic})_{CO2}$ = 5.24E-4 Day^{-1}, $(K_{mac})_{CO2}$ = 1.0E-2 Day^{-1}.

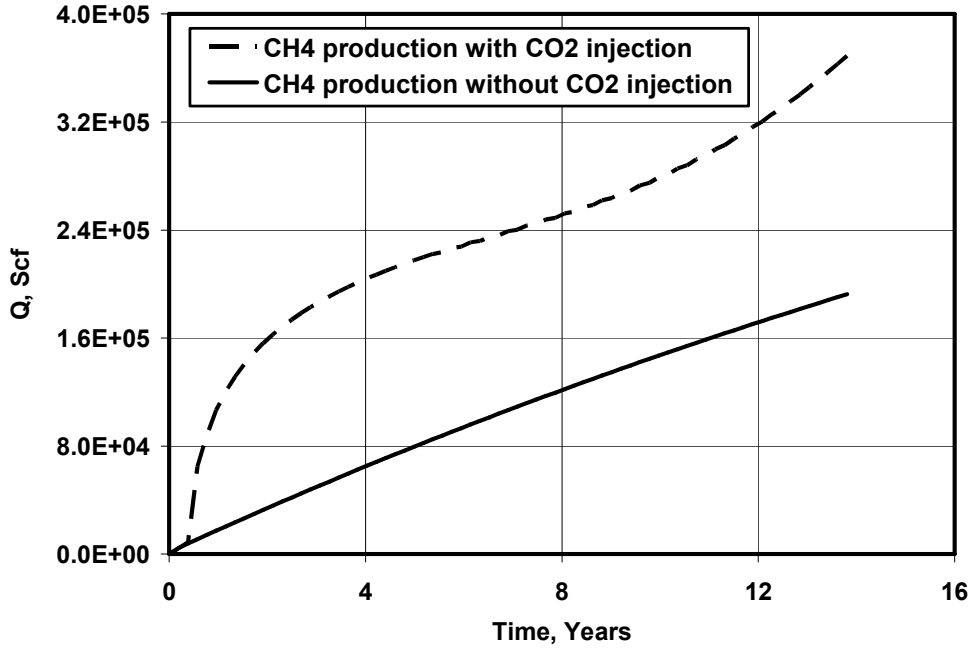

Figure 7. 26. Methane production with (WI) and without (WOI) carbon dioxide injection, $(K_{mic})_{CH4}$ = 1.05E-4 Day^{-1}, $(K_{mac})_{CH4}$ = 1.0E-2 Day^{-1}, $(K_{mic})_{CO2}$ = 5.24E-4 Day^{-1}, $(K_{mac})_{CO2}$ = 1.0E-2 Day^{-1}.

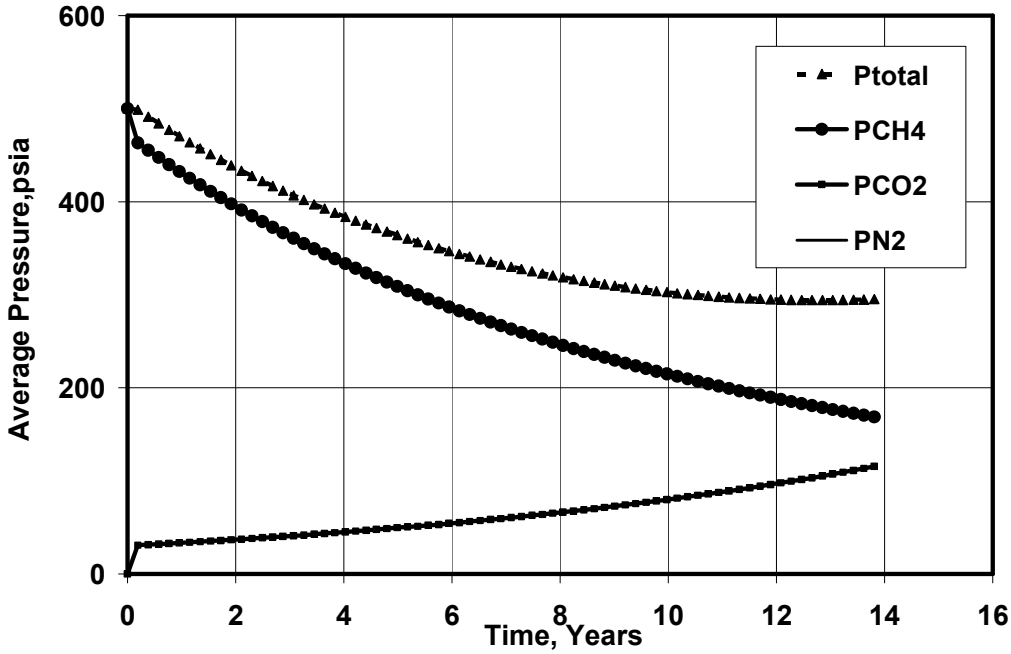

Figure 7. 27. Methane, carbon dioxide and system total pressure versus time, $(K_{mic})_{CH4}$ = 1.05E-4 Day^{-1}, $(K_{mac})_{CH4}$ = 1.0E-2 Day^{-1}, $(K_{mic})_{CO2}$ = 5.24E-4 Day^{-1}, $(K_{mac})_{CO2}$ = 1.0E-2 Day^{-1}.

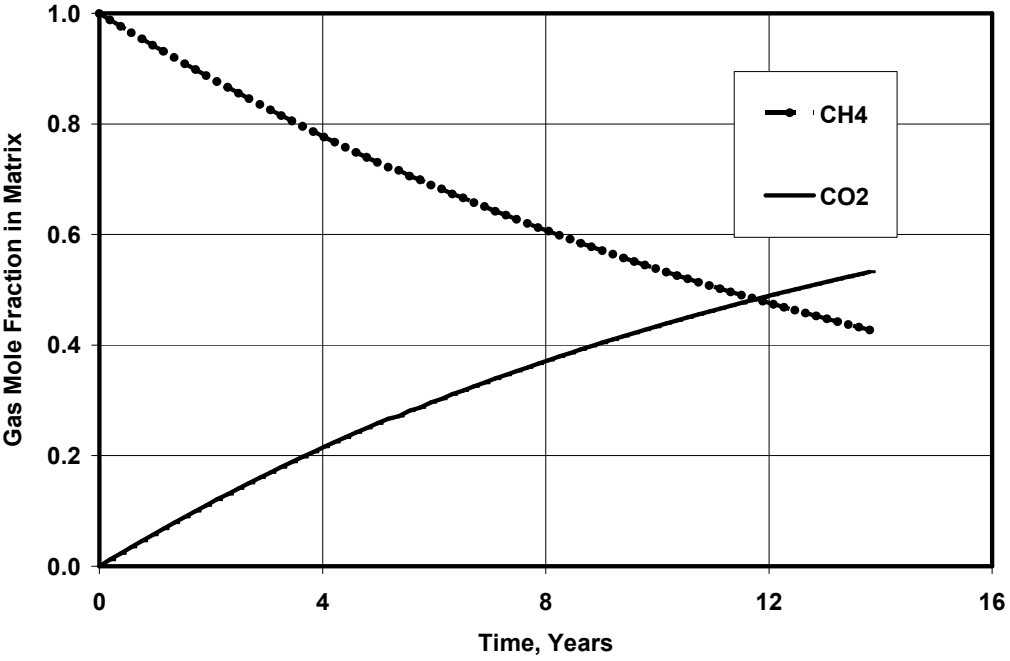

Figure 7. 28. Matrix methane and carbon dioxide mole fractions versus time, $(K_{mic})_{CH4}$ = 1.05E-4 Day^{-1}, $(K_{mac})_{CH4}$ = 1.0E-2 Day^{-1}, $(K_{mic})_{CO2}$ = 5.24E-4 Day^{-1}, $(K_{mac})_{CO2}$ = 1.0E-2 Day^{-1}.

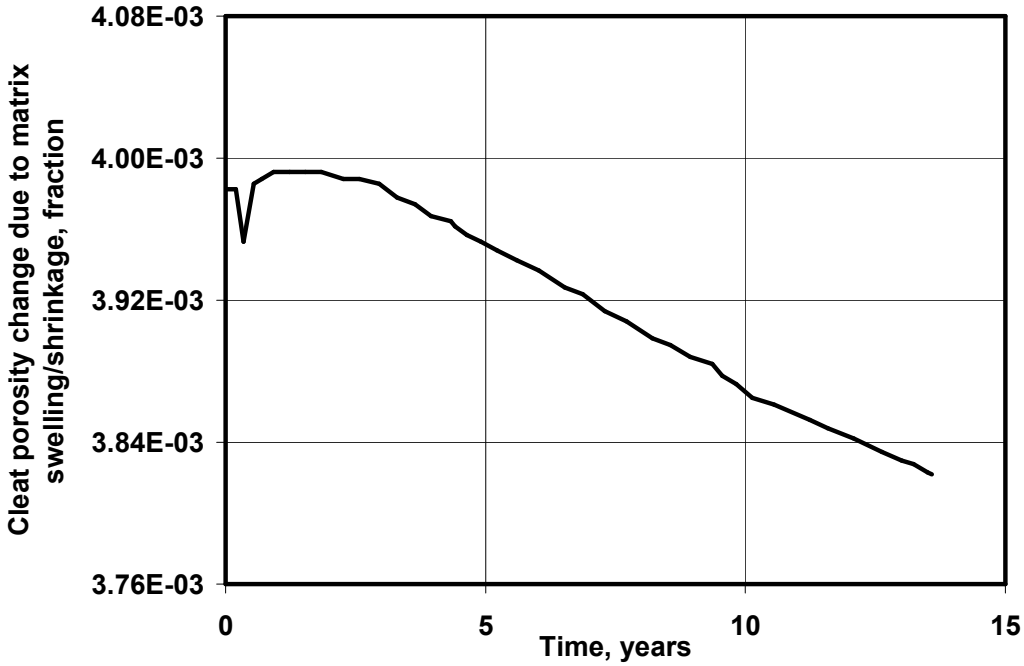

Figure 7. 29. Coal cleat porosity change due to the matrix swelling/shrinkage versus time, $(K_{mic})_{CH4}$ = 1.05E-5 Day^{-1}, $(K_{mac})_{CH4}$ = 1.0E-2 Day-1, $(K_{mic})_{CO2}$ = 5.24E-4 Day-1, $(K_{mac})_{CO2}$ = 1.0E-2 Day^{-1}.

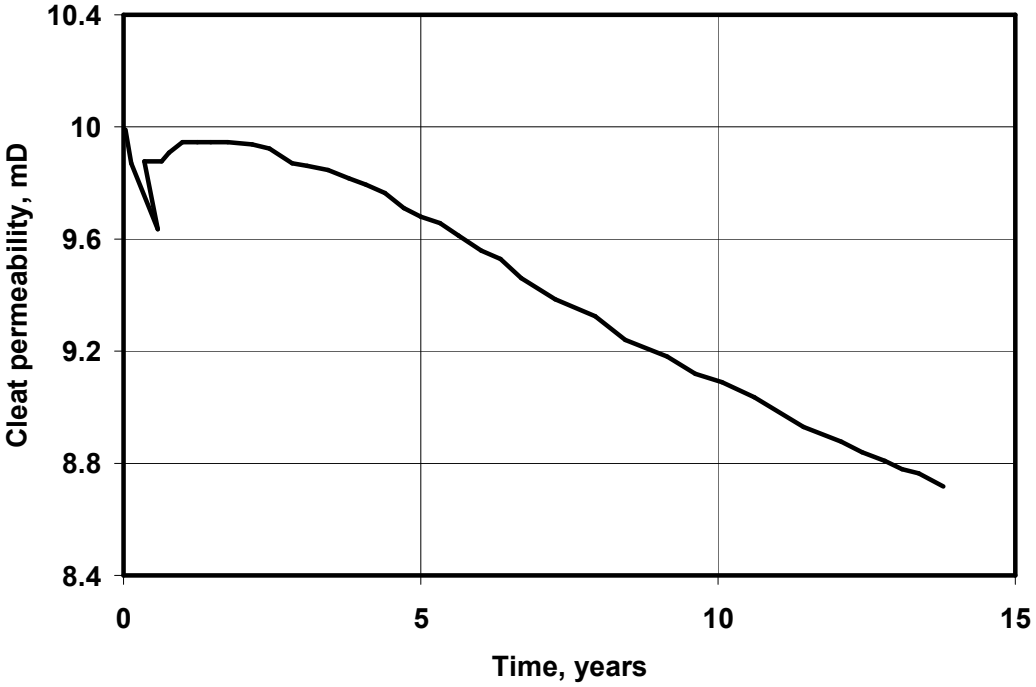

Figure 7. 30. Coal cleat permeability change due to the matrix swelling/shrinkage versus time, $(K_{mic})_{CH4}$ = 1.05E-4 Day^{-1}, $(K_{mac})_{CH4}$ = 1.0E-2 Day^{-1}, $(K_{mic})_{CO2}$ = 5.24E-4 Day^{-1}, $(K_{mac})_{CO2}$ = 1.0E-2 Day^{-1}.

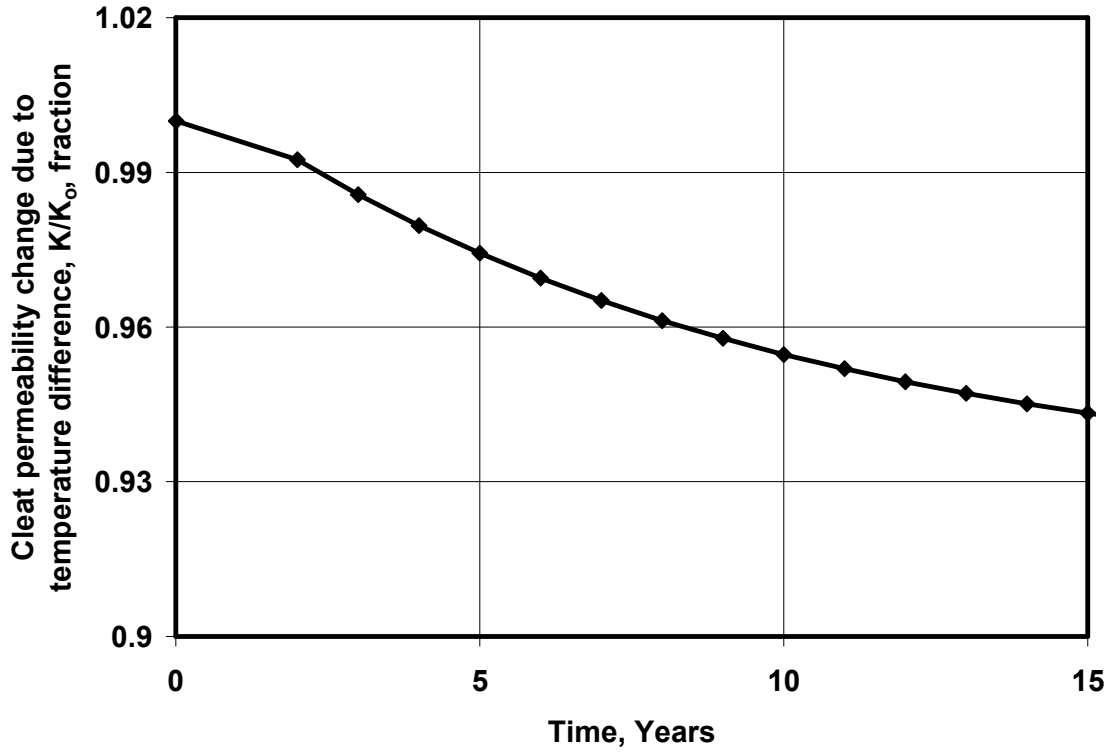

Figure 7. 31. Coal cleat permeability change due to the temperature difference versus time, $(K_{mic})_{CH4}$ = 1.05E-4 Day^{-1}, $(K_{mac})_{CH4}$ = 1.0E-2 Day^{-1}, $(K_{mic})_{CO2}$ = 5.24E-4 Day^{-1}, $(K_{mac})_{CO2}$ = 1.0E-2 Day^{-1}.

Among all mentioned parameters, there are some parameters that we can control and some that depend on the physical properties of the coal and the materials in contact with them and therefore are out of our control. Some of the parameters that we can control are the carbon dioxide injection rate and pressure. Change in the injection rate and pressure will affect the rate of the permeability and porosity reduction and also carbon dioxide sequestration and methane production. However, an economical analysis is necessary to investigate the optimum injection rate and injection pressure for carbon dioxide.

2.b. Low Rank Coals and Shale with Relatively Higher Matrix Porosity

When the coal or shale matrix porosity is significant, like in low rank coals and most of the shale reservoirs, the injected carbon dioxide first fills the pore space of the coal or shale and then adsorbs on the coal internal surfaces. This mechanism can be expressed:

$$\left(q_{m\,\mathrm{csc}}\right)_i = \frac{\left(K_{mic}\right)_i V_b R T_{sc}}{P_{sc}} \left(\Delta C\right)_i = \frac{V_b T_{sc}}{T P_{sc}} \frac{d}{dt}\left[\frac{P_{matrix}\left(y_{mac}^{matrix}\right)_i}{Z_i}\phi_{matrix}\right] + \frac{d\left(\overline{\overline{V}}_{dsc}\right)_i}{dt} \quad \text{.....(7.35)}$$

The matrix pressure and gas mole fractions in the coal matrix are divided into two categories, including micropores and macropores. These values are needed to be calculated for each time step.

$$q_{m\,\mathrm{csc}\,i}(t) = -\frac{\left(K_{mic}\right)_i V_{matrix} R T_{sc}}{P_{sc}} \begin{Bmatrix} \frac{P_{sc}\overline{\rho}_{matrix}}{R T_{sc}} \overline{V}_{mi} \exp\left\{-\left[-\overline{D}_i \ln(X)\right]^{r_i}\right\} \\ -\left(\overline{S}_{gasi}^{cleat} - S_{wc}\right) \frac{\overline{P}_i^{cleat}}{\overline{Z}_{gasi}^{cleat} R \overline{T}_{cleat}} \end{Bmatrix} \quad \text{.....(7.36)}$$

where:

$$X = \frac{\overline{P}_{mic}^{matrix}\left(y_{mic}^{matrix}\right)_i \phi_i^{matrix}}{P_{oi}} \tanh\left[2\frac{\overline{P}_{mic}^{matrix}\left(y_{mic}^{matrix}\right)_i \phi_i^{matrix}}{P_o}\left(K_{mac}\right)_i t\right] \quad \text{.....(7.37)}$$

Like the previous case various scenarios can be considered for this case. However, the results are very similar to the previous section. Therefore, to avoid the repetition, the results of this section are not presented.

Case 3. Mixture of carbon Dioxide and Nitrogen Injection and Methane Production

Carbon dioxide is sequestrated in coal seams to enhance coal gas recovery and reduce the harmful green house gases. Nitrogen is also usually injected with carbon dioxide to improve the coal gas recovery further. Carbon dioxide is adsorbed on the coal internal surface and hence expels out the portion of the previously adsorbed methane. Coal affinity to adsorb nitrogen is significantly less than methane and carbon dioxide. Therefore, the unadsorbed nitrogen in the cleat reduces cleat methane partial pressure, and hence increases the methane potential difference between the cleats and coal adsorption sites.

Coal cleat permeability and porosity alterations by coal matrix shrinkage/swelling due to the coal gas adsorption/desorption process and temperature difference between coal and the injected gas are some of the important parameters that may influence the final coal gas recovery. The success of the simultaneous carbon dioxide and nitrogen injection into the coal seam depends on several parameters including gas mixture injection rate, pressure, mole fraction, and the prevailing reservoir temperature and pressure conditions. For illustration purposes, a portion of the coalbed methane reservoir described in the previous sections is considered for the CO_2/N_2 injection. Various scenarios are discussed in the following section.

Scenario 1. Effect of the Injected CO_2/N_2 Mole Fraction in the Coal Gas Recovery

Figure 7.32 exhibits the equilibrium CO_2, CH_4, and N_2 isotherms utilized in this example. Figure 7.32 indicates that the specified coal in this scenario adsorbs preferentially more carbon dioxide than methane and nitrogen. Figure 7.33 shows

the methane gas production for various mole ratios of CO_2/N_2 gases in the injected gas mixture. The figure indicates that the optimum mole fraction of the nitrogen gas in the CO_2/N_2 mixture is 0.2 for the given system. Any other mole fraction of the nitrogen gas will not result in the optimum cumulative methane production. For the optimum case (20% N_2 and 80% CO_2) the methane recovery factor by as much as 19% in compared with the pure carbon dioxide injection.

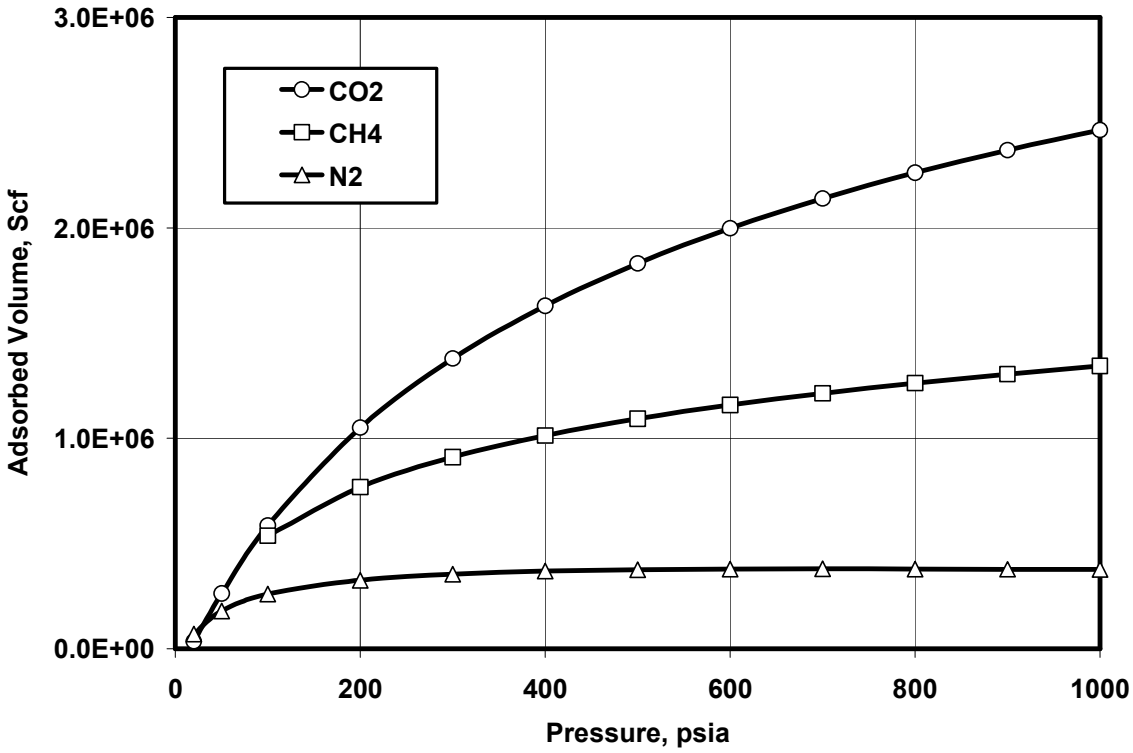

Figure 7. 32. CO_2, CH_4, N_2 adsorbed volumes versus the equilibrium pressure.

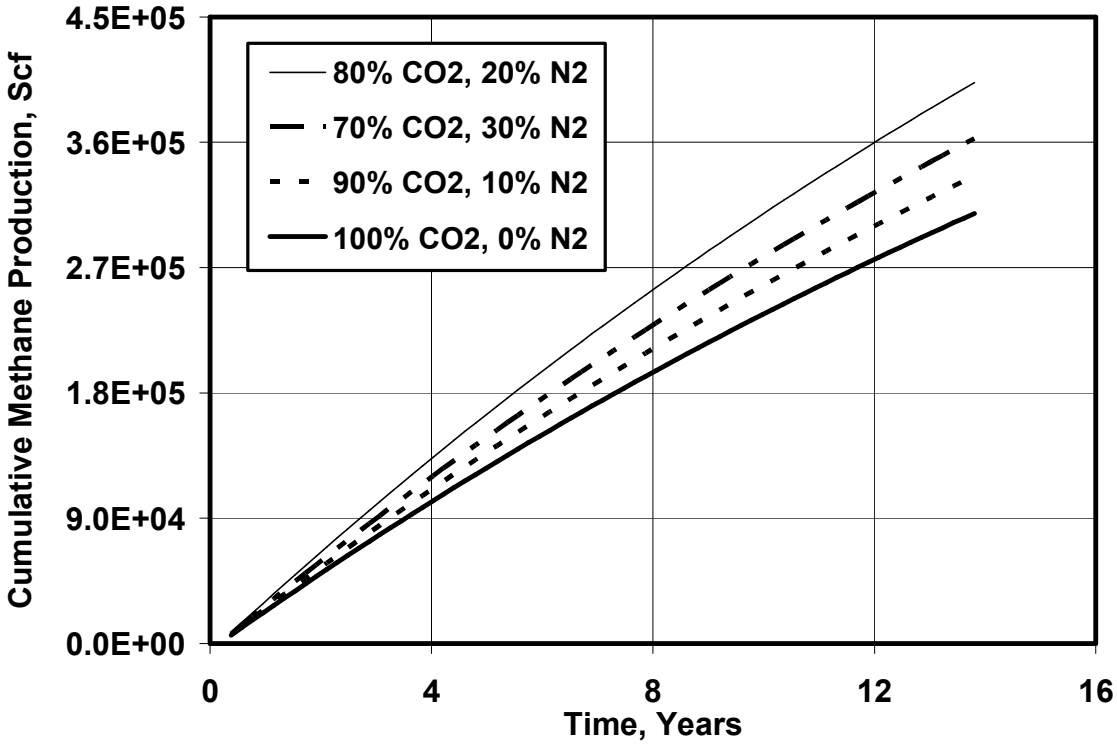

Figure 7. 33. Methane production versus time for various injected CO_2/N_2 ratio. $(K_{mic})_{CH4}$ = 1.05E-4 Day^{-1}, $(K_{mac})_{CH4}$ = 1.0E-2 Day^{-1}, $(K_{mic})_{CO2}$ = 5.24E-4 Day^{-1}, $(K_{mac})_{CO2}$ = 1.0E-1 Day^{-1} $(K_{mic})_{N2}$ = 3.55E-5 Day^{-1}, (K_{mac})N2 = 1.0E-82 Day^{-1}

Scenario 2. Effect of the Injected CO_2/N_2 Ratio in the Coal Gas Recovery

In this example it is considered that the total CO_2/N_2 injection rate remains constant throughout the operation. Therefore, the bottomhole pressure changes due to the constant injection rate. The total methane production is also a function of the initial injection rate. Figure 7.34 shows that the total methane production increases as the injection rate increases. However, there is a limitation in the injection rate. Because, the bottomhole pressure increases as the injection rate increases, indicating that the injection pressure has to increase to overcome the bottomehole pressure. Increasing the injection pressure will result in higher energy requirements and hence will increase the injection operation costs. Moreover, increasing the injection pressure

will decrease the total injected gas temperature. Reduction in the temperature will cause severe damage to the cleat permeability and porosity. Therefore, an optimum injection rate can be found to minimize the cost and damage, and hence, maximize the gas recovery.

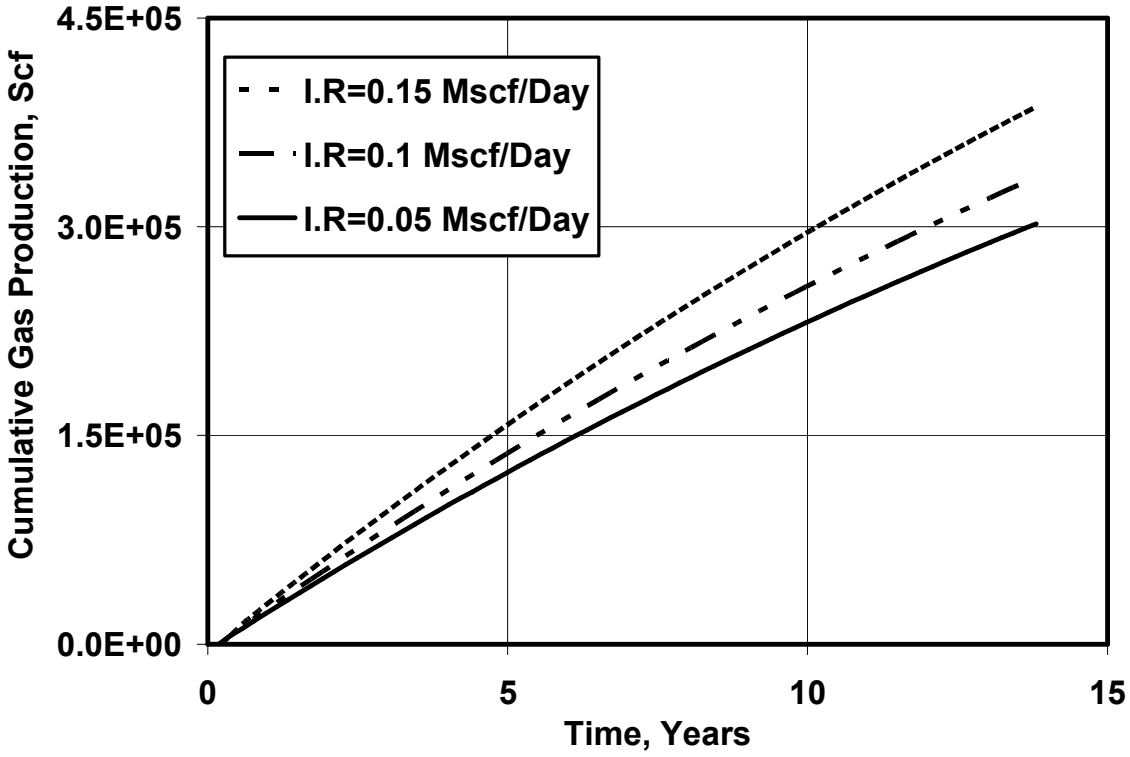

Figure 7. 34. Effect of the injection rate (I.R) on the methane production($K_{mic})_{CH4}$ = 1.05E-4 Day^{-1}, $(K_{mac})_{CH4}$ = 5.01.0E-1 Day^{-1}, $(K_{mic})_{CO2}$ = 5.24E-4 Day^{-1}, $(K_{mac})_{CO2}$ = 1.0E00 $Day^{-1}$$(K_{mic})_{N2}$ = 3.55E-5 Day^{-1}, (K_{mac})N2 = 1.0E-82 Day^{-1}

Figure 7.35 shows the relationships between the final nitrogen gas adsorption in coal, the diffusion and desorption rates. According to this figure, the coal is saturated with nitrogen and does not adsorb the nitrogen gas any further after 5 years of nitrogen injection. However, the gas diffusion appears to be the dominant

N_2 transport mechanisms for the first 5 years and adsorption becomes the limiting process after 5 years. It is also indicated that after 5 years the unadsorbed gas remains free in the cleat structure. The free gas keeps the total pressure in the cleat high and hence prevents matrix swelling due to CO_2 adsorption. Moreover, the partial pressure and hence the concentration of methane gas in the cleat reduces resulting in more methane diffusion to the cleat. For the same system Figure 7.38 shows the relationships between the final carbon dioxide gas adsorption on coal, the diffusion and adsorption rates. According to this figure, carbon dioxide adsorption rate in coal is so high that is out of the range of this figure. However, it is also indicated that, the carbon dioxide injection rate is the limiting process for first 5 years. The gas diffusion becomes the limiting process after 5 years. As a result, some of the injected carbon dioxide remains free and unadsorbed in the cleat after 5 years. However, the ratio of the unadsorbed to adsorbed CO_2 is very small and almost negligible for this system. Figure 7.39 also indicates that the methane production is mainly limited by methane gas diffusion throughout the matrix structure. However, the obtained curves and the limiting mechanisms will be different for various values of matrix macropore and micropore apparent diffusivities. Figures 7.36 and 7.37 show that the cleat permeability and porosity remain constant for first five years. However, they increase after five years because of the unadsorbed nitrogen gas that remains free in the cleat.

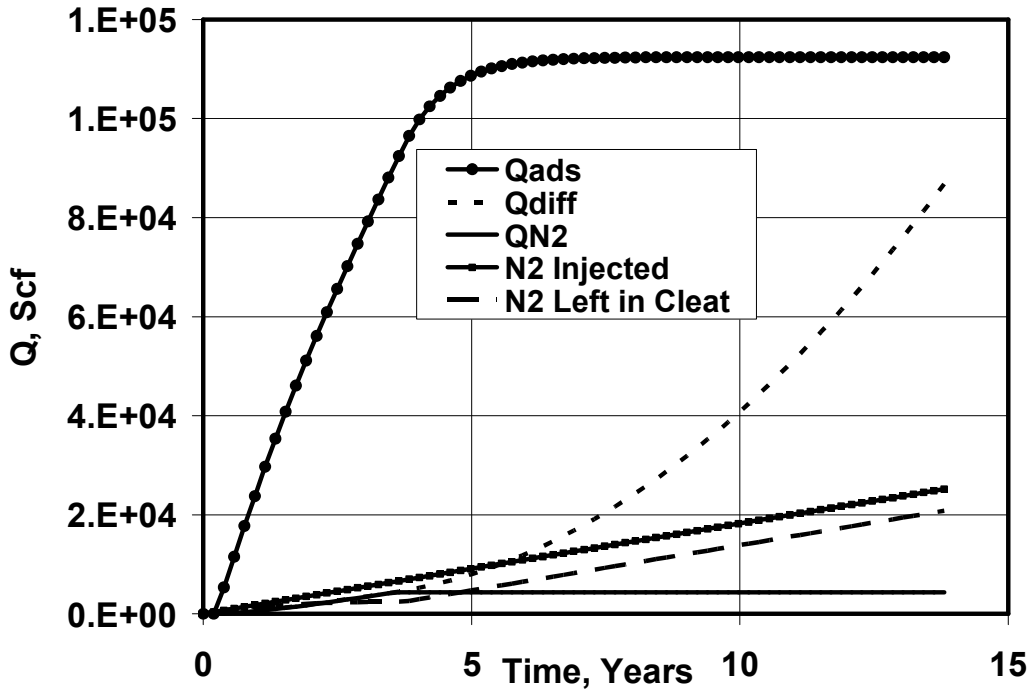

Figure 7. 35. Nitrogen gas diffusion, adsorption, injection rates vs. time. $(K_{mic})_{CH4}$ = 1.05E-4 Day^{-1}, $(K_{mac})_{CH4}$ = 5.01.0E-1 Day^{-1}, $(K_{mic})_{CO2}$ = 5.24E-4 Day^{-1}, $(K_{mac})_{CO2}$ = 1.0E00 $Day^{-1}$$(K_{mic})_{N2}$ = 3.55E-5 Day^{-1}, $(K_{mac})_{N2}$ = 1.0E-82 Day^{-}

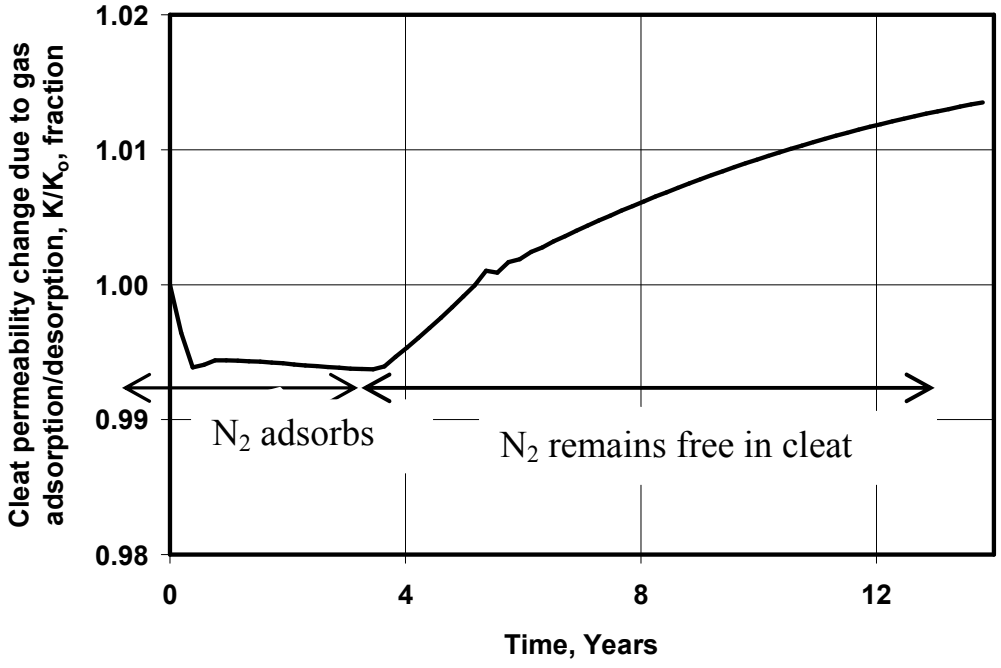

Figure 7. 36. Coal cleat permeability change versus time, $(K_{mic})_{CH4}$ = 1.05E-4 Day^{-1}, $(K_{mac})_{CH4}$ = 5.01.0E-1 Day^{-1}, $(K_{mic})_{CO2}$ = 5.24E-4 Day^{-1}, $(K_{mac})_{CO2}$ = 1.0E00 $Day^{-1}$$(K_{mic})_{N2}$ = 3.55E-5 Day^{-1}, $(K_{mac})_{N2}$ = 1.0E-82 Day^{-1}

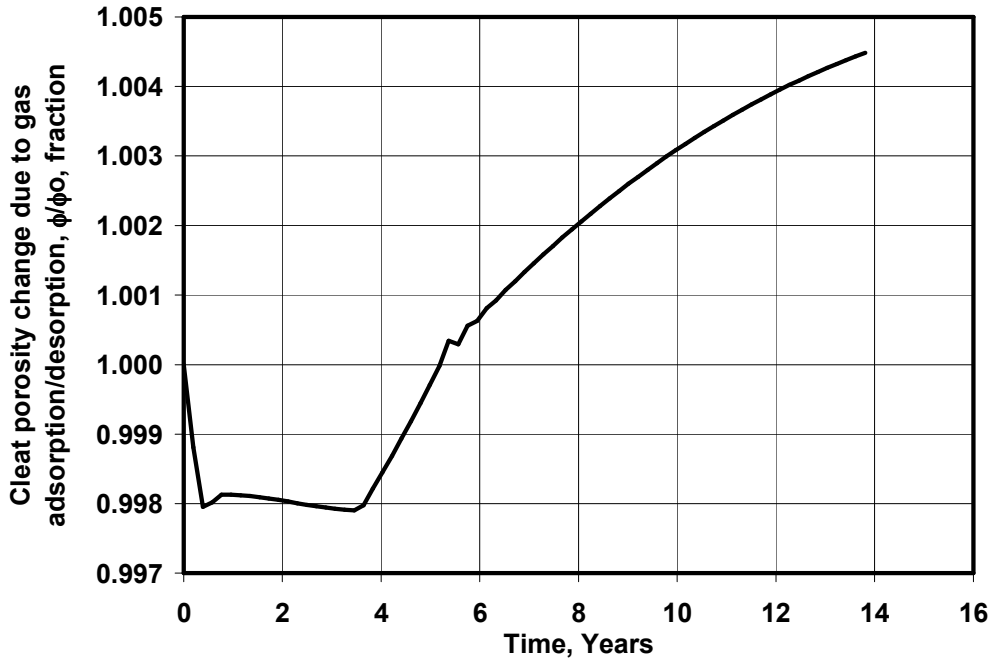

Figure 7. 37. Coal cleat porosity change versus time, $(K_{mic})_{CH4}$ = 1.05E-4 Day^{-1}, $(K_{mac})_{CH4}$ = 5.01.0E-1 Day^{-1}, $(K_{mic})_{CO2}$ = 5.24E-4 Day^{-1}, $(K_{mac})_{CO2}$ = 1.0E00 Day^{-1} $(K_{mic})_{N2}$ = 3.55E-5 Day^{-1}, $(K_{mac})_{N2}$ = 1.0E-82 Day^{-1}

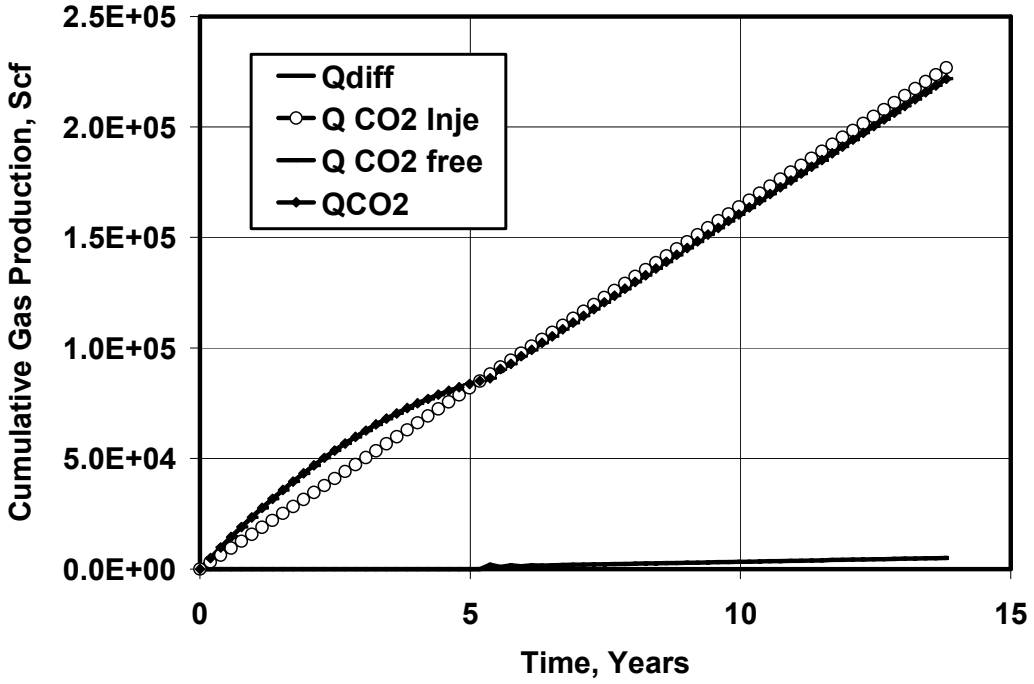

Figure 7. 38. Carbon dioxide gas diffusion, adsorption, injection rates vs. time. $(K_{mic})_{CH4}$ = 1.05E-4 Day^{-1}, $(K_{mac})_{CH4}$ = 5.01.0E-1 Day^{-1}, $(K_{mic})_{CO2}$ = 5.24E-4 Day^{-1}, $(K_{mac})_{CO2}$ = 1.0E00 Day^{-1} $(K_{mic})_{N2}$ = 3.55E-5 Day^{-1}, $(K_{mac})_{N2}$ = 1.0E-82 Day^{-1}

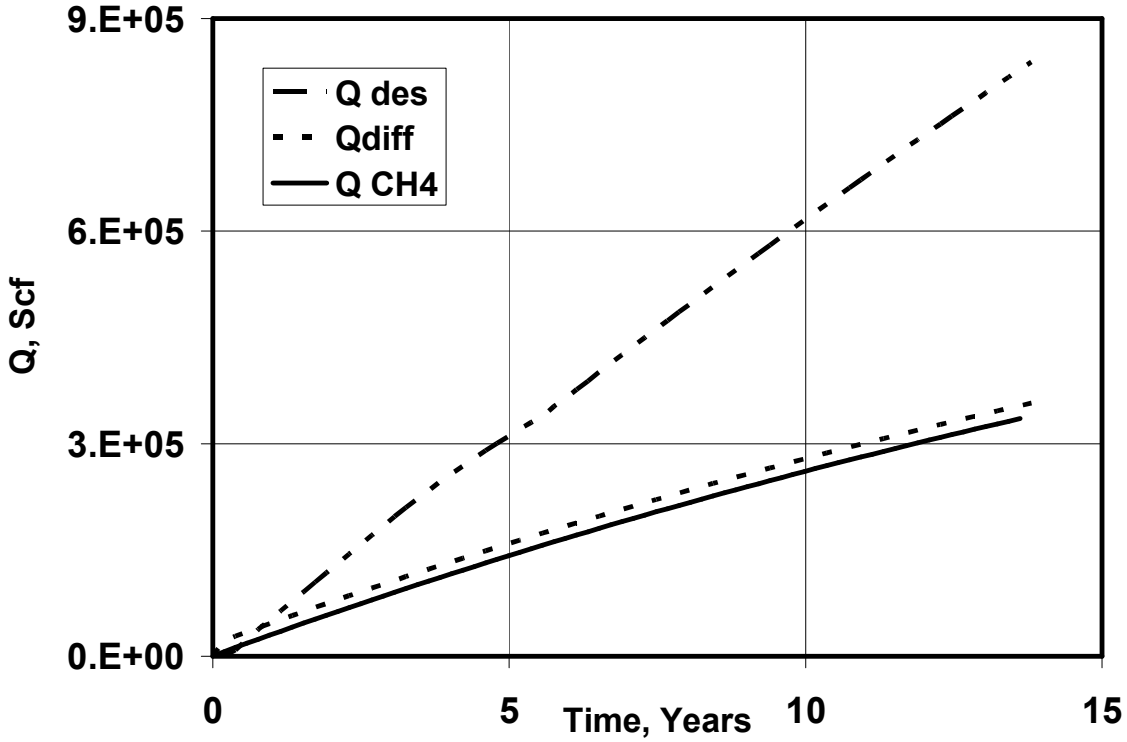

Figure 7. 39. Methane gas diffusion, adsorption and cumulative production vs. time. $(K_{mic})_{CH4}$ = 1.05E-4 Day^{-1}, $(K_{mac})_{CH4}$ = 5.01.0E-1 Day^{-1}, $(K_{mic})_{CO2}$ = 5.24E-4 Day^{-1}, $(K_{mac})_{CO2}$ = 1.0E00 $Day^{-1}$$(K_{mic})_{N2}$ = 3.55E-5 Day^{-1}, $(K_{mac})_{N2}$ = 1.0E-82 Day^{-1}

CHAPTER 8

CONCLUSIONS AND RECOMENDATIONS

Conclusions

The coalbed methane and shale gas reservoirs are water saturated unconventional gas reservoirs. The majority of the stored gas in both reservoirs (98% in coalbed methane and 50% in shale) is the adsorbed gas. Therefore, to accurately estimate the initial gas reserves and simulate the reservoir primary and enhanced gas recovery by carbon dioxide and nitrogen injection, a thorough knowledge of the sorption and isotherm development mechanisms is essential.

This study presented a novel technique to construct multi-component gas-coal/shale equilibrium and non-equilibrium isotherms under the reservoir prevailing conditions with the presence of water. The applications of the non-equilibrium in rapid determinations of the equilibrium isotherm and coalbed methane/shale gas reservoir simulation were discussed. Based on the results of this study the following may be concluded:

1. The feasibility of developing the non-equilibrium isotherms with and without the presence of water has been demonstrated. The Dubinin–Radushkevich (D-R) relationship was extended to model the multi-component gas adsorption/desorption phenomenon. The extended D-R isotherm parameters were modified for the effects of the pressure and coal particle size. It was determined that the D-R exponent (r) is independent of the pressure and coal

particle size. The D-R coefficient (D) changes linearly with the pressure and coal particle size. The theoretical maximum adsorbed volume (V_m) logarithmically depends on the system pressure and grain size.

2. The experimental results indicated that the presence of water in the sorption system reduces the carbon dioxide adsorption rates by 30%-40% and 40%-55% for high rank coal A and low rank coal B, respectively. The results also indicate that the presence of water reduces the nitrogen adsorption rate by 25%-35% for high rank coal A and 30%-50% for lower rank coal B, respectively. Comparing the effects of water on the nitrogen and carbon dioxide adsorption rates on high and low rank coals illustrates that the presence of water significantly reduces the adsorption ability of low rank coals. One of the reasons for this phenomenon is that the high rank coal contains tighter matrix structure and smaller pore spaces than the low rank coals. Therefore, the water molecules cannot diffuse and adsorb on the coal internal structure as freely as in the low rank coals.
3. The experimental results indicated that the solubility rate of carbon dioxide in water is approximately 5-10 times higher than the solubility rate of the nitrogen in water. Therefore, presence of water in the sorption system has more effects on the ability of the coal to adsorb carbon dioxide than nitrogen.
4. The multi-component gas (CO_2/N_2) adsorption experimental results indicate that increasing the initial mole fraction of the nitrogen gas in the initial CO_2/N_2 mixture will increase the net carbon dioxide sequestration rate on wet coals. However, there is an optimum nitrogen mole fraction beyond which

increasing the initial nitrogen mole fraction will not increase the sequestration rate further. The reason is that, carbon dioxide dissolves and reacts with the resident water in the reservoir condition. Presence of nitrogen in the injected carbon dioxide will decrease the effect of water on carbon dioxide and change the gas mixture critical pressure and temperature. These changes may result in more carbon dioxide adsorption in the coal structure.

5. The feasibility of the rapid determination of the single and multi-component gas adsorption equilibrium and non-equilibrium isotherms with and without the presence of water was demonstrated and validated using the literature and in-house experimental data. The results indicate that, for low pressure range (less than 150 psia), only one set of the non-equilibrium sorption isotherms at one pressure is needed to construct both the equilibrium and non-equilibrium isotherms for other pressure levels. For the high pressure ranges (over 150 psia), two sets of the non-equilibrium isotherms are necessary for construction of both the equilibrium and non-equilibrium isotherms for other pressure levels. Therefore, the time required to construct an isotherm is reduced by a factor of 70 times less than the time required using the equilibrium techniques.
6. The implementation of the developed non-equilibrium multi-component gas isotherms for coalbed methane and shale gas reservoirs simulations was illustrated. The simulation results show that ignoring the time-dependency of the sorption phenomenon in the coalbed/shale primary gas production can lead to 30%-50% prediction error depending on the prevailing reservoir conditions and coal/shale characteristics.

7. Series of gas production rate equations based on the two diffusivity parameters were developed under various scenarios. These are the apparent matrix macropore and micropore diffusivity coefficients representing the time-dependency of the gas adsorption/desorption through the matrix macropores and gas diffusion through the matrix micropores, respectively. This model has demonstrated more flexibility in modeling of the CO_2/N_2 sequestration rates and CH_4 production rates than the models based on only one diffusivity coefficient.
8. The simulation results indicate that coal cleat permeability and porosity may significantly decrease due to the matrix swelling by carbon dioxide adsorption and cleat contraction by mixing of the injected low temperature carbon dioxide and the cleat resident fluid (water and gas). The simulation results also indicated that adding some nitrogen to the injected carbon dioxide will prevent the cleat permeability and porosity reduction. In fact the cleat permeability may increase due to the availability of some free nitrogen in the cleat structure.
9. The simulation results for simultaneous CO_2/N_2 injection indicated that sequestrating a mixture of CO_2 and N_2 in coalbed methane/shale gas reservoirs instead of pure CO_2 will result in more methane production. However, there is always an optimum initial N_2/CO_2 injection ratio beyond which increasing the amount of nitrogen will not increase the methane production rate. For the cases considered in this study, the optimum CO_2/N_2 ratio was found to be in the range from 2 to 5.

10. It can be concluded from both the experimental and simulation results that various parameters including the effect of the resident water, time-dependency of the sorption phenomenon, cleat permeability/porosity alterations, and economical conditions have to be taken into account to successfully design an effective CO_2/N_2 sequestration project.

Recommendations

The non-equilibrium multi-component, multi-phase isotherm development technique introduced in this study may be modified and tested further for various gas-solid systems. Therefore, the following are recommended for future work purposes:

1. Enhance the experimental procedure for the systems of methane, ethane, carbon dioxide, nitrogen, and water in various coals and shale particles, for various pressure levels and grain sizes to test the model applicability for these systems.
2. Repeat the experimental procedure at various temperatures to modify the model parameters for the temperature effects. The Arrhenius equation may be applicable for the model parameters.
3. The model needs to be tested and modified for pressures higher than the carbon dioxide critical pressure. Because, in the enhanced coal gas recovery by carbon dioxide injection, the injected pressures are usually higher than the CO_2 critical pressure.

NOMENCLATURE

A	:	P-R constant	dimensionless
a_D	:	constant	dimensionless
a_{Vm}	:	Constant	dimensionless
b	:	P-R constant	dimensionless
B	:	P-R constant	dimensionless
$b^{/}$	:	Constant	dimensionless
b_D	:	constant	dimensionless
b_o	:	Constant	dimensionless
b_{Vm}	:	Constant	dimensionless
c	:	constant	dimensionless
C	:	concentration	$mole/ft^3$
$c^{/}$	:	Constant	dimensionless
c_c	:	Coal compressibility	psi^{-1}
$c_{cleat\ grain}$	:	cleat grain compressibility	psi^{-1}
c_{gas}	:	cleat gas compressibility	psi^{-1}
C_P	:	fluid heat capacity	
c_s	:	swelling coefficient	psi^{-1}
c_w	:	Cleat water compressibility	psi^{-1}
D	:	D-R isotherm coefficient	dimensionless
D_o	:	dissolution energy of the diatomic molecule at 0 K	Joule
E	:	Adsorption energy	Joule
E	:	Young's modulus	psi
E_o	:	characteristic adsorption	Joule
f	:	fugacity	psi
F(θ)	:	fraction of surface available for adsorbing molecules	dimensionless
G	:	Gibbs Free Energy	Joule
G	:	D-R isotherm parameters	dimensionless
G(θ)	:	function related to the surface coverage θ	dimensionless
H	:	Enthalpy	Joule
H	:	Henry constant	psi
J	:	Net adsorption rate	sec^{-1}
k	:	permeability	md
K	:	thermal conductivity	
Ka	:	Adsorption coefficient	
Kd	:	Desorption coefficient	

$k_{d\infty}$	:	rate desorption constant at infinite temperature	dimensionless
K_{gs}	:	equilibrium exchange rate	dimensionless
K_{gw}	:	Solubility coefficient (gas in water)	min^{-1}
k_{mac}	:	Apparent diffusivity of gas in the macropores	min^{-1}
k_{mic}	:	Apparent diffusivity of gas in the micropores	min^{-1}
K_o	:	temperature depended parameter	dimensionless
K_{wg}	:	Solubility coefficient (water in gas)	min^{-1}
k_{ij}^{AQ}	:	binary interaction coefficients for various gases and brine with various salinities	dimensionless
m	:	masses of the atoms in the molecule	gram
M	:	available adsorption sites on the solid surface	dimensionless
Mw	:	Molecular weight	lb/lbmole
$\overline{\overline{m}}$	:	desorbed gas mass	lb
n	:	Number of moles	lbmole
N^s	:	number or moles of the adsorbed molecules	dimensionless
P	:	Pressure	psi
P*	:	Saturation pressure	psi
Pc	:	Capillary pressure	psia
Q	:	heat of adsorption	Joule
q	:	parameters	dimensionless
q	:	heat flux	
q^s	:	molecular partition function	dimensionless
R	:	Universal gas constant	psi ft^3 $lbmole^{-1}K^{-1}$
q_o^s	:	molecular partition function of the adsorbed molecules	dimensionless
r	:	D-R isotherm exponent	dimensionless
R_a	:	Adsorption rate	scf/sec/ton
R_d	:	Desorption rate	scf/sec/ton
r_e	:	distance of separation of the two nuclei at the	cm

		lowest energy	
s	:	number of adsorption sites	dimensionless
S	:	Sticking coefficient	dimensionless
So	:	constant	dimensionless
S_w	:	Water saturation	dimensionless
t	:	time	sec
T	:	Temperature	K
u	:	velocity	ft/sec
V_m	:	Langmuir constant	scf/ton
W	:	pore volume occupied by the gas	ft^3
W_o	:	total pore volume that can be filled in relative pressure equal to 1.0	ft^3
x	:	Liquid mole fraction	dimensionless
y	:	Gas mole fraction	dimensionless
z	:	Pressure ratio	dimensionless
Z	:	Gas compressibility	dimensionless
θ	:	Surface coverage	dimensionless
α	:	coefficient related to non-perfect sticking	dimensionless
χ	:	constant	dimensionless
δ_{gs}	:	related to the chemical potential of the adsorbed and gas phase	dimensionless
ε_a	:	Activated energy of desorption	Joule
ε_d	:	Activated energy of desorption	Joule
γ	:	constant	dimensionless
φ	:	constant	dimensionless
ω	:	fundamental frequency of the vibratory modes	rev/min
ξ	:	constant	dimensionless
α			
β	:	similarity constant	dimensionless
Δ	:	dispersion	dimensionless
δ_i	:	binary interaction coefficients	dimensionless
μ^g	:	Chemical potential of the gas phase	Joule
μ^s	:	chemical potential of the adsorbed phase	Joule

ρ	:	Density	lb/ft^3
υ	:	poison ratio	dimensionless

Subscript

g	:	Gas phase
a	:	Adsorbed
b	:	Bulk
c	:	Coal
f	:	Fracture
G	:	Gas component
i	:	Component
in	:	Initial
m	:	Matrix
mac	:	Macropore
mic	:	Micropore
nb	:	Normal boiling point
sc	:	Standard condition
t	:	Total
w	:	Water phase
W	:	Water component

REFERENCES

1. Allardice, D. J., and Evans, D. G.: "The Brown Coal/Water System: Part 2. Water Sorption Isotherm on Bed-Moist Yallourn Brown Coal", Fuel, 1971, 50(3), 236-53.

2. Apol, M. E. F., Amadei A., and Berendsen, H. J. C.: "Application of Quasi-Guassian Entropy Theory to the Calculation of Thermodynamic Properties of Water and Methane in the Liquid and Gas Phase", Journal of Physical Chemistry, 1996, 104(17), 6666-78.

3. Arnaud, M., Bose, T. K., Okambawa, R., and Ingrain, D.: "Precise Determination of the Compressibility Factor by Using Dielectric Constant Measurements", Journal of Fluid Phase Equilibria, 1993, 88, 137-49.

4. Berlier, K., Frere, M., "Adsorption of CO_2 on Microporous Materials. 1. On Activated Carbon and Silica Gel", J. Chem. Eng. Data, 1997, 42, 533-537.

5. Berry, J. P., Good, W. K.: "Cogeneration Potential in Western Canada", SPE International Heavy Oil Symposium, 19-21 June 1995, Calgary, Alberta, Canada.

6. Boer J. H. de.: "The Dynamic Character of Adsorption", 2^{nd} ed, 1899, 20-35.

7. Brunauer, S., Emmett, P. H., and Teller, E.: "Adsorption Gases in Multi-Molecular Layers", Fuel, Feb, 1938, 309-319.

8. Brunauer, S., Deming, L. S., Deming, W. E., and Teller, E.: "On the Theory of the van der Waals Adsorption of Gases", Fuel, July 1940, 62, 1723-1732.

9. Busch, A., Gensteblum, Y., kross, B. M., and Littke, R.: "Methane and Carbon Dioxide-Diffusion experiments on Coal: Upscaling and Modeling", International Journal of Coal Geology, 2004, 60, 151-68.

10. Cerofolini, G. F.: "Extension of the Asymptotically-Correct Approximation to Fowler-Guggenheim Adsorption", Surface Science, Sep 1975, 52(1), 195-8.

11. Clarkson, C. R.: "Application of a New Multicomponent Gas Adsorption Model to Coal Gas Adsorption Systems" Society of Petroleum Engineers Journal, Sep. 2003, 236-251.

12. Clarkson, C. R., and Bustin, R. M.: "Binary Gas Adsorption/Desorption Isotherms: Effect of Moisture and Coal Composition upon Carbon Dioxide Selectivity over Methane", International Journal of Coal Geology, 2000, 42, 241-71.

13. Chaback, J. J., Morgan, W. D., and Yee, D.: "Sorption of Nitrogen, Methane, Carbon Dioxide and their Mixtures on Bituminous Coals at in-situ Conditions" Fluid Phase Equilibria, Mar 1996, 117(1-2), 289-296.

14. Chapoy, A., Mohammadi, A. H., Tohidi, B., and Richon, D., "Gas Solubility Measurements and Modeling for the Nitrogen + Water System from 274.18 K to 363.02 K", J. Chem. Eng. Data, 2004, 49, 1110-15.

15. Chaudhary, V. R., and Mayadevi, S.: "Adsorption of Methane, Ethane, Ethylene, and Carbon Dioxide on Silicalite-I", Zeolites, 1996, 17, 501-507.

16. Chen, J. H., Wong, D. S. H., Tan, C. S., Subramanian, R., Lira, C. T., and Orth, M.: "Adsorption and Desorption of Carbon Dioxide onto and from Activated Carbons at High Pressures", Ind. Eng. Chem. Res, 1997, 36, 2808-2815.

17. Cheng, A., and Huang, W.: "Selective Adsorption of Hydrocarbon Gases on Clays and Organic Matter", Organic Geochemistry, April 2004, 35(4), 413-423.

18. Choi, B., Choi, D., Lee, Y.W., and Lee, B.K.: "Adsorption Equilibria of Methane, Ethane, Ethylene, Nitrogen, and Hydrogen onto Activated Carbon", Journal of Chemical Data, 2003, 48, 603-607.

19. Chopy, A., Mohammadi, A. H., Richon, D., and Tohidi, B.: "Gas Solubility Measurements and Modeling for Methane-Water and Methane-Ethane-n-Buthane-Water Systems at Low Temperature Conditions", Journal of Fluid Phase Equilibria, 220(1), 111-119.

20. Coquelet, C., Chareton, A., Valtz, A., Baba-Ahmed, A., and Richon, D.: "Vapor-liquid equilibrium data for the Azeotropic Difluoromethane + Propane System at Temperatures from 294.83 to 343.26 K and Pressures up to 5.4 MPa", Journal of Chemical and Engineering Data, March/April 2003, 48(2), 317-323.

21. Ciembroniewicz, A., Marecka, A.: "Kinetics of CO_2 Sorption for two Polish Hard Coals", Fuel, Mar 1993, 72(3), 405-408.

22. Crawshaw, J. P., John, J. H.: "Experimental Determination of Binary Sorption and Desorption Kinetics for the System Ethanol, Water, and Maize at 90°C", Industrial & Engineering Chemistry Research, Mar 1992, 31(3), 887-892.

23. DeGance, A. E.: Multicomponent High-Pressure Adsorption Equilibria on Carbon Substrates: Theory and Data. Fluid Phase Equilibria, 1992, 78, 99-137.

24. Ding, L. P., and Bhatia, S. K.: "Analysis of Multicomponent Adsorption Kinetics on Activated Carbon", AIChE Journal, Apr 2003, 49(4), 883-895.

25. Dhima, A., de Hampinne, J. C., and Jose, J.: "Solubility of Hydrocarbons and CO_2 Mixtures in Water under High Pressure", Ind. Eng. Chem. Res, 1999, 38, 3144-61.

26. Do, D. D.: "Adsorption Science and Technology", World Scientific, 2000, 30-1000.

27. Dreisbach, F., Staudt, R., Keller, J. U.: "High Pressure Adsorption Data of Methane, Nitrogen, Carbon Dioxide and Their Binary and Ternary Mixtures on Activated Carbon". Adsorption, 1999, 5, 215-227.

28. Dubinin, M. M., "Chemistry and Physics of Carbon", Vol. 2, 1966, Edward Arnold Ltd., New York.

29. Elliot, J. A. W., and Ward, C. A.: "Temperature Programmed Desorption: A Statistical Rate Theory Approach", Journal of Chemical Physics, 1997, 106 (13), 5678-5684.

30. Evelein, K. A., and Moore, R. G.: "Prediction of Phase Equilibria in Sour Natural Gas Systems Using the Soave-Redlich-Known Equation of State", Ind. Eng. Chem. Process Des. Dev., 1979, 18(4), 618-24.

31. Fawzi, B. A., Jana, S.: "Removal of Benzene Traces from Contaminated Water by Vacuum Membrane Distillation", Chemical Engineering Science, April 1996, 51(8), 1257-1265.

32. Frére, M. G., De Weireld, G. F.: "High-Pressure and High-Temperature Excess Adsorption Isotherms of N_2, CH_4, and C_3H_8 on Activated Carbon", J. Chem. Eng. Data, 2002, 47, 823-829.

33. Gamson, P., Beamish, B., and Johnson, D.: "Coal Microstructure and Secondary Mineralization: their Effects on Methane Recovery", Coalbed Methane and Coal Geology, 1996, 165-179.

34. Gasem K A M, Robinson R L., Reeves, S. R.: "Adsorption of Pure Methane, Nitrogen, and Carbon Dioxide and Their Mixtures on San Juan Basin Coal", A Topical Report Contract No#DE-FC26-00NT40924, Oklahoma State University, May 2002.

35. George, J. D., and Barakat, M. A.: "The Change in Effective Stress Associated with Shrinkage from Gas Deportation in Coal", International Journal of Coal Geology, 2001, 45(2-3), 105-113.

36. Glasstone, S., Laidler, J. J., and Eyring, H.: "The Theory of Rate Progresses", McGraw-Hill, New York, 1941, 347.

37. Gosiewska, A., Drelich, J.; Laskowski, J.S.; Pawlik, M.: "Mineral Matter Distribution on Coal Surface and its Effect on Coal Wettability", Journal of Colloid and Interface Science, 2002, 247(1), 107-116.

38. Gray, I.: "Reservoir Engineering in Coal Seams: Part 1- The Physical Process of Gas Storage and Movement in Coal Seams", SPERE, 1987, 2, 28.

39. Gunther, J.: "Investigation of the Gas-Coal Bond", Rev. Ind. Min., 1978, Vol 47, 693-708.

40. Lane, H. S., Watson, A.T., Lancaster, D. E.: "Identifying and Estimating Desorption from Devonian Shale Gas Production Data", SPE Annual Technical Conference and Exhibition, 8-11 October, San Antonio, Texas, 1989.

41. Larsen, B. L., Rasmussen, P., and Fredenslund, A. A.: "Modified UNIFAC Group Contribution Model for the Prediction of Phase Equilibria and Heats of Mixing", Ind. Eng. Chem. Res 1987, 26, 2274-86

42. Larsen, J. W.: "The Effects of Dissolved CO_2 on Coal Structure and Properties", International Journal of Coal Geology, 2004, 57, 63-70.

43. Li, Y. H., Lu, G. Q., and Rudolph, V.: "Compressibility and Fractal Dimension of Fine Coal Particles in Relation to Pore Structure Characterization Using Mercury Porosimetry", Particle and Particle Systems Characterization, May 1999, 16(1), 25-31.

44. Li, J., Vanderbeken, I., Ye, S., Carrier, H., and Xans, P.: "Prediction of the Solubility of Gas-Liquid Equilibria for Gas-Water and Light Hydrocarbon-Water Systems at High Temperatures and Pressures with a Group Contribution Equation of State", Fluid Phase Equilibria, 1997, 131, 107-118.

45. Jahediesfanjani, H., and Civan, F.: "Rapid Determination of Equilibrium Gas Isotherms in Wet Coalbeds from Non-equilibrium State Measurements. paper 521, the 2005 International Coalbed Methane Symposium held in Tuscaloosa, Alabama USA, May 10-12, 2005.

46. Jahediesfanjani, H., and Civan, F.: "Rapid Determination of Equilibrium Gas Isotherms in Wet Coalbeds from Early-Time Measurements", Fuel, In the Review.

47. Jahediesfanjani, H., and Civan, F.: "Effects of the Resident Water in Enhanced Coal Gas Recovery by Simultaneous CO_2/N_2 Injection", SPE 102634, To be presented in the 2006 SPE Annual Technical Conference and Exhibition to be held in San Antonio, Texas, USA, September 24-27, 2006.

48. Juntgen, H.: "Research for Future in Situ Conversion of Coal", Fuel, 1990, 66, 443.

49. Kapoor, A., Ritter, J. A., and Yang, R. T.: "On the Dubinin-Radushkevich Equation for Adsorption in Microporous Solids in the Henry's Law Region", Langmuir, 1989, 5, 1118-1121.

50. Karacan, C. O.: "Heterogeneous Sorption and Swelling in a Confined and Stressed Coal during CO_2 Injection" Energy & Fuels, 2003, 17, 1595-1608.

51. Karacan, C. O., and Okandan, E.: "Adsorption and Gas Transport in Coal Microstructure: Investigation and Evaluation by Quantitative X-ray CT Imaging", Fuel, Mar 2001, 80(4), 509-520.

52. Keenan, J.H.: "Steam Tables; Thermodynamic Properties of Water, Including Vapor, Liquid, and Solid Phases (English units)", New York, Wiley [1969], 1-200.

53. Kisliuk, P.: "Using Constant Resistance to Measure Adsorption of Gases on Metals", Bell System Technical Journal, July 1958, 37, 925-949.

54. Krooss, B. M., Bergen, F., Gensterblum, Y., Siemons, N., Pagnier, H. J. M., and David, P.: "High-Pressure Methane and Carbon Dioxide Adsorption on Dry and Moisture-Equilibrated Pennsylvanian Coals", International Journal of Coal Geology 2002, 51, 69– 92.

55. Hall, F. E., Zhou, C., Ghasem, K. A. M., Robinson, R. L., and Yee, D.: "Adsorption of Pure Methane, Nitrogen and Crbon Dioxide, and their Binary Mixtures on the Fruitland Coal", SPE 29194, Proceedings from the Eastern Regional Conference and Exhibition held in WV, USA, 8-10 November, 1984.

56. Harpalani, S., and Chen, G.: "Estimation of Changes in Fracture Porosity of Coal with Gas Emission", Fuel, 1995, 74(10), 1491-1498.

57. Haydel, J. J., and Kobayashi, R.: "Adsorption Equilibria in the Methane-Propane Silica Gel System at High Pressures", I&E C Fundamentals, Nov. 1967, no 4, 546-554.

58. Mohammadi, A. H., Chapoy, A., Tohidi, B., and Richon, D.: "Water Content Measurement and Modeling in the Nitrogen-Water System", J. Chem. Eng. Data, 2005, 50, 541-45.

59. Maggs, F. A. P.: "The Adsorption-Swelling of Several Carbonaceous Solids", Transactions of the Faraday Society, 1946(42B), 284-8.

60. Masel, R.I.: "Principles of Adsorption and Reaction on Solid Surfaces," John Wiley & Sons, Inc., New York, (1996).

61. Moffat, D. H., and Weale, K. E.: "Sorption by Coal of Methane at High Pressures", Fuel, 1955, 34, 449.

62. Monazam, E. R.: 'Water Ddsorption and Desorption by Coals and Chars", Energy and Fuels, 1998, 12, 1299-1304.

63. Mofarahi, M., Sadrameli, M., and Towfighi, J.: "Characterization of Activated Carbon by Propane and Propylene Adsorption", Journal of Chemical and Engineering Data, 2003, 48(5), 1256-61.

64. Muster, T.H., Prestidge, C.A., Hayes, R.A.: "Water Adsorption Kinetics and Contact Angles of Silica Particles", Colloids and Surfaces A (Physicochemical and Engineering Aspects), Jan 2001, 176, 2-3, 30, 253-66.

65. Nagai, K., and Hirashima, A.: "Reply to "On one of the Ways of Application of the Lattice-Gas Model to Describe the Kinetics of Desorption" by Zhdanov, V.P"., Surface Science, 171, 1986, 464-468.

66. Nordon, P., and Bainbridge, N. W.: "Heat of Wetting of a Bituminous Coal", Fuel, 1983, Vol 62, 619-621.

67. Owen, M. J., Terra L. B., Pratt, T.: "Measurement and Evaluation of Coal Sorption Isotherm Data". Proceedings from the SPE Annual Technical Conference and Exhibition, 23-26 September, New Orleans, Louisiana, 1990.

68. Pattison, C. I., Fielding, C. R., McWatters, R. H., and Hamilton, L. H.: "Nature and Origin of Fractured in Permian Coals from the Bowen Basin, Queensland, Australia", Coalbed Methane and Coal Geology, The Geological Society, 1996, 133-149.

69. Peng, D. Y., and Robinson, D. B.: "A New Two-Constant Equation of State", Ind. Eng. Chem., Fundam., 1976, 15(1), 59-64.

70. Reich, R., Ziegler, W. T., Rogers, K. A.:" Adsorption of Methane, Ethane, and Ethylene Gases and Their Binary and Ternary Mixtures and Carbon Dioxide on Activated Carbon at 212-301 and Pressures to 35 Atmospheres, Ind. Eng. Chem. Processes Des. Dev., 1980, 19, 336.

71. Reucroft, P. J., and Patel, H.: "Gas-Induced Swelling in Coal", Fuel, June 1986, 65, 816-820.

72. Reucroft, P. J., and Sethuraman, A. R.: 'Effect of Pressure on Carbon Dioxide Induced Coal Swelling', Energy & Fuels 1987, 1, 72-75.

73. Reeves, S., and Pekot, L.: "Advanced Reservoir Modeling in Desorption-Controlled Reservoirs", Proceedings - SPE Rocky Mountain Petroleum Technology Conference, Petroleum Technology - Leads the Way, Proceedings - SPE Rocky Mountain Petroleum Technology Conference, Petroleum Technology - Leads the Way, 2001, p 455-468

74. Ritter, J. A., Yang, R. T.: “Equilibrium Adsorption of Multicomponent Gas Mixtures at Elevated Pressures”, Ind. Chem. Res., 1987, 26, 1679-1686.

75. Rudzinski, W., and Panczyk, T.: “Kinetics of Gas Adsorption in Activated Carbons, Studied by Applying the Statistical Rate Theory of Interfacial Transport’, Journal of Physical Chemistry B, 2001,105, 6858-66.

76. Rudzinski, W., and Panczyk, T., “The Langmuirian Adsorption Kinetics Revised: A Farewell to the XXth Century Theories?” Fuel, 2000, 1963-1974.

77. Rudzinski, W., Borowiecji, T., Panczyk, T., and Dominko, A.: “On the Applicability of Arrhenius Plot Methods to Determine Surface Energetic Heterogeneity of Adsorbents and Catalysts Surfaces from Experimental TPD Spectra”, Adv. Coll. And Interface Sci., 84, 1-26, 2000.

78. Rudzinski, W., and Aharoni, C.: “Multi-Site-Occupancy Adsorption on Heterogeneous Solid Surfaces: Effects of Surface Topography on Adsorption Kinetics”, Polish J. Chemi., 1995, 69, 1066-1071.

79. Rutherford, S.W. and Coons, J.E.: “Adsorption Equilibrium and Transport Kinetics for a Range of Porbe Gases in Tekeda 3A Carbon Molecular Sieve”, Journal of Colloid and Interface Science, April 2005, 284(2), 432-439.

80. Schettler Jr., P. D., Parmely, C. R., Juniata C.: “Contributions to Total Storage Capacity in Devonian Shales”, SPE Eastern Regional Meeting, 22-25 October, Lexington, Kentucky, 1991

81. Soreide, I., and Whitson, C. H.: “Peng-Robinson Predictions for Hydrocarbons, CO_2, N_2, and H_2S with Pure Water and NaCl Brine”, Fluid Phase Equilibria, Sep 1992, 77, 217-240.

82. Spitzer, Z.: “Mercury Porosimetry and its Application to the Analysis of Coal Pore Structure”, Powder Technology, May-June 1981, 29(1), 177-86.

83. Stamm, L. J.: “Diffusion of Water into Uncoated Cellophane. II. From Steady-State Diffusion Measurements”, Ind. Eng. Chem., Anal., Jan.1956, 60, 83-86.

84. Stoeckli, F.: “Recent Developments in Dubinin's Theory”, Carbon, 1998, 36(4), 363-368.

85. Sutton, J. B., and Davis, E.C.H.: “The Adsorption of Methane by Coal”, Fuel, 1935, 57, 1785-1787.

86. Syahrial, E.: “Coalbed Methane Simulator Development for Improved Recovery of Coalbed Methane and CO_2 Sequestration”, Paper SPE 93160, proceeding from the 2005 Asia Pacific Oil and Gas Conference and Exhibition, held in Jakarta, Indonesia, 5-7 April 2005.

87. Talu, O., Zwiebel, I., "Multicomponent Adsorption Equilibria of Non-ideal Mixtures", AIChE J, 1986, 32, 1263-1276.

88. Toda, Y., Toyoda, S.: "Densities of Coals Measured with Various Liquids", 1972, Fuel, 51(2), 108-112.

89. Vaart, R. V. D., Huiskes, C., Bosch, H., and Reith, T.: "Single and Mixed Gas Adsorption Equilibria of Carbon Dioxide/Methane, on Activated Carbon, Adsorption, 2000, 6, 311–323.

90. Vyas, S. N., Patwardhan, S. R., Vijayalakshimi, S., and Ganesh, K. S.: "Adsorption of Gases on Carbon Molecular Sieves", Journal of Colloid and Interface Science, 1994, 168, 275-80.

91. Wakasugi, Y., Ozawa, S., Ogino, Y., "Physical Adsorption of Gases at High Pressure, V. An Extension of a Generalized Adsorption Equation to System with Polar Adsorbents", Journal of Colloid and Interface Science, 1981, 79, 399-409.

92. Ward, C. A., Findlay, R. D., and Rizk, M.: J. Chem. Phys. 76, 5599, 1982.

93. Ward, C. A., Elmoselhi, M.: "Molecular Adsorption at a Well Defined Gas-Solid Interphase: Statistical Rate Theory Approach", Surface Science, 1986, 176, 457-475.

94. Ward, C. A.: J. Chem. Phys., 1983, 79, 5605.

95. Ward, C. A., Finadlay, R. D., and Rizk, M., J. Chem. Phys. 76, 1982, 5599.

96. Weidlich U., and Gmehling J. A.: "Modified UNIFAC Model. 1. Prediction of VLE, h^E and the Activity Coefficients at Infinite Dilution", Ind. Chem. Res., 1987, 26, 1327-81.

97. Wubben, P., Seewald, H., and Jurgen, K.: "Permeation and Sorption Behavior of Gas and Water in Coal", Proceedings of the 12th Annual Underground Coal Gasification Symposium, August 24-28, 1986.

98. Xiao-Chun, L., Fan-Chang, L., and Ted, W.A.: "Adsorption Studies of Natural Gas Srorage in Devonian Shales", SPE Formation evaluation, 10, 2, Jun 1995, 109-113.

99. Xijun, H., Gade, R. N., and Duong, D. D.: "Multicomponent Sorption Kinetics of Ethane and Propane in Activated Carbon: Simultaneous Adsorption", Gas Separation & Purification, Mar 1993, 7(1), 39-45.

100. Yong, Q., Fu, X; Ye, J; Line, D., and Tang, S.: "Geological Controls and their Mechanisms of Coal-Reservoir Petrography and Physics of Coalbed Methane

Occurrence in China", Zhongguo Kuangye Daxue Xuebao/Journal of China University of Mining & Technology, 1999, 28(1), 1999, 14-19.

101. Zhou, C., "Modeling and Prediction of Pure and Multicomponent Gas Adsorption," Ph.D. Dissertation, Oklahoma State University, Stillwater, Oklahoma (1994).

102. Zhou, L., Zhou, Y., Li, M., Chen, P., and Wang, Y.: "Experimental and Modeling Study of the Adsorption of Supercritical Methane on a High Surface Activated Carbon", Langmuir, 2000, 16, 5955-5959.

.

APPENDIX 1

REVIEW OF THE EQUILIBRIUM ADSORPTION MODELS

Numerous theories and models have been developed to correlate the pure adsorption data and predict the gas mixture adsorption. Among them are the extended Langmuir model, ideal adsorbed solution (IAS) theory, heterogeneous ideal adsorbed solution (HIAS), vacancy solution model (VSM), theory of volume filling micropores (TVFM), 2-D equations of state, simplified local density (SLD) model, and Ono-Kondo (OK) lattice model. Here, a number of relevant adsorption models and various carbon adsorbents are reviewed briefly. Appendix 1 reviews only three major adsorption models including: (1) Langmuir Model. (2) BET Model. (3) Dubinin–Radushkevich–Stoeckli theory.

A1.1. Langmuir Model

The most basic theory in adsorption is the Langmuir theory (1918). This theory describes the monolayer surface adsorption on an ideal surface. As depicted in Figure A1.1, an ideal surface means that the energy fluctuations, E, on the surface are periodic with the same magnitude, and the magnitude of this fluctuation is larger than the thermal energy of a molecule, kT. Hence, the energy fluctuation is acting as the adsorption site. If the distance between the two neighboring sites is much larger than the diameter of the adsorbate molecule, the adsorption process is called localized and each adsorbate molecule will occupy only one site. Although

the Langmuir model can be derived from the equilibrium thermodynamic point of view, the best way to describe this model is by using kinetic theory.

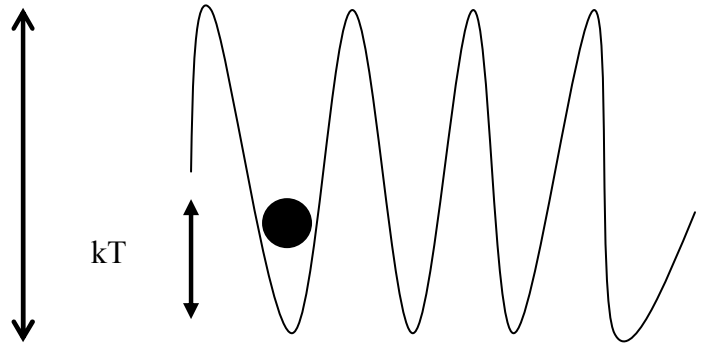

Figure A1.1. Surface energy fluctuation (After Masel, 1996).

When a molecule hits the surface, the molecule might be adsorbed or reflected, as shown in Figure A1.2. The molecule will be reflected if a molecule hits a site that is already occupied by a molecule. Thus, the adsorption rate will be proportional to the fraction of empty sites. After a certain time, this adsorbed molecule may evaporate. The rate of evaporation therefore depends on the occupied sites. Equating the rates of adsorption and desorption (evaporation), we can obtain the Langmuir isotherm written in terms of fractional loading:

$$\theta = \frac{V}{V_m} = \frac{bP}{1+bP} \quad \text{.....(A1.1)}$$

This equation will follow Henry's law at low pressure: $\theta = bP$, and for mixture adsorption, the Langmuir model takes the following form:

$$V_i = \frac{L_i(T) b_i(T) P y_i}{1 + \sum_j b_j(T) P y_j} \quad \text{(A1.2)}$$

The parameter b is called the affinity constant or the Langmuir constant. It is a measure of how strongly an adsorbate molecule is attached onto a surface. This parameter is related to the heat of adsorption, Q, as shown in the following expression:

$$b = b_o \exp(\frac{Q}{RT}) \quad \text{(A1.3)}$$

where b_o is temperature dependent as shown below,

$$b_o = \frac{\alpha}{k_{d\infty}\sqrt{2\pi MRT}} \quad \text{(A1.4)}$$

where α is a coefficient related to non-perfect sticking, and $k_{d\infty}$ is the rate desorption constant at infinite temperature.

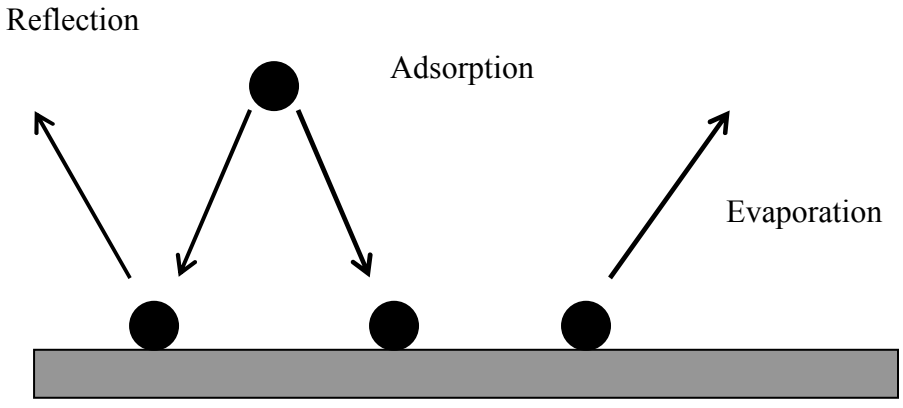

Figure 3.1. Schematic diagram for the Langmuir adsorption mechanism (After Do, 2000).

A1.2. The Brunauer-Emmett-Teller (BET) theory

Langmuir isotherm is based on the monolayer adsorption assumptions. Brunauer-Emmett-Teller (1938) extended the Langmuir isotherm for the case of multilayer adsorption isotherm that is named after them as BET isotherm. However, their multilayer model was itself developed under several assumptions and simplifications. The BET isotherm is developed for the case of the adsorption of sub-critical adsorbents. The molecules are adsorbed onto the solid surface in a layering process and multiple layers are formed when the pressure is sufficiently high. The general form of the BET isotherm is given by:

$$\theta = \frac{c\frac{P}{P_o}}{\left(1-\frac{P}{P_o}\right)\left[1-(1-c)\frac{P}{P_o}\right]} \quad \text{(A1.15)}$$

where P is pressure and P_o is the saturation pressure of the gas and c is a constant given by:

$$c = \exp\left(\frac{\Delta H_{des} - \Delta H_{vap}}{RT}\right) \quad \text{(A1.6)}$$

Here ΔH_{des} and ΔH_{vap} are the enthalpies of desorption from the monolayer and of vaporization of the liquid adsorbate, respectively. The assumptions made in developing the BET model are (Brunauer 1940):

1. The surface is homogeneous; the adsorption energy is constant over all sites.
2. Adsorption on a surface is localized; the adsorbed atoms or molecules are adsorbed at definite, localized sites.

3. Each site accommodates only one molecule or atom.
4. The number of layers is infinite.

A1.3. The Dubinin–Radushkevich–Stoeckli Theory

The Dubinin–Radushkevich–Stoeckli theory, also known as the Theory of Volume Filling of Micropores (TVFM), was first introduced by Dubinin et al. (1947) as an extension of the Polany's (1914) adsorption theory. Unlike Langmuir and several other adsorption theories that express the adsorption process as layer-by-layer formation of a adsorbed film on the adsorbent wall, the TMFM theory assumes that adsorption is a phenomenon in which the gas or liquid molecules fill the pores of the adsorbent. The following concept is the base for the Dubinin et al. theory.

$$A = RT \ln\left(\frac{P^o}{p}\right) \quad \text{(A1.7)}$$

where P is the equilibrium pressure at temperature T, P^o is the saturation vapor pressure, and A is referred as the adsorption potential. Dubinin used the term relative pore filling described as the following equation to express the pore volume filled by gas or liquid ratio to the total pore volume on the solid surface:

$$\theta = \frac{W}{W_o} \quad \text{(A1.8)}$$

where θ is the surface coverage, W is the pore volume occupied by the gas or liquid when the relative pressure is P/P_o, and W_o is the total pore volume that can be filled

in relative pressure equal to 1.0. Dubinin also applied the concept of adsorption energy E and related this concept to the adsorption potential by:

$$\theta = f\left(\frac{A}{E_o\beta}\right) \quad \text{(A1.9)}$$

where E_o is the characteristic adsorption for a reference vapor, and β is the similarity constant. Dubinin and Radushkevich (1966) modified Equation 3.10 for the case of Gaussian pore size distribution as the following expression:

$$\theta = \exp\left[-\left(\frac{A}{E_o\beta}\right)^2\right] \quad \text{(A1.10)}$$

Using Equations 3.7-3.10, the general form of the D-R equation is expressed as:

$$W = W_o \exp\left\{-B\left[\frac{T}{\beta}\log\left(\frac{P^\circ}{P}\right)\right]^2\right\} \quad \text{(A1.11)}$$

where E_o and B are related to each other according to the following relationship:

$$E_0 = 0.00195\sqrt{(1/B)} \quad \text{(A1.12)}$$

Due to the several deficiencies of the D-R equation in describing adsorption of gas or solids in lower coverage and in tight solid materials, Dubinin and Astakhov (1971) modified the D-R equation by adding one more parameter, n. Therefore, the degree of pore filling was related to two different parameters named as A/E and n. The two-parameter Weibull distribution was used, expressed as:

$$\theta = \exp\left[-\left(\frac{A}{E_o\beta}\right)^n\right] \quad \text{(A1.13)}$$

Equation A1.13 is well-known as the D-A equation. D-A equation was more generalized than D-R and therefore could overcome some of the D-R equation

deficiencies. However, one of the major assumptions in developing D-R and D-A isotherm was still unsolved. It assumes a homogenous solid surface. In reality, the solid surface is very heterogeneous. To overcome this problem Cerofolini (1975) and latter Stoeckli (1998) divided the heterogeneous surface into several homogeneous sites in which the adsorbed phase follows a local isotherm (θ_i) trend. By applying the normal Gaussian distribution of microspores and the following equation was obtained after some mathematical adjustments that is well-known as the Dubinin–Radushkevich–Stoeckli (D-R-S) equation:

$$W = 0.5W_o \exp(-B_o y)\exp(0.5y^2\Delta^2)[1 - erf(z)] \quad \text{(A1.14)}$$

where:

$$y = \left[\frac{T}{\beta}\log\left(\frac{P^\circ}{P}\right)\right]^2 \quad \text{(A1.15)}$$

Δ is the dispersion (or variance) and z is defined as:

$$z = \left(y - \frac{B_\circ}{\Delta^2}\right)\frac{\Delta}{\sqrt{2}} \quad \text{(A1.16)}$$

Equation A1.16 has gained significant attention in the adsorption industry.

APPENDIX 2

EXPERIMENTAL DATA FOR VARIOUS SYSTEMS OF GAS-WATER, COAL-WATER, COAL-GAS, AND COAL-GAS-WATER DESCRIBED IN CHAPTER 4

In Chapter 4 we described the experimental procedure to conduct the sorption experiments. Some of the experimental data were also reported. In this section, the additional figures of the experimental data re presented for the system of coal-single component gas, coal-water-single component gas, coal-multi-component gas, and coal-water-multi-component gas.

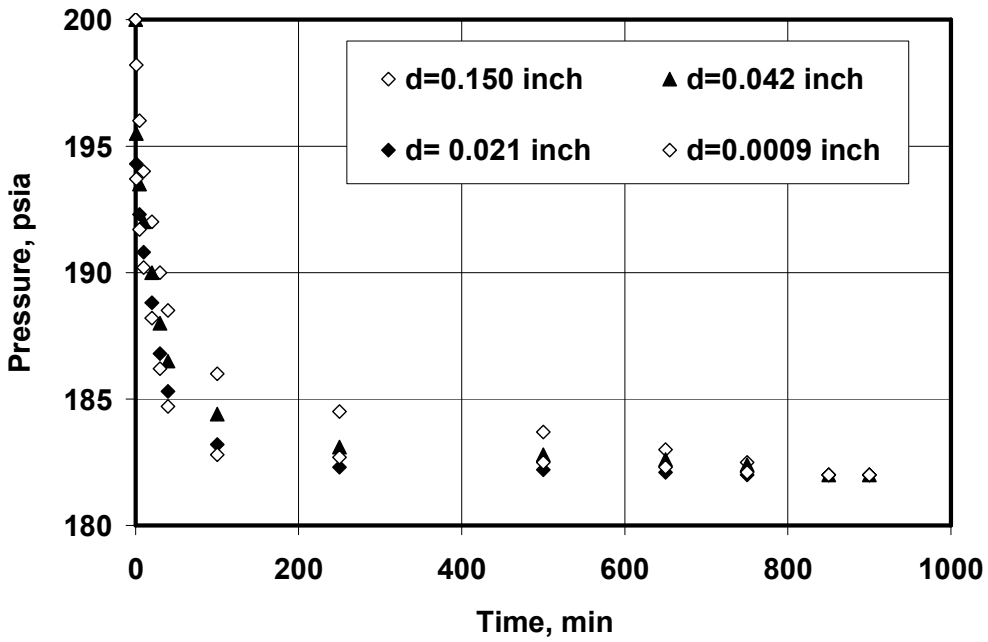

Figure A2. 1. Pressure versus time for various average coal A grain size and N_2 system (Pin = 200 psia)

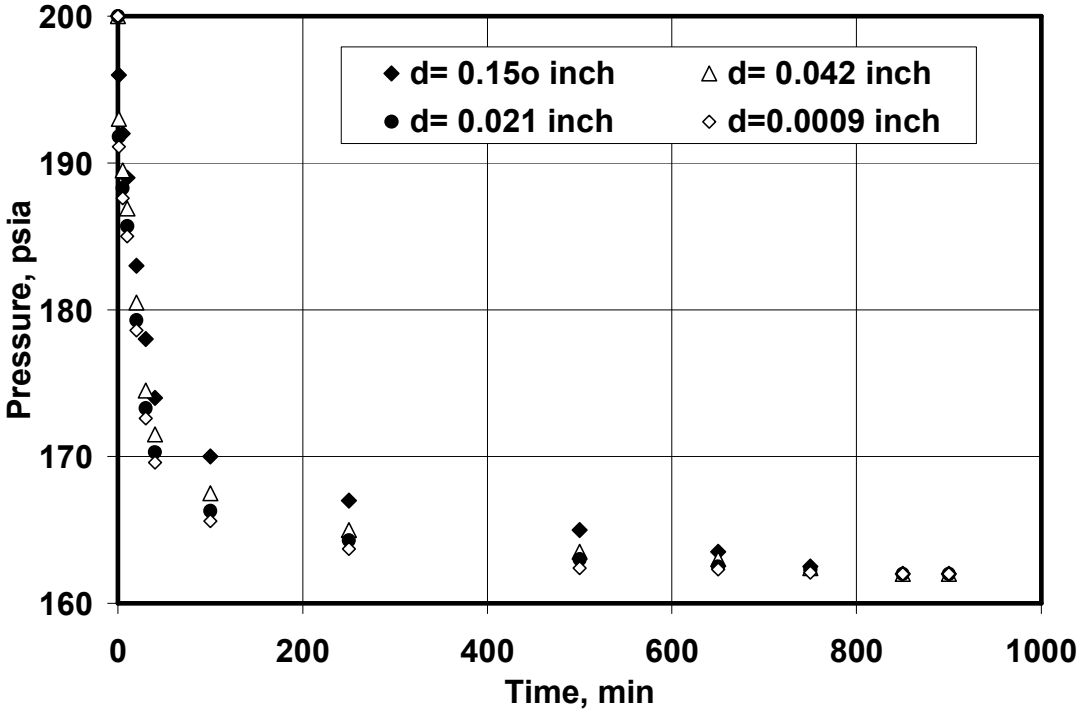

Figure A2. 2. Pressure versus time for various average coal A grain size and CO_2 system (P_{in} = 200 psia)

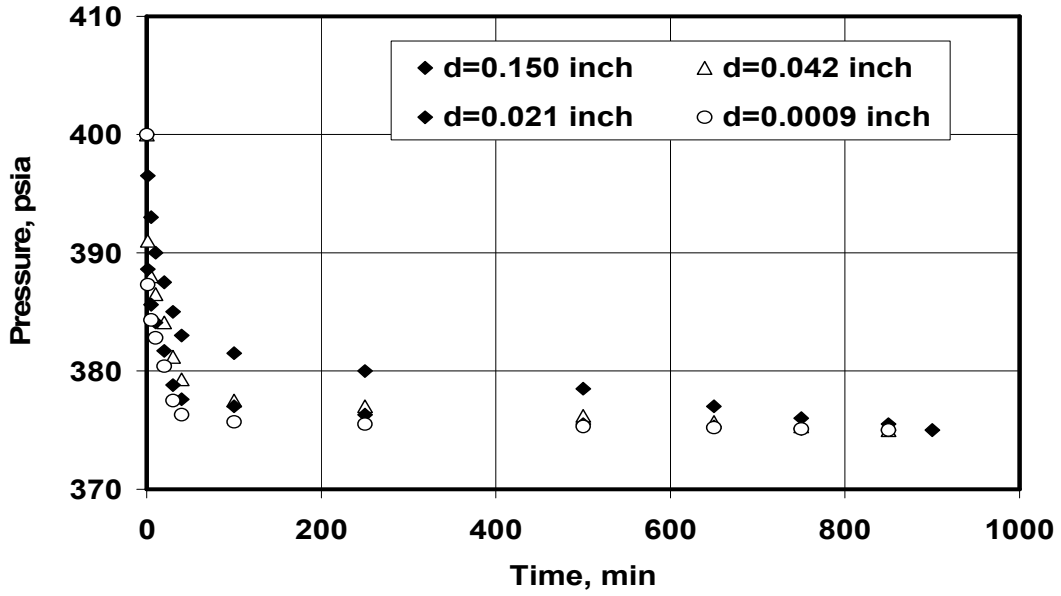

Figure A2. 3. Pressure versus time for various average coal A grain size and N_2 system (P_{in} = 400 psia)

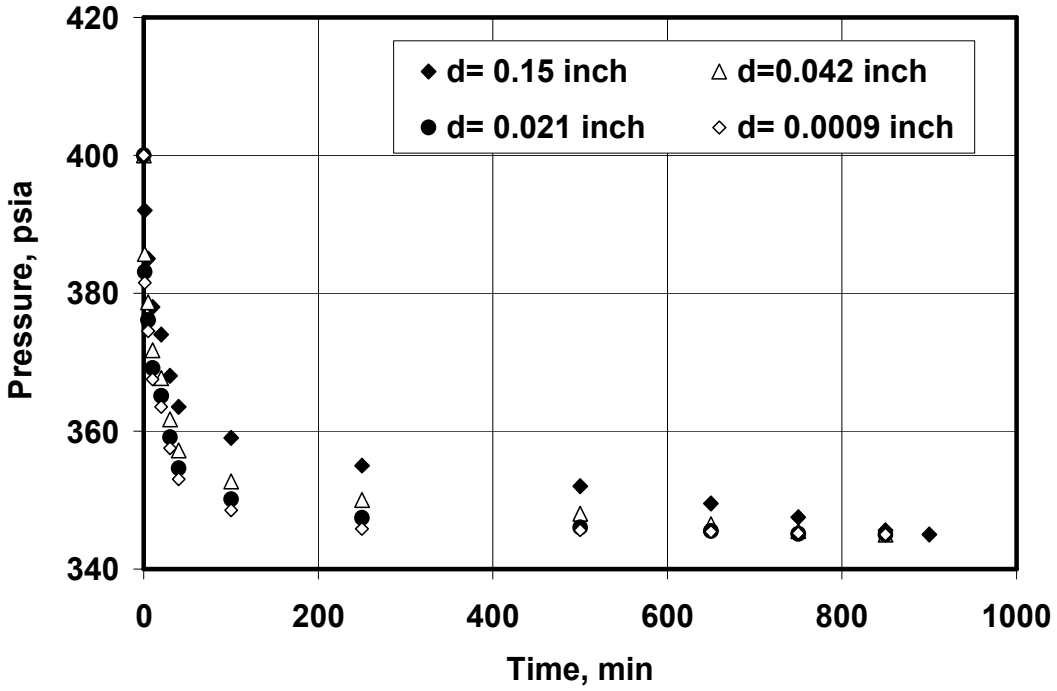

Figure A2. 4. Pressure versus time for various average coal A grain size and CO_2 system (P_{in} = 400 psia)

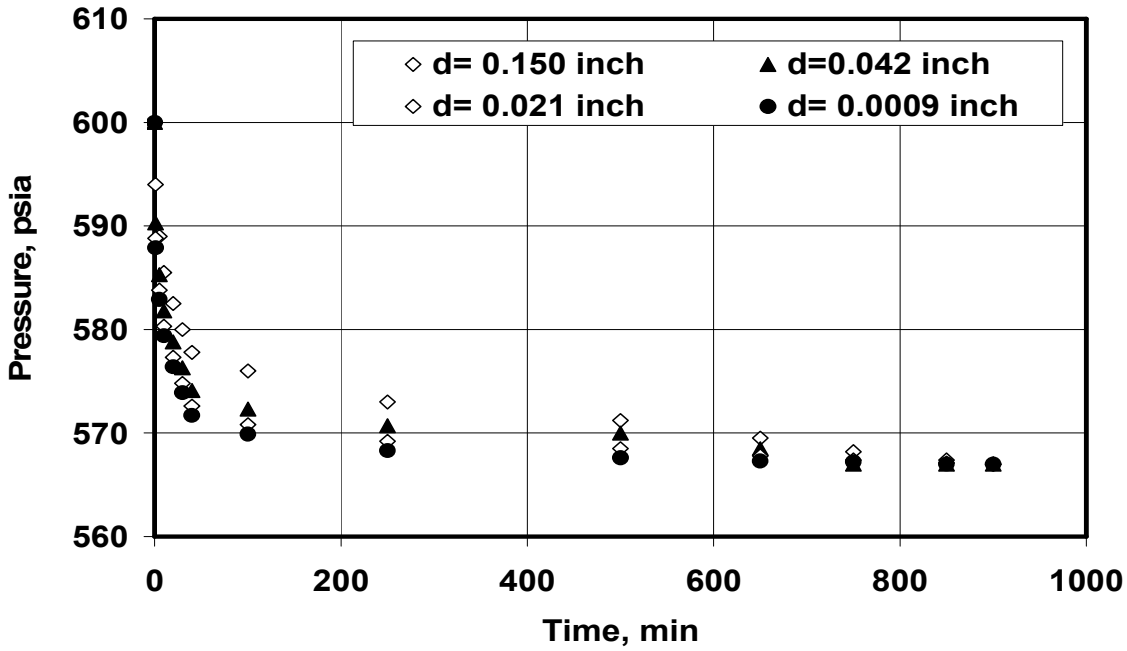

Figure A2. 5. Pressure versus time for various average coal A grain size and N_2 system (P_{in} = 600 psia)

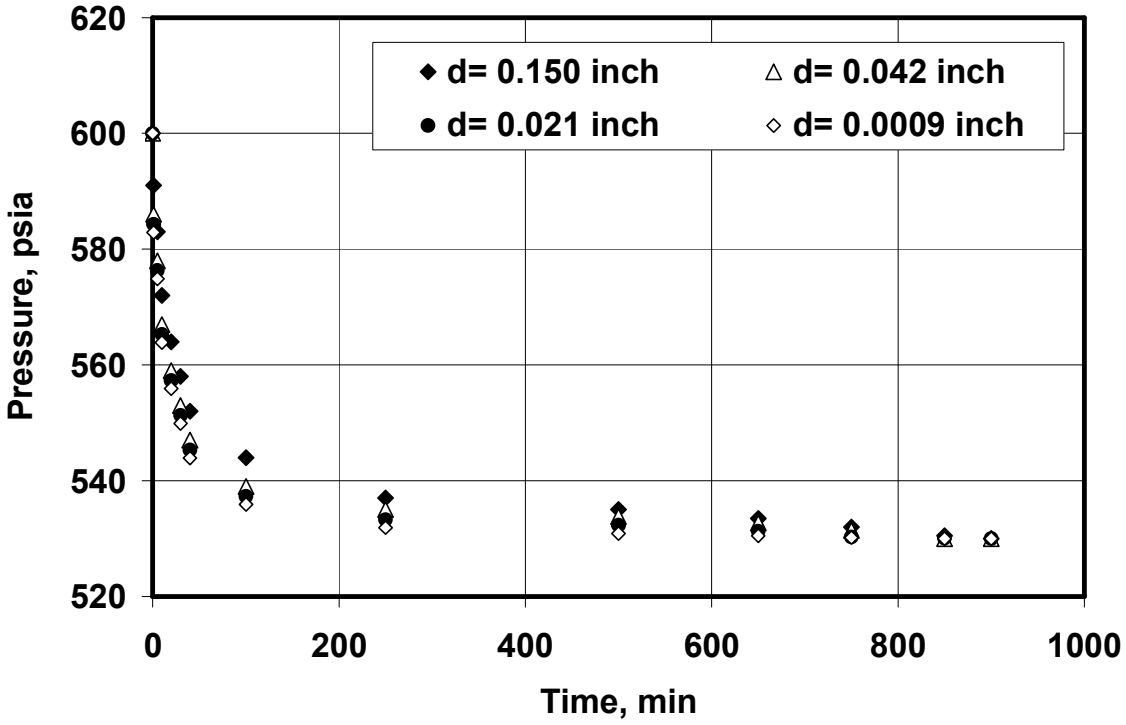

Figure A2. 6. Pressure versus time for various average coal A grain size and CO_2 system (P_{in} = 600 psia)

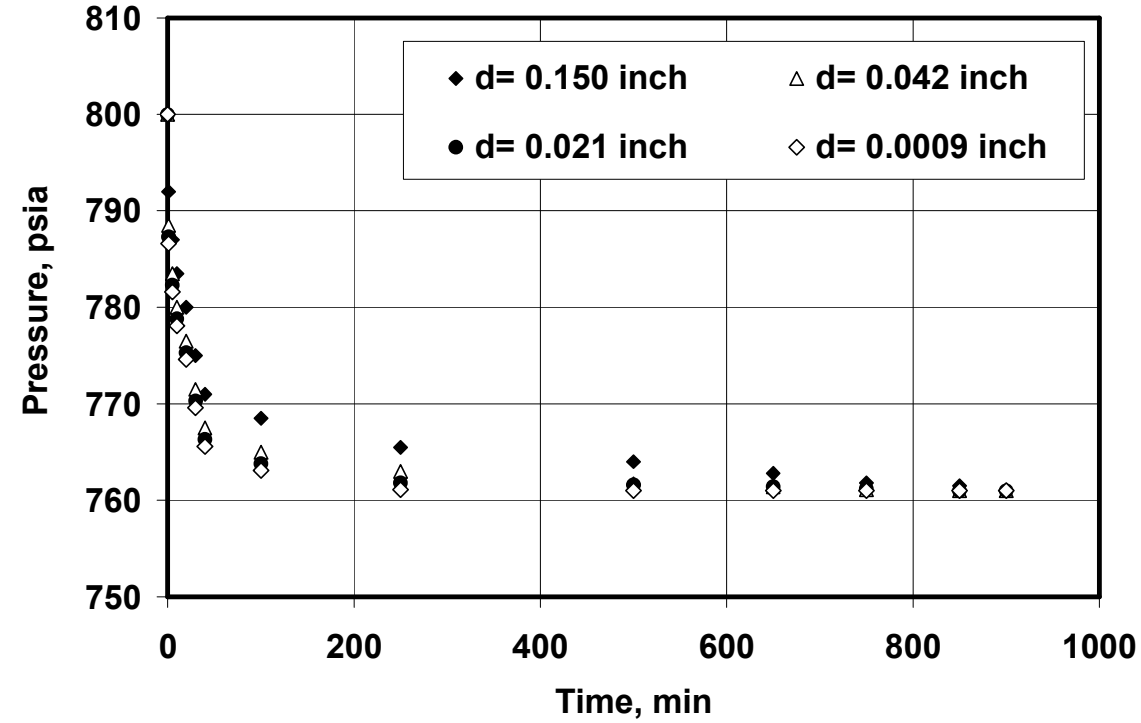

Figure A2. 7. Pressure versus time for various average coal A grain size and N_2 system (Pin = 800 psia)

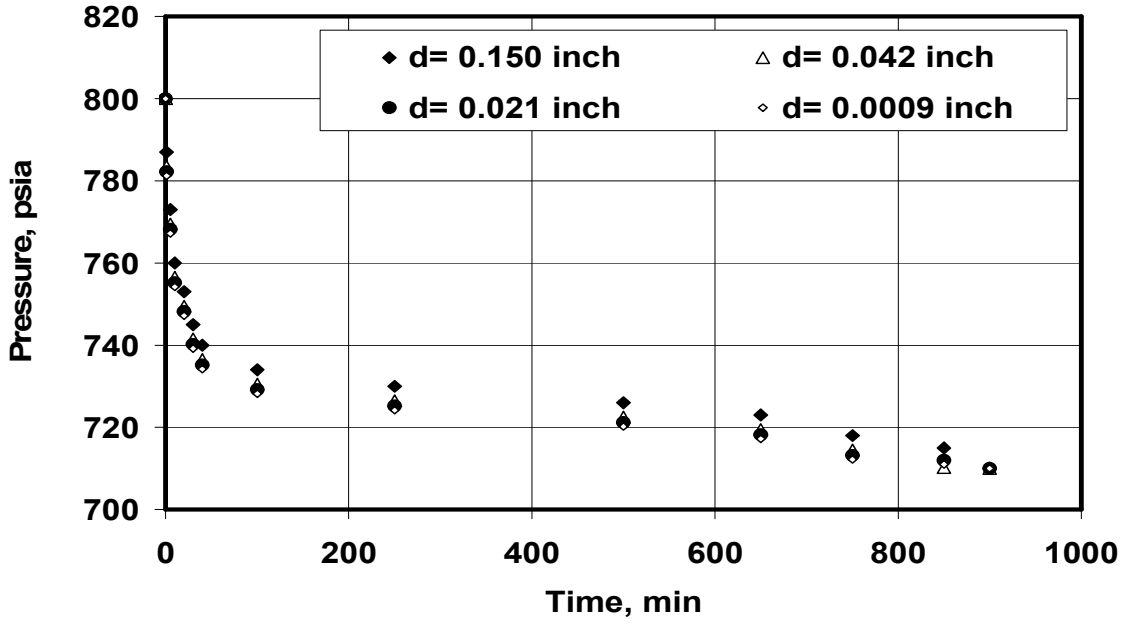

Figure A2. 8. Pressure versus time for various average coal A grain size and CO_2 system (P_{in} = 800 psia).

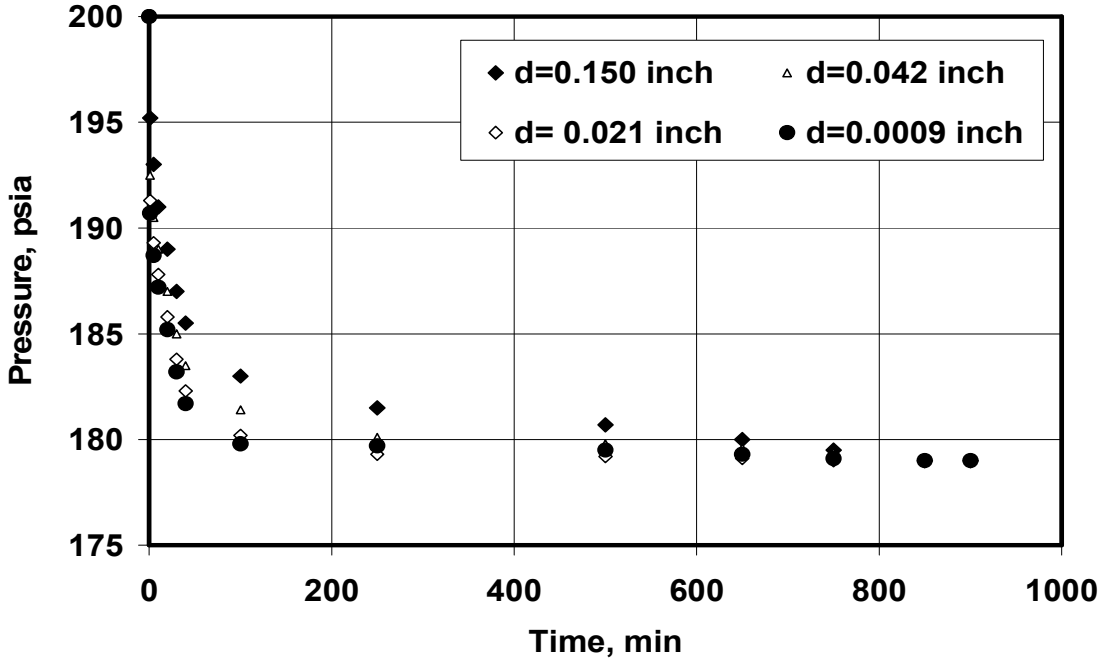

Figure A2. 9. Pressure versus time for various average coal B grain size and N_2 system (P_{in} = 200 psia)

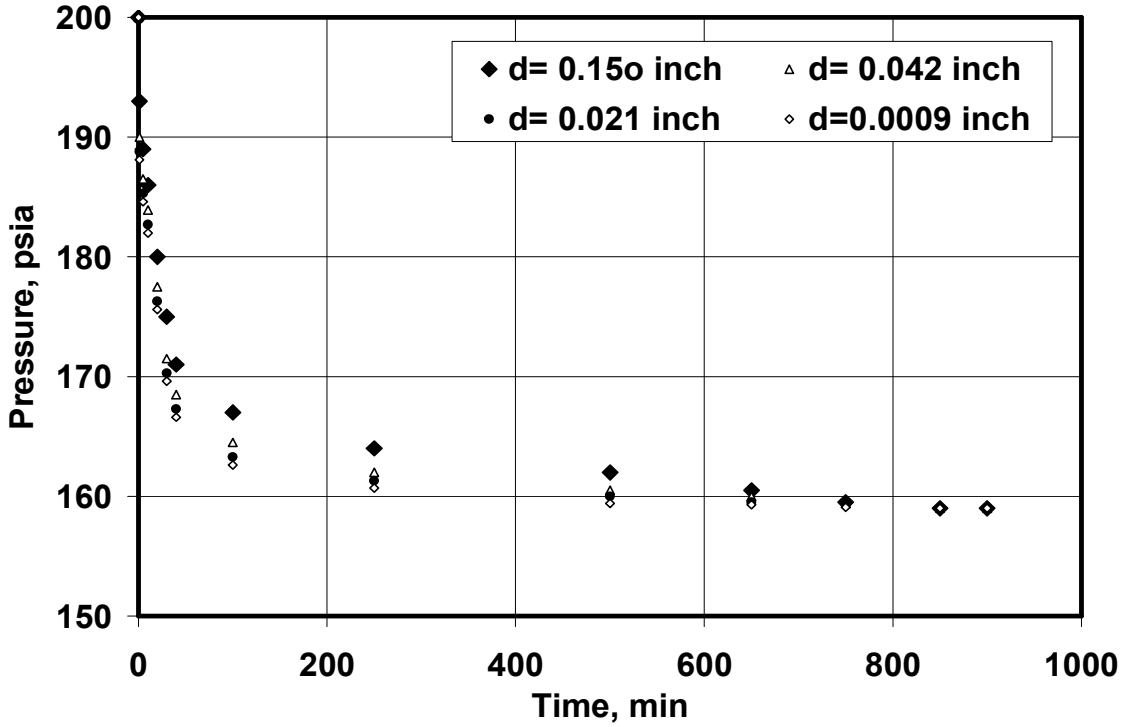

Figure A2. 10. Pressure versus time for various average coal B grain size and CO_2 system (P_{in} = 200 psia)

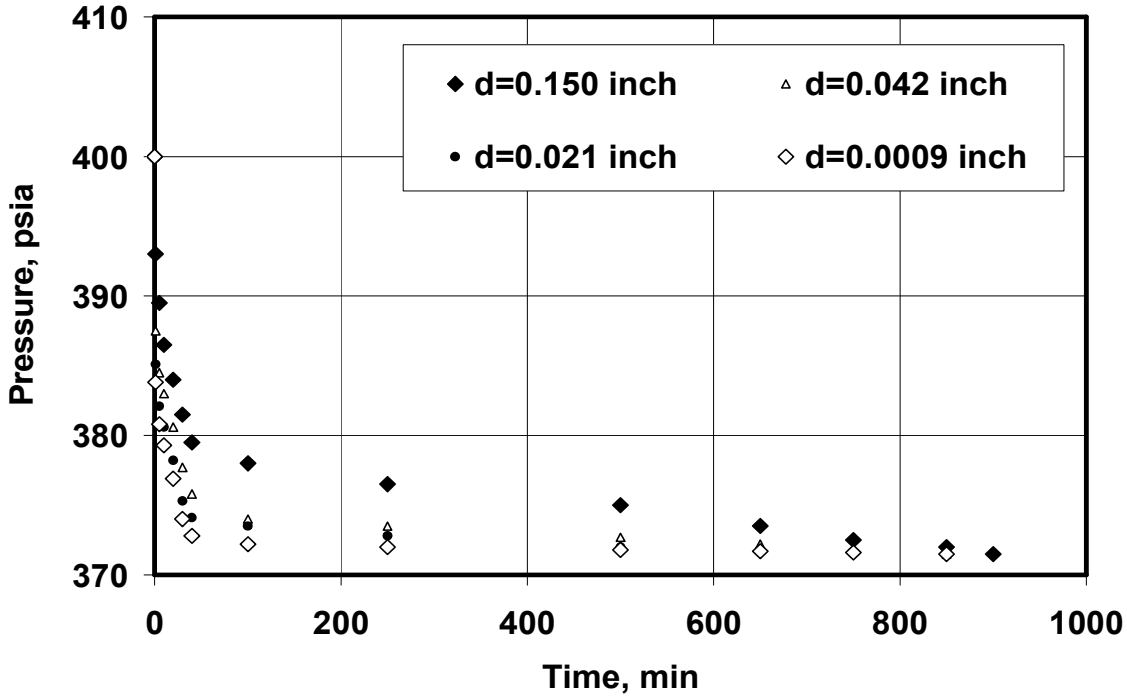

Figure A2. 11. Pressure versus time for various average coal B grain size and N_2 system (P_{in} = 400 psia)

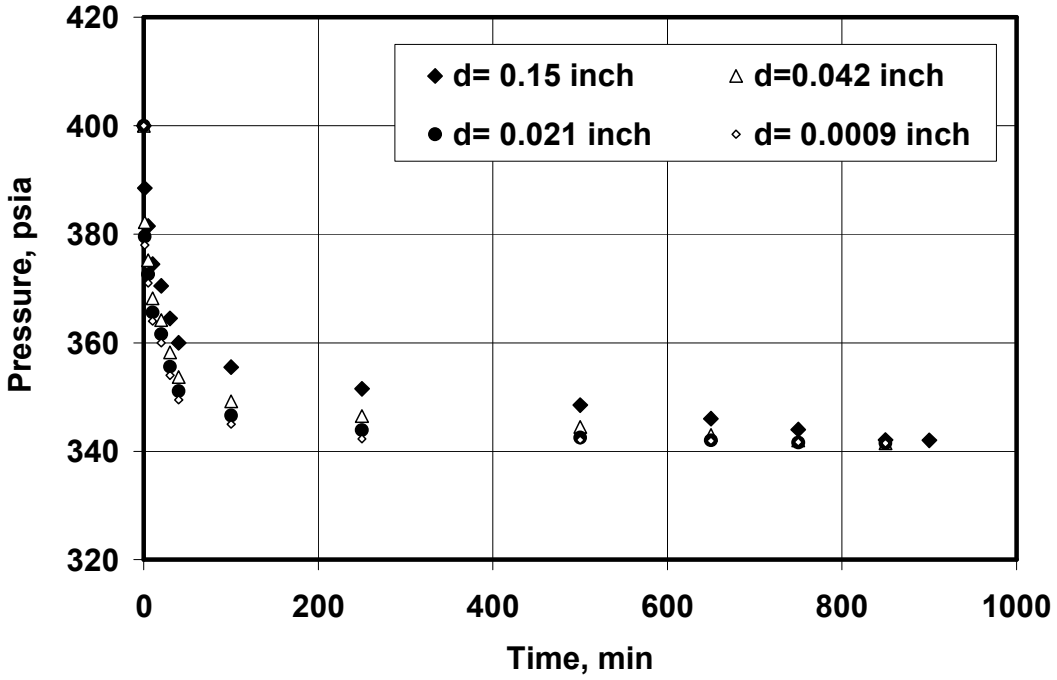

Figure A2. 12. Pressure versus time for various average coal B grain size and CO_2 system (P_{in} = 400 psia)

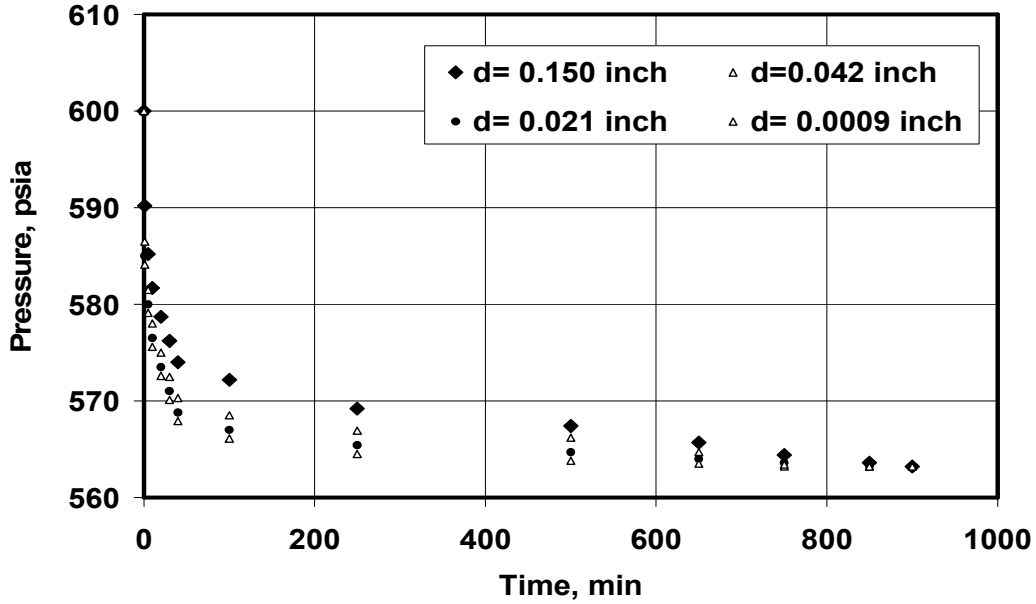

Figure A2. 13. Pressure versus time for various average coal B grain size and N_2 system (P_{in} = 600 psia)

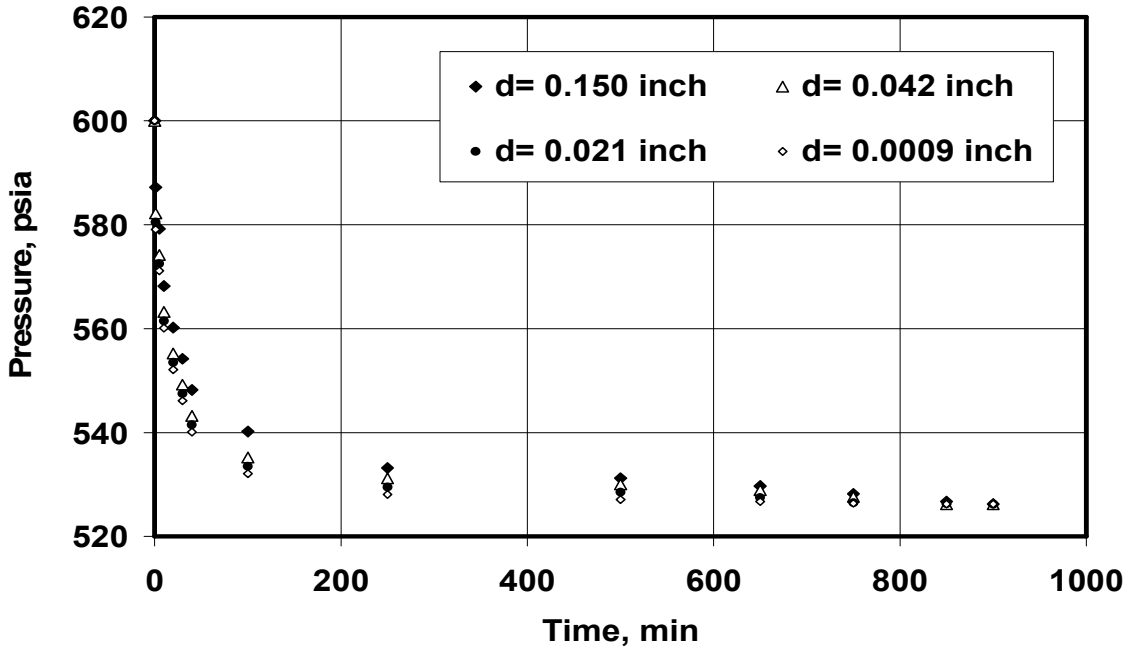

Figure A2. 14. Pressure versus time for various average coal B grain size and CO_2 system (P_{in} = 600 psia).

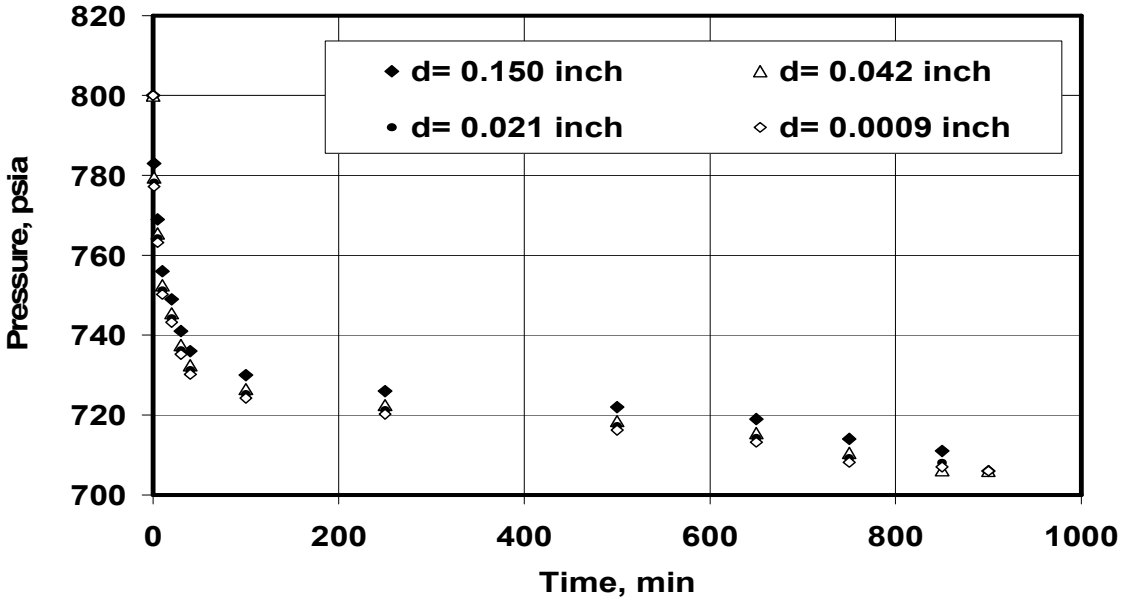

Figure A2. 15. Pressure versus time for various average coal B grain size and N_2 system (P_{in} = 800 psia)

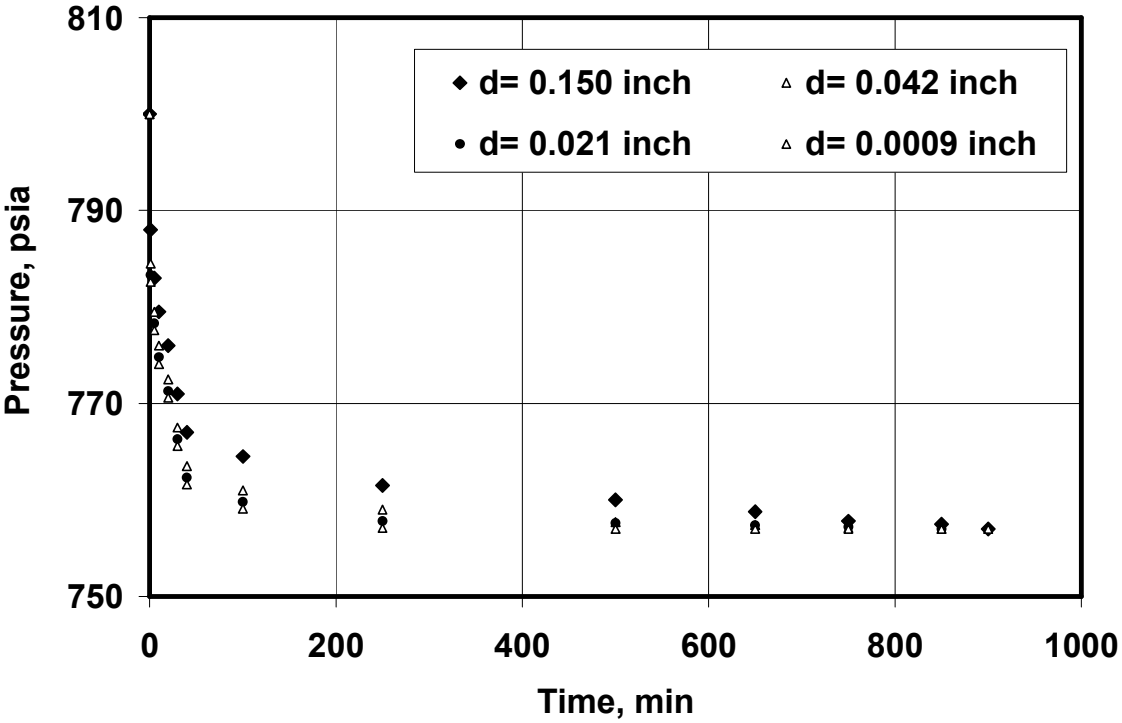

Figure A2. 16. Pressure versus time for various average coal B grain size and CO_2 system (P_{in} = 800 psia)

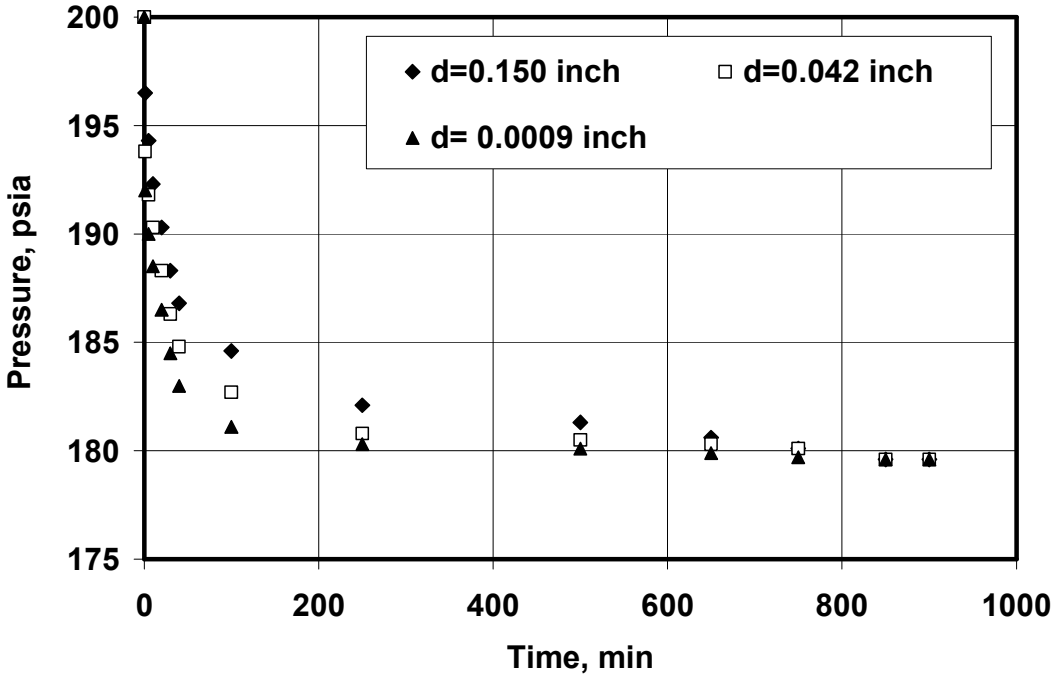

Figure A2. 17. Pressure versus time for coal A-N_2-Water, for different grain sizes (P_{in} = 200 psia)

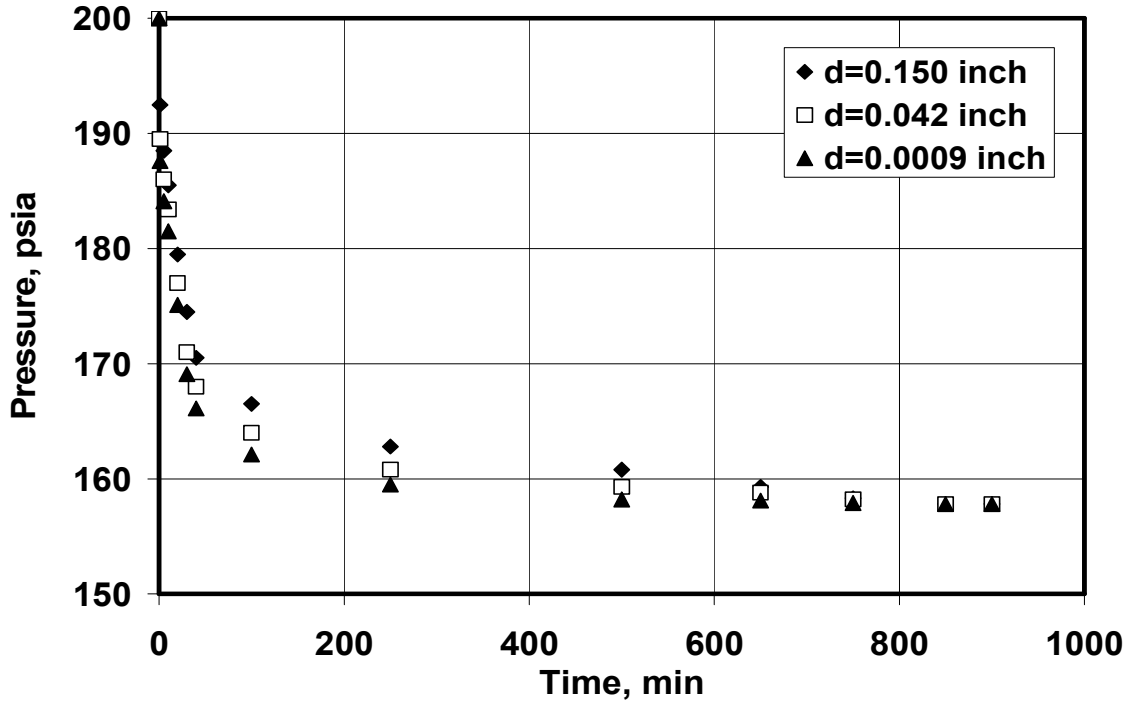

Figure A2. 18. Pressure versus time for coal A-CO_2-Water, for different grain sizes (P_{in} = 200 psia)

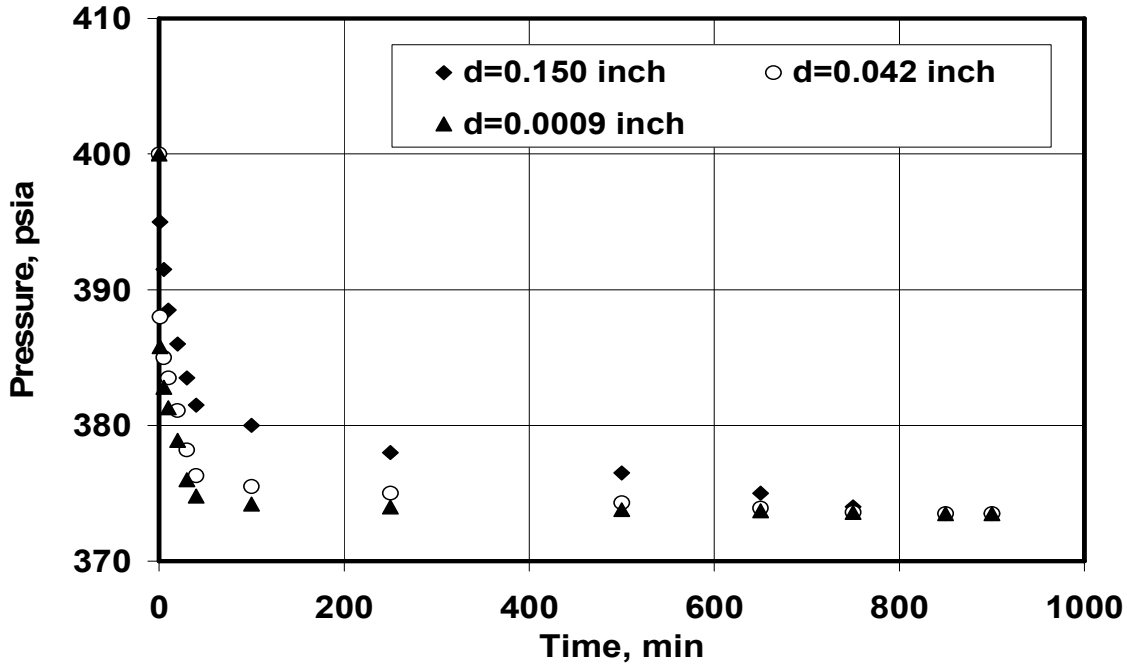

Figure A2. 19. Pressure versus time for coal A-N_2-Water, for different grain sizes (Pin = 400 psia)

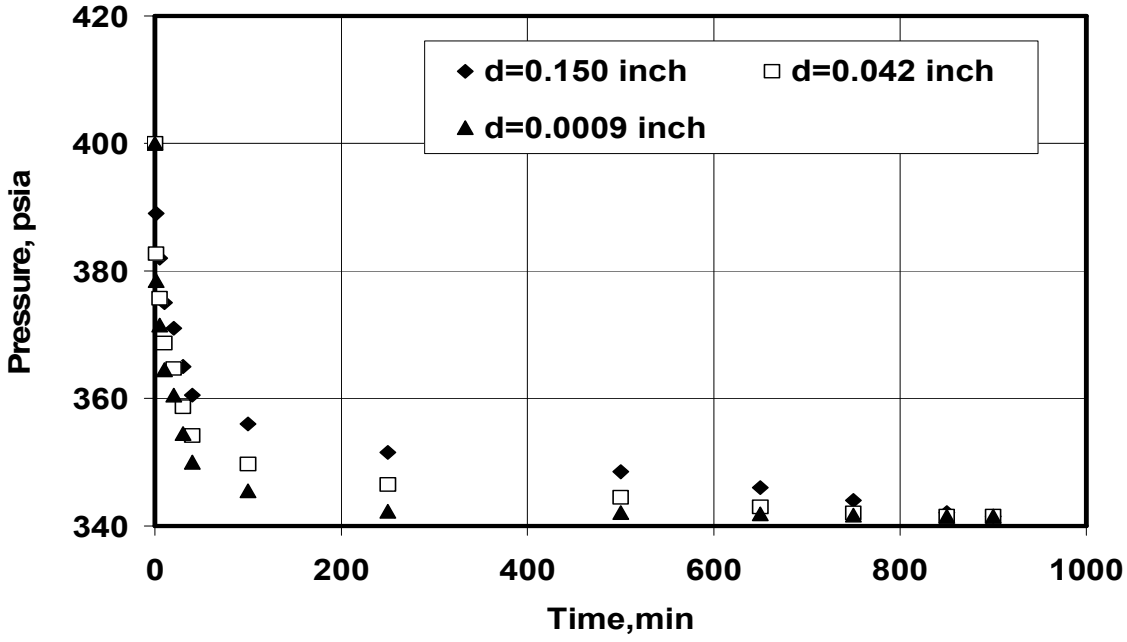

Figure A2. 20. Pressure versus time for coal A-CO_2-Water, for different grain sizes (P_{in} = 400 psia)

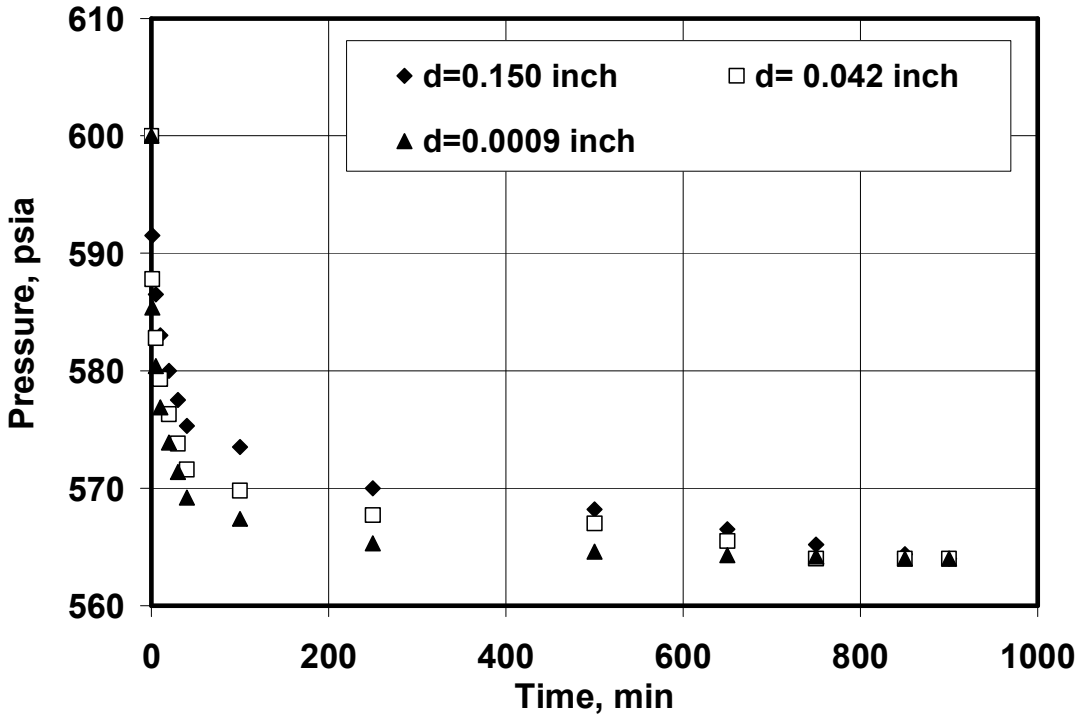

Figure A2. 21. Pressure versus time for coal A-N_2-Water, for different grain sizes (P_{in} = 600 psia)

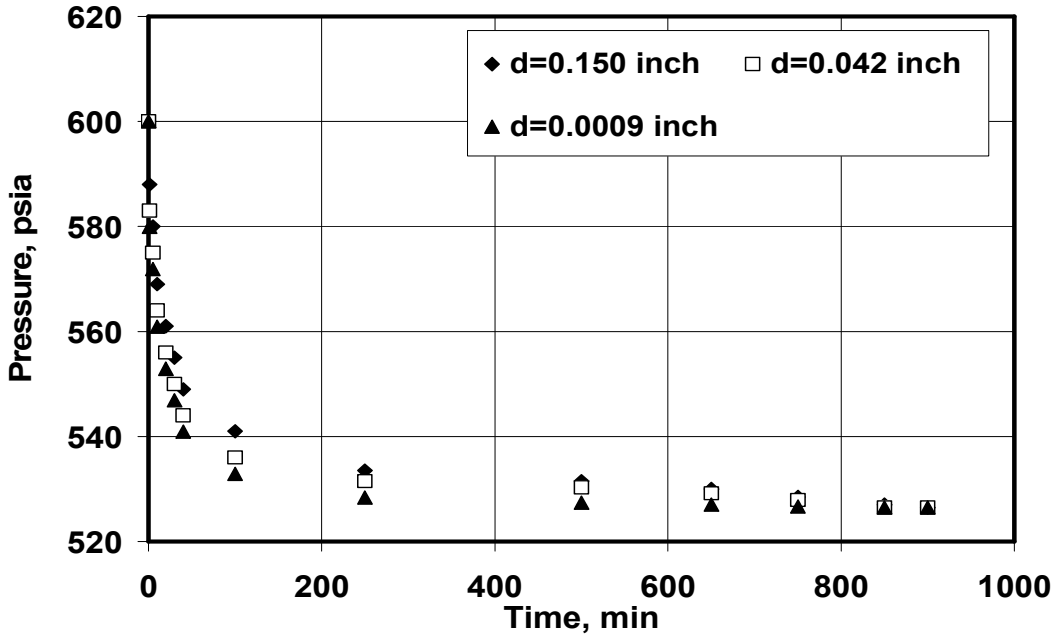

Figure A2. 22. Pressure versus time for coal A-CO_2-Water, for different grain sizes (P_{in} = 600 psia)

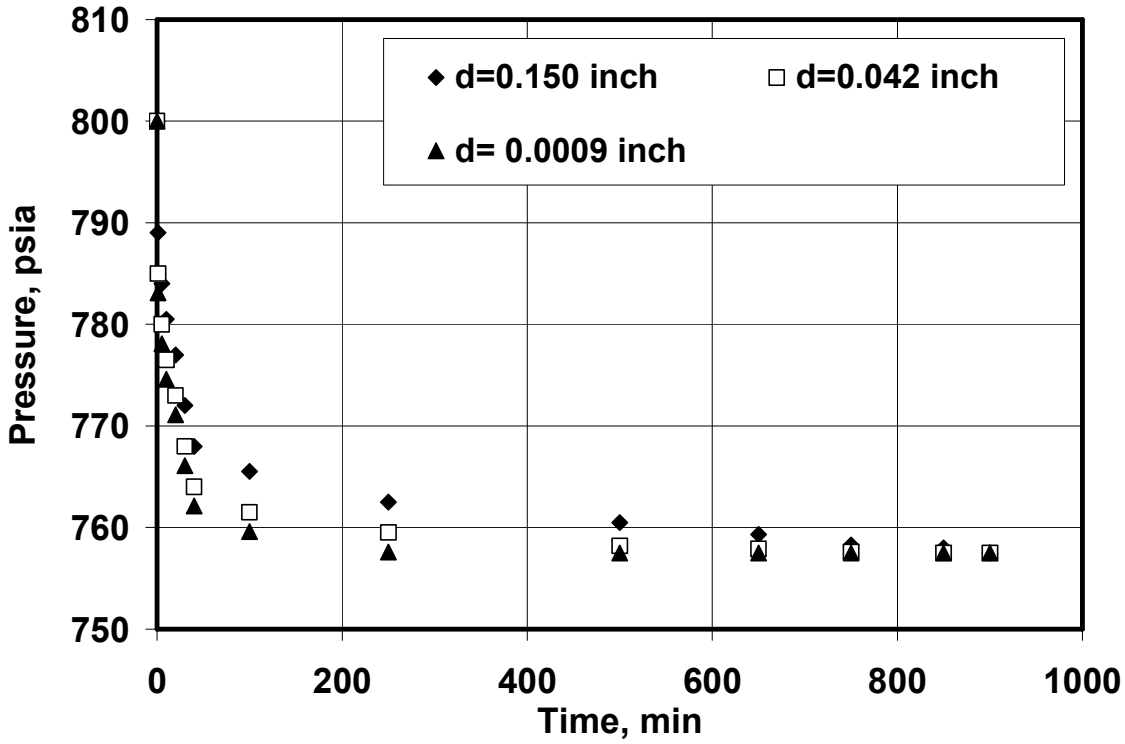

Figure A2. 23. Pressure versus time for coal A-N_2-Water, for different grain sizes (P_{in} = 800 psia)

APPENDIX 3

TABLES AS SUPPLEMENT TO CHAPTER 3- PARAMETERS OF THE DUBININ-RADUSHKEVICH (D-R) OBTAINED BY THE LEAST-SQUARES CURVE FITTING METHODS FOR VARIOUS GASES AND CARBONACEOUS MATTER

The single-component and multi-component equilibrium and non-equilibrium curve fitting procedures were explained in Chapter 5. The mentioned curve fitting procedures are applied for a series of the literature data to investigate the applications of the equilibrium, and non-equilibrium D-R, and Extended D-R isotherms. Appendix 3 contains three tables presenting the D-R isotherm curve fitting results for various equilibrium single-component gas-solid, non-equilibrium single-component gas-solid, and equilibrium multi-component gas-solid.

Table A3. 1.D-R Isotherm Curve fitting results for various literature data.

Data Sources	Tem. K	Pres. psia	Gas	R^2	r	D	V_m Scf/ton
Rutherford, and Coons, (2003)[α]	323	0-400	CH_4	0.99	0.002	2	23
Rutherford, and Coons, (2003)[α]	333	0-400	CH_4	1.0	0.0037	2	22
Berlier and Frere (1997) [β]	298	0-450	CO_2	1.0	0.079	2	28
Berlier and Frere (1997)[β]	303	0-450	CO_2	1.0	0.0046	2	25
Berlier and Frere (1997)[β]	318	0-450	CO_2	1.0	0.006	2	28
Berlier and Frere (1997)[β]	328	0-450	CO_2	1.0	0.15	2	17
Berlier and Frere (1997)[γ]	303	0-450	CO_2	1.0	0.094	1.5	29
Berlier and Frere (1997)[γ]	328	0-450	CO_2	1.0	0.10	1.5	30

[α] Tekeda Coal
[β] Activated carbon
[γ] Norit

Dreisbach et al. (1999)[δ]	298	0-850	CH_4	1.0	.086	1.5	84
Dreisbach et al. (1999)[δ]	298	0-850	N_2	1.0	0.128	1.5	57
Dreisbach et al. (1999)[δ]	298	0-850	CO_2	1.0	0.0066	2	12
Reich et al. (1980)[β]	301	0-550	CH_4	1.0	0.095	1.5	65
Reich et al. (1980)[β]	301	0-550	C_2H_6	1.0	0.181	2	65
Reich et al. (1980)[β]	301	0-550	C_2H_4	1.0	0.00243	2	66
Reich et al. (1980)[β]	301	0-550	CO_2	1.0	0.0076	2	88
Wakasugi et al., (1981)[β]	348	0-200	CH_4	1.0	0.003	2	48
Wakasugi et al. (1981)[β]	323	0-200	CH_4	0.99	0.0067	3	53
Wakasugi et al. (1981)[β]	298	0-200	CH_4	1.0	0.0026	3	60
Wakasugi et al. (1981)[β]	348	0-200	N_2	0.99	0.01136	2	49
Wakasugi et al. (1981)[β]	323	0-200	N_2	1.0	0.00627	3	57
Wakasugi et al.	298	0-200	N_2	1.0	0.011	2	42

[δ] Silicate

(1981)[β]							
Wakasugi et al. (1981)[β]	348	0-200	C_2H_6	1.0	0.00467	3	47
Wakasugi et al. (1981)[β]	323	0-200	C_2H_6	0.97	0.00586	2	55
Wakasugi et al. (1981)[β]	298	0-200	C_2H_6	0.95	0.00328	3	56
Wakasugi et al. (1981)[β]	348	0-200	CO_2	0.95	0.0027	3.2	86
Wakasugi et al. (1981)[β]	323	0-200	CO_2	0.99	0.0026	2	96
Wakasugi et al. (1981)[β]	298	0-200	CO_2	0.99	0.00156	2	100
Zhou et al. (2000)[β]	333	0-1200	CH_4	0.99	0.148	1.5	120
Zhou et al. (2000)[β]	313	0-1200	CH_4	1.0	0.017	2	115
Zhou et al. (2000)[β]	293	0-1200	CH_4	0.92	0.0095	2	49
Choudhary and Mayadevi (1996)[γ]	304	0-200	CO_2	1.0	0.0031	2	32
Choudhary and Mayadevi (1996)[γ]	354	0-200	CO_2	1.0	0.89	1	90
Choudhary and Mayadevi (1996)[γ]	306	0-200	C_2H_4	1.0	0.0015	3	24

Choudhary and Mayadevi (1996)[γ]	353	0-200	C_2H_4	1.0	0.736	1	87
Choudhary and Mayadevi (1996)[γ]	305	0-200	CH_4	0.97	0.0028	3.2	11
Choudhary and Mayadevi (1996)[γ]	353	0-200	CH_4	1.0	1.76	0.5	66
Choudhary and Mayadevi (1996)[γ]	305	0-200	C_2H_6	1.0	0.0036	3	25
Choudhary and Mayadevi (1996)[γ]	353	0-200	C_2H_6	1.0	0.0017	3.6	21
Choudhary and Mayadevi (1996)[γ]	413	0-200	C_2H_6	0.99	0.023	2	15
Chaback et al., (1996)[θ]	319	0-1600	CH_4	1.0	0.141	1.5	621
Chaback et al. (1996)[θ]	319	0-1600	N_2	1.0	0.287	1.5	273
Chaback et al. (1996)[θ]	319	0-1600	CO_2	1.0	0.017	1.9	894
Chaback et al. (1996)[σ]	319	0-1600	CH_4	1.0	0.185	1.5	282
Chaback et al.	319	0-1600	N_2	1.0	0.687	1.0	109

[θ] Fruit-Land Coal A
[σ] Fruit-Land Coal B

(1996)[σ]							
Chaback et al. (1996)[σ]	319	0-1600	CO_2	1.0	0.126	1.5	610
Chaback et al. (1996)[ω]	300	0-1600	CH_4	1.0	0.193	0.3	910
Chaback et al. (1996)[ω]	300	0-1600	N_2	1.0	0.193	1.5	307
Sutton and Davies (1935)[ε]	283	0-20	CH_4	1.0	0.168	1.9	84
Sutton and Davies(1935)[ε]	291	0-20	CH_4	1.0	0.206	1.5	66
Sutton and Davies(1935)[ε]	297	0-20	CH_4	1.0	0.627	1.1	83

[ω] Mary-Lee Coal
[ε] Char Coal

Table A3. 2. Curve fitting procedure for gas mixtures CH_4, CO_2, N_2, C_2H_6, and C_2H_4.

Data Sources	Tem. K	Pres. psia	Gas Mixture (component mole fraction)	R^2	D_i	r_i	Vm_i Scf /ton	ϕ_i
Dreisbach et al.(1999)[β]	298	0-1000	CH_4(9)/N_2(91) i = CH_4	0.99	0.62	1.0	30	0.91
Dreisbach et al.(1999)[β]	298	0-1000	CH_4(9)/N_2(91) i = N_2	0.99	0.01	2.0	35	0.76
Dreisbach et al.(1999)[β]	298	0-1000	CH_4(21)/CO_2(79), i = CH_4	0.99	0.15	1.0	23	0.90
Dreisbach et al.(1999)[β]	298	0-1000	CH_4(21)/CO_2(79), i = CO_2	0.99	0.06	1.5	103	0.89
Dreisbach et al.(1999)[β]	298	0-1000	CO_2(47)/N_2(53), i = CO_2	0.99	0.12	1.5	104	0.90
Dreisbach	298	0-1000	CO_2(47)/N_2(53)	0.99	0.01	2.0	115	0.82

[β] Activated Carbon

et al.(1999) [β]			, i = N_2					
Dreisbach et al.(1999) [β]	298	0-1000	CH_4(48)/CO_2(8)/N_2(44), i = CH_4	0.99	0.01	1.0	42	0.97
Dreisbach et al.(1999) [β]	298	0-1000	CH_4(48)/CO_2(8)/N_2(44), i = CO_2	0.99	0.10	1.5	21	0.92
Dreisbach et al.(1999) [β]	298	0-1000	CH_4(48)/CO_2(8)/N_2(44), i = N_2	0.99	0.02	2.0	20	0.84
Reich et al. (1980) [β]	301	0-300	CH_4(27)/C_2H_6(73), i = CH_4	1.0	0.05	1.5	23	0.94
Reich et al. (1980) [β]	301	0-300	CH_4(27)/C_2H_6(73), i = C_2H_6	1.0	0.002	2.0	60	0.98
Reich et al. (1980) [β]	301	0-300	CH_4(50)/C_2H_6(50), i = CH_4	1.0	0.004	1.5	78	0.94
Reich et al. (1980) [β]	301	0-300	CH_4(50)/C_2H_6(50), i = C_2H_6	0.99	0.002	2.0	140	0.99
Reich et al. (1980) [β]	301	0-300	CH_4(74)/C_2H_6(26), i = CH_4	1.0	0.05	1.5	18	0.90
Reich et al.	301	0-300	CH_4(74)/C_2H_6(	1.0	0.00	2.0	63	0.96

(1980)[β]			26), i = C_2H_6		3			
Reich et al. (1980)[β]	301	0-300	CH_4(26)/C_2H_4(74), i = CH_4	1.0	0.06	1.5	33	0.90
Reich et al. (1980)[β]	301	0-300	CH_4(26)/C_2H_4(74), i = C_2H_4	0.99	0.04	1.5	60	0.91
Reich et al. (1980)[β]	301	0-300	CH_4(76)/C_2H_4(24), i = CH_4	1.0	0.06	1.5	43	0.9
Reich et al. (1980)[β]	301	0-300	CH_4(76)/C_2H_4(24), i = C_2H_4	1.0	0.01	1.5	41	0.92
Reich et al. (1980)[β]	301	0-450	CH_4(62)/C_2H_6(18)/C_2H_4(20), i = CH_4	0.97	0.49	1.5	74	0.97
Reich et al. (1980)[β]	301	0-450	CH_4(62)/C_2H_6(18)/C_2H_4(20), i = C_2H_6	0.99	0.002	2.0	25	0.91
Reich et al. (1980)[β]	301	0-450	CH_4(62)/C_2H_6(18)/C_2H_4(20), i = C_2H_4	0.99	0.002	2.0	26	0.94
Reich et al. (1980)[β]	301	0-450	CH_4(23)/C_2H_6(52)/C_2H_4(25), i = CH_4	1.0	0.002	1.5	27	0.96
Reich et al.	301	0-450	CH_4(23)/C_2H_6(	1.0	0.00	2.0	46	0.95

(1980)[β]			52)/C_2H_4(25), i = C_2H_6		1			
Reich et al. (1980)[β]	301	0-450	CH_4(23)/C_2H_6(52)/C_2H_4(23), i = C_2H_4	0.99	0.21	1.5	54	0.95
Reich et al. (1980)[β]	301	0-450	CH_4(20)/C_2H_6(20)/C_2H_4(60), i = CH_4	1.0	0.003	1.5	15	0.97
Reich et al. (1980)[β]	301	0-450	CH_4(20)/C_2H_6(20)/C_2H_4(60), i = C_2H_6	0.99	0.006	2.0	16	0.92
Reich et al. (1980)[β]	301	0-450	CH_4(20)/C_2H_6(20)/C_2H_4(60), i = C_2H_4	0.99	0.23	1.5	71	0.98
Chaback et al. (1996)[ω]	300	300-1500	CH_4(70)/N_2(30) i = CH_4	1.0	0.002	1.5	59	0.92
Chaback et al. (1996)[ω]	300	300-1500	CH_4(70)/N_2(30) i = N_2	0.85	0.0003	3.0	44	0.83
Chaback et al. (1996)[ω]	300	300-1500	CH_4(9)/N_2(91) i = CH_4	1.0	0.002	1.5	200	0.93
Chaback et	300	300-	CH_4(9)/N_2(91)	0.99	0.00	3.0	277	0.94

[ω] Mary-Lee Coal

al. (1996) [ω]		1500	i = N_2		2			
Chaback et al. (1996) [ω]	300	300-1500	CH_4(15)/N_2(85) i = CH_4	1.0	0.16	1.5	288	0.95
Chaback et al. (1996)[ω]	300	300-1500	CH_4(15)/N_2(85) i = N_2	1.0	0.002	3.0	250	0.93
Chaback et al. (1996)[θ]	300	300-1500	CH_4(40)/CO_2(40)/N_2(15), i = CH_4	1.0	0.08	1.5	361	0.96
Chaback et al. (1996) [θ]	300	300-1500	CH_4(40)/CO_2(40)/N_2(15), i = CO_2	1.0	0.33	1.0	182	0.90
Chaback et al. (1996) [θ]	300	300-1500	CH_4(40)/CO_2(40)/N_2(15), i = N_2	1.0	0.38	1.0	591	0.83
Chaback et al. (1996) [θ]	300	300-1500	CH_4(65)/CO_2(20)/N_2(15), i = CH_4	1.0	0.11	1.5	567	0.95
Chaback et al. (1996) [θ]	300	300-1500	CH_4(65)/CO_2(20)/N_2(15), i = CO_2	1.0	0.35	1.0	432	0.91
Chaback et	300	300-	CH_4(65)/CO_2(2	1.0	0.05	1.0	204	0.87

[θ] Fruit-Land Coal

al. (1996) [θ]		1500	0)/N_2(15), i = N_2					
Chaback et al. (1996) [θ]	300	300-1500	CH_4(55)/CO_2(42)/N_2(3), i = CH_4	0.99	0.83	0.5	943	0.99
Chaback et al. (1996) [θ]	300	300-1500	CH_4(55)/CO_2(42)/N_2(3), i = CO_2	0.88	1.5	0.5	1300	0.93
Chaback et al. (1996) [θ]	300	300-1500	CH_4(55)/CO_2(42)/N_2(3), i = N_2	0.98	1.4	0.5	2200	0.88
Chaback et al. (1996) [θ]	300	300-1500	CH_4(89)/CO_2(8)/N_2(3), i = CH_4	1.0	0.4	1.0	66	0.94
Chaback et al. (1996) [θ]	300	300-1500	CH_4(89)/CO_2(8)/N_2(3), i = CO_2	0.99	3.5	0.5	76	0.91
Chaback et al. (1996) [θ]	300	300-1500	CH_4(89)/CO_2(8)/N_2(3), i = N_2	1.0	0.08	2.0	50	0.87
Chaback et al. (1996) [θ]	300	300-1500	CH_4(7)/CO_2(90)/N_2(3), i = CH_4	1.0	0.12	1.5	51	0.99
Chaback et al. (1996) [θ]	300	300-1500	CH_4(7)/CO_2(90)/N_2(3), i = CO_2	1.0	0.48	1.5	58	0.93
Chaback et al. (1996) [θ]	300	300-1500	CH_4(7)/CO_2(90)/N_2(3), i = N_2	1.0	0.59	1.0	175	0.88

DeGance (1992) θ	320	200-1600	CH_4(20)/N_2(80) i = CH_4	1.0	0.56	1.0	14	0.97
DeGance (1992) θ	320	200-1600	CH_4(20)/N_2(80) i = N_2	1.0	0.16	1.5	26	0.90
DeGance (1992) θ	320	200-1600	CH_4(80)/N_2(20) i = CH_4	1.0	0.43	1.0	10	0.99
DeGance (1992) θ	320	200-1600	CH_4(80)/N_2(20) i = N_2	1.0	1.48	0.5	10	0.92
DeGance (1992) θ	320	200-1600	CH_4(80)/CO_2(20), i = CH_4	1.0	0.45	1.0	11	0.98
DeGance (1992) θ	320	200-1600	CH_4(80)/CO_2(20), i = CO_2	1.0	0.39	1.0	25	0.92
DeGance (1992) θ	320	200-1600	CH_4(9)/CO_2(84)/N_2(7), i = CH_4	1.0	0.11	1.5	201	0.99
DeGance (1992) θ	320	200-1600	CH_4(9)/CO_2(84)/N_2(7), i = CO_2	1.0	0.52	1.0	483	0.92
DeGance (1992) θ	320	200-1600	CH_4(9)/CO_2(84)/N_2(7), i = N_2	1.0	0.01	3.0	435	0.88
DeGance (1992)θ	320	200-1600	CH_4(87)/CO_2(7)/N_2(6), i = CH_4	1.0	0.01	3.0	14	0.98
DeGance (1992)θ	320	200-1600	CH_4(87)/CO_2(7)/N_2(6), i = CO_2	1.0	0.004	1.5	20	0.93

DeGance (1992)[θ]	320	200-1600	CH_4(87)/CO_2(7)/N_2(6), i = N_2	1.0	0.0007	3.0	18	0.88

Table A3. 3. Curve fitting non-equilibrium D-R isotherm parameters for various gases non-equilibrium sorption data on different adsorbents

Data Source	Tem. K	Pres. psia	Gas	R^2	D	r	Vm scf/ton	k_{gs}
Clarkson (2003)[ζ]	300	115	CH_4	1.0	0.346	1.0	30	10^{-8}
Clarkson (2003)[ζ]	300	130	CH_4	1.0	0.213	1.0	18	10^{-8}
Clarkson (2003)[ζ]	300	144	CH_4	0.96	0.18	1.0	10	10^{-8}
Clarkson (2003)[ζ]	300	160	CH_4	1.0	0.11	1.0	5	10^{-8}
Clarkson (2003)[ζ]	300	29	CO_2	1.0	0.21	3.0	15	10^{-7}
Clarkson (2003)[ζ]	300	43	CO_2	0.96	0.18	3.0	13	10^{-7}
Clarkson (2003)[ζ]	300	73	CO_2	0.98	0.14	3.0	11	10^{-7}
Clarkson (2003)	300	89	CO_2	1.0	0.09	3.0	9	10^{-7}
Clarkson (2003)[ζ]	300	216	CH_4	1.0	0.17	2.0	12	10^{-6}
Clarkson (2003)[λ]	300	216	CH_4	1.0	0.14	2.0	10	10^{-6}
Clarkson (2003)[λ]	300	216	CH_4	1.0	0.08	2.0	8	10^{-6}
Zhou (1994)[υ]	302	15	Fluore	1.0	0.5	2.5	11	10^{-6}
Fawzi et al. (1996)[ς]	298	15	Benzene	0.99	0.32	2.5	35	10^{-8}

[ζ] Dry Coal
[λ] Wet Coal
[υ] Polymer
[ς] Zeolite

Crawshaw and John (1992)[б]	300	14	Water	0.98	0.31	1.0	35	10^{-5}
Crawshaw and John (1992)[б]	300	14	Methanol	0.98	0.22	2.5	19	10^{-6}
Xijun (1993)[β]	283	10	Ethane	0.99	0.192	3.0	10	10^{-5}
Xijun (1993)[β]	308	10	Ethane	0.99	0.15	2.0	8.0	10^{-5}
Xijun (1993)[β]	323	10	Ethane	0.97	0.11	1.0	5.0	10^{-5}
Xijun (1993)[β]	283	10	Propane	1.0	0.18	3.5	20	10^{-6}
Xijun (1993)[β]	308	10	Propane	0.99	0.14	3.0	15	10^{-6}
Xijun (1993)[β]	323	10	Propane	0.99	0.08	2.0	10	10^{-6}
Xijun (1993)[β]	283	15	n-Butane	1.0	0.35	2.5	38	10^{-7}
Xijun (1993)[β]	308	15	n-Butane	0.99	0.29	1.5	31	10^{-7}
Xijun (1993)[β]	323	15	n-Butane	0.99	0.21	0.5	27	10^{-7}
Ciembroniewicz and Marecka (1993)[κ]	289	15	CO2	0.98	0.25	1.5	32	10^{-8}
Cheng and Huang (2004)[í]	300	14.6	CH_4	0.98	0.45	2.0	56	10^{-7}
Cheng and Huang (2004)[í]	300	14.6	C_2H_6	0.95	0.42	1.5	50	10^{-7}
Cheng and Huang (2004)[í]	300	14.6	C_3H_8	0.99	0.35	1.5	47	10^{-7}
Cheng and Huang (2004)[í]	300	14.6	n-C_4H_{10}	0.98	0.30	2.0	43	10^{-7}
Cheng and Huang (2004)[í]	300	14.6	n-C_5H_{12}	0.97	0.25	3.0	38	10^{-7}
Cheng and Huang (2004)[í]	300	14.6	C_6H_{14}	1.0	0.19	1.5	31	10^{-7}
Cheng and Huang (2004)[ξ]	300	14.6	CH_4	0.95	0.34	2.5	43	10^{-6}
Cheng and Huang (2004)[ξ]	300	14.6	C_2H_6	0.98	0.31	2.0	33	10^{-6}

[б] Maize
[β] Activated Carbon
[κ] Polish Coal
[í] Shaly Coal
[ξ] Green River Shale

Cheng and Huang (2004) [ξ]	300	14.6	C_3H_8	0.97	0.26	1.5	25	10^{-6}
Cheng and Huang (2004) [ξ]	300	14.6	n-C_4H_{10}	0.99	0.21	2.5	28	10^{-6}
Cheng and Huang (2004) [ξ]	300	14.6	n-C_5H_{12}	0.99	0.17	3.0	12	10^{-6}
Cheng and Huang (2004) [ξ]	300	14.6	C_6H_{14}	0.98	0.12	3.5	6	10^{-6}
Ding and Bhatia (2003)[β]	310	15	C_2H_6	0.99	0.32	2.0	43	10^{-7}
Ding and Bhatia (2003)[β]	310	15	C_3H_8	0.99	0.23	1.5	32	10^{-7}

[β] Activated Carbon

APPENDIX 4

INTERPRETATION OF THE EXPERIMENTAL DATA-SUPPLEMENT TO CHAPTER 5

This appendix contains several examples illustrating the step-by-step calculation of the adsorbed volume and mole fraction of any component in the gas-water, single component gas-coal, single component gas-coal-water, and multicomponent gas-coal systems under non-equilibrium conditions.

4.1. Water-Gas System

This section presents the experimental data interpretation procedure to interpret and convert the obtained experimental pressure versus time data to the volume and mole fraction versus time. First the water-gas systems are examined using series of examples describing the data interpretation procedure. Figure A4.1 shows the PVT experiment cell dimensions.

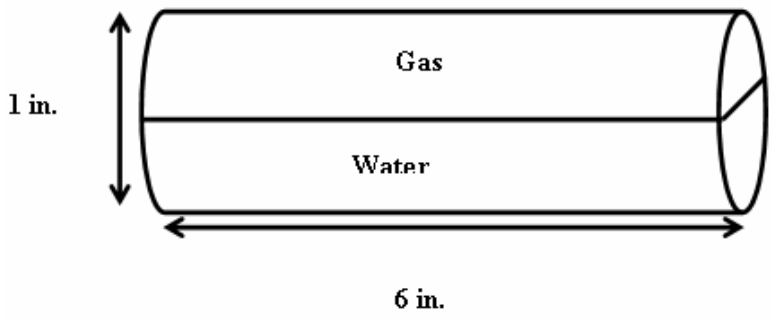

Figure A4.1. The dimensions of the PVT cell and gas-water system (Volume of PVT cell=340 cc=19 in^3, Volume of water= 100 cc= 6.1 in^3)

Step 1. The first step in evaluating the experimental data is to calculate the injected gas moles at various pressure levels using the real gas EoS stated as the following:

$$n(t=0)=\frac{P(t=0)V_{gas}}{R\,T\,Z(t=0)}$$

where:

$$V_{gas}=V_{cell}-V_{water}=340-100=240cc=8.476\times10^{-3}\,ft^3$$

An example below describes the computational procedure for N_2-water system at 100 psia and 28^o C.

$$T_r=\frac{T}{T_c}=\frac{28+273.3}{126}=2.391$$

$$P_r=\frac{P}{P_c}=\frac{100}{490}=0.204$$

The Peng-Robinson EoS is used to estimate the gas compressibility factor at the given pressure and temperature.

Equation 5.59 : $k(\omega)=0.37464+1.54226(0.0403)-0.26992(0.0403)^2=0.4364$

Equation 5.56: $a=0.45724\frac{(19.31)^2(126)^2}{490}\sqrt{1+0.4364\left(1-(2.391)^{1/2}\right)}=4821$

Equation 5.57: $b=0.0778\frac{(19.31)(126)}{(490)}=0.386$

Equation 5.60: $A=\frac{(4821)(100)}{(19.31)^2(301.3)^2}=0.014$

Equation 5.60: $B=\frac{(0.386)(100)}{(19.31)(301.3)}=6.63\times10^{-3}$

Equation 5.52:

$$Z^3-\left(1-\left(6.63\times10^{-3}\right)\right)Z^2+\left(0.014-3\left(6.63\times10^{-3}\right)^2-2\left(6.63\times10^{-3}\right)\right)Z-$$
$$\left((0.014)\left(6.63\times10^{-3}\right)-\left(6.63\times10^{-3}\right)^2-\left(6.63\times10^{-3}\right)^3\right)=0$$

Therefore the gas compressibility factor is obtained by solving the following equation:

$$Z^3-\left(0.99337\right)Z^2+\left(6.081\times10^{-4}\right)Z-4.851\times10^{-5}=0$$

By solving the above third degree polynomial the N_2 compressibility factor at 100 psia and 301 K is equal to 0.9975. The initial nitrogen moles in the PVT cell are estimated using the following relationship:

$$n\left(t=0\right)=\frac{P\left(t=0\right)V_{gas}}{R\,T\,Z\left(t=0\right)}$$

Tables 6.6 and 6.7 summarize the gas compressibility factors and initial gas moles for both N_2 and CO_2 using the Peng Robinson EoS.

Table A4. 1. The nitrogen compressibility factor and initial injected moles for various pressures and temperature of 28°C.

P, psia	Z	lbmole
50	0.9987	7.290E-05
100	0.9975	1.404E-04
200	0.9953	2.927E-04
300	0.9935	4.399E-04
400	0.9725	6.009E-04
500	0.9665	7.558E-04
600	0.9610	9.122E-04
700	0.9558	1.070E-03
800	0.9510	1.229E-03
900	0.9467	1.389E-03
1000	0.9427	1.550E-03

Table A4. 2. The carbon dioxide compressibility factor and initial injected moles for various pressures and temperature of 28°C.

P, psia	Z	lbmole
50	0.9818	7.2440E-04
100	0.9633	1.517E-04
200	0.9251	3.158E-04
300	0.8852	4.951E-04
400	0.8433	6.930E-04
500	0.7986	9.147E-04
600	0.7505	1.168E-04
700	0.6977	1.466E-03
800	0.6376	1.833E-03
900	0.5646	2.329E-03
1000	0.4550	3.211E-03

For the same system of N_2-water (100 psia, 301.3 K), the system pressure drops to 98 psia from the initial 100 psia after 1 minute. The compositions of both phases change as function of time due to the thermodynamic and chemical interactions between gas and water phases,

Step 2. The next step is to calculate the mole fractions of the water and nitrogen components in both the water and gas phases at the new time step. Majority of the EoSs fail to describe the phase behavior of the gaseous mixtures (especially polar gases) containing water. Therefore, the solubility of gaseous phase in water at various time steps is calculated using the P-R EoS with Alpha function modifications following the Coquelet et al. (2003) approach. The following example explains the procedure of obtaining gas and water phase composition changes versus time.

$$n_{initial\ N_2} = 0.00014719\ \ lbmoles$$

$$n_{initial,H_2O} = 100cc \times \frac{3.531466672 \times 10^{-5}\ ft^3}{cc} \times \frac{lb}{0.01606\ ft^3} \times \frac{lbmole}{18lb}$$

$$n_{initial,H_2O} = 1.22162 \times 10^{-2}\ lbmole$$

The mass conservation law indicates that the summation of the nitrogen component moles in the gas and water phases must be equal to the initial injected nitrogen moles. Therefore, the following relationships are true:

$$n_{initial\ N_2} = n_{Gg}(t) + n_{Gw}(t)$$

$$n_{initial\ H_2O} = n_{Ww}(t) + n_{Wg}(t)$$

To start, the following guesses are made:

$$n_{N_2-W} = 1.00\times10^{-9}\, lbmole$$

$$n_{W-N_2} = 1.00\times10^{-9}\, lbmole$$

Then, the mole fractions are calculated as:

$$x_{N2-w} = \frac{1.00\times10^{-9}}{1.00\times10^{-9} + 1.221622\times10^{-2}} = 8.1858375\times10^{-8}$$

$$x_{Ww} = 1.00 - x_{Gw} = 1.00 - 1.26\times10^{-6} = 0.99999874$$

$$x_{Ww} = 1.00 - 8.85375\times10^{-8} = 0.9999999181$$

$$y_{wG} = \frac{1.00\times10^{-9}}{1.00\times10^{-9} + 1.47189\times10^{-4}} = 6.794\times10^{-06}$$

$$y_{Gg} = 1.00 - 6.794\times10^{-6} = 0.9999932$$

For the gas phase the P-R EoS is used as following:

Table 5.4 contains necessary information about nitrogen and water critical temperature, pressure, acentric function, binary interaction coefficients, and other relevant parameters.

$$T_{rN_2} = \frac{T}{T_c} = \frac{28+273.3}{126} = 2.391$$

$$P_{rN_2} = \frac{P}{P_c} = \frac{98}{490} = 0.200$$

$$T_{rH_2O} = \frac{T}{T_c} = \frac{28+273.3}{647.3} = 0.465$$

$$P_{rH_2O} = \frac{P}{P_c} = \frac{98}{3219} = 0.0.0304$$

Equation 5.54 for nitrogen we have: $\alpha(T) = \left[1 + 0.4495\left(1 - \sqrt{2.391}\right)\right]^2 = 0.56934$

Equation 5.54 for water we have:

$$\alpha(T) = \left[1 + 0.9141\left(1 - \sqrt{0.465}\right) - 0.2357\left(1 - \sqrt{0.465}\right)^2 + 0.5411\left(1 - \sqrt{0.465}\right)^3\right]^2$$

$$\alpha(T) = 1.6486$$

Equation 5.56 for nitrogen:

$$a_{N_2} = 0.45724\frac{(19.31)^2(126.05)^2}{490}(0.569336) = 3147.505886$$

Equation 5.56 for water:

$$a_{H_2O} = 0.45724\frac{(19.31)^2(647.3)^2}{3219}(1.6486) = 36586.43$$

Equation 5.57 for nitrogen:

$$b_{N_2} = 0.07780\frac{(19.31)(126.05)}{(490)} = 0.386464$$

Equation 5.57 for water:

$$b_{N_2} = 0.07780\frac{(19.31)(647.3)}{(3219)} = 0.302097$$

Equation 5.54:

$$b = (0.9999931)(0.386464) + \left(6.79 \times 10^{-6}\right)(0.302097) = 0.386463$$

Equation 5.55:

$$a_{N_2-H_2O} = (1 - 0.425)\sqrt{(4171.406)(36586.43)} = 7165.215$$

Equation 5.53:

$$a = (2)(0.9999931)(6.69\times10^{-6})(7165.215) + (0.9999931)(3147.82422) + (6.69\times10^{-6})(36586.43) = 3147.82422$$

Equation 5.60:

$$A = \frac{(3147.82422)(98)}{(19.31)^2(301.3)^2} = 0.00911326$$

Equation 5.60:

$$B = \frac{(0.386463)(98)}{(19.31)(301.3)} = 0.006509575$$

Equation 5.52:

$$Z^3 - (1 - 0.006509575)Z^2 + (0.00911326 - 3(0.006509575)^2 - 2(0.006509575))Z - ((0.00911326)(0.006509575) - (0.006509575)^2 - (0.006509575)^3) = 0$$

$$Z^3 - (0.99349)Z^2 - (0.00403)Z - (1.70\times10^{-5}) = 0$$

Solving the above equation, the calculated value of Z is equal to:

Z= 0.99755

Therefore, the occupied volume by the gas phase is calculated as:

$$V_g = \frac{Zn_gRT}{P} = \frac{(0.99755)(1.00\times10^{-9} + 1.47189\times10^{-4} - 1.00\times10^{-9})(19.31)(301.3)}{(98.00)}$$
$$= 8.517\times10^{-3}\ ft^3$$

Step 3. The next step is to calculate the volume occupied by the liquid phase. For this purpose the modified Peng-Robinson method is used. Peng and Robinson (1976) modified their previous equation for the liquid phase by introducing a new parameter for the aqueous phase. They introduced the following expression for the aqueous phase:

$$a_{ij}^{AQ} = \sum_i \sum_j x_i x_j \left(a_i a_j\right)^{1/2} \left(1 - k_{ij}^{AQ}\right) \quad \text{(A4.1)}$$

Soreide and Whitson (1992) introduced series of expressions for the binary interaction coefficients for various gases and brine with various salinities (k_{ij}^{AQ}). This expression for hydrocarbon/brine mixture is:

$$k_{ij}^{AQ} = A_o\left(1 + \alpha_o c_{SW}\right) + A_1 T_{ri}\left(1 + \alpha_1 c_{SW}\right) + A_2 T_{ri}^2\left(1 + \alpha_2 c_{SW}\right) \quad \text{(A4.2)}$$

where the coefficients expressed in Equation 6.8 are given as:

Table A4. 3. Parameters used in Eq. 6.8 for the aqueous mixture of hydrocarbon/water.

A_0	$1.1120\text{-}1.7369\omega i^{-}_{0.1}$
A_1	$1.1001+0.8360\omega i$
A_2	-0.15742-1.0988ωi
α_0	$4.7863\times10^{-13}\,\omega_i^4$
α_1	1.4380×10^{-2}
α_2	2.1547×10^{-3}

Similarly for the aqueous mixture of N_2/brine we have:

$$k_{ij}^{AQ} = -1.70235\left(1 + 0.25587 c_{SW}^{0.75}\right) + 0.44338\left(1 + 0.8125 c_{SW}^{0.75}\right) T_{ri}$$

For CO_2/brine:

$$k_{ij}^{AQ} = -0.31092\left(1 + 0.15587 c_{SW}^{0.7505}\right) + 0.23580\left(1 + 0.17837 c_{SW}^{0.979}\right) T_{ri}$$
$$- 21.2566 \exp\left(-6.7222 T_{ri} - c_{SW}\right)$$

For H_2S/brine:

$$k_{ij}^{AQ} = -0.20441 + 0.23426T_{ri} \quad \text{(A4.3)}$$

Therefore, considering that the water salinity is zero ($c_{SW} = 0$), the volume of the aqueous solution is calculated as:

$$k_{N_2-water}^{AQ} = -(1.70235) + (0.44338)(2.390321) = -0.642529$$

$$a_{ij}^{AQ} = \left(1.26\times10^{-6}\right)^2(4171.406) + (0.999998743)^2(36586.43) + \left(1.26\times10^{-6}\right)(0.999998743)(1 + 0.642529) = 36586.337$$

The calculated Z_{max}= 0.99311. However Z_{min} is not a real number. Therefore, the mentioned approach is not applicable for this scenario. It could be due to the extremely low solubility of N_2 in water at low pressures. The alternative approach is to assume an infinite dilute solution by applying the Coquelet et al. (2003)'s approach. The following expressions are given:

$$v_i^{\infty} = \frac{RT_{c,i}}{P_{c,i}}\left[0.095 + 2.35\frac{TP_{c,i}}{cT_{c,i}}\right] \quad \text{(A4.4)}$$

where:

$$c = \frac{\Delta H_w - RT}{v_w^{sat}} \quad \text{(A4.5)}$$

where ΔH_w is the water enthalpy change due to vaporization of water, and v_w^{sat} is the saturated molar volume of water at 298.15 K. These values can be found in water property handbooks such as by Keenan (1969). For temperatures rather than 298.15 K, the volume term needs to be adjusted. However, for this study, the experiments were performed at the room temperature and therefore, the temperature adjustments are not required.

For water at 98 psia and 301.3 K from the water thermodynamic properties tables (Keenan, 1969) the following information are obtained: $v_w^{sat} = 0.016077 \frac{ft^3}{lb}$

$$\begin{cases} h_l = 50.08 \frac{Btu}{lb} \\ h_v = 1097.3 \frac{Btu}{lb} \end{cases}$$

Therefore the value of c in Equation A4.5 is calculated and substituted in Equation A4.4 to estimate the infinite dilution volume of nitrogen in water.

$$\Delta H_w(301.3K) = h_v - h_l = 1097.3 - 50.08 = 1047.22 \frac{Btu}{lb} \times 18 \frac{lb}{lbmole} = 18{,}849.96 \frac{Btu}{lbmole}$$

$$c = \frac{18{,}849.96 - (3.57458)(301.3)}{(0.016077) \times 18 \frac{lb}{lbmole}} = 61416.0293 \frac{Btu}{ft^3}$$

$$v_{N_2}^{\infty} = \frac{\left(3.57458 \frac{Btu}{lbmoleK}\right)(126.05K)}{490.0\,psia} \left[0.095 + 2.35 \frac{(301.3)K(490.0\,psia)}{\left(61416.0293 \frac{Btu}{ft^3}\right)(126.05K)} \right]$$

$$v_{N_2}^{\infty} = 0.4719 \frac{ft^3}{lbmole} + 0.04121 \frac{ft^3}{lbmole} = 0.51311 \frac{ft^3}{lbmole}$$

The liquid water volume is also obtained from the same table (Keenan, 1969):

$$v_w(301.3K, 98\,psia) = 0.0160 \frac{ft^3}{lb} \times 18 \frac{lb}{lbmole} = 0.2880 \frac{ft^3}{lbmole}$$

The dissolved nitrogen volume is estimated as:

$$V_{N_2} = n_{N_2-w} \times v_{N_2}^{\infty} = (1.0 \times 10^{-9}) \times (0.51311) = 5.1311 \times 10^{-10}\, ft^3$$

The water volume in the aqueous phase is calculated as:

$$V_{Ww} = n_{Ww} \times v_{Ww} = (0.2880) \times (1.22162 \times 10^{-2}) = 3.51826 \times 10^{-3}\ ft^3$$

The nitrogen volume in water in compare with water volume is negligible. Because the gas and water system is below their critical temperature and pressure, the summation of both volumes in the PVT cell is equal to the total PVT cell volume. Therefore:

$$V_{PVT-cell} = V_g(t) + V_w(t) = (8.517 \times 10^{-3}) + (3.51826 \times 10^{-3}) = 1.2052 \times 10^{-3}\ ft^3$$

The PVT cell volume is already measured and is equal to 1.2007ft^3. The percentage error for this problem is equal to:

$$P.E = \left| \frac{V_{cell-Measured} - V_{cell-Calculated}}{V_{cell-measured}} \right| \times 100 = \left| \frac{1.2052 - 1.2007}{1.2052} \right| \times 100 = 0.37522\%$$

The error margin may be acceptable. However, for the illustration purposes this process is repeated for other possible initial guesses. Because, the calculated volume is more than the PVT cell volume and the water volume does not change significantly, the moles of the dissolved gas in water should increase and also the moles of the evaporated water in gas phase should decrease. Table A4.4 summarizes the error percentage obtained by applying various initial guesses. Therefore, the best guessed mole fractions with the least percentage error are obtained from Table A4.4. Using the obtained values the fugacity values can be calculated using the following procedure.

The fugacity of any component in gaseous phase is calculated using the Peng-Robinson EoS. The following information is obtained from the previous procedure for the obtained values.

Z=0.994602, A= 0.01207672, B= 0.006509584, b_{N2}= 0.386464, b_w= 0.30209706, a_{N2}= 4171.406, a_w= 36586.43.

Table A4. 4. The calculated values for various values of the initial guess.

n_{N2-w}	n_{w-N2}	x_{N2-w}	y_{wN2}	PE, %
1.00E-09	1.00E-08	8.19E-08	6.05E-05	-0.3990
1.00E-10	1.00E-08	8.19E-09	6.95E-05	-0.3795
1.00E-08	1.00E-08	8.19E-07	6.95E-06	-0.3747
1.00E-08	7.80E-08	8.38E-06	6.79E-07	0.0003
1.00E-06	1.00E-07	8.19E-06	6.79E-06	0.0695

Equation 5.51:

$$\ln\left(\frac{\hat{f}_{N_2}}{y_{N_2}P}\right)=\frac{(0.386464)}{(0.38646358)}(0.994602-1)-\ln(0.994602-0.006509584)$$

$$-\frac{0.01207672}{2\sqrt{2}(0.006509584)}\left(\frac{2(0.99999321)(3147.406)+2\left(6.7944\times10^{-07}\right)(36586.43)}{4171.437816}-\frac{0.38646358}{0.38646358}\right)$$

$$\ln\left(\frac{0.994602+2.414(0.006509584)}{0.994602-0.414(0.006509584)}\right)=-0.194$$

$$\hat{f}_{N_2-N_2}=(0.999931)(98.0)[\exp(-0.194)]=80.6\,psia$$

Similarly for water:

$$\ln\left(\frac{\hat{f}_w}{y_w P}\right) = \frac{(0.302097)}{(0.38646358)}\left(6.7944\times10^{-7} - 1\right) - \ln(0.994602 - 0.006509584)$$
$$-\frac{0.01207672}{2\sqrt{2}(0.006509584)}\left(\frac{2(0.99999321)(3147.406) + 2\left(6.7944\times10^{-07}\right)(36586.43)}{4171.437816} - \frac{0.302097}{0.38646358}\right)$$
$$\ln\left(\frac{0.994602 + 2.414(0.006509584)}{0.994602 - 0.414(0.006509584)}\right) = -0.0069366$$

$$\hat{f}_{W-N_2} = \left(6.7944\times10^{-7}\right)(98.0)\left[\exp(-0.00693664)\right] = 6.61248\times10^{-5}\ psia$$

Step 4. The next step is to calculate the fugacity values of each component in the water phase. The following procedure describes the necessary steps. The Henry's constant for the system of nitrogen in water is calculated using the following expression (table 5.8):

$$H^{\circ}_{N_2-w}(psia) = (13791.0)(301.3) - 2.85\times10^{6} = 1.30523\times10^{6}\ psia$$

From the water thermodynamic properties data the corresponding water saturation pressure at 301.3 K is $P_w^{sat} = 15.2414\ \ psia$. The nitrogen fugacity in water phase is then calculated.

Equation 5.63:

$$\ln\gamma_{N_2} = \ln\gamma^{C}_{N_2} + \ln\gamma^{R}_{N_2}$$

The structure N_2 in N_2 is repeated only one time, therefore:

Equation 5.65:

$$v^{(N_2)}_{N_2} = 1 \rightarrow r_{N_2} = (1)(1.8680) = 1.8689$$

Equation 5.65:

$$v^{(w)}_{w} = 1 \rightarrow r_{w} = (1)(0.9200) = 0.9200$$

Equation 5.67:

$$V'_{N_2} = \frac{(1.8680)^{3/4}}{(8.18584\times10^{-7})(1.8689)^{3/4} + (0.99999918)(0.9200)^{3/4}} = 1.770144$$

Equation 5.67:

$$V_{N_2} = \frac{(1.8680)}{(8.18584\times10^{-7})(1.8689) + (0.99999918)(0.9200)} = 2.141302$$

Equation 5.67:

$$q_{N_2} = (1.9700)(1.0) = 1.9700$$

Equation 5.67:

$$q_w = (0.9200)(1.0) = 0.9200$$

Equation 5.67:

$$F_{N_2} = \frac{(1.9700)}{(8.18584\times10^{-7})(1.9700) + (0.99999918)(1.400)} = 2.141302$$

Equation 5.66:

$$\ln\gamma^C_{N_2} = 1 - 1.770144 + \ln(1.770144) - 5(1.9700)\left(1 - \frac{1.770144}{2.141302} + \ln\frac{1.770144}{2.141302}\right)$$

$$\ln\gamma^C_{N_2} = -0.03143$$

Equation 5.68:

$$\ln\gamma^R_{N_2} = \sum \upsilon^{(N_2)}_{N_2}\left(\ln\Gamma_{N_2} - \ln\Gamma^{(N_2)}_{N_2}\right)$$

$$\Gamma_{N_2} = \Gamma_{N_2}^{N_2}$$

Therefore, the residual activity coefficient for this system is equal to zero:

$\ln \gamma_{N_2}^{R} = 0$.

$$\ln \gamma_{N_2} = (-0.03143) + (0.0) = -0.03143 \rightarrow \gamma_{N_2} = 0.969056$$

Equation 5.61:

$$\ln\left(\frac{\hat{f}_{N_2w}}{x_{N_2w}}\right) = \ln\left[\left(1.30523 \times 10^{6}\right)(0.969056)\right] + \frac{0.08840}{(19.31)(301.3)}(98.00 - 15.2414) = 14.0517$$

$$\hat{f}_{N_2w} = \left(6.376 \times 10^{-6}\right)\left(1.2664142 \times 10^{6}\right) = 8.07212 \text{ psia}$$

To calculate the fugacity of water component in water phase, the activity coefficient of the water component is calculated according to the following procedure:

Equation 5.67:

$$V_w' = \frac{(0.9200)^{3/4}}{\left(8.18584 \times 10^{-7}\right)(1.8689)^{3/4} + (0.99999918)(0.9200)^{3/4}} = 0.99999937$$

$$V_w = \frac{(0.9200)}{\left(8.18584 \times 10^{-7}\right)(1.8689) + (0.99999918)(0.9200)} = 0.999999066$$

$$q_w = (0.9200)(1.0) = 0.9200$$

$$F_w = \frac{(1.400)}{\left(8.18584 \times 10^{-7}\right)(1.9700) + (0.99999918)(1.400)} = 0.999999667$$

Equation 5.66:

$$\ln\gamma_w^C = 1 - 0.99999937 + \ln(0.99999937) - 5(0.9200)\left(1 - \frac{0.99999937}{0.999999667} + \ln\frac{0.99999937}{0.999999667}\right)$$

$$\ln\gamma_w^C = 1.10318\times10^{-13}$$

$$\ln\gamma_w^R = \sum \upsilon_w^{(w)}\left(\ln\Gamma_w - \ln\Gamma_w^{(w)}\right)$$

$$\Gamma_w = \Gamma_w^w$$

Therefore, the residual activity coefficient for this system is equal to zero ($\ln\gamma_w^R = 0$).

$$\ln\gamma_w = \left(1.103\times10^{-13}\right) + (0.00) \approx 0.00 \rightarrow \gamma_w = 1.00$$

Step 5. The next step is to estimate the vapor fugacity coefficient of saturated pure water. This parameter is calculated using Redlich-Kwong EoS as described below (Li et al. 1997):

$$\ln\phi_w^{sat} = \ln\left(\frac{v}{v-b}\right) + \frac{b}{v-b} - 2\frac{y_w a_{ww}}{RT^{1.5}b}\left(\frac{v+b}{v}\right) + \frac{ab}{RT^{1.5}b^2}\left[\ln\left(\frac{v+b}{v}\right) - \frac{b}{v+b}\right] - \ln\left(\frac{Pv}{RT}\right) \quad \text{.....(6.12)}$$

where:

$$a_{ww} = \begin{cases} 3493.75 - 16.2791(T) + 0.0207716(T)^2 & T \le 323.15K \\ 5518.64 - 37.4866(T) + 0.100081(T)^2 - 1.19610\times10^{-4}(T)^3 + & \text{.....(A4.6)} \\ 5.34185\times10^{-8}(T)^4 & 323.15 < T < 647.3 \end{cases}$$

$$a = 2y_w^2 a_{ww} \quad \text{.....(A4.7)}$$

$$b_w = 0.0867\frac{RT_c}{P_c} \quad \text{.....(A4.8)}$$

$$b = y_w b_w \quad \text{.....(A4.9)}$$

where v is the pure saturated water vapor molar volume is obtained from the water thermodynamic property table. For T=301.3 K, this value is:

$$v_v^{sat} = 10710 \frac{ft^3}{lbmole}$$

$$a_{ww} = 3493.95 - 16.2791(301.3) + 0.0207716(301.3)^2 = 474.5238$$

$$b_w = 0.0867 \frac{(19.31)(647.3)}{(3219)} = 0.3367$$

$$b = (1.00)(0.3367) = 0.3367$$

$$a = 2(1.00)^2 (474.5238) = 949.0476$$

Equation 6.12:

$$\ln \phi_w^{sat} = \ln\left(\frac{10710}{10710 - 0.3367}\right) + \frac{0.3367}{10710 - 0.3367} - 2\frac{(1.00)(474.5288)}{(19.31)(301.3)^{1.5}(0.3367)}$$
$$\left(\frac{10710 + 0.3367}{10710}\right) + \frac{(949.0476)(0.3367)}{(19.31)(301.3)^{1.5}(0.3367)^2}\left[\ln\left(\frac{10710 + 0.3367}{10710}\right) - \frac{0.3367}{10710 + 0.3367}\right]$$
$$- \ln\left(\frac{(98.00)(10710)}{(19.31)(301.3)}\right) = -5.24575$$

$$\phi_w^{sat} = 0.00527$$

Equation 5.62:

$$\ln\left(\frac{\hat{f}_{Ww}}{x_{Ww}}\right) = \ln[(1.0)(0.00527)(15.2414)] + \frac{0.289386}{(19.31)(301.3)}(98.0 - 15.2414) = -2.51762$$

$$\hat{f}_{Ww} = (0.999991815)(\exp(-2.5176)) = 0.080651 psia$$

The parameters obtained thus far are summarized in the following table.

Table A4. 5. Summarized parameters obtained for N_2-water system (301.3K and 98.0 psia).

P, psia	x_{N2-w}	y_{w-N2}	$\hat{f}_{N_2-}$ psi	$\hat{f}_{w-N_2}$ psi	$\hat{f}_{N_2-w}$ psi	$\hat{f}_{Ww}$ psi
98.00	6.376E-06	6.794E-07	80.61	6.6125E-5	8.07212	0.080651

A4.2. Single-Component Gas-Coal System

Similar to the previous case (nitrogen-water), the initial injected moles of nitrogen and carbon dioxide at various pressures are calculated. The coal volume is calculated using the coal density and coal mass as following:

$$V_{Coal} = m_{coal} \times \frac{1}{\rho_{coal}}$$

For coal A and B:

$$V_{CoalA} = (100gr)\left(\frac{1}{1.45gr/cc}\right)\left(\frac{ft^3}{28631.847cc}\right) = 2.409\times10^{-3}\,ft^3$$

$$V_{CoalB} = (100gr)\left(\frac{1}{1.35gr/cc}\right)\left(\frac{ft^3}{28631.847cc}\right) = 2.587\times10^{-3}\,ft^3$$

$$V_{gasA} = V_{cell} - V_{water} = 0.0120069 - 0.003881 = 0.0080803\,ft^3$$

$$V_{gasB} = V_{cell} - V_{water} = 0.0120069 - 0.004366 = 0.007593\,ft^3$$

Table A4. 6. The initial injected gas (nitrogen and carbon dioxide) moles to the PVT cell for various pressure levels.

P, psia	$n_{N2\text{-}CoalA}$, lbmole	$n_{N2coalB}$, lbmole	$n_{CO2coalA}$, lbmole	$n_{CO2coalB}$, lbmole
50	8.2462E-05	8.081E-05	8.38E-05	8.222E-05
200	0.0003306	0.0003243	0.000356	0.0003493
400	0.0006634	0.0006509	0.0007824	0.0007677
600	0.0009973	0.000978536	0.00132	0.0012972
800	0.00133	0.001306	0.002087	0.002047

2. For an instance, the nitrogen gas is injected to the PVT cell at 200 psia and 30.3 K. The system shows 2 psia net pressure drops after 2 minutes. This pressure drop is due to the gas adsorption on the coal internal surfaces.

3. The coal volume undergoes some changes. Coal volume reduces due to the external pressure (overburden pressure in the reservoir condition) and increases due to gas adsorption. For illustration purposes, it is assumed that the coal swelling parameter for the coal-N_2 system is approximately 3.40E-7 /psia. This value is the

same as the coal swelling parameter for helium adsorption in coal reported in Table 5.1. The coal compressibility value is taken from Table 5.2 is equal to 2.14E-06 psi^{-1}.

4. The adsorbed gas moles are guessed and the coal new volume and also the remaining gas new volumes are calculated:

$n_{N2\text{-}coal}$=1.00E-6 lbmole

Equation 5.30 is applied to estimate the coal new volume as:

$$V_c^{t+1}(t) = \left[1 + \left(3.40 \times 10^{-7}\right)(182) - \left(2.14 \times 10^{-6}\right)(198.0)\right]\left(2.409 \times 10^{-3}\right) = 0.00243463 \text{ ft}^3$$

Applying the Peng-Robinson EoS for the volume of the nitrogen component at 198 psia and 301.3K is calculated as:

V_{N2}= 0.009638926 ft^3

If the sum of the calculated nitrogen gas and coal volumes is equal to the cell volume, the initial guess is correct. Otherwise, a new value for the moles of the adsorbed gas is guessed and the same procedure is repeated.

$V_{coal}+V_{N2}$=0.009638926+0.00243263 =0.0120735 ft^3

The percent error is calculated by:

$$P.E = \left|\frac{V_{Cell} - V_{Cell_{New}}}{V_{Cll}}\right| \times 100 = \left|\frac{0.012006987 - 0.0120735}{0.012006987}\right| \times 100 = 0.56 > 1.0 \times 10^{-6}$$

The acceptable error percentage (PE) is 1.0E-06. Therefore the same procedure is repeated until the correct value of the adsorbed nitrogen moles is obtained as following:

$n_{N2\text{-}coal}$=3.276E-6 lbmole

The corresponding gas volume in the standard conditions (T= 298.3K and P= 14.6 psia) is calculated as:

$$V_{sc} = \frac{(3.276\times10^{-06})(19.31)(298.3)}{(14.6)} = 1.2924\times10^{-3}\ scf$$

The calculated adsorbed volume is based on 100 gm coal. The adsorbed volumes are usually expressed as scf/ton. Therefore we have:

$$V(scf/ton) = (1.2924\times10^{-3}\ scf/100 gm\ coal)\frac{10^6\ gr\ coal}{1.0\ ton\ coal} = 12.92\ \ scf/ton$$

Repeating the same procedure for all pressure drop values the single component non-equilibrium isotherm for the pressure range of 200-182 psia establishes.

A4.3. Coal-water-Single Component Gas System

To explain the calculation procedure for coal-water-single component gas consider the system of CO_2 gas in the PVT cell in contact with coal A (d_g=0.15 inch) and water. The system is pressurized to an initial pressure of 200 psia. First, the volume and lbmoles of each component at time zero are calculated.

$$V_{coal} = (100gr)\left(\frac{cm^3}{1.45gr}\right)\left(\frac{1ft^3}{28361.84cm^3}\right) = 0.0024355\,ft^3$$

$$n_{initial,H_2O} = 40cc \times \frac{3.531466672\times10^{-5}\,ft^3}{cc} \times \frac{lb}{0.01606\,ft^3} \times \frac{lbmole}{18lb}$$

$$n_{initial,H_2O} = 0.0048865\ \ lbmole$$

$$n_{initial,CO_2} = \frac{PV_{CO_2}}{ZRT} = \frac{(200)(340.0-40.0-68.97)}{(0.92411)(19.31)(301.3)} = 0.0003493\ \ lbmole$$

The system pressure drops to 193.0 psia from initial pressure of 200 psia after one minute. The time-dependency of the solubility of CO_2 in water and dissolution of water in CO_2 follow a series of equations that are already obtained. According to the parameters reported in Table 6.12 these equations (Equation 6.17 and 6.18 for CO_2-water system) are:

$$\frac{y^{t+1}_{CO_2-CO_2} - y^{t}_{CO_2-CO_2}}{\Delta t} = \left(4.11\times10^{-04}\right)\exp\left[\left(8.50\times10^{-2}\right)\frac{\hat{f}_{CO_2-CO_2}}{\hat{f}_{CO_2-w}} - (32.0)\frac{\hat{f}_{CO_2-w}}{\hat{f}_{CO_2-CO_2}}\right]$$

$$\frac{x^{t+1}_{W-w} - x^{t}_{W-w}}{\Delta t} = \left(2.70\times10^{-08}\right)\exp\left[\left(2.74\times10^{-02}\right)\frac{\hat{f}_{w-W}}{\hat{f}_{w-CO_2}} - (90.0)\frac{\hat{f}_{w-CO_2}}{\hat{f}_{w-W}}\right]$$

To calculate the fugacity values the lbmole of gas in water and coal phases, the lbmoles of water in gas and coal phases must be known. Therefore, some initial guess for these values are made as:

$$n_{w-coal} = 1.0\times10^{-6}\,lbmole$$
$$n_{CO_2-coal} = 1.0\times10^{-6}\,lbmole$$

$$n_{CO_2-w} = 1.0\times10^{-6}\,lbmole$$
$$n_{w-CO_2} = 1.0\times10^{-6}\,lbmole$$

The mole fractions of water component in the gas phase and carbon dioxide in the water phase are calculated. The new coal, gas, and water phase volumes are calculated. The percent error is 2.13%. This value is greater than 1.0E-06. The deviations could be due to the error in the initial guess of the lbmoles of the adsorbed water and carbon dioxide on coal or in the initial guess of the gas and water lbmoles in gas and water phases. To investigate this issue, using these values the fugacity values of the water and gas components in water and gas phases are calculated:

$$f_{CO_2-CO_2} = 138.156\,psia$$
$$f_{w-CO_2} = 2.36\times10^{-4}\,psia$$
$$f_{CO_2-w} = 23.97\,psia$$
$$f_{W-w} = 4.32\times10^{-2}\,psia$$

Substituting these values in Equations 6.17 and 6.18 the new mole fractions of water and carbon dioxide in the gas and water phases are calculated.

$$\frac{y_{W-CO_2}^{t+1} - 0.0}{(1.0)} = \left(6.50\times10^{-04}\right)\exp\left\{\left(8.50\times10^{-2}\right)\frac{138.156}{23.97} - (32.0)\frac{23.97}{138.156}\right\}$$
$$= 4.11\times10^{-06}$$

$$\frac{x_{CO_2-w}^{t+1} - 0.0}{\Delta t} = \left(2.74\times10^{-08}\right)\exp\left\{\left(2.74\times10^{-02}\right)\frac{4.32\times10^{-02}}{2.36\times10^{-04}} - (90.0)\frac{2.36\times10^{-04}}{4.32\times10^{-02}}\right\}$$
$$= 2.52\times10^{-06}$$

Therefore the new mole fractions at the new time are obtained as:

$$y_{W-CO_2} = 4.11\times10^{-06} < 2.04688\times10^{-05}$$
$$x_{CO_2-w} = 2.52\times10^{-06} < 3.316\times10^{-04}$$

The old guessed values are replaced with the new calculated ones. The new calculated values are used in the same procedure to estimate the fugacity values. After some iteration, the final mole fraction values are:

$$y_{W-CO_2} = 2.1\times10^{-06}$$
$$x_{CO_2-w} = 3.53\times10^{-05}$$

The next step is to calculate the adsorbed moles of water and carbon dioxide in the coal phase using:

$$y_{W-CO_2} = \frac{n_{W-CO_2}}{n_{CO_2-CO_{2_{initial}}} + n_{W-CO_2} - n_{CO_2-coal} - n_{CO_2-w}}$$

$$x_{CO_2-w} = \frac{n_{CO_2-w}}{n_{W-w_{initial}} + n_{CO_2-w} - n_{W-coal} - n_{W-CO_2}}$$

The initial guessed values of $n_{W\text{-}coal}$ and $n_{CO2\text{-}coal}$ are applied in above equations and the corresponding values of $n_{CO2\text{-}w}$ and $n_{W\text{-}CO2}$ are calculated. These values are used to estimate the volume of each phase. The sum of the volumes of each phase below the system critical temperature and pressure (T = 304 K and P = 1064 psia) is equal to the PVT cell volume. After some iteration the corrected final values are calculated as:

$$n_{w-coal} = 9.80\times10^{-05}\, lbmole/100gm\ coal$$
$$n_{CO_2-coal} = 1.10\times10^{-05}\, lbmole/100gm\ coal$$

These values are equivalent to the following:

$$m_{w-coal} = 17.64 lb/ton\ coal = 8{,}000 gm/ton-coal = 0.8\%wt$$
$$V_{CO_2-coal} = 43.398\ \ scf/ton$$

A 4.4. Coal-Water-Multi-Component Gas system

For instance, a gas mixture with initial $P_r = \frac{P_{N_2}}{P_{CO_2}} = 0.25$ is injected to the PVT cell up to the initial pressure of P_{tin}=200 psia. The mole fraction of each component in the gas phase at the initial time is calculated by:

$$n_{N_2-gas} = \frac{(V_{cell} - V_{coal})P_r P_{\text{int}}}{Z_{N_2} RT} = \frac{(9.556\times10^{-03})(0.25)(200.0)}{(0.9953)(19.31)(301.3)} = 8.23\times10^{-05}\, lbmole$$

The lbmoles of the injected carbon dioxide is guessed and then the mole fractions are calculated. The gas volume is calculated applying the Peng-Robinson EoS with the system total pressure equal to 200 psia. This volume is compared with the PVT cell free volume. The comparison is made and the mentioned process is repeated until a good agreement is achieved between the calculated and measured gas volumes. This value is calculated as:

$$n_{CO_2-gas} = 2.66\times10^{-04}\, lbmole$$

Therefore, the initial gas mole fraction in gas phase is obtained as:

$$y_{N_2-gas} = 0.2377 \quad y_{CO_2-gas} = 0.7625$$

The system total pressure drops to 193.3 psia from the initial pressure of 200 psia after 1.0 minute. Following the previously explained procedure, the lbmoles of both N_2 and CO_2 components in the coal phase are guessed. The coal and gas phase new volumes are calculated. The procedure is repeated until the sum of both phase volume is equal to the total cell volume. Therefore, the adsorbed volumes of each component in the coal phase can be calculated using the corresponding lbmoles of each component in the coal phase at the specified pressure. After several trial and errors these values are calculated to be:

$$n_{N_2-coal} = 1.80 \times 10^{-06}\, lbmole = 7.094\ \ scf/ton$$
$$n_{CO_2-coal} = 1.10 \times 10^{-05}\, lbmole = 43.36\ \ scf/ton$$

The critical point is that the obtained values may not be the unique values. To determine the best approximation, this process is repeated for other possible pairs that may satisfy the above conditions. The V_{CO2} values are plotted versus the V_{N2} values. Investigating the pure N_2 and CO_2 adsorption on coal for the new pressure value of 193.3 psia indicates that the 6.7 psia pressure drop for the case of pure nitrogen and carbon dioxide are equivalent to 43.75 scf/ton and 50.84 scf/ton, respectively. These two points are also a part of the above plot. Therefore, the intersection of two lines will provide the best possible versus of V_{CO2} and V_{N2}. Figure 6.42 shows the process of obtaining the best possible values. For the above example the best pair is obtained as V_{CO2}= 39.41 scf/ton and V_{N2}= 9.80 scf/ton.

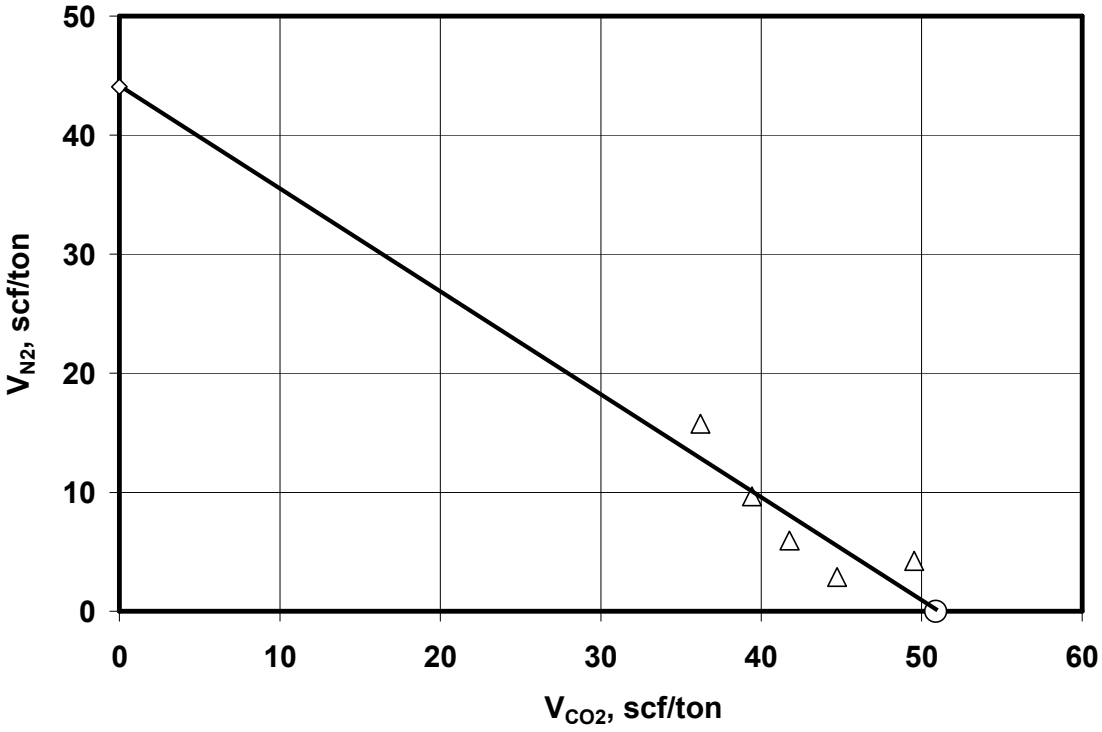

Figure A4. 1. Obtaining the best possible pair of adsorbed volume of nitrogen and carbon dioxide from a binary mixture by plotting the calculated nitrogen volume versus the calculated carbon dioxide volume.

APPENDIX 5

INCORPORATIN THE NON-EQUILIBRIUM ADSORPTION ISOTHERM IN COALBED METHANE/SHALE GAS RESERVOIR SIMULATION (DERIVATIONS OF THE EQUATIONS)- SUPPLEMENT TO CHAPTER 7

Appendix 5 describes a series of the simulation procedures considered to incorporate the time-dependency of the adsorption phenomenon to improve the quality and the flexibility of the current coalbed methane/shale gas reservoirs.

A5.1. High Rank Coal with Extremely Low Matrix Porosity (Close to Zero)

Assuming an average diffusivity coefficient for the entire matrix block (Figure 7.1) Equation 7.11 becomes:

$$\frac{\partial C}{\partial t} = -\overline{D}_{gm}\left[\frac{\partial^2 C}{\partial x^2} + \frac{\partial^2 C}{\partial y^2} + \frac{\partial^2 C}{\partial z^2}\right] \quad \text{(A5.1)}$$

Using the reservoir matrix grid block average properties Equation A5.1 becomes (F_S is the shape factor):

$$\frac{d\overline{C}}{dt} = -\overline{D}_{gm}(\Delta C)F_S\left[\frac{1}{\Delta x^2} + \frac{1}{\Delta y^2} + \frac{1}{\Delta z^2}\right] \quad \text{(A5.2)}$$

The mean-fracture spacing, S_f, is defined as:

$$\frac{1}{S_f} = \left[\frac{1}{\Delta x^2} + \frac{1}{\Delta y^2} + \frac{1}{\Delta z^2}\right]^{1/2} \quad \text{(A5.3)}$$

Substituting Equation A5.3 into Equation A5.2 yields:

$$\frac{d\overline{C}}{dt} = -\frac{\overline{D}_{gm} F_S}{S_f^2}(\Delta C) \quad \text{(A5.4)}$$

The gas concentration is defined according to Equations 7.6 and 7.7. Substituting Equation 7.6 into Equation 7.15, after some rearrangements results in:

$$\frac{dV_{sc}}{dt} = -\frac{\overline{D}_{gm} F_S V_{matrix} RT_{sc}}{S_f^2 P_{sc}}\left(\Delta\overline{C}\right) \quad \text{(A5.5)}$$

The following relationship is applicable:

$$q_{m\,\mathrm{csc}}(t) = \frac{dV_{sc}}{dt} \quad \text{(A5.6)}$$

Therefore Equation A5.6 becomes:

$$q_{m\,\mathrm{csc}}(t) = -\frac{\overline{D}_{gm} F_S V_{matrix} RT_{sc}}{S_f^2 P_{sc}}\left(\Delta\overline{C}\right) \quad \text{(A5.7)}$$

where:

$$\Delta\overline{C} = \overline{C}_{gas}^{\,matrix} - \overline{C}_{gas}^{\,cleat} \quad \text{(A5.8)}$$

The gas concentration in the matrix is defined as:

$$\overline{C}_{gas}^{\,matrix} = \frac{\overline{n}_{gas}^{\,matrix}}{V_{matrix}} = \frac{1}{V_{matrix}} \frac{P_{sc}\overline{V}_{gas}^{\,matrix}}{RT_{sc}} \quad \text{(A5.9)}$$

The volume of the gas in the matrix is a function of time for a specific matrix pressure and is estimated using the non-equilibrium isotherm:

$$V_{gas}^{\,matrix}(t) = \overline{V}_m \exp\left\{-\left[-\overline{D}\ln\frac{\overline{P}_{matrix}}{P_o}\tanh\left(2P_{matrix}K_{gs}t\right)\right]^r\right\} V_{matrix}\rho_{matrix} \quad \text{(A5.10)}$$

The gas concentration in the cleat is defined as:

$$\overline{C}_{gas}^{\,cleat} = \left(\overline{S}_g^{\,cleat} - S_{wc}\right)\frac{\overline{P}_{gas}^{\,cleat}}{\overline{Z}_{gas}^{\,cleat} R\overline{T}_{cleat}} \quad \text{(A5.11)}$$

Therefore Equation A5.11 becomes:

$$q_{m\,\mathrm{csc}}(t) = -\frac{\overline{D}_{gm} F_S V_{matrix} RT_{sc}}{S_f^2 P_{sc}}$$

$$\left\{ \begin{array}{l} \dfrac{P_{sc}\overline{\rho}_{matrix}}{RT_{sc}} \overline{V}_m \exp\left\{ -\left[-\overline{D} \ln\left(\dfrac{\overline{P}_{matrix}}{P_o} \tanh\left(2\overline{P}_{matrix} K_{gs} t\right)\right)\right]^r \right\} \\ -\left(\overline{S}_{gas}^{cleat} - S_{wc}\right) \dfrac{\overline{P}_{cleat}}{\overline{Z}_{gas}^{cleat} R\overline{T}_{cleat}} \end{array} \right\} \quad \text{.....(A5.12)}$$

Two parameters of K_{mic} and K_{mac} are defined as following to describe the diffusivity factor of the gas component in the matrix micropores and macropores respectively:

$$K_{mic} = \frac{\overline{D}_{gm} F_S}{S_f^2} \quad \text{.....(A5.13)}$$

$$K_{mac} = K_{gs} P_O \quad \text{.....(A5.14)}$$

Therefore Equation 7.A5.12 becomes:

$$q_{m\,\mathrm{csc}}(t) = -\frac{K_{mic} V_{matrix} RT_{sc}}{P_{sc}}$$

$$\left\{ \begin{array}{l} \dfrac{P_{sc}\overline{\rho}_{matrix}}{RT_{sc}} \overline{V}_m \exp\left\{ -\left\{ -\overline{D} \ln\left[\dfrac{\overline{P}_{matrix}}{P_o} \tanh\left(2\dfrac{\overline{P}_{matrix}}{P_o} K_{mac} t \right)\right]\right\}^r \right\} \\ -\left(\overline{S}_{gas}^{cleat} - S_{wc}\right) \dfrac{\overline{P}_{cleat}}{\overline{Z}_{gas}^{cleat} R\overline{T}_{cleat}} \end{array} \right\} \quad \text{.....(A5.15)}$$

A 5.2. Low Rank Coals and Shale with Relatively Higher Matrix Porosity

The low rank coals and shale reservoirs contain higher matrix porosity and therefore, the free methane stored in the matrix pore spaces is comparable with the

adsorbed methane in the matrix coal internal surfaces. For this case the governing equations are explained in the following.

The cleat-matrix gas flow rate for low rank coals and shale gas reservoirs is expressed by:

$$-\frac{d\overline{\overline{\tau}}_{mc}}{dt}=\frac{\overline{D}_{gm}F_S V_b Mw}{S_f^2}\Delta C=\frac{V_b Mw}{RT}\frac{d}{dt}\left(\frac{P_{gas}^{matrix}}{Z}\phi\right)+\frac{d\overline{\overline{m}}}{dt} \quad \text{(A5.16)}$$

The gas volume entering the cleat structure is also expressed as:

$$q_{m\,\mathrm{csc}}=\frac{\overline{D}_{gm}F_S V_b RT_{sc}}{S_f^2 P_{sc}}\Delta C=\frac{V_b T_{sc}}{TP_{sc}}\frac{d}{dt}\left(\frac{P_{gas}^{matrix}}{Z}\phi_{matrix}\right)+\frac{d\overline{\overline{V}}_{dsc}}{dt} \quad \text{(A5.17)}$$

The apparent gas diffusivity in the matrix microspores and macropores are defined as:

$$K_{mic}=\frac{\overline{D}_{gm}F_S}{S_f^2} \quad \text{(A5.18)}$$

$$K_{mac}=K_{gs}P_O \quad \text{(A5.19)}$$

Therefore Equation A5.17 becomes:

$$q_{m\,\mathrm{csc}}=\frac{K_{mic}V_b RT_{sc}}{P_{sc}}\Delta C=\frac{V_b T_{sc}}{TP_{sc}}\frac{d}{dt}\left(\frac{P_{gas}^{matrix}}{Z}\phi_{matrix}\right)+\frac{d\overline{\overline{V}}_{dsc}}{dt} \quad \text{(A5.20)}$$

Equation A5.21 shows that the matrix gas production rate is initially due to the matrix pore volume gas diffusion through the matrix. The diffused gas is replaced by the desorbed gas. If the diffusion coefficient is high enough then the desorption

rate is the limiting process in matrix gas production and transportation. However, if the matrix gas diffusion coefficient is relatively small, the matrix gas production will be limited by diffusion process.

The gas concentration in the matrix to be used in Equation A5.20 is defined as:

$$\overline{C}_{gas}^{matrix} = \frac{\overline{n}_{gas}^{matrix}}{V_{matrix}} = \frac{1}{V_{matrix}}\left[\frac{P_{sc}\overline{V}_{des,gas}^{matrix}}{RT_{sc}} + \frac{\overline{P}_{matrix}V_{\phi}}{\overline{Z}_{mtrix}R\overline{T}_{matrix}}\right] \quad \text{(A5.21)}$$

The volume of the gas in the matrix is a function of time for a specific matrix pressure and is estimated using the non-equilibrium isotherm:

$$V_{gas}^{matrix}(t) = \overline{V}_m\left(V_{matrix} - V_{\phi}\right)\rho_{matrix}\exp\left\{-\left[-\overline{D}\ln\frac{\overline{P}_{matrix}}{P_o}\tanh\left(2P_{matrix}K_{gs}t\right)\right]^r\right\} \quad \text{(A5.22)}$$